DYNAMIC MODELLING AND EXPERIMENTAL STUDIES OF TURBULENT BUBBLY FLOW IN BUBBLE COLUMN REACTORS

by

Xinyue CAI

A thesis submitted to the University of Nottingham in fulfilment of the requirements for the degree of

Doctor of Philosophy

Under the supervision of

Prof Xiaogang Yang

Dr Guang Li

JUNE 2022

DEDICATION

To my parents for their endless love, support and encouragement.

Thank you for everything.

ACKNOWLEDGEMENT

This is a pretty emotional moment for me when I write down the first sentence of this acknowledgement. Look back my PhD study, I only have endless gratitude to everyone who supported me over this long journey.

First, I would like to express my deepest gratitude to my supervisor, Professor Xiaogang Yang, for his consistent help, encouragement, physical insight, creative influence and patient guidance in my entire PhD study. I have known Prof. Yang for 7 years since my undergraduate study, his constructive criticise, expertise guidance and diligence to work harder than students encourage me all the time. I still can remember my first lecture from Prof. Yang was about vector and Taylor Expansion, which was the motivation of my PhD study. He is not only the best supervisor for academic studies but also acts as a mentor of life, I have been touched with and benefited a lot from his words many times as Prof. Yang always gave me tolerance and understanding.

Also, my thanks go to the thesis' two examiner, Professor Bin Chen, Xi'an Jiao-tong University and Dr. Yong Ren, the University of Nottingham Ningbo China, for their valuable time in reviewing my PhD thesis.

This work was financially supported by the National Natural Science Foundation of China and the Deutsche Forschungsgemeinschaft (DFG, German Research Foundation) (Grant Nos. 91534118, 21761132026). I would also like to acknowledge the Ph.D. scholarship of the International Doctoral Innovation Centre

(IDIC) of the University of Nottingham Ningbo China and the support of EPSRC (Grant no. EP/G037345/1). My sincerest thanks to Ms. Jessica Wang for her administrative support.

I would like to thank the FAST group members, Dr. Guang Li, Dr. Jie Yang, Dr. Weibin Shi, Dr. Luming Chen, Dr. Bin Dong, Dr. Xiani Huang, Dr. Chenyang Xue, Dr. Lu Liu, Dr. Yanqing Guo, Dr. Bin Li, Dr. Shanshan Long, Ms. Lulu Wang, Ms. Jiaying Lu and Ms. Rui Jiang for their assistance and pleasurable discussions. It has been a great pleasure to work with all of you. I also wish to express my thanks to my fellow colleagues, especially Mr. Jiarui Gao and Mr. Zeping Wang for your generous help and support.

I would especially like to thank my best friend, Ms. Dan Ge. Thank you for sailing through this journey with me, loving me and always cheering me during the most difficult days. You have been my greatest support and companion. I also owe my sincere gratitude to my friends, particularly Dr. Bin Li and Dr. Shiyuan Liu, for their constant help and encouragement. Thank you for standing by me so I can stand on mountains.

Special thanks are given to my parents, Mr. Angang Cai and Mrs. Yuan Hu, for their love, support and encouragement. You are my everything.

The doctoral life is a hard but precious experience, I wish this milestone could support, guide and shine on my way forward.

SYNOPSIS

The bubble column reactors are intensively used as multiphase contactors for carrying out gas-liquid two-phase or gas-liquid-solid three-phase reactions in various industries, such as chemical, biochemical, pharmaceutical industries and nuclear power engineering, due to their high efficiencies of heat and mass transfer and simple structure. Investigation on hydrodynamic properties of gas-liquid two-phase flow and gas-liquid-solid three-phase flow in bubble column reactors is important for reactor design, optimization and scale-up, and expanding the scope of application of bubble columns. With the development of computational fluid dynamics in recent years, considerable progress in numerical simulation of turbulent bubbly flow in bubble column reactors has been advanced, Computational Fluid Dynamics (CFD) has become an important tool. However, the strong interfacial interactions and turbulence results in a very complex phenomenon, there are still remaining many modelling difficulties to make achieve the accurate numerical prediction, for example, the turbulent model closures and the breakup and coalescence process. Turbulent model is the basis of CFD modelling as serving a modelling framework. The momentum and mass transfer between bubble and bubble and bubble and continuous phase is the key issue in CFD modelling of bubble column, therefore, the breakup and coalescence process needs to be considered thoroughly. The present project investigates the hydrodynamics inside the bubble column based on CFD modelling in Eulerian-Eulerian approach and experimental method.

Current research status of CFD modelling in bubble column together with related models and corresponding experimental studies, has been comprehensively reviewed in Chapter 1. A fundamental understanding of the complicated mechanisms of multiphase flow in bubble columns has been extracted from both numerical and experimental studies, serving as the background for this project.

The bubble size distribution is a crucial parameter in CFD modelling for gas-liquid flow, as it is essential for force closure and plays an important role in mass and heat transfer. In order to obtain this parameter, the Population Balance Model (PBM) coupling CFD can be implemented to investigate the bubble breakup and coalescence. However, the bubble breakup models with different consideration result in multiple integral, a tricky issue in numerical simulation due to the difficulty of achieving numerical integration and the high computational demand. In Chapter 2, a numerical method for bubble breakup model is proposed. This method adopted for numerical integrations has been used for the acceleration of CFD-PBM modelling. The proposed model is successfully implemented into Eulerian-Eulerian bubbly flow and compared simulation results and computational time with the use of the direct integral method. Two cases of bubble columns with different column diameters have been simulated for validations to check the reliability under different flow characteristics. The results show that this numerical method is time-saving with good performance of prediction in different scale of bubble column. This has provided a basis for the modification and validation of bubble breakup model when PBM is coupled in CFD simulation of bubble column.

As bubble breakup event mainly occurs when bubble is bombarded by the eddy with same size, most of researches assumed the bubble velocity is same as that of the bombarding eddy, however, bubbles do not response the liquid eddy movement faithfully. Chapter 3 evaluated the effect of eddy-bubble interactions and proposed a modified turbulent viscosity model involving bubble response to the surrounding eddies. The proposed model is successfully implemented into Eulerian-Eulerian bubbly flow, while the bubble size distribution is predicted by a breakup model considering the bubble-induced turbulence kinetic energy spectrum. Comparing the simulations results using the proposed model and standard model and the experimental data from literature, the modified viscosity model demonstrates great improvements in the predictions of gas holdup, liquid velocity and bubble size distribution. The importance of taking into account the additional viscosity due to the response of bubble to turbulent eddies and the bubble-induced turbulent energy spectrum is clearly revealed, which has been ignored in previous studies on CFD modelling of multiphase flow in bubble column.

The experimental study of the multiphase flow in the bubble column through 2D-PIV in Chapter 4. Different hydrodynamics including velocity, velocity fluctuation and turbulent kinetic energy are well captured and studied. Most current researches on CFD modelling of gas-liquid-solid three-phase flow employ pseudo-three-phase simulation, assuming the mixture of liquid and solid phase as slurry phase, because the effect of solid phase in three-phase flow does still not clear. The experimental results demonstrate the particle modulation in three-phase flow by comparing different hydrodynamic properties and turbulent

characteristics between gas-liquid two-phase flow and gas-liquid-solid three-phase flow, which provides the basis of the CFD modelling of three-phase flow in the future work. The turbulent energy spectrum of gas-liquid two-phase flow is also presented, it clearly shows the existence of the κ^{-3} scaling law by bubble-induced turbulence. The need of consideration of bubble-induced turbulence power law in bubbly flow is demonstrated.

To sum up, gas-liquid two-phase flow and gas-liquid-solid three-phase flow in bubble column are investigated numerically and experimentally. The implication is that the eddy-bubble interaction and the addition of particle strongly affect the flow behaviour within bubble column. The effect of eddy-bubble interaction is considered numerically in the modified viscosity model and in modified bubble breakup model, with an experimental study. The effect of solid particle on flow behaviours is investigated by the comparison between the experimental results of gas-liquid two-phase flow and gas-liquid-solid three-phase flow. The critical importance of including the eddy/bubble interaction in CFD-PBM modelling of bubble column bubbly flows is highlighted.

TABLE OF CONTENT

LIST OF FIGURES

CHAPTER 1: A LITERATURE REVIEW ON CFD MODELLING OF TURBULENT BUBBLY FLOWS AND EXPERIMENTAL STUDIES OF BUBBLE COLUMN REACTORS

CHAPTER 2: CFD MODELLING OF THE POPULATION BALANCE FOR GAS-LIQUID TWO-PHASE FLOW IN BUBBLE COLUMN

CHAPTER 3: CFD-PBM MODELLING OF GAS-LIQUID TWO-PHASE FLOW IN BUBBLE COLUMN REACTOR ACCOUNTING THE EFFECT OF EDDY-BUBBLE INTERACTION AND BUBBLE-INDUCED TURBULENCE

CHAPTER 4: EXPERIMENTAL INVESTIGATION OF MULTI-PHASE FLOW IN THE BUBBLE COLUMN BY PIV

LIST OF TABLES

NOMENCLATURE

C_D = effective drag coefficient for a bubble around a swarm, dimensionless

C_L = lift coefficient, dimensionless

C_f = increase coefficient of surface area, dimensionless

C_{TD} = turbulent dispersion coefficient, dimensionless

C_{VM} = virtual mass coefficient, dimensionless

C_{wl} = wall lubrication coefficient, dimensionless

D = bubble column diameter, m

d = bubble diameter, m

d_{32} = equivalent bubble diameter, m

d_{eq} = equivalent bubble diameter, m

d_h = long axis of deformable bubble, m

Eo = Eötvös number, dimensionless

F = force, N

F_D = drag force, N/m^3

F_{Lift} = lift force, N/m^3

F_{td} = turbulent dispersion force, N/m^3

F_{VM} = virtual mass force, N/m^3

F_{wl} = wall lubrication force, N/m^3

Fr = Froude number, dimensionless

f_V = breakage volume fraction, dimensionless

f_i = fraction of i-th bubble class of total fraction

f_λ = number density of bombarding eddies, m^{-4}

g = gravity acceleration, m/s^2

G = production of turbulent kinetic energy

H = distance from the bottom surface, m

k = turbulence kinetic energy, m^2/s^2

L = length scale, m

Mo = Morton number, dimensionless

n = number density per unit volume, m^{-3}

N = number of bubbles per unit volume, dimensionless

r = radius, m

Re = Reynolds number, dimensionless

S = surface area, m^2

Sc

St = Stokes number, dimensionless

S_{ij} = mean strain rate tensor, dimensionless

t = time, s

U = superficial velocity, m/s

U_r = rising velocity, m/s

U_{Slip} = slip velocity, m/s

U_t = terminal velocity, m/s

$\bar{u}_\lambda$ = mean velocity of turbulent eddies, m/s

u = velocity vector, m/s

u' = fluctuation velocity in u-direction, m/s

V = volume, m^3

v' = fluctuation velocity in v-direction, m/s

We = Weber number, dimensionless

w' = fluctuation velocity in w-direction, m/s

x_{ij} = size ratio of colliding bubbles, dimensionless

Greek letters

α = phase volume fraction, dimensionless

ε = turbulence dissipation rate, m^2/s^3

η = Kolmogorov length scale, m

κ = wave number, m^{-1}

λ = eddy length scale, m

Λ = characteristic length scale, m

μ = molecular dynamic viscosity, Pa·s

μ_t = turbulence dynamic viscosity, Pa·s

μ_{eff} = effective turbulence dynamic viscosity, Pa·s

υ = kinematic viscosity, m^2/s

ξ = ratio of eddy length scale to bubble diameter, dimensionless

ρ = phase density, kg/m^3

σ = surface tension, N/m

σ_{TD} = Turbulent Schmidt number of gas phase, dimensionless

τ = shear stress, Pa

Superscripts/Subscripts

b = bubble

B = breakage

C = coalescence

coal = coalescence

col = collision

eff = effective

g = gas

i = i-th class bubble

j = daughter bubble

k = phase indicator / turbulent kinetic energy

l = liquid

m = mixture

R = Reynolds stress

rel = relative

s = surface

td = turbulent dispersion

vm= virtual mass

w = wake

wl = wall lubrication

z = vertical direction

Abbreviation

BIT = Bubble-induced turbulence

CARPT = Computer aided radioactive particle tracing

CCD = Charged coupled device

CFD = Computational fluid dynamics

CT =Computational tomography

DGD = Dynamic gas disengagement

DM = Discrete method

DQMOM = Direct quadrature method of moments

DNS = Direct numerical simulation

HFA = Hot film anemometer

E-E = Eulerian-Eulerian

E-L = Eulerian-Lagrangian

ECT = Electric capacitance tomography

ERT = Electric resistance tomography

FFT = Fast Fourier transform

LDA = Laser Doppler velocimetry

LES = Large eddy simulation

MIC = Marker-and-Cell

PBM = Population balance model

PDF = Possibility density function

PIC = Particle-In-Cell

PIV = Particle imaging velocimetry

PMMA = Polymethyl methacrylate

QMOM = Quadrature method of moments

RSM = Reynolds stress model

TKE = Turbulent kinetic energy

VOF = Volume of fluid

CHAPTER 1: A LITERATURE REVIEW ON CFD MODELLING OF TURBULENT BUBBLY FLOWS AND EXPERIMENTAL STUDIES OF BUBBLE COLUMN REACTORS

SUMMARY

The experimental and numerical investigations of bubble column reactors have made significant progress over the past few decades. At early stages, the researchers focused on the experimental investigation of the global-averaged parameters, e.g. gas holdup, and time-averaged characteristics, which have formed the fundamental understanding of the gas-liquid two-phase flow and gas-liquid-solid three-phase flow in bubble columns. Due to the rapid development of experimental measurements since 1990s, the capture accuracy of dynamic structures and behaviour of local flow field has enhanced significantly, providing the possibility to study the multiphase nature within bubble column reactors in depth. Recently, with the urgent demands of carbon neutrality, the interest of bubble column has increased due to its high efficiency of heat and mass transfer. Numerous correlations and phenomenal models have been developed and implemented into the CFD modelling under the discovery of experiments, which accelerates the development of theoretical understanding of the flow nature in the bubble column reactors. Despite the general simplicity of bubble columns in mechanical design, the fluid dynamics in bubble columns are very complex. The multi-scale behaviours, the gas-liquid two-phase interactions particularly, have not

been fully revealed, which has become a crucial problem in the design and scale-up of the bubble columns. To develop a better understanding of turbulent flow characteristics of the multiphase flow within bubble column, this chapter will review prior efforts according to the available literatures in two veins, experimental investigations and CFD modelling.

1. **INTRODUCTION**

The bubble column reactors are intensively used as multiphase contactors for carrying out gas-liquid two-phase or gas-liquid-solid three-phase reactions in various industries, such as chemical, biochemical, pharmaceutical industries and nuclear power engineering. Comparing with other multiphase reactors such as stirred tanks and fixed beds, bubble columns have the following advantages, i) lower cost of both the capital cost in construction and the labour cost in operation; ii) simpler structure, easy to maintenance; iii) relatively higher liquid retention which allows the reactions with long residence time; iv) higher interphase mass and heat transfer capacity under the same energy consumption.

One important application of bubble column reactor in the energy industry is the Fischer-Tropsch process, which is a collection of gasification and liquefaction reactions to produce synthetic lubrication oil, low-sulphur transportation fuels and other synthetic fuels from coal, natural gas or biomass, addressing environmental advantageous over petroleum derivatives (Krishna and Sie, 2000, Degaleesan et al., 2001). Typical examples can also be found in p-xylene oxidation (Jin et al., 2005), wine fermentation (Schmidt and Velten, 2016), wastewater treatment (Smith et al., 1996), and algae growing for high-value products extraction (Manjrekar et al., 2017). The typical structure of bubble column is consisted of a vessel with a gas distributor, after passing through the distributor located at the bottom of the reactor, the gas rises in the form of bubbles in the continuous liquid phase in the main body of the column. Some bubble columns have equipped with different kinds of internals for their specific industrial applications, which includes

vertical or horizontal tube bundles, draft tubes, rotating disks and multi-layer seize plates (Youssef et al., 2013). The types of gas distributors that are commonly found include nozzles, perforated plates, seize plates, porous media, membrane, ring type distributors and arm spargers (Kulkarni and Joshi, 2005).

Despite the general simplicity of bubble columns in mechanical design, the complex flow dynamic in bubble column and the presence of dispersed bubbles within continuous phase cause the difficulties of fully understanding of multiphase flow in bubble column which affects the optimisation of scale-up and process. The main concerns focus on the physical mechanisms of the multiphase interaction, including the interface forces, the turbulence interactions, and the bubble size distribution caused by bubble breakup and coalescence phenomenon. In the last few decades, the interphase interactions have been widely studied by many researchers and different models have been developed and validated based on well-designed experiments and computational fluid dynamics (CFD) modelling. The developments in the open literature that attempts to understand the flow characteristics in the bubble column reactors are reviewed in this chapter. Section 2 reviews the flow regime and flow pattern in bubble column. Section 3 reviews the numerical modelling of bubbly flow in the aspect of simulation approaches, interfacial forces, turbulence model and bubble breakup and coalescence events, while Section 4 focus on the experimental measurements of bubble columns.

2. FUNDAMENTALS OF BUBBLE COLUMN REACTORS

The bubble column reactor is a typical multiscale system, which consists of macroscale or reactor scale structures such as large-scale liquid circulation, mesoscale interactions such as bubble-eddy or bubble-bubble collision, and microscale behaviours such as mass or momentum transfer across the bubble surface. Although the complicated multiphase and multiscale nature has not yet been fully and thoroughly revealed due to the limitations of the more advanced experimental device and the development of turbulence theory, the fundamental understandings of turbulent bubbly flow in the bubble columns have been established and generally accepted on the basis of experimental studies. Some common understandings of the turbulent bubbly flows in bubble column reactors include the flow structures and flow regime transitions, as well as bubble deformations and interfacial mass transfer.

2.1 Flow Structures

According to the different superficial gas velocity and the diameter of column, the flow regimes in the bubble column can be defined as homogeneous bubbly flow, transition range, slug flow and the heterogeneous churn-turbulent range. The approximate distinction of the flow regimes in the bubble columns is shown in Figure 1-1. For the study of the flow regime transitions in the bubble columns, Figure 1-2 identifies the flow regimes as dispersed bubble, vortical-spiral flow and turbulent flow. As illustrated in Figure 1-2, a typical 3-D macroscopic flow structures in the vortical-spiral flow regime is in consist of central plume, descending flow, vortical-spiral flow and fast bubble flow. These illustrations have important influence on the understandings in the dynamic characteristics and the

coherent eddy structures in the bubble columns and on the guidelines of the design and scale-up of bubble columns. It seems that the flow regime transitions are affected by various parameters such as bubble column diameter, liquid dispersion height, liquid phase properties, the type of gas distributors and operating conditions. Recent studies found that a further clarification of the homogeneous flow could be made by the different superficial velocities and bubble size distributions, and the classes are the mono-dispersed homogeneous regime and the poly-dispersed homogeneous flow regime (Besagni and Inzoli, 2016b). In the case of gas sparger with large diameter orifices, the mono-dispersed homogeneous regime may not exist due to the aeration of the large bubbles (Besagni and Inzoli, 2016a). This presence of large bubbles causes the transition from the homogeneous regime to the transition region. The transition flow regime is characterised according to the macroscopic flow structures, large eddies and a widened bubble size distribution (Guedon et al., 2017). In this case, the turbulent eddies and the "coalescence-induced" large bubble within eddies significant enhanced the generation of turbulence in the bubble column.

2.2 Critical Issues on Studies of Bubble Column Reactors

Although numerous research efforts have been made, the complex multiscale and multiphase nature of the bubble column reactors have not been fundamentally revealed. It seems that the key issues focus on the mechanism of gas-liquid interactions, such as different interfacial momentum transfer or bubble coalescence and breakage phenomena. In particular, the understanding of turbulence in the bubble columns is still very limited from both CFD modelling and experimental

point of views. In general, the description of turbulence in the bubble columns is usually based on the analogy to isotropic homogeneous single-phase turbulence in pipe flows. This is due to the ongoing debates on the experimental findings of bubble motions, surface oscillations and deformations, bubble wakes and the turbulence generated in the wakes of bubbles. Therefore, the research works including CFD modelling and experimental studies on these critical issues of bubble column reactors will be presented in section 3 and section 4 respectively. A short recapitulation and implication will be presented in section 5.

3. NUMERICAL SIMULATION OF FLOW IN BUBBLE COLUMN REACTORS

Flow characteristics in the bubble columns, e.g. velocity, temperature and volume fraction, will fluctuate greatly both in space and time accordingly, which further affect momentum, heat and mass transfer. To simulate gas-liquid two-phase flow in bubble column, numerical methods are generated as two groups, time-averaged models and time-dependent models. There are also two ways of calculating the dispersed phase variables: Lagrangian tracking or Eulerian two-fluid methods.

3.1 Simulation Approaches

Direct numerical simulation (DNS)

The direct numerical simulations for two-phase flows solve the governing equations for the continuous phase and dispersed phase in every single bubble. The interface between two phases should be represented explicitly with sharp interfacial properties and should be free to move, deform, breakup and coalesce as how an actual interface would behave. Therefore, the two-phase coupling and the momentum exchange rely on the interface-tracking methods. The interface-tracking methods that have been developed mainly include Particle-In-Cell method (PIC) (Harlow, 1988), Marker-and-Cell method (MIC) (Harlow and Welch, 1965), volume of fluid method (VOF) (Hirt and Nichols, 1981), level-set method (Hirt and Nichols, 1981), boundary-fitted grid method and front tracking method (Tryggvason et al., 2001). It is one of the greatest advantages of the DNS method for gas-liquid two-phase flow simulations that the changes on the bubbles interface

can be clearly illustrated, such as Krishna and van Baten (1999). Also, the DNS method for two-phase flow can be used as a tool to study the liquid phase turbulence under the influence of gas bubbles, such as Metrailler et al. (2017). Although there are not interphase force model or turbulence models required as model closure, the computational demanding is so high that DNS is limited to low Reynolds numbers and few bubbles, which makes the simulation of real industrial processes almost impossible.

Eulerian-Lagrangian approach

The Eulerian-Lagrangian method is a more promising approach. This method considers the dispersed phase as discrete particles and each particle is tracked by appropriate equation of motions in Lagrangian frame of reference through the continuum flow field (Chen, 2004). The particle-particle interactions can be clearly described, such as hard-sphere models or soft-ball model for bubble collision and coalescence. For continuous phase, a single set of conservation equations is solved using a grid-based Eulerian method. It can be assumed that the influence of the dispersed phase movement on the flow field of continuous phase is neglectable if the dispersed phase particles are in small size and in low concentration. However, once the particle concentration can no longer be neglected, the the discrete particles and the continuous phase can be coupled by using a source term of interphase momentum exchange equations. This method had been used to simulate the gas-liquid two-phase flow in bubble columns and have been verified by the more promising results in recent researches (Delnoij and Kuipers (2000), Sokolichin et al. (1997), Lain and Sommerfeld (2003), Deen et al. (2004) and Buwa et al. (2006)). Because turbulence description in the continuous phase under Eulerian method

only provides averaged-velocity and turbulence statistics, assumptions have to be made to obtain the instantaneous velocity of the continuous phase at bubble position from its mean value for solving the equation of motion. The Euler-Lagrangian method is quite suitable for fundamental investigations because of the possibility of considering various effects related to bubble-bubble and bubble-liquid interactions directly.

The use of this method is often limited by the two main factors, the spatial resolution of the meshes and the number of bubbles being tracked. Although the computational cost is still very high for industrial-scale simulations, the physical interpretations still make sense while the considered models in this method are simpler than the DNS method.

Eulerian-Eulerian approach

The Eulerian-Eulerian method, also called two-fluid model, is the most widely used approach in numerical simulations of multiphase flow. Both the continuous phase and the dispersed phase are treated as interpenetrating continua. The motion of each phase is described in a macroscopic sense in two-fluid model. As there are two 'fluids' present, the void fraction is used to represent the concentration of each phase. Although the void fraction is not possible to resolve every point in time or space, it is rather necessary to average over a specific time and space. The separate differential equations of the conservation of mass and momentum is derived for each phase, as shown in Equation (1-1) and Equation (1-2) (Drew, 1983, Drew and Passmann, 1999).

The mass balance equation:

$$\frac{\partial(\rho_k \alpha_k)}{\partial t} + \nabla \cdot (\rho_k \alpha_k u_k) = 0 \tag{1-1}$$

The momentum equation:

$$\frac{\partial(\rho_k \alpha_k \boldsymbol{u_k})}{\partial t} + \nabla \cdot (\rho_k \alpha_k \boldsymbol{u_k} \boldsymbol{u_k}) = -\alpha_k \nabla p + \nabla \cdot \bar{\bar{\tau}}_k + \alpha_k \rho_k \boldsymbol{g} + \boldsymbol{F_k} \tag{1-2}$$

where ρ_k, α_k, $\boldsymbol{u}_k$, $\bar{\bar{\tau}}_k$, $\boldsymbol{g}$ and $\boldsymbol{F}_k$ are the symbol of density, volume fraction, velocity vector, viscous stress tensor, gravity vector and the exchange term for the *k* (liquid or gas) phase respectively. The sum of the volume fractions for both phases is equal to 1.

The governing equations of the two-fluid model can be treated based on averaging methods. For example, the most commonly used averaging method that has been accepted by many commercial CFD codes is the Reynolds (ensemble) averaging, which decomposes instantaneous flow variable into the time-averaged mean component and the fluctuating component. The averaged governing equations and the different turbulent correlations of fluctuation terms have been discussed by Joshi (2001) in details. The information regarding the microscopic scale is lost after the averaging process, which inevitably leads to the closure problems that have been extensively studied by many researchers.

When implementing two-fluid model, it seems that the most required terms for solving the governing equations numerically are the interphase forces and the Reynolds stresses terms, thus different closure models have been developed to close these two terms. In addition, some of the interphase force closures, e.g. drag force and lift force, are the function of the bubble diameter, which further arises the need of appropriate closure of the bubble size distributions. It is acceptable to

use a volume-averaged bubble diameter if the bubble column is operated at the homogeneous regime and the bubble size distribution is very narrow. However, in most industrial processes, the bubble columns are operated at the churn-turbulent flow regime, the bubble sizes are broadly distributed due to intensive bubble coalescence and breakage phenomenon. In this case, the uniform bubble diameter assumption is no longer appropriate, and the local bubble sizes can be calculated using bubble population balance equations.

3.2 Interphase Forces

The interphase forces term is required for the closure of momentum exchange between the gas phase and the liquid phase when using Eulerian-Eulerian two-fluid models. The interphase forces include the drag force, lift force, virtual mass force, turbulent dispersion force, wall lubrication force and Basset force. All these forces are essentially generated from the local pressure variations and stress distribution on the bubble surface. If a bubble is motionless in a static liquid, the forces acting on the bubble only pressure and gravity.

If there is a relative motion between the bubble and liquid, the motion results in a shear stress which makes more forces act on bubble through the liquid-gas interface (Drew and Passmann, 1999, Zhang and Prosperetti, 1997). If the slip velocity is uniform, the force acting on the bubbles is only the drag force. If the bubbles are accelerated with respect to the liquid phase, the virtual mass force takes effect. If the bubbles flow in non-uniform liquid phase flow field, there are also the lateral lift forces. Due to the turbulent fluctuations of the liquid phase, the bubble

moves transversely under the influence of turbulent dispersion force. When the bubble is approaching the column wall, the higher pressure gradient caused by the low velocity in the boundary layer makes the direction of the wall lubrication force towards the centre of the bubble column. Basset force is a historical force, which greatly affects the bubble motion in a very short time. However, the time step is usually much larger than the influencing time of the Basset force. Therefore, the Basset force is usually neglected in the Eulerian-Eulerian simulations. The schematic of various force acting on bubble are shown in Figure 1-6. From the study of Muniz and Sommerfeld (2020), the contributions of each force in fully development bubble column flows are evaluated and compared with ratio to the buoyancy force, as shown in Figure 1-7, the drag force contributes approximately up to 90%, while the 60%, 2-7%, 3%, 2% for added mass force, Basset force, transverse lift force and wall lubrication force, respectively.

Drag force

Drag force is generated due to the relative motion of bubbles and the surrounding liquid flow, which is one of the most important interphase forces. The accurate estimation of the drag force is the crucial for simulating gas-liquid two-phase flow in the bubble column.

For a single spherical bubble rising at steady state, the drag force can be expressed by

$$\boldsymbol{F_{D,bubble}} = C_D \left(\frac{\pi}{4} d_b^2\right) \frac{\rho_l}{2} \left(\boldsymbol{u_l} - \boldsymbol{u_g}\right) \left|\boldsymbol{u_l} - \boldsymbol{u_g}\right| \tag{1-3}$$

where C_D is the drag coefficient, d_B is the bubble diameter and $\left(\boldsymbol{u_l} - \boldsymbol{u_g}\right)$ is the

slip velocity. It appears that the drag coefficient and the bubble diameter are required to calculate the drag force.

For a bubble swarm, the drag force formulation is comparable complicated due to the presence of other surrounding bubbles. The idealised drag force for a bubble swarm can be considered as linear superposition of single bubbles. Assume the number of bubbles per unit volume within the swarm is ***N***, the drag force of the bubble swarm can be expressed as

$$\boldsymbol{F_{D,swarm}} = N \cdot C_D \left(\frac{\pi}{4} d_b^2\right) \frac{\rho_l}{2} \left(\boldsymbol{u_l} - \boldsymbol{u_g}\right) \left|\boldsymbol{u_l} - \boldsymbol{u_g}\right| \tag{1-4}$$

Since N is the number of bubbles per unit volume, which can be expressed by $N = {\alpha_g}/{\frac{\pi}{6} d_b^3}$, Equation (1-4) can be rewritten as

$$\boldsymbol{F_{D,swarm}} = C_D \frac{3\alpha_g}{4} \frac{\rho_l}{d_b} \left(\boldsymbol{u_l} - \boldsymbol{u_g}\right) \left|\boldsymbol{u_l} - \boldsymbol{u_g}\right| \tag{1-5}$$

To ensure the drag force returns to zero when the gas holdup in a computational cell is 1 or 0, Equation (1-9) should be multiplied by α_l, which gives

$$\boldsymbol{F_{D,swarm}} = C_D \frac{3\alpha_g \alpha_l}{4} \frac{\rho_l}{d_b} \left(\boldsymbol{u_l} - \boldsymbol{u_g}\right) \left|\boldsymbol{u_l} - \boldsymbol{u_g}\right| \tag{1-6}$$

The drag coefficient is affected by bubble size, shape and physical conditions of liquid phase, which is dependent on the parameters: bubble Reynolds number, Eotvos number and Morton number. These relative parameters are summarized in Table 1-1.

Table 1- 1 Parameter related in calculating the drag coefficient

Dimensionless number	Expression	Phase Meaning	Relation
Reynolds number	$Re = \frac{\rho_l u_b d_b}{\mu_l}$	The ratio of inertial forces to viscous forces	-
Eötvös number	$Eo = \frac{g d_b^2 (\rho_l - \rho_g)}{\sigma}$	The ratio of gravitational forces to surface tension forces	-
Weber number	$We = \frac{\rho_l u_b^2 d_b}{\sigma}$	The ratio of inertial to surface tension	$We = \frac{Re^2 Mo^{1/}}{Eo^{1/2}}$
Froude number	$Fr = \frac{u_b}{\sqrt{g d_b}}$	The ratio of inertia to gravitational forces	-
Morton number	$Mo = \frac{g \mu_l^4 (\rho_l - \rho_g)}{\rho_l^3 \sigma^3}$	Combination of physical properties	$Mo = \frac{We^3}{Fr^2 Re^4}$

Although the drag coefficient has been extensively studied by many researchers, the formulations are mostly still based on empirical or semi-empirical correlations. The most commonly used models of drag coefficients in CFD studies of bubble columns include Schiller and Naumann (1935), Ishii and Zuber (1979), Grace et al. (1978) and Tomiyama (1998). The expressions for popular drag models are presented in Table 1-2.

Table 1- 2 Popular drag force coefficient models (Khan et al., 2020)

Model	Equation	Parametric Dependence
Analytical	$C_D = 24/\mathrm{Re}_b \; 0 \le \mathrm{Re}_b \le 0.2$	Re_b
Schiller and Naumann (1935)	$C_D = \begin{cases} \frac{24}{Re_b}(1+0.15\mathrm{Re}_b^{0.687}) & \mathrm{Re}_b \le 1000 \\ 0.44 & \mathrm{Re}_b > 1000 \end{cases}$ $C_D = \max\{0.44, 24/Re_b(1+0.15\mathrm{Re}_b^{0.687})\}$	Re_b
Moore (1963)	$C_D = \frac{48}{Re_b}\left(1-\frac{2.2}{Re_b^{0.5}}+f(Re_b^{-5/6})\right) \; \mathrm{Re}_b \tilde{} 100$	Re_b
(Morsi and Alexander, 1972)l	$C_D = a_1 + \frac{a_2}{Re_b} + \frac{a_3}{Re_b^2}$ $a_1, a_2, a_3 = \begin{cases} 0, 24, 0 & 0 < \mathrm{Re}_b < 0.1 \\ 3.690, 22.73, 0.0903 & 0.1 < \mathrm{Re}_b < 1 \\ 1.222, 29.1667, -3.8889 & 1 < \mathrm{Re}_b < 10 \\ 0.6167, 46.50, -116.67 & 10 < \mathrm{Re}_b < 10^2 \\ 0.3644, 98.33, -2778 & 10^2 < \mathrm{Re}_b < 10^3 \\ 0.357, 148.62, -47500 & 10^3 < \mathrm{Re}_b < 5\times10^3 \\ 0.46, -490.546, 578700 & 5\times10^3 < \mathrm{Re}_b < 10^4 \\ 0.5191, -1662.5, 5416700 & \mathrm{Re}_b \ge 10^4 \end{cases}$	Re_b
Clift et al. (1978)	$C_D = 3/16 + 24/\mathrm{Re}_b \; \mathrm{Re}_b < 0.01$ $C_D = 24/\mathrm{Re}_b[1+0.1315Re_b^{(0.82-0.05w)}] \; 0.01 < \mathrm{Re}_b \le 20$ $C_D = 24/\mathrm{Re}_b[1+0.1935Re_b^{0.0305}] \; 20 \le \mathrm{Re}_b \le 260$ $C_D = 24/\mathrm{Re}_b[44.005\times10^{-1.1242w+0.1558w^2}] \; 260 \le \mathrm{Re}_b \le 1500$ Where, $w = \log_{10}\mathrm{Re}_b$	Re_b
Ishii and Zuber (1979)	$C_D = \max(\min(C_{D-ellipse}, C_{D-cap}), C_{D-sphdere})$ $C_{D-ellipse} = 24/\mathrm{Re}_b(1+0.15\mathrm{Re}_b^{0.75}) \; 0 \le \mathrm{Re}_b < 1000$ $C_{D-\mathrm{ellipse}} = \frac{2}{3}Eo^{1/2} \; \mathrm{Re}_b \ge 1000$ $C_{D-cap} = \frac{8}{3}$	Re_b, Eo
Mei et al. (1994)	$C_D = \frac{24}{\mathrm{Re}_b}\left\{\frac{2}{3}+\left[\frac{12}{\mathrm{Re}_b}+0.75\left(1+\frac{3.315}{\sqrt{\mathrm{Re}_b}}\right)\right]^{-1}\right\}$	Re_b
Grevskott et al. (1996)	$C_D = \begin{cases} \frac{5.645}{\frac{1.0}{Eo}+2.385}, & d_s \ge 2.0\mathrm{mm} \\ \frac{8}{3}(1-\alpha_g)^2, & d_s < 2.0\mathrm{mm} \end{cases}$ Where: $d_s$is solid particle diameter and $\alpha_g$is the volume fraction of gas.	$\mathrm{Re}_b, Eo, \alpha_g$
Tomiyama et al. (1998)	For contaminated system $C_D = \max\left[\frac{24}{\mathrm{Re}_b}(1+0.15\mathrm{Re}_b^{0.687}), \frac{8}{3}\frac{Eo}{Eo+4}\right]$ For a slightly contaminated system $C_D = \max\left\{\min\left[\frac{24}{Re}(1+0.15Re_b^{0.687}), \frac{72}{Re}\right], \frac{8}{3}\frac{Eo}{Eo+4}\right\}$ For pure system $C_D = \max\left\{\min\left[\frac{16}{Re}(1+0.15Re_b^{0.687}), \frac{48}{Re}\right], \frac{8}{3}\frac{Eo}{Eo+4}\right\}$ $10^{-2} < Eo < 10^3, 10^{-3} < \mathrm{Re}_b < 10^6, 10^{-14} < Mo < 10^7$	Re_b, Eo
Lain et al. (1999)	$C_D = \begin{cases} 24/Re_b(1.0+0.15Re_b^{0.68}), & Re_b < 500 \\ 9.5\times10^{-5}Re_b^{1.397}, & 500 < Re_b < 1500 \\ 2.61, & Re_b \ge 1500 \end{cases}$	Re_b
Kurose et al. (2001)	$C_D = \begin{cases} \frac{16}{Re_b} & Re_b < 1 \\ 16/Re_b(1+0.15\mathrm{Re}_b^{0.5}) & 1 \le Re_b \end{cases}$	Re_b
Zhang and VanderHeyden (2002)	$0.5 \le \mathrm{Re}_b \le 200$ $C_D = 0.44 + \frac{24}{Re_b} + \frac{6}{1+\sqrt{Re_b}}$	Re_b
Tomiyama (2004)	$C_D = \frac{8}{3}\frac{Eo(1-\chi^2)}{\chi^{2/3}Eo+16\chi^{4/3}(1-\chi^2)}f(\chi)^{-2}$ Where: $f(E) = \frac{\sin^{-1}(\sqrt{1-\chi^2})-\chi\sqrt{1-\chi^2}}{(1-\chi^2)}$, $\chi = \frac{1}{1+0.163Eo^{0.757}}$	Eo, χ
Simonnet et al. (2007)	$C_D = C_{D\infty}E'$ $E' = (1-\alpha_{\mathrm{loc}})\left[(1-\alpha_{\mathrm{loc}})^m + \left(4.8\frac{\alpha_{\mathrm{loc}}}{1-\alpha_{\mathrm{loc}}}\right)^m\right]^{-2/m}$, $\mathrm{m} = 25\; C_{D\infty} = \frac{4}{3}\frac{\rho_l-\rho_g}{\rho_l}gd_b\frac{1-\alpha_{\mathrm{loc}}}{\lvert\mathbf{U}_{\mathrm{relative}}\rvert^2}$ $\mathbf{U}_{\mathrm{relative}} = \mathbf{U}_g - \mathbf{U}_l$	$\alpha_{\mathrm{loc}}, d_b, \rho_{liquid}, \rho_{gas}, g$
Snyder et al. (2007)		Re_b

(continued on next page)

Table 1- 2 Popular drag force coefficient models (continued)

Model	Equation	Parametric Dependence
	$C_D = \begin{cases} \frac{24}{Re_b}, & Re_b < 1 \\ \left(\frac{24}{Re_b}\right)\left(1+\frac{3.6}{Re_b^{0.313}}\left(\frac{Re_b-1}{19}\right)^2\right), & 1 \le Re_b \le 20 \\ \left(\frac{24}{Re_b}\right)\left(1+.15Re_b^{0.687}\right), & Re_b > 20 \end{cases}$	
Loth (2008)	$C_D \approx \max(C_{D,1}, C_{D,2})$ for $Re_b > 100$ $C_{D,1} \approx 2.5\tanh(0.2We) - 1.5$ $C_{D,2} = 48/\mathrm{Re}_b G(\chi)(1 - 2.21H(\chi)/\mathrm{Re}_b)$ For $\chi > 0.5$ $G(\chi) \approx 0.1287 + 0.4256/\chi + 0.4466/\chi^2$ $H(\chi) \approx 0.8886 + 0.5693/\chi - 0.4563/\chi^2$	Re_b, We, χ
Roghair et al. (2011)	$C_{D,\text{swarm of bubble}} = (1-\alpha)C_{D\infty}f(\alpha)$ Where: $f(\alpha) = [(1-\alpha_{loc})^m + (4.8\alpha_{loc}/(1-\alpha_{loc}))^m]^{-2/m}$ $C_{D,\infty} = \sqrt{C_D(Eo)^2 + C_D(\mathrm{Re}_b)^2}$ $C_D(Eo) = 4Eo/(9.5+Eo)$ $C_D(\mathrm{Re}_b) = \frac{16}{\mathrm{Re}_b}\left(1+2/\left(1+\frac{16}{\mathrm{Re}_b}+\frac{3.315}{\sqrt{\mathrm{Re}_b}}\right)\right)$ $1 \le Eo \le 5$, $4\times10^{-12} < Mo < 2\times10^{-9}$ For transition, $m = 25$	$\mathrm{Re}_b, \chi, \alpha, \alpha_{loc}, Eo$
Rastello et al. (2011)	$C_D(\chi) = \frac{16}{\mathrm{Re}_b}\left[\frac{1+8/15(\chi-1)+0.015(3G(\chi)-2)\mathrm{Re}_b}{1+0.015\mathrm{Re}_b} + \left[\frac{8}{\mathrm{Re}_b}+\frac{1}{2}\left(1+\frac{3.315H(\chi)G(\chi)}{\mathrm{Re}_b}\right)\right]^{-1}\right]\left(1+\frac{0.3}{Ro^{2.5}}\right)$ $G(\chi) = \frac{\chi^{-4/3}(\chi^{-2}-1)^{3/2}[(\chi^{-2}-1)^{1/2} - (2-\chi^{-2})\operatorname{arcsec}\chi^{-1}]}{3[\chi^{-2}\operatorname{arcsec}\chi^{-1} - (\chi^{-2}-1)^{1/2}]^2}$ $H(\chi) = 0.0108\chi^{-4} - 0.157\chi^{-3} + 1.5725\chi^{-2} - 2.0195\chi^{-1} - 1.617$ $\chi = 1 + 5/32We + O(We^2)$ $0.7 \le \mathrm{Re}_b \le 380$, $0.58 \le Ro \le 26$, $1 \le \chi \le 3$	$\mathrm{Re}_b, We, \chi, Ro$
Roghair et al. (2013)	$C_{D,\text{swarm of bubble}} = (1-\alpha_g)C_{D\infty}\left(1+\alpha_g\left(\frac{22}{0.4+Eo}\right)\right)$ Where: $C_{D,\infty} = \sqrt{C_D(Eo)^2 + C_D(\mathrm{Re}_b)^2}$ $C_D(Eo) = 4Eo/(9.5+Eo)$ $C_D(\mathrm{Re}_b) = \frac{16}{\mathrm{Re}_b}\left(1+2/\left(1+\frac{16}{\mathrm{Re}_b}+\frac{3.315}{\sqrt{\mathrm{Re}_b}}\right)\right)$ $0.13 < Eo < 4.83$, $6.6 < Mo < 10.6$ and $\alpha = 45\%$	$\mathrm{Re}_b, \alpha_g, Eo$
Aoyama et al. (2016)	$C_D(\chi) = \frac{16}{\mathrm{Re}_b}\left[\frac{1+8/15(\chi-1)+0.015(3G(\chi)-2)\mathrm{Re}_b}{1+0.015\mathrm{Re}_b} + \left[\frac{8}{\mathrm{Re}_b}+\frac{1}{2}\left(1+\frac{3.315H(\chi)G(\chi)}{\mathrm{Re}_b}\right)\right]^{-1}\right]\left(1+\frac{0.3}{Ro^{2.5}}\right)$ $G(\chi) = \frac{\chi^{-4/3}(\chi^{-2}-1)^{3/2}[(\chi^{-2}-1)^{1/2} - (2-\chi^{-2})\operatorname{arcsec}\chi^{-1}]}{3[\chi^{-2}\operatorname{arcsec}\chi^{-1} - (\chi^{-2}-1)^{1/2}]^2}$ $H(\chi) = 0.0108\chi^{-4} - 0.157\chi^{-3} + 1.5725\chi^{-2} - 2.0195\chi^{-1} - 1.617$ $\chi = \frac{1}{[1+0.016Eo^{1.12}\mathrm{Re}_b]^{0.388}}$ $-11 \le \log Mo \le 0.63$, $3.2\times10^{-3} \le \mathrm{Re}_b \le 1.3\times10^2$, $4.2\times10^{-2} < Eo < 2.9\times10^1$	$\mathrm{Re}_b, We, \chi, Ro$
Buffo et al. (2016)	$C_D = C_{D,o}(Re_{b-\mathrm{mod}})f(\alpha_g)$ $f(\alpha_d) = \begin{cases} (1-\alpha_g)^{C_A} & \text{if } \alpha_g \le 0.8 \\ 1 & \text{if } \alpha_g > 0.8 \end{cases}$ $C_{D,o}(Re_{b-\mathrm{mod}}) = \max\left[\frac{24}{\mathrm{Re}_{b-\mathrm{mod}}}(1+0.15\mathrm{Re}_{b-\mathrm{mod}}^{0.687}), \frac{8}{3}\frac{Eo}{Eo+4}\right]$ $\mathrm{Re}_{b-\mathrm{mod}} = \frac{d_b\rho_g\lvert U_g - U_l\rvert}{\mu_{\mathrm{eff}}}$ $\mu_{\mathrm{eff}} = \mu_g + C_B\rho_g\frac{k^2}{\varepsilon}$ C_A, C_B are model constants.	d_b, ρ_g, U_g, U_l μ_g, k, ε
Feng and Bolotnov (2016)	$C_D = \min[48/Re_b(1+3\times110^{-10}Re_b^{3.319}), 16/Re_b(1+0.15Re_b^{0.687})]$ Where $Re_b < 900$	Re_b

In the CFD simulations using two-fluid model, the drag coefficient has been considered in different ways according to the nature of the two-fluid flows. For example, using the drag coefficient of the single bubble by ignoring the bubble interactions and the bubble deformations. Alternatively, to modify the drag

coefficient of the spherical bubble by taking the shape factors into account or to consider the bubble interactions by assuming the drag coefficient of bubble swarm to that of the single bubble as a function of the gas holdup. However, it is noticed that none of these drag models is applicable to all complex flow conditions in real industrial processes, and different kinds of lumping parameters are proposed to adjust the drag coefficients from case to case.

Added mass force

When a single bubble accelerates or decelerates, some volume of the surrounding liquid must be moved or deflected as the bubble moves through it. The surrounding liquid is exerted an extra force by the acceleration induced b bubble motion, which is like the mass of bubble has been added.

The mathematical expressions of virtual mass force have derived by Auton et al. (1988). The virtual mass force model implanted in most CFD codes can be expressed as

$$\boldsymbol{F_{VM,l}} = \alpha_g \rho_l C_{VM} \left(\frac{D\boldsymbol{u_g}}{Dt} - \frac{D\boldsymbol{u_l}}{Dt} \right) \tag{1-7}$$

where C_{VM} is the virtual mass coefficient. The value of the virtual mass coefficient of spherical bubble in potential flow is 0.5. However, in the reality, the bubbles are not perfectly spherical and the interactions among neighbouring bubbles make the virtual mass coefficient deviated from the theoretical value. For example, Cook and Harlow (1986) have used a value of 0.25 and Tomiyama (2004) has used a tensor for C_{VM} for ellipsoidal bubbles to describe the different values in horizontal and vertical directions.

It seems that a concrete conclusion has not yet been made regarding the effect of added mass force in the CFD studies of gas-liquid two-phase flows in the bubble columns (Krishna and Van Baten, 2001b, Joshi, 2001, Tabib et al., 2008). Mudde and Simonin (1999) have shown that the simulation considering the drag and virtual mass force together has satisfactorily comparable with experimental results of the amplitude and time period of bubble plume. However, from the same research group, Oey et al. (2003) investigated the influence of interfacial closures and numerics on the hydrodynamics of the same bubble column, but they could not reproduce the same results.

Lift force

Lift force is one of the most key forces driving the radial motion of bubble and is a difficult part of gas-liquid two-phase simulation (Joshi, 2001). The mechanisms for the lift force are quite complicated, including the Magnus lift force due to the bubble rotation, the Saffman lift force due to the velocity gradient of the carrier fluid, and the lift force due to the bubble deformation. The different flow conditions that lead to the generation of lift forces have been clearly illustrated by Tomiyama et al. (1995) and summarised by Chen (2004), as shown in Figure 1-9.

It is generally accepted that the lift force acting on the bubbles mainly due to the liquid-phase velocity gradient in the bubble columns, thus the lift force acting on the dispersed phase can be derived as

$$\boldsymbol{F_{lift}} = -C_L \rho_l \alpha_g \left(\boldsymbol{u_l} - \boldsymbol{u_g}\right) \times (\nabla \times \boldsymbol{u_l}) \qquad (1\text{-}8)$$

where C_L is the lift coefficient. In the open literature, successful simulations

Some studies have shown great simulation results both for including lift (Tabib et al., 2008, Zhang et al., 2006, Rampure et al., 2007, Deen et al., 2001) and isolating the effect of lift force (Deen et al., 2000b, Krishna and van Baten, 2001a, Ranade and Tayalia, 2001). The values of lift coefficient varies considerably from the open literature, such as Zhang et al. (2006) and Bhole et al. (2008). It is generally accepted that more significant effect of lift coefficient with high superficial velocities. The positive value of lift force makes the bubbles move outwards towards the column wall, which causes lower centreline velocity and a comparably flat gas holdup profile. The effect of lift force is illustrated in Figure 1-10. Thus, the bubble size distribution should be taken into account when choosing the value of lift coefficient, rather than using a constant value for averaged bubble size for the entire bubble column.

Based on large numbers of experimental statistics, Tomiyama (1998) has correlated the lift coefficient with the bubble size, which considers the bubble shape variations by using the bubble Eotvos number.

$$C_L = \begin{cases} \min[0.288\tanh(0.121Re)\,,\ f(Eo')] & Eo < 4 \\ 0.00105Eo'^3 - 0.0159Eo'^2 - 0.0204Eo' + 0.474 & 4 \le Eo \le 10 \\ -0.29 & Eo > 10 \end{cases} \quad (1\text{-}9)$$

where the $Eo' = \frac{g(\rho_l - \rho_g)d_h^2}{\sigma}$ and the long axis of deformable bubble

$d_h = d_b(1 + Eo^{0.757})^{\frac{1}{3}}$.

From Equation (1-9), that value of lift coefficient becomes negative when the bubble diameter larger than 5.8 mm in the air-water system, which drives the large ellipsoidal bubbles to move towards the core region of the bubble column.

Turbulent Dispersion force

Turbulence dispersion force describes the effect of turbulent fluctuation of liquid velocity on the bubbles. Yang et al. (2002) have demonstrated the turbulent eddies with approximately the same size as the bubble affect significantly the entrapment and transport of bubbles, as shown in Figure 1-11. However, the turbulent fluctuations at small scales have lost in the two-fluid model.

The turbulent diffusion of the bubbles by the turbulent eddies can be approximated by Lopez de Bertodano (1992),

$$\boldsymbol{F_{td,l}} = -\boldsymbol{F_{td,g}} = C_{TD}\rho_l k_l \nabla\alpha_g \tag{1-10}$$

where C_{TD} is the turbulent dispersion coefficient with recommended values between 0.1 and 0.5, k_l is the liquid phase kinetic energy per unit mass, $\nabla\alpha_g$ is the gradient of gas phase volume fraction.

Based on the Favre averaging the interfacial drag froce, Burns et al. (2004) proposed an explicit expression of the turbulent dispersion force.

$$\boldsymbol{F_{td,l}} = -\boldsymbol{F_{td,g}} = C_{TD}\frac{3\alpha_g}{4}\frac{\rho_l}{d_b}\left(\boldsymbol{u_l} - \boldsymbol{u_g}\right)\frac{\nu_t}{\sigma_{TD}}\left(\frac{\nabla\alpha_l}{\alpha_l} - \frac{\nabla\alpha_g}{\alpha_g}\right) \tag{1-11}$$

where ν_t is the turbulent kinematic viscosity, and σ_{TD} is Schmidt number.
Due to the absence of a deeper understanding, a constant value of $\sigma_{TD} = 0.9$ is typically used.

Wall lubrication Force

When rising bubbles move approaching to the bubble column wall, wall lubrication force is generated by the asymmetric fluid flow surrounding bubbles in the vicinity of the way because of the fluid boundary layer. The wall lubrication force tends to push the bubbles away from the wall. The general form of the wall lubrication force can be expressed by

$$\boldsymbol{F_{wl}} = C_{wl}\rho_l\alpha_g \left|\left(\boldsymbol{u_l} - \boldsymbol{u_g}\right)_{||}\right|^2 \boldsymbol{n_w} \tag{1-12}$$

where C_{wl} the wall lubrication coefficient, $\left|\left(\boldsymbol{u_l} - \boldsymbol{u_g}\right)_{||}\right|$ the phase relative velocity component tangential to the wall surface, and n_w the unit normal pointing away from the wall.

The wall lubrication can be expressed from Antal et al. (1991) as

$$C_{wl} = max\left(0, \frac{C_{w1}}{d_b} + \frac{C_{w2}}{y_w}\right) \tag{1-13}$$

where commonly used values for the dimensionless coefficients C_{w1} = -0.01 and C_{w2} = 0.05, and y_w the distance to the nearest wall.

The wall lubrication force is only effective in a thin layer adjacent to the wall, as a model cut-off, $y_w \leq \left(\frac{C_{w2}}{C_{w1}}\right) d_b$.

Based on the correlations developed in the experiments, Tomiyama (1998) have improved the model for wall lubrication coefficient and make the formulation associated with pipe diameter. Also, based on Tomiyama (1998), Frank et al. (2008) have further improved the model of wall lubrication coefficient by removing the dependence of the pipe diameter and achieved better agreements with experimental data.

3.3 Turbulence Models

Turbulence widely exists in the fluid flows of industrial processes, thus the turbulence flow is one of the most important factors in computational fluid dynamics (CFD). However, its behaviour is extremely complex, especially in multiphase turbulence, the accurate modelling of turbulence is quite difficult. Since the bubble column reactors are usually operated in heterogeneous regime with high superficial gas velocities to achieve high productivity, the turbulence in the bubble columns is multiphase turbulences. Theoretically, direct numerical simulation (DNS) can predict the turbulence behaviour in all scales with the help of sufficient small grid size and time-step. However, Kolmogorov (1991) shows that the minimum turbulent eddy scale is inversely proportioned to $Re^{3/4}$, which means the higher turbulence intensity requires smaller grid size. It is obvious that the computational demanding of using DNS for turbulence in practical engineering systems is tremendous and nearly impossible with current technology. The DNS is only capable of low Reynolds number flows and with few numbers of bubbles, such as DNS of individual bubble. Therefore, engineering solutions are needed to deal with turbulence modelling in industrial processes.

To avoid resolving the all-scale turbulence structures, approximate treatment has been employed to model the contributions of turbulent eddies at specific length scales, e.g. larger eddy simulations (LES) and Reynolds averaging. The LES only computes large-scale turbulent eddies directly while removing information of eddies at small length scales by filtering operation. Instead of computing directly, the sub-grid models is employed to model the effect of these eddies smaller than

the cut-off width. Some researchers have used LES for numerical modelling of bubble columns, such as Deen et al. (2001), Dhotre et al. (2008), Niceno et al. (2008), Ma et al. (2016), and Liu and Li (2018). Comparing with the DNS, the computational demanding of LES is much reduced. It is likely that the pace of developments of LES for industrially relevant complex flows will increase as computing resources become more powerful.

Reynolds averaging is the most preferred method in the studies of industry-relevant reactors because its computational cost is relatively low. The Reynolds stress term τ, resulting from the Reynolds averaging, is the main concern. In order to achieve accurate results, the Reynolds stress term needs to be modelled correctly. Different models have been developed to model the Reynolds stress term, such as one equation model (Spalart-Allmaras), two-equation models and Reynolds stress models. Two-equation models are the most widely studied and commonly used method, which include Algebraic stress model, $k \sim \omega$ model, $k \sim \varepsilon$ model and their variants such as shear stress transport (SST) $k \sim \omega$, RNG $k \sim \varepsilon$ and Realizable $k \sim \varepsilon$ models.

Two-equation k ~ ε model

The two-equation $k \sim \varepsilon$ model includes two extra transport equations, which considers the convection and diffusion of turbulent energy. The transported variable k is the turbulent kinetic energy and ε is the turbulent dissipation rate. The standard $k \sim \varepsilon$ model for the liquid phase flow can be expressed by

$$\frac{\partial(\alpha_l\rho_l k_l)}{\partial t} + \nabla\cdot(\alpha_l\rho_l k_l \boldsymbol{u_l}) = \nabla\cdot\left[\alpha_l\left(\mu_l + \frac{\mu_t}{\sigma_k}\right)\nabla k_l\right] + \alpha_l\left(G_{k,l} - \rho_l\varepsilon_l\right) + S^k \tag{1-14}$$

$$\frac{\partial(\alpha_l\rho_l \varepsilon_l)}{\partial t} + \nabla\cdot(\alpha_l\rho_l \varepsilon_l \boldsymbol{u}_l) = \nabla\cdot\left[\alpha_l\left(\mu_l + \frac{\mu_t}{\sigma_k}\right)\nabla\varepsilon_l\right] + \alpha_l\frac{\varepsilon_l}{k_l}\left(C_{1\varepsilon}G_{k,l} - C_{2\varepsilon}\rho_l\varepsilon_l\right) + S^\varepsilon \tag{1-15}$$

where the eddy viscosity $\mu_t = C_\mu k^2/\varepsilon$. S^k and S^ε are the source terms for the turbulence generation in the wakes of bubbles. Only the liquid shear turbulence is considered without source terms in above two equations. On the contrary, by adding the source terms S^k and S^ε, the effects of the bubble induced turbulence can be partially included in the turbulence model, even though the source term S^k is still limited to the isotropic turbulence assumption set by the two-equation turbulence model. The detailed expressions of source terms S^k and S^ε will be discussed in the bubble induced turbulence section.

G_k in Equation (1-14) and (1-15) represents the production of turbulent kinetic energy, which is expressed by

$$G_k = -\rho\overline{u'_\iota u'_J}\frac{\partial u_j}{\partial x_i} \tag{1-16}$$

The Reynolds stress terms are new unknowns that are introduced into the averaged equations by the Reynolds averaging, which inevitably lead to the closure problem. The Reynolds stress terms are not solved directly in the two-equation model but being approximated by using the Boussinesq's turbulent viscosity hypothesis, which can be expressed by

$$-\rho\overline{u'_\iota u'_J} = 2\mu_t S_{ij} - \frac{2}{3}\rho k\delta_{ij} \tag{1-17}$$

where S_{ij} is the mean strain rate tensor, and δ_{ij} is the Kronecker delta.

The mean strain rate tensor is defined by

$$S_{ij} = \frac{1}{2}\left(\frac{\partial U_i}{\partial x_j} + \frac{\partial U_j}{\partial x_i}\right) \tag{1-18}$$

Therefore, the production of turbulent kinetic energy in Equation (1-16) can be rewritten as

$$G_k = 2\mu_t S_{ij} S_{ij} \tag{1-19}$$

The Boussinesq hypothesis is one of the fundamental basis of solving the two-equation models. However, by rewriting Equation (1-16) into Equation (1-19), the isotropic assumption of the normal Reynolds stresses has been used implicitly, which may not be necessarily true in the multiphase turbulence in the bubble column. It is true in simple flows like straight boundary layers, but in complex flows, such as flows with strong curvature, or strongly accelerated or decelerated flows, the Boussinesq hypothesis is simply not valid. Therefore, the Reynolds stress model and the LES model, which considers anisotropic turbulence, have higher accuracy in bubble column simulations.

Reynolds Stress Model

When the flow features of interest are the result of anisotropy, the Reynolds stress cannot be described under the Boussinesq hypothesis of isotropic turbulent eddy viscosity. Hence, the Reynolds stress model (RSM) is implemented to reflect the anisotropic nature. The RSM model solves seven equations, six Reynolds stress transport equations and an equation for the turbulence dissipation rate, which are used to calculate the individual Reynolds stresses $\overline{u'_\iota u'_j}$. The exact transport equations for the transport of the Reynolds stresses may be expressed as

$$\frac{\partial\left(\alpha_l\rho_l\overline{u_i'u_j'}\right)}{\partial t}+\frac{\partial\left(\alpha_l\rho_l u_k\overline{u_i'u_j'}\right)}{\partial x_k}=\frac{\partial}{\partial x_k}\left(\alpha_l\left(\mu_l+\frac{\mu_t}{\sigma_k}\right)\frac{\partial\overline{u_i'u_j'}}{\partial x_k}\right)$$
$$+\alpha_l P_{ij}+\alpha_l\phi_{ij}-\frac{2}{3}\delta_{ij}\alpha_l\rho_l\varepsilon \quad (1\text{-}20)$$

where ϕ_{ij} is the pressure-strain correlation and P_{ij} is the extra turbulence production term that is given by

$$P_{ij}=-\rho_l\left(\overline{u_i'u_k'}\frac{\partial u_j}{\partial x_k}+\overline{u_j'u_k'}\frac{\partial u_i}{\partial x_k}\right) \quad (1\text{-}21)$$

As the scalar turbulence dissipation rate appeared in Equation (1-20), a related transport model is used to calculate ε, as shown as

$$\frac{\partial(\alpha_l\rho_l\varepsilon)}{\partial t}+\frac{\partial}{\partial x_i}(\alpha_l\rho_l\varepsilon\boldsymbol{u}_i)=\frac{\partial}{\partial x_j}\left[\alpha_l\left(\mu_l+\frac{\mu_t}{\sigma_\varepsilon}\right)\frac{\partial\varepsilon}{\partial x_j}\right]$$
$$+\alpha_l\rho_l\frac{\varepsilon}{k}\left(C_{1\varepsilon}\overline{u'_i u'_j}\frac{\partial\boldsymbol{u_i}}{\partial x_k}-C_{2\varepsilon}\varepsilon\right) \quad (1\text{-}22)$$

where the turbulent kinetic energy k can be obtained from the solved values of normal stress using the Reynolds stress transport equation, as

$$k=\frac{1}{2}\left(\sum_{i=1,2,3}u'_i u'_j\right) \quad (1\text{-}23)$$

The RSM model have been employed to simulate flow characteristics in the bubble column reactors in some studies. Comparing with $k\sim\varepsilon$ model, RSM can predict the swirling behaviours of the flow more appropriately. RSM is also able to better address the characteristics of the turbulent bubbly flow in the bubble columns where the bubble-induced turbulence and anisotropy of turbulence are significant (Gupta and Roy, 2013, Tabib et al., 2008, Silva et al., 2012, Bhole et al., 2008, Ekambara et al., 2008, Parekh and Rzehak, 2018, Liu and Hinrichsen, 2014, Chahed et al., 2003). Tabib et al. (2008) have compared various turbulence models, e.g. $k\sim\varepsilon$ model, RSM and LES model in the simulation of flow within the cylindrical bubble column. In this study, the RSM demonstrates good accuracy of

simulation of anisotropic flows, involving swirls, acceleration and deceleration and buoyancy, in the bubble column. In addition, the RSM can predicts the averaged liquid velocity profiles more successfully comparing with the $k \sim \varepsilon$ model.

3.4 Bubble-induced Turbulence

Due to the momentum transfer occurring at the bubble interphase, the multiphase turbulence in the bubble column reactors becomes more complicated. In bubble column, liquid fluctuations are induced when bubbles go up through the column, which is called as bubble induced turbulence or pseudo-turbulence. The dispersed bubbles in the bubble columns surely affect the liquid phase turbulence, even though the effects have not been fully understood. Therefore, developing a suitable model for bubble-induced turbulence is a crucial for the simulation of bubbly flow because bubble-induce turbulence is the main difference between the dynamic behaviour of bubble column and other type of reactors, and it has significant influence on momentum, heat and mass transfer rates.

Bubble-induced turbulence fluctuations are reflected in energy spectrum, as the energy cascade of bubble-induced turbulence is different from that of homogeneous single-phase turbulence, especially for large-scale system (Roghair et al., 2011). Lance and Bataille (1991) measured the energy spectrum of the fluctuations caused by a swarm of bubbles rising through an imposed turbulent flow using constant-temperature anemometry (CTA) and laser Doppler anemometry (LDV). They found the behaviour of energy spectrum in high wave number range obeys -8/3 scaling law, in contrast to the classical -5/3 energy

spectrum scaling for homogeneous single-phase turbulence. They attributed the change of scaling to the wake dissipation effect, in which eddies produced were dissipated rapidly before the spectral transfer has even taken place. They also have done scaling analysis and got an exponent of -3 which is close to the experimental value. The view of κ^{-3} in pseudo-turbulence is established in many research works (Mercado et al., 2010, Riboux et al., 2013, Roghair et al., 2011, Risso, 2011a, Prakash et al., 2016, Bouche et al., 2014, Mendez-Diaz et al., 2013).

In modelling, Bunner and Tryggvason (2002) modelled an energy spectrum for a swarm of ellipsoidal bubbles and the scaling of slop of spectrum was -3.6. In contrast to Lance and Bataille (1991), they founded a strong anisotropic flow, which might be caused by large-scale convection induced by rising bubbles. The view that the bubble wakes is the main origin of the -3 spectrum scaling has been established in the difference of the following two works. Mazzitelli and Lohse (2009) conducted numerical analysis on bubble column and observed that a slope of -5/3 of energy spectrum and a transfer of energy from small scales to large scales which called as an inverse energy cascade. However, as bubble was assumed as point-like particles, thus the finite-size effects and capillary phenomena are ignored, this limitation makes the “wrong” -5/3 scaling is not suitable for real/experimental bubble columns. Roghair et al. (2011) carried out a fully resolved simulation of freely rising bubbles with finite-size and deformable shapes and compared the numerical simulation results with experimental results. They quantified the influence of bubble wake on energy spectrum scaling and found -3 as the spectral scaling exponent.

The research on turbulence models for bubbly flow is still at the beginning stage, and there is still no a generally acceptable model for bubbly flows (Sokolichin et al., 2004). Some reported CFD simulation work consider the effect of bubble-induced turbulence on the effective viscosity, a typical model from Sato and Sekoguchi (1975) predicts the turbulent viscosity due to BIT by the bubble size and slip velocity. However, Shu et al. (2020) indicated that the total turbulence kinetic energy might be underestimated without the consideration of the contribution of bubble-induced turbulence on turbulence kinetic energy. In contrast, a source-term generated by bubble-induced turbulence is added directly in the transport equations of turbulent variables (Pfleger and Becker, 2001, Troshko and Hassan, 2001, Rzehak and Krepper, 2013).

There are different expressions of the source-terms of the contribution of BIT in transport equations, but most of them are proposed by assuming the contribution to turbulence kinetic energy from BIT is equal to power input generated by interfacial forces. The generation of turbulent kinetic energy leads to additional dissipation, thus the source-term representing the generation of turbulence dissipation rate due to the contribution of BIT is added by assuming that turbulence kinetic energy is dissipated at the characteristic timescale. Pfleger and Becker (2001) calculated that the characteristic timescale from the Kolmogorov length scale and the velocity scale from overall turbulent fluctuations. While Troshko and Hassan (2001) and Liao et al. (2019) proposed the model at macroscopic scale which employed bubble diameter and slip velocity as characteristic scale to find the characteristic timescale.

3.5 Bubble Size Distribution

Since not only the interphase force closure, such as drag and lift force, but also the turbulence closure requires bubble size, the prediction of bubble sizes is essential in the numerical studies of bubble columns. In earlier stage, CFD simulation have used the averaged bubble size, which can only be obtained from experimental measurements or determined by repetitive trial-and-error simulations. However, the averaged bubble size cannot show the predictive nature of CFD modelling and the real inhomogeneity of bubble sizes in time and space aspects. Especially when the bubble columns are operated at the heterogeneous regime with high gas holdup and superficial velocity, the bubble sizes can be widely distributed. Different models have been developed to cope with this issue. For example, instead of explicitly using the bubble diameter, Thakre and Joshi (1999), Vitankar et al. (2002), and Dhotre and Joshi (2007) have used the ratio of drag coefficient and bubble diameter C_D / d_B as a lumping coefficient to close the interphase momentum exchange term. However, the values of the lumping coefficient are usually determined based on semi-empirical or empirical correlations that developed from experiments, and which causes further difficulties for other closure terms. Krishna and Baten (1999) have proposed the two bubble groups model based on experimental observations by using dynamic gas disengagement (DGD) technique. The two bubble groups concept has also been adopted by Guedon et al. (2017) which explicitly divides the bubbles into large and small groups in the simulations. The two bubble groups model has significantly improved the simulation results especially at high superficial velocities (Krishna and van Baten, 2001a, Krishna et

al., 1999), however, it still cannot properly reflect dynamic changes of the bubble sizes and the momentum exchange between the large and small bubble.

In recent years, the bubble size distribution is determined by applying the population balance model (PBM). The population balance model, which with kernel functions accounting for the bubble coalescence and breakage phenomenon, can be used in CFD modelling to describe the dynamic changes of the number density of bubble groups. During the development and implementation of the population balance models, many researchers have made significant contributions (Fu and Ishii, 2003a, Fu and Ishii, 2003b, Sun et al., 2004, Ishii et al., 2004, Lehr and Mewes, 2001, Olmos et al., 2001, Buwa and Ranade, 2002, Wang et al., 2006, van den Hengel et al., 2005, Jakobsen et al., 2005, Liao et al., 2015, Bhole et al., 2008, Hagesaether et al., 2002, Kumar and Ramkrishna, 1996).

Wu et al. (1998) and Fu and Ishii (2003b) have developed the interfacial area transport models by simplifying population balance model. Two assumptions are made in the simplification: firstly, the difference in sub-bubble breakup and coalescence rates within the same bubble group is not considered; secondly, the difference in velocity between sub-bubbles is ignored. Using the similar way, Lehr et al. (2002) developed a bubble volume transport model. Both the interfacial area transport models and the bubble volume transport model are the simplification of the population balance model, which have lower computational cost due to fewer equations to be solved. Thus these models can be used conveniently in the bubble column with large diameter such as Schlegel et al. (2015). However, the effect of sub-bubble size on the rate of bubble breakup and coalescence cannot be described

in the derivation and the bubble size distribution cannot be predicted. With the development of computational resources, it becomes possible that solving the complete population balance equations for the grids with a large number of cells, for example, the work by Yang and Xiao (2017) have performed CFD-PBM modelling with approximately 400-thousand cells and 20 discrete bubble classes.

Population Balance Model

The population balance equations can be numerically solved via different solution methods, such as the discrete method (DM) (Hounslow et al., 1988, Lister et al., 2004), the quadrature method of moments (QMOM) (Marchisio et al., 2003), and the direct quadrature method of moments (DQMOM) (Fan et al., 2004). It seems that all these solution methods are capable of mathematically resolving the population balance equations with different levels of complexity for each method. Therefore, the main concerns of the population balance modelling of bubble columns still fall on the understanding and description of the physical phenomenon of bubble coalescence and breakup, with the nature of which are recognised as the bubble-bubble and the eddy-bubble interactions respectively.

When using population balance models to model bubble size distribution, bubble coalescence and breakage phenomena are taken into account, the bubbles are classified into groups with different size d_i for the discrete method. The population balance equation is

$$\frac{\partial n_i}{\partial t} + \nabla \cdot \left(\boldsymbol{u}_{b,i} \cdot n_i \right) = S_i \tag{1-24}$$

where n is the number density of bubbles for, $\boldsymbol{u}_b$ is the bubble velocity vector, and S is the source term. The subscript i means the i-th group.

Due to coalescence and breakage events, the source term can be expressed by the birth and death of bubbles due to coalescence, which shown as

$$S_i = B_{coalescence,i} - D_{coalescence,i} + B_{breakup,i} - D_{breakup,i}$$
$$= \sum_{V_j=V_{min}}^{\frac{V_i}{2}} \Omega_C\left(V_j : V_i - V_j\right) - \sum_{V_j}^{V_{max}-V_i} \Omega_C\left(V_j : V_i\right) + \sum_{V_j=V_i}^{V_{max}} \Omega_B\left(V_j : V_i\right) - \Omega_B(V_i) \quad (1\text{-}25)$$

where V_i is the volume for the i-th class.

The local gas volume fraction and the Sauter mean diameter d_{32} can be calculated as follows:

$$\alpha_g f_i = n_i V_i \quad (1\text{-}26)$$

$$d_{32} = 1/\left(\sum_{i=1}^{N} \frac{f_i}{d_i}\right) \quad (1\text{-}27)$$

where f_i is the i-th class fraction of total volume fraction.

Bubble Breakage

The bubbles in turbulent dispersion are subject many forces which lead to bubble deformation or breakage, such as viscous force and turbulence stress. On the other hand, the bubbles are also subject to surface tension which is the most important force of the stabilisation of bubbles. Table 1-3 summarized various forces and relative influences on bubbles.

Table 1- 3 Various forces that act to break up and stabilize the bubble (adapted from (Chen, 2004))

Force for Breakage/Deformation	Force for Stabilization/Restoration
Turbulence stress/Eddy bombarding	Surface tension
Viscous force (negligible)	Liquid acceleration along the bubble surface
Kelvin-Helmholtz instability	
Rayleigh-Taylor instability	
Centrifugal force induced by gas internal circulation	

Based on the understanding of turbulent nature, a pioneering phenomenological model was proposed by Coulaloglou and Tavlarides (1977) with the assumption that the bubble breakup event occurs when the eddy-carried energy impacting on the bubble is greater than the bubble surface energy. As bubble collision is the main reason of bubble breakup, Prince and Blanch (1990) proposed that only the eddies with approximately same size as bubbles can lead bubble breakup, while the eddies at a much larger length scale have the tendency to transport bubbles rather than to break bubbles. Based on Prince and Blanch (1990) model, Tsouris and Tavlarides (1994) proposed a modified breakup model which defined the critical energy for breaking bubbles as the mean value of the surface energy increase for breakage into daughter bubbles with the same size and into a smallest and a biggest one. Luo and Svendsen (1996) proposed a bubble breakup model accounting the length scale and the energy containing of the arriving eddies based on the kinetic gas theory. The minimum length scale of eddies which can lead to bubble breakup equals to 11.4 times those eddies corresponding to the dissipation with the Kolmogorov scale. The model introduced the probability of bubble breakup which was the critical ratio of surface energy increased by bubble breakup and the mean turbulent

kinetic energy of the eddies colliding to bubble. It seems that eddies at very small scales do not contain sufficient energy to cause bubble breakup.

The Luo and Svendsen (1996) breakup model can be expressed as

$$\Omega_{B,L\&S}(d_i:d_j) = 0.923(1-\alpha_g)n_i\left(\frac{\varepsilon}{d_i^2}\right)^{\frac{1}{3}}\int_{\xi_{min}}^{1}\frac{(1+\xi)^2}{\xi^{11/3}}\exp\left(-\frac{12\sigma C_f}{\beta\rho_l\varepsilon^{2/3}d_i^{5/3}\xi^{11/3}}\right)d\xi \tag{1-28}$$

where $\xi = \lambda / d_i$, the increase coefficient of surface area $C_f = f_V^{2/3} + (1 - f_V)^{2/3} - 1$, the breakage volume fraction $f_V = d_j^3 / d_i^3$.

Unlike studies at earlier stage, rather than using a predefined daughter bubble size distribution, the daughter bubble size distribution can be calculated directly by Luo and Svendsen (1996) model, as given by

$$\beta(d_i:d_j) = \frac{\Omega(d_i:d_j)}{\int_0^1 \Omega_B(d_i:d_j)df_V} \tag{1-29}$$

Based on the study of Luo and Svendsen (1996), Wang et al. (2003) proposed the model for bubble breakup with the constraints of energy and capillary pressure. The energy constrain is that bubble breakup occurs only when energy contained by bombarding eddies contains greater than or equal to the energy increased by bubble breakup. The capillary constraint is that the dynamic pressure of the arriving eddy is greater than the capillary pressure of the bubble. This model improved the accuracy of simulation results to practical observation in comparison of Luo and Svendsen (1996) model because the two breakup criteria add the restriction of the minimum size of the bubble that can breakup. The constraints of energy and capillary pressure have also been adopted and extended in the recent studies reported by Zhao and Ge (2007) and Liao et al. (2015).

Bubble Coalescence

Because the probability of the collision of three or more bubbles is very small, coalescence model normally only considers binary collision. In order to study the bubble coalescence process, Shinnar and Church (1960) proposed the classic film drainage model, the coalescence between two bubbles in turbulent flow can be considered in three steps. As shown in Figure 1-19, at the first stage, bubbles collide and result in the deformation of the surface of colliding surfaces, which called the "dimple" formation. Then, liquid between two bubble drains thinning the film. Finally, when the attractive pressures can overcome the negative pressure along the film surface and the film is ruptured, coalescence between two bubbles happens.

If the surrounding pressure cannot the viscous force of the thin film, coalescence will not happen and bubbles will bounce back. Therefore, the coalescence probability is determined by the period of contacting time and the period of draining time. Prince and Blanch (1990) proposed a collision model taking the effects of liquid viscous shear, buoyancy-driven and turbulent eddy fluctuation into account, which can be expressed as

$$\Omega_{C,P\&B} = n_i n_j \frac{\pi}{4}\left(\frac{d_i+d_j}{2}\right)^2 \left(\bar{u}_i^2 + \bar{u}_j^2\right)^{1/2} \exp\left(-\frac{t_{coal}}{\tau_{col}}\right) \quad (1\text{-}30)$$

where t_{coal} the coalescence time, τ_{col} the collision time

It has been accepted that the influence of turbulence fluctuation is much greater than that of liquid viscous shear and buoyancy-driven in several cases. Therefore, Luo (1993) proposed a collision model, which encounters the deduction of liquid

viscous shear and buoyancy-driven and considers that the relative position of the mass centres of the two colliding bubble changes during the liquid film drainage. The Luo (1993) coalescence model is

$$\Omega_{C,Luo} = n_i n_j \frac{\pi}{4}\left(d_i + d_j\right)^2\left(\bar{u}_i^2 + \bar{u}_j^2\right)^{\frac{1}{2}} \exp\left(-c_1 \frac{\left[0.75\left(1+x_{ij}^2\right)\left(1+x_{ij}^3\right)\right]^{1/2}}{\left(\rho_g/\rho_l+0.5\right)^{1/2}\left(1+x_{ij}\right)^3} We_{ij}^{1/2}\right) \quad (1\text{-}31)$$

where the size ratio of two colliding bubbles $x_{ij}=d_i / d_j$ and We_{ij} the Weber number.

When both coalescence model and breakage model are implemented together in CFD simulations, it is often found that the bubble breakage rate and bubble coalescence rate are mismatch. In work of Chen (2004) and Chen et al. (2005), the predicted bubble breakage rate is about one order of magnitude lower than the predicted coalescence rate in churn-turbulent flow. Therefore, empirical correlations are requires to prevent over or under prediction in the comparison of experimental results. Yao and Morel (2004) and Mukin (2014) showed the need of coefficient adjusting the predicted bubble coalescence rate in dense bubbly flows. Bhole *et al.* (2008) have considered the slip between the bubble and eddies in liquid phase, which proposed a coefficient related to the bubble Stokes number.

4. EXPERIMENTAL VALIDATION

The fundamental understandings of turbulent bubbly flow in the bubble columns come from numerous experimental studies at early stages. The experimental studies of bubble column reactors have been through the development from overall characteristics to local characteristics and from steady state to dynamic behaviours. Early-stage investigations focus more on the time-averaged overall characteristics, such as large-scale liquid circulation. The experimental approaches are simple, for example, measuring the increase of liquid height to measure total gas holdup, conductivity or optical fibre probe for local gas holdup measurement and Pitot tube for time-average liquid velocity. However, many new measurement devices have been rapidly developed since the 1980s, such as hot-wire/film anemometry, Particle Imaging Velocimetry (PIV), Laser Doppler Velocimetry (LDV), High-Speed Camera, Computational Tomography (CT), Electric Resistance Tomography (ERT) /Electric Capacitance Tomography (ECT), and Computer Aided Radioactive Particle Tracing (CARPT). Although different limitations still exist on these new devices and measurement techniques, the in-depth study of flow structures and dynamic behaviours under various conditions can be satisfyingly achieved by choosing the appropriate experimental tools.

4.1 Measure of Gas Holdup

The overall gas holdup in the bubble columns can be measured with simple techniques. Comparing the dynamic liquid height with the static liquid height is

the commonly used one, especially when the flow regime is within the bubbly and the transition ranges. For a simple bubble column operation procedure, the liquid is not fully filled into the bubble column and remains static before the gas phase is injected. Once the gas phase has been pumped into the column, the bubbles will be formed and occupy the spaces that are originally full of the carrier fluid. In this case, the gas-liquid interface at the top surface will be lifted up to a dynamic height that keeps fluctuating slightly. Since the cross-sectional area of the bubble column is constant, the volume of the gas being injected into the volume of the liquid phase can be calculated by their heights respectively. The overall gas holdup measured by this method can be expressed by

$$\alpha = \frac{H_{dynamic} - H_{static}}{H_{dynamic}} \tag{1-32}$$

where $H_{dynamic}$ and H_{static} are the dynamic and static liquid height respectively. Since the gas-liquid interface at the top surface keeps oscillating all the time, the dynamic liquid height can only be obtained from taking average of the readings by multiple observations. Although the errors are partially reduced by averaging the recorded data, a specific height seems to be difficult to determine only by eye observations, especially when the gas-liquid interface at the top surface is changing quickly and intensely.

A pressure-based method can also be used to obtain the overall gas holdup in the bubble columns. Two pressure sensors are mounted at the side wall of the top and the bottom of the testing section, away from each other for a certain distance ΔH. The pressure difference ΔP of the testing section can also be measured by a simpler instrument, U-tube pressure gauge, with its two ends respectively connected to the

same positions as the pressure sensors. The schematic diagram of using the U-tube to measure the pressure difference of the testing section is shown in Figure 1-21. Since the density of the gas phase is much smaller than the liquid phase, the pressure changes resulting from the gas phase in the testing section can often be neglected under this circumstance. Thus, the change in pressure difference is mainly owing to the volumes that originally occupied by the liquid phase are now replaced by the gas bubbles. Therefore, the overall gas holdup measured by this method can be expressed by

$$\alpha = \frac{\Delta P}{\rho_L g \Delta H} \tag{1-33}$$

where ρ_L is the density of the liquid phase.

There are more complex techniques for total gas holdup measurement, such as dynamic gas disengagement technique (DGD), imaging analysis and cross-sectional averaging from local gas holdup. For example, DGD requires measuring the liquid level or the pressure at different levels in the bubble column when the aeration is stopped. If the dispersion is axially homogeneous when the gas feed is interrupted and no bubble coalescence and breakup happening during disengagement, the liquid level decreases as a function of time can be interpreted as caused by the bubbles disengaged in different rise velocities that corresponding to their bubble classes (Camarasa et al., 1999). However, this method can only be applied when the bubble column is operated in homogeneous regime mainly due to the complex assumptions (Lee et al., 1999). It seems that small relative errors have always existed within these methods. Yet still, the measurement results will be reasonably accurate if a suitable method is chosen for different testing conditions.

It is found that the influencing factors for overall gas holdup include gas superficial velocity, column diameter, gas distributor design, height to diameter ratio, physical properties and operating conditions. The overall gas holdup increases with the gas superficial velocity almost linearly at homogeneous regime while the increasing rate becomes lower at heterogeneous regime due to the large bubbles with higher rising velocities that are formed by the bubble-bubble interactions. A typical example of the increase in overall gas holdup with superficial velocity is shown in Figure 1-22.

Daly et al. (1992) have used DGD method for bubble columns with diameters 0.05 m and 0.21 m respectively and finds that the overall gas holdup in the small column is slightly larger in the large column under the same superficial velocity. The experimental results of Forret et al. (2003) have shown that the overall gas holdup increases with the column diameter while the differences are within 5%. Shah et al. (1982) claim that the effect of column diameter on the overall gas holdup can be neglected once the column diameter is larger than 10 to 15 cm. Vandu and Krishna (2004) finds that the overall gas holdup reduces with the increase of column diameter. They conclude that this is due to the enhanced liquid circulation in bubble columns with large diameters has fastened the bubble rising velocity. It seems that there are different conclusions on the effect of column diameter on the overall gas holdup. However, it is generally believed that the influence is not very significant if the column diameter is larger than 10 cm. Thorat et al. (1998) have comprehensively investigated the effect of sparger design and liquid dispersion height to bubble column diameter ratio on the averaged gas holdup. It is found that

the averaged gas holdup decreases as the *H/D* ratio increases from 1 to 5 for perforated plate with hole diameter smaller than 3 mm, but no significant changes when *H/D* > 5. It seems that the *H/D* ratio has almost no effect on the averaged gas holdup for the spargers with hole diameters from 3 mm to 6 mm. For the sparger hole diameter larger than 10 mm, the overall gas holdup increases with the *H/D* ratio due to the large initial bubble size that requires sufficient liquid height to allow bubble breakage. It seems that the free area has not much effect on the overall gas holdup for perforated plate with smaller hole diameters. Yet still, for spargers with larger holes, the overall gas holdup increases reversely with the free area. It seems that the overall gas holdup is increased as the elevated pressure leads to smaller average bubble size(Luo et al., 1999). Also, experimental results show that electrolyte can suppress the bubble coalescence and hence increase the gas holdup (Zahradnik et al., 1995). The liquid viscosity is a parameter that greatly affects the gas holdup. The overall gas holdup is obviously lower in high viscosity systems, such as air-oil system (Chen et al., 1999) or Air-Aqueous Solution of Carboxymethyl Cellulose (Thorat et al., 1998).

The local gas holdup distribution can be measured in different ways, including probes, Computational Tomography (CT), Electric Resistance Tomography (ERT) /Electric Capacitance Tomography (ECT) and high-speed imaging. Among these methods, using needle probes is one of the simplest and the most cost-effective ways to obtain the local gas holdup at the queasy-steady state. Depending on the types of signals that the probes based on, single-tip optical fibre or conductivity probes lead to the measurement of gas fraction and bubbling frequency. In addition to the results that can be obtained by single-tip probes, dual-tip conductivity probes

allow measurements of bubble velocity, time-average local interfacial area, and mean bubble chord length. A typical configuration of the dual-tip conductivity probe is shown in Figure 1-23.

The measurement of the local gas holdup by the conductivity probe is based on the conductivity difference between the gas and the liquid phase. Since the conductivity probe has to be inserted into the bubble column and fixed at the radial positions that are about to be measured, the two tips of the probe are supposed to be as thin as possible (0.5 mm – 5 μm) to avoid causing too much interference to the flow field (Thang and Davis, 1979). The two tips are separated from each other with a short distance (0.5 - 5 mm) and the sampling frequency should be fast enough (1-10 kHz) to capture the instant transition of the gas and liquid phase without causing long delays and hence large measuring errors (Boyer et al., 2002). Also, the sampling time should be long enough in order to reflect the time-averaged characteristics. When a tip of the probe is immersed in the liquid, due to the high conductivity of the liquid, the signal should appear to be near 1. When the tip is in contact with a gas bubble, the signal will drop to 0 almost instantly. Once the gas bubble leaves the tip, the conductivity signal recovers to 1. Ideally, if no deformation or distortion happened and the gas bubble passes the two tips through the same path, the time durations obtained from two tips for the gas bubble should be exactly the same. However, the reality is far more complicated than the assumptions. For instance, the gas bubble may not come from the normal direction to hit the measuring tips or the gas bubble that attacked the first tip may not necessary hit the second tip. Therefore, the signals obtained from both tips can be used for statistical analysis to reduce the system errors. Output signals for bubble

detection by dual-tip probe under different conditions are shown in Figure 1-24.

The conductivity probe should be placed at several radial locations, and the collection of data should be repeated sufficiently for each location. Once the conductivity signals have been properly processed, the gas holdup for each local position can be expressed by

$$\alpha_g = \frac{\sum \Delta T_0}{\Delta T_n} \tag{1-34}$$

where ΔT_0 is the time duration for the probe surrounded by the gas bubbles and ΔT_n is the total time duration of each measurement.

Some researchers have proposed multi-point probes, such as Burgess and Calderbank (1975), Yao et al. (1991) and Manjrekar and Dudukovic (2015). Theoretically, all components of the velocity vectors can be obtained by using multi-point probes and hence the measurements become more accurate. However, practical problems have limited the application of these multi-point probes. For instance, multiple tips may cause bubble deformation easily when some of them piercing through the liquid film at the same time. Also, the interaction of trapping of the bubbles with the multiple tips can no longer be neglected. Furthermore, the algorithm for calibration and signal processing is inevitable complicated due to the numbers of the measuring tips.

Although the tips are made as thin as possible, using the probes are still an intrusive method that inevitably affects the surrounding flow field. Also, the measurement results can only represent the gas holdup for a small range around the measuring

point. However, non-intrusive measurements on the entire flow field are required for the interest of both the industry and academia. These non-intrusive methods for gas holdup measurement include X-ray/γ-ray CT, ERT, ECT, and high-speed imaging. By using these methods, the spatial distribution of gas holdup for an entire (horizontal or vertical) cross-section can be obtained in time sequence. The non-intrusive measurements have no interference to the fluid flow and as well as not being affected by the operating conditions such as high temperature, high pressure and corrosive fluid, and hence made the accurate on-line measurement of local characteristics possible.

Electrical Capacitance/Resistance Tomography is widely used for void fraction measurement of two-phase flow systems. Based on the differences in capacity/resistivity of the gas-phase and liquid-phase, the ECT/ERT measurement system uses an array of electrodes that attach to the bubble column wall to receive the electrical signals. A data acquisition system is directly connected to the electrodes. The collected data are processed by image reconstruction algorithms to plot the cross-sectional distribution of void fractions. Circumferential arrangement of electrodes, calibration images of different fluids and typical results of a 2-layer ECT/ERT measurement are shown in Figure 1-25.

It seems that the resolution of ECT/ERT is largely depended on the number of electrodes being deployed, the diameter of the vessel to be measured, and the image reconstruction algorithm. Theoretically, the more electrodes are used the higher resolution will be obtained for the same bubble column. However, in practice, the number of electrodes to be used is limited to the diameter of the bubble column to

be measured. Also, increasing the number of electrodes means more time and computing effort for the image reconstruction algorithm, usually linear back projection algorithm, to convert the collected data into the final void fraction images. Moreover, most of these ECT/ERT systems are 2-D based measurement. Although 3-D plots can be obtained such as Al-Masry et al. (2010), it seems that these 3-D plots are generated from interpolation of 2-D measurements. Considering all these disadvantages, a 3-D real-time electrical capacitance volume tomography (ECVT) has been developed recently (Warsito et al., 2007). The ECVT system uses upgraded 3-D capacitance sensors with different shapes and configurations and a volume image reconstruction technique called the neural-network multi-criterion optimisation image reconstruction (NN-MOIRT). The sensor designs and the reconstruction results for the ECVT system are shown in Figure 1-26.

The ECT/ERT measurement systems have used the electrical signals measured on the vessel wall to inversely estimate the image in the centre. It is believed that this is not a direct measurement in the core region of the flow field. However, Computational Tomography uses a narrow beam of X-ray/γ-ray to penetrate the multiphase system along a straight path. Radiative decay flies off during this process primarily by absorption and scattering, and resultant intensity can be detected by scintillation detectors placed on the opposite side of the source (Chen et al., 1998, Patel and Thorat, 2008, Kumar et al., 1997, Hubers et al., 2005).

Figure 1-27 (a) presents a typical source-detector configuration of CT systems, the source and detectors are mounted on a gantry that is capable of being rotated about the axis of the test section through a stepper motor. The spatial resolution based on

the rotational scanning of CT measurement is generally higher than ECT/ERT. However, different from the instantaneous measurement with some delays from the image reconstruction of ECT/ERT, the gas holdup profile measured by CT can only reflect the time-averaged characteristics, as the maximum rotational speed is limited by the weights of the scanning assembly and the number of projection measurements required for a complete 360-degree rotation.

With the development of those measurement devices, the local characteristics of the bubble columns have been widely studied. For example, an early study by Hills (1974) has used conductivity probe to investigate the radial distribution of time-averaged gas holdup under different superficial velocities and with perforated plate distributors that have different size and number of holes. It is found that the local gas holdup is generally shown to be a normal distribution and it is strongly affected by the distributor configurations. In order to further study the effect of free area and hole diameter of gas distributors, Patel and Thorat (2008) measured radial distribution of gas holdup in a 0.2 m diameter bubble column. It seems that the gas holdup distribution is strongly associated with the flow regime of bubbles at the outlet of gas distributor. When the free area is decreased, the flow regime of bubbles is easier to transform into bubble jetting. In this case, the high-velocity jets will disappear quite quickly under the influence of liquid-phase, large coalesced bubbles are easier to be formed due to the downstream interaction of jets, and hence the gas holdup will be reduced. When the free area is kept the same, increase the hole diameter will also decrease the gas holdup, because of the increased initial bubble size (Kumar et al., 1997). Veera and Joshi (2000) comprehensively measured the local gas holdup distribution for different sparger hole diameters,

liquid dispersion height, and liquid phase properties. Similar conclusion with Kumar et al. (1997) has been drawn on the gas distributor design, and they further show that the decrease of gas holdup distribution is due to the bubble coalescence by comparing the measurement results for coalescence inhabiting and coalescence promoting liquids. These experimental findings are shown in Figure 1-28.

The gas holdup distribution is also associated with the axial height position and bubble column diameter. The experimental results of Veera and Joshi (2000) have shown that the gas holdup in the centre of the bubble column increases along the axial direction for a large bubble column with a diameter of 0.38 m. Chen et al. (1998) have found a similar trend for a larger bubble column with a diameter of 0.44 m and at a superficial velocity of 0.1 m/s. Kumar et al. (1997) have measured gas holdup distribution for both large and small bubble columns (diameters of 0.26 m and 0.1 m). Different from the large bubble columns, the evolution of gas holdup distribution in the small bubble column at high superficial velocity is shown to be increased with the axial position in an entry region and then decrease gradually until it reaches an equilibrium state. The effects of axial distance to the gas distributor for both small and large bubble columns are shown in Figure 1-29.

The local gas holdup is also influenced by the operating pressure of the bubble columns. It is found by Kemoun et al. (2001) the effect of operating pressure becomes significant especially at high superficial velocities. As shown in Figure 1-30(d), the gas holdup is about 70% higher at 0.7 MPa than at atmospheric pressure, even though the elevated pressure decreases the radial gradient of the gas holdup distribution.

4.2 Bubble Dynamics

The bubble characteristics in gas-liquid two-phase flows have been intensively studied. In the bubble column reactors, the rising of bubbles leads to the large-scale circulation of the liquid phase, and the turbulence is generated due to the liquid shear and the wake formed by shedding vortices from the bubbles. The bubble motions in the liquid flow can be considered as flow over moving objects that are under dynamic oscillation and deformation due to the surrounding pressure. The dynamic behaviour of the bubbles is closely associated with the flow of the bubble's boundary layer and the shedding of vortices. It seems that there are very strong interactions between the bubbles and the carrier fluid. Therefore, investigations on the bubble characteristics lead to understandings of the gas-liquid interactions in the bubble columns.

For a specific gas-liquid system, such as air-water system, the physical properties of the liquid phase can be regarded as constants. Under this circumstance, the shape of bubbles is only related to the bubble diameters. Mendelson Harvey (1967) specified the shape of bubbles according to the bubble diameters while classifying the terminal velocities into 4 regions. The bubbles are in spherical shape when they are smaller than 1.4 mm. When bubbles become larger, they are no longer spherical and tend to follow a zigzag or helical rising path. According to Mendelson Harvey (1967), the bubbles begin to assume a spherical cap shape when they are larger than 6 mm. However, it has been argued that this transition size to spherical-cap bubble is not accurate. Clift et al. (1978) present that the bubbles are shown to be spherical-capped

when the diameter is approximately large than 20 mm, which makes a better agreement with the experimental observations by Batchelor (1967). The terminal velocity map of air bubbles of different sizes has been presented in Figure 1-31. Based on a large number of experimental statistics, Tomiyama (1998) proposed a semi-empirical model for bubble shapes variations, which has given 1.36 mm and 17.3 mm as the boundaries between spherical/ellipsoidal bubbles and ellipsoidal/spherical capped bubbles respectively in a slightly contaminated air-water system.

It seems that a large proportion of the bubbles in the bubble column reactors are in ellipsoidal shapes. These medium-size ellipsoidal bubbles have very significant surface oscillations and also the most complex rising trajectories. Reichardt and Sommerfeld (2008) present the oscillation and rising characteristics of single ellipsoidal air-bubble in the stagnant liquid by applying particle tracking velocimetry, as shown in Figure 1-32.

It is believed that the rising of non-spherical bubbles is largely affected by the bubble wakes. Mendelson Harvey (1967) considers that the drag force being imposed on the non-spherical bubbles is increased due to the vortices or eddies induced in the bubble's wake. Since the spherical-cap bubbles vertically rise in water almost along a straight line with relatively constant speed, the flow behind the spherical-cap bubbles seems to be easier to be captured, as shown in Figure 1-33. For Reynolds number less than about 360, the wake behind the bubble is laminar and takes the form of a toroidal vortex; while the Reynolds number is larger than 360, the wake behind the bubble becomes turbulent. It seems that

this kind of bubble-induced turbulence decays quite quickly due to liquid viscosity in the downstream of bubbles, which may be very different from the turbulence generated due to the liquid shear. In the bubble columns, the wake of bubbles not only affects the drag force but also interacts very strongly with the subsequent bubbles. To be more specific, both the bubble coalescence and breakup phenomena, which are due to bubble-bubble collision and eddy-bubble collision, will be greatly affected due to the eddies or bubbles that are under the influence of bubble-induced turbulence. Therefore, understanding the bubble-induced turbulence must be one of the key points for accurately describing the gas-liquid interactions in the bubble columns.

4.3 Liquid Flow Field Characteristics

There are many studies on the liquid flow field characteristics in the bubble column reactors, and most of the early studies focus on the time-averaged liquid velocity distribution, flow structures, and flow regime transitions. The time-averaged liquid velocity distributions can be simply measured by modified Pitot tube, such as Hills (1974). One of the key findings of these studies is the large-scale liquid circulation driven by rising bubbles. However, in-depth understandings of the transient behaviour of the both the local and the entire flow field, such as instantaneous liquid velocity and dynamic flow regime transitions, are still insufficient at this stage.

With the development of Particle Imaging Velocimetry (PIV), Laser Doppler Anemometry (LDA), Computer Aided Radioactive Particle Tracing (CARPT)

and high speed imaging, as well as in combined with other measurement techniques including pressure measurements, bed expansion method, and optical probes, the flow regime transitions have been systematically studied by various researchers (Chen et al., 1994, Zahradnik et al., 1997, Camarasa et al., 1999, Ruzicka et al., 2001, Ruzicka et al., 2003, Ruzicka et al., 2008, Reilly et al., 1994, Krishna and Ellenberger, 1996, Manjrekar and Dudukovic, 2015, Thorat and Joshi, 2004). It seems that the flow regime transitions are influenced by various parameters including bubble column diameter, liquid dispersion height, liquid phase properties, operating pressure, and gas distributor designs.

The flow regimes in the bubble column can be defined as homogeneous bubbly flow, transition range, slug flow the heterogeneous churn-turbulent range, depending on the superficial velocity of the gas phase and the column diameter. The sketch of approximate distinction of the flow regimes in the bubble columns has been shown in Figure 1-1. A very comprehensive study on the flow regime transitions in the bubble columns has been presented by Chen et al. (1994), which identifies the flow regimes as dispersed bubble, vortical-spiral flow, and turbulent flow. The typical 3-D macroscopic flow structures in the vortical-spiral flow regime have been clearly illustrated, which include descending flow, vortical-spiral flow, fast bubble flow, and central plume. These illustrations have greatly extended the understandings in the dynamic characteristics and the coherent eddy structures in the bubble columns, which further provide very important guidelines to the design and scale-up of bubble columns. It seems that the transition of the flow regimes and the macroscopic flow structures are found to be analogous to the Taylor instabilities, which characterised flow between

two concentric rotating cylinders. Besagni and Inzoli (2016b) further distinguished the homogeneous flow regime into the mono-dispersed homogeneous regime and the poly-dispersed homogeneous flow regime, depending on the superficial velocities and the associated bubble size distributions. The presence of the large bubbles leads to the transition from the homogeneous regime to the transition region. The transition flow regime is characterised by macroscopic flow structures with large eddies and a widened bubble size distribution (Guedon et al., 2017), in which case, the turbulent eddies induced by the "coalescence-induced" large bubbles may make increasingly significant contributions to the turbulence generated in the column.

The turbulence in the bubble columns is different from the single-phase turbulence in pipe flows. With the gas phase and liquid phase simultaneously existed in the bubble columns, the two-way interactions are inevitable between the liquid phase flow and the gas bubbles of different sizes and shapes. Apart from the shear turbulence due to the velocity gradient of the liquid phase flow, the interactions between the gas bubbles and the carrier fluid certainly make great contributions to the turbulence in the bubble columns. From a slightly different perspective, bubbles are the energy source of the bubble columns. There is no turbulence when the liquid is remained static before the bubble column start operation. Once the bubbles are aerated into the column, the turbulent eddies are induced at the wake of bubbles. This kind of bubble-induced turbulence is expected to decay in a different way from the single-phase turbulence. However, different from individual bubbles, the structures and behaviours of the turbulent eddies are more difficult to be described, which

leads to more problems in understanding the influence of gas bubbles on the liquid-phase turbulence. Therefore, a statistic tool, the turbulence energy spectrum, can be used to characterise different behaviours of the turbulence in the bubble columns.

The turbulence energy spectrum can be approximately divided into energy-containing range and universal equilibrium range, which includes inertial subrange and dissipation range, based on the frequency or wave number of turbulent eddies. The turbulent kinetic energy cascades from large eddies to small eddies in sequence. The Kolmogorov -5/3 law for the inertial subrange, which can be expressed as $E(\kappa) \sim \varepsilon^{2/3}\kappa^{-5/3}$, has already been widely accepted for homogeneous and isotropic turbulence in single-phase flow. The experimental work from Mudde *et al.* (1997) and Cui and Fan (2004) have shown the pseudo-turbulence energy spectrum follows the -5/3 scaling law. However, it can be found in more experimental studies that the energy spectrum of bubble-induced turbulence is different from that of single-phase turbulence. Lance and Bataille (1991) measured the energy spectrum of the fluctuations caused by a swarm of bubbles rising through an imposed turbulent flow using hot-wire and laser Doppler anemometry (LDV). They found the behaviour of energy spectrum in high wave number range obeys -8/3 scaling law, in contrast to the classical -5/3 energy spectrum scaling for homogeneous single-phase turbulence. They attributed the change of scaling to the wake dissipation effect, in which eddies produced were dissipated rapidly before the spectral transfer has even taken place. Mercado et al. (2010) conducted single-point measurements using phase-sensitive constant-temperature anemometry (CTA)

probe and found the slope of power spectrum in bubble-induced turbulence was near -3 for various void fractions ranging from 0.8-2.2% in the very dilute system. Moreover, Mendez-Diaz et al. (2013) observed a decayed power scaling close to -3 for energy distributions of a wide range of Reynolds and Weber numbers using a hot film anemometer (HFA) system. They also suggested the specific details of the pseudo-turbulent fluctuation does not depend strongly on hydrodynamic interactions among bubbles. As pointed out by Risso (2011b), the κ^{-3} scaling obtained from CTA measurements is based on the time fluctuation of velocities. For the spatial fluctuation of velocities, it requires simultaneous measurements of the liquid velocity insufficient number of locations, which cannot be done by using LDA or CTA probes. Therefore, Riboux et al. (2013) measured energy spectrum using PIV in the wake of a bubble swarm due to the light reflection at interface of bubble within swarm and measured liquid velocity inside bubble swarm using LDA. They found that the power was close to -3 for larger scales (i.e. length scale greater than bubble diameter) and was -5/3 for small scale. This result did not depend on bubble size and distribution. The value of scaling of large scale confirmed the result of Lance and Bataille (1991).

The phase-sensitive CTA was developed by van den Berg (2006), who has used optical an optical fibre attached to the hot-film probe. When a bubble collides with the hot-film sensor, it can also be detected by the optical fibre. The detection of bubbles is similar to that by using conductive probes, only the objective signal is the light intensity rather than conductivity. It should be noticed that the measurements of Riboux et al. (2013) focus on the unsteady

flow that evolves as the bubbles just rise away from the fixed measuring window of one high-speed PIV camera. Another synchronised camera is placed at a perpendicular position to trace the bubble trajectories so that the exact timing of the bubbles rise away from the measuring window can be found. Although this technique has successfully measured the velocities induced at the bubbles rising passage, it is essentially the measurement of the single phase. Therefore, the measured velocities are with short delays and whether the characteristics of the bubble swarm's wake are significant of the flow within the homogeneous swarm are hard to be determined. A typical two-camera PIV system for simultaneous 2-D measurement of the bubbles and the liquid phase in the bubble columns has been presented by Broder and Sommerfeld (2002). The working principle has been explained in details by Poelma et al. (2007).

The neutral buoyant fluorescing particles are added into the bubble column as tracer particles. The testing section is illuminated by a pulsed Nd:YAG laser (New Wave Gemini, @532nm, 2×30 MJ, light sheet thickness approx. 0.5 mm). The two CCD cameras are usually placed at non-perpendicular positions, with one records the tracer particles signal and the other records the bubbles. The emission spectrum of the fluorescing particles should be different from the wavelength of the scattered light from the bubbles so that different filters can be applied to both cameras to allow light with a different particular wavelength to pass through for each camera. By doing so, the signals for both phases can be separated. Classic iterative algorithms incorporating a successive refinement of the interrogation area can be used for the image pairs of the tracer particles while the bubble detection algorithm can be applied along with the Particle Tracking

Velocimetry (PTV) algorithm to obtain the bubbles velocity vectors (Sommerfeld and Broder, 2009). Deen et al. (2000a) used a similar two-camera PIV to measure the velocity field in a square bubble column and compare the results with that of a single-camera ensemble-averaged PIV measurement. The results revealed clearly a proper discrimination of the displacement vectors for both phases is not possible in a single-camera setup, as the velocity difference between the phases is relatively small in the bubble columns. Therefore, it is emphasised that the separation of the signals from two phases is very important as the main concern is to only investigate the statistical characteristics of liquid phase turbulence (under the influence of bubbles). Based on the separation concept, similar PIV measurement results of -3 scaling turbulence energy spectrum have been obtained by Murai et al. (2000) and Bouche et al. (2014) in both 2-D and 3-D bubble columns.

Although the simultaneous measurement of both phases can be obtained by using the two-camera PIV system, the velocity vectors for the liquid phase at the regions that being occupied by the bubbles are still very difficult to obtain. However, the spatial resolution is strongly required to obtain the turbulence energy spectrum, because the length of the smallest interrogation cell should be small enough to represent the highest wavenumber that intended to be covered. In other words, limited to the resolution of PIV cameras, the measuring window cannot be too big. Therefore, the liquid velocity signals are often blocked by the existence of bubbles in this small measuring window, which may be a difficult problem for obtaining the turbulence energy spectrum from two-camera simultaneous measurements. Considering all these difficulties, a special camera

with even higher resolutions and high capturing speed may be required to allow sufficient spatial resolution in a larger measuring window for completed and simultaneous measurements.

Apart from the limitations of experimental devices, the understanding of the -3 pow law scaling behaviour of the bubble-induced turbulence is still insufficient. Theories formed based on the experimental observations and measurements are mostly speculations or conjectures. Arguments and debates on the existence, the active range, the characteristic length and time scales and the energy cascade processes of the -3 power scaling behaviours are still lasting, which has become an obstacle from applying these characteristics of the bubble-induced turbulence into numerical studies, such as coupling with the bubble coalescence and breakup kernels or including the contribution of bubble-induced turbulence into turbulence modelling in gas-liquid two-phase flows.

5. RECAPITULATION AND IMPLICATIONS

This chapter has reviewed recent researches of the turbulent bubbly flow in the bubble column reactors both in the experimental and numerical method. Various experimental techniques on the measurements of the gas holdup, bubble characteristics, and liquid phase flow fields have been outlined. It seems that the investigations on the gas holdup, bubble behaviours, and the liquid flow field have trended towards the dynamic and local characteristics. With the development of high-speed and high-resolution measurement device and technique, the importance of the structures of bubbles and eddies that are under the influence of each other has been gradually recognised. For CFD modelling, the two-fluid model is considered as the most cost-effective numerical modelling method for the simulation of turbulent bubbly flows in the bubble columns, especially with the requirement of describing a large number of bubble's coalescence and breakage phenomenon. However, closure problems such as interphase forces, turbulence modelling, and bubble size distribution have been brought into concern in this case. The most crucial conclusion to be drawn from both experimental and numerical studies reviewed in this chapter is that the understanding of gas-liquid interactions in the bubble column reactors is still limited. In particular, the response of bubble to the surrounding eddy and the effect of the bubble-induced turbulence have not been appropriately considered in the CFD modelling, and the modulation of particle in three-phase flow have not been fully revealed from an experimental point of view.

In the following chapters, the studies focusing on the effect of bubble dynamic in multiphase flows in bubble column reactors are carried out. An acceleration numerical method will be presented in Chapter 2. Chapter 3 will investigate the effect of the eddy-bubble response in turbulent viscosity model. Chapter 4 will present experimental study of gas-liquid-solid three-phase flow in bubble column. Finally, Chapter 5 will present the main conclusions derived from previous chapters to deepen the understanding of the turbulent bubbly flows in the bubble column reactors and provide recommendations for future works on this aspect.

6. AIMS AND LIST OF OBJECTIVES

In general, after the comprehensive literature review about the current status of turbulent bubbly flows and experimental studies of bubble column reactors, this research work aims to investigate on gas-liquid two-phase and gas-liquid-solid three-phase flow in bubble column from both numerical and experimental aspects to fill in the gap of fundamental understanding of the complicated mechanisms of multiphase flow in bubble column.

The objectives of this work can be summarized as follows:

i. Investigation on the CFD modelling of gas-liquid two-phase bubble column coupling Population Balance Model.
ii. Proposed a numerical method for bubble breakup model to calculate the bubble size distribution in a more effective numerical scheme, which provides the basis of any modification of bubble breakup model in numerical modelling.
iii. Investigation on the bubble-induced turbulence and the bubble response to the eddies with similar turbulence length scale, thus development of a modified turbulent viscosity model to simulate the effect of bubble-eddy response on different hydrodynamic properties in gas-liquid two-phase flow.
iv. Conduction of the experiments of gas-liquid two phase flow and gas-liquid-solid three-phase flow in the bubble column through 2D PIV.
v. Produced a turbulent energy spectrum of two-phase flow with experimental data, and further indicated the importance of taking into account bubble-

induced turbulence.

vi. Investigation on the particle modulation in three-phase flow by comparing different hydrodynamic properties between gas-liquid two-phase flow and gas-liquid-solid three-phase flow, which provides the basis of the CFD modelling of three-phase flow in the future, for example, how to develop a proper interphase force model between gas and solid phase and how to evaluate the viscosity of solid phase in turbulence models.

REFERENCES

AL-MASRY, W. A., ALI, E. M., ALSHEBEILI, S. A. & MOUSA, F. M. 2010. Non-invasive imaging of shallow bubble columns using electrical capacitance tomography. *Journal of Saudi Chemical Society,* 14**,** 269-280.

ANTAL, S. P., LAHEY, R. T. & FLAHERTY, J. E. 1991. Analysis of phase distribution in fully developed laminar bubbly two-phase flow. *International Journal of Multiphase Flow,* 17**,** 635-652.

AUTON, T. R., HUNT, J. C. R. & PRUDHOMME, M. 1988. The Force Exerted on a Body in Inviscid Unsteady Non-Uniform Rotational Flow. *Journal of Fluid Mechanics,* 197**,** 241-257.

BATCHELOR, G. K. 1967. *An Introduction to Fluid Dynamics*, Cambridge University Press.

BESAGNI, G. & INZOLI, F. 2016a. Bubble size distributions and shapes in annular gap bubble column. *Experimental Thermal and Fluid Science,* 74**,** 27-48.

BESAGNI, G. & INZOLI, F. 2016b. Comprehensive experimental investigation of counter-current bubble column hydrodynamics: Holdup, flow regime transition, bubble size distributions and local flow properties. *Chemical Engineering Science,* 146**,** 259-290.

BHOLE, M. R., JOSHI, J. B. & RAMKRISHNA, D. 2008. CFD simulation of bubble columns incorporating population balance modeling. *Chemical Engineering Science,* 63**,** 2267-2282.

BOUCHE, E., ROIG, V., RISSO, F. & BILLET, A.-M. 2014. Homogeneous swarm of high-Reynolds-number bubbles rising within a thin gap. Part 2. Liquid dynamics. *Journal of Fluid Mechanics,* 758**,** 508-521.

BOYER, C., DUQUENNE, A. M. & WILD, G. 2002. Measuring techniques in gas-liquid and gas-liquid-solid reactors. *Chemical Engineering Science,* 57**,** 3185-3215.

BRODER, D. & SOMMERFELD, M. 2002. An advanced LIF-PLV system for analysing the hydrodynamics in a laboratory bubble column at higher void fractions. *Experiments in Fluids,* 33**,** 826-837.

BUNNER, B. & TRYGGVASON, G. 2002. Dynamics of homogeneous bubbly flows Part 2. Velocity fluctuations. *Journal of Fluid Mechanics,* 466**,** 53-84.

BURGESS, J. M. & CALDERBANK, P. H. 1975. The measurement of bubble parameters in two-phase dispersions—I: The development of an improved probe technique. *Chemical Engineering Science,* 30**,** 743-750.

BURNS, A. D., FRANK, T., HAMILL, I. & SHI, J.-M. The Favre Averaged Drag Model for Turbulent Dispersion in Eulerian Multi-Phase Flows. Fifth International Conference on Multiphase Flow, ICMF-2004, 2004 Yokohama, Japan.

BUWA, V. V., DEO, D. S. & RANADE, V. V. 2006. Eulerian-Lagrangian simulations of unsteady gas-liquid flows in bubble columns. *International Journal of Multiphase Flow,* 32**,** 864-885.

BUWA, V. V. & RANADE, V. V. 2002. Dynamics of gas-liquid flow in a rectangular bubble column: experiments and single/multi-group CFD simulations. *Chemical Engineering Science,* 57**,** 4715-4736.

CAMARASA, E., VIAL, C., PONCIN, S., WILD, G., MIDOUX, N. & BOUILLARD, J. 1999. Influence of coalescence behaviour of the liquid and of gas sparging on hydrodynamics and bubble characteristics in a bubble column. *Chemical Engineering and Processing,* 38**,** 329-344.

CHAHED, J., ROIG, V. & MASBERNAT, L. 2003. Eulerian-Eulerian two-fluid model for turbulent gas-liquid bubbly flows. *International Journal of Multiphase Flow,* 29**,** 23-49.

CHEN, J. H., YANG, N., GE, W. & LI, J. H. 2009. Modeling of Regime Transition in Bubble Columns with Stability Condition. *Industrial & Engineering Chemistry Research,* 48**,** 290-301.

CHEN, J. W., GUPTA, P., DEGALEESAN, S., AL-DAHHAN, M. H., DUDUKOVIC, M. P. & TOSELAND, B. A. 1998. Gas holdup distributions in large-diameter bubble columns measured by computed tomography. *Flow Measurement and Instrumentation,* 9**,** 91-101.

CHEN, J. W., LI, F., DEGALEESAN, S., GUPTA, P., AL-DAHHAN, M. H., DUDUKOVIC, M. P. & TOSELAND, B. A. 1999. Fluid dynamic parameters in bubble columns with internals. *Chemical Engineering Science,* 54**,** 2187-2197.

CHEN, P. 2004. *Modeling the fluid dynamics of bubble column flows. Ph.D. Thesis.* Ph.D. Thesis.

CHEN, P., SANYAL, J. & DUDUKOVIC, M. P. 2005. Numerical simulation of bubble columns flows: effect of different breakup and coalescence closures. *Chemical Engineering Science,* 60**,** 1085-1101.

CHEN, R. C., REESE, J. & FAN, L. S. 1994. Flow Structure in a 3-Dimensional Bubble-Column and 3-Phase Fluidized-Bed. *Aiche Journal,* 40**,** 1093-1104.

CLIFT, R., GRACE, J. R. & WEBER, M. E. 1978. *Bubbles, Drops, and Particles*, Academic Press.

COOK, T. L. & HARLOW, F. H. 1986. Vortices in Bubbly 2-Phase Flow. *International Journal of Multiphase Flow,* 12**,** 35-61.

COULALOGLOU, C. A. & TAVLARIDES, L. L. 1977. Description of Interaction Processes in Agitated Liquid-Liquid Dispersions. *Chemical Engineering Science,* 32**,** 1289-1297.

CUI, Z. & FAN, L. S. 2004. Turbulence energy distributions in bubbling gas-liquid and gas-liquid-solid flow systems. *Chemical Engineering Science,* 59**,** 1755-1766.

DALY, J. G., PATEL, S. A. & BUKUR, D. B. 1992. Measurement of Gas Holdups and Sauter Mean Bubble Diameters in Bubble Column Reactors by Dynamic Gas Disengagement Method. *Chemical Engineering Science,* 47**,** 3647-3654.

DEEN, N., HJERTAGER, B. & SOLBERG, T. 2000a. *Comparison of PIV and LDA Measurement Methods Applied to the Gas-Liquid Flow in a Bubble Column*.

DEEN, N. G., SOLBERG, T. & HJERTAGER, B. H. 2000b. Numerical simulation of gas–liquid flow in a square cross section bubble column. *14th International congress of chemical and process engineering (CHISA).* Praha, Czech Republic.

DEEN, N. G., SOLBERG, T. & HJERTAGER, B. H. 2001. Large eddy simulation of the gas-liquid flow in a square cross-sectioned bubble column. *Chemical Engineering Science,* 56**,** 6341-6349.

DEEN, N. G., VAN SINT ANNALAND, A. & KUIPERS, J. A. M. 2004. Multi-scale modeling of dispersed gas-liquid two-phase flow. *Chemical Engineering Science,* 59**,** 1853-1861.

DEGALEESAN, S., DUDUKOVIC, M. & PAN, Y. 2001. Experimental study of gas-induced liquid-flow structures in bubble columns. *Aiche Journal,* 47**,** 1913-1931.

DELNOIJ, E. & KUIPERS, J. A. M. 2000. Reply to comments on "Dynamic simulation of dispersed gas-liquid two-phase flow using a discrete bubble model". *Chemical Engineering Science,* 55**,** 2345-2346.

DHOTRE, M. T. & JOSHI, J. B. 2007. Design of a gas distributor: Three-dimensional CFD simulation of a coupled system consisting of a gas chamber and a bubble column. *Chemical Engineering Journal,* 125**,** 149-163.

DHOTRE, M. T., NICENO, B. & SMITH, B. L. 2008. Large eddy simulation of a bubble column using dynamic sub-grid scale model. *Chemical Engineering Journal,* 136**,** 337-348.

DREW, D. A. 1983. Mathematical modeling of two-phase flow. *Ann. Rev. Fluid Mech., 15, 261-291.*

DREW, D. A. & PASSMANN, S. L. 1999. *Theory of Multicomponent Fluids.,* New York`, Springer.

EKAMBARA, K., NANDAKUMAR, K. & JOSHI, J. B. 2008. CFD Simulation of Bubble Column Reactor Using Population Balance. *Industrial & Engineering Chemistry Research,* 47**,** 8505-8516.

FAN, J. R., ZHOU, D. D., HUA, Q. & CEN, K. F. 1994. Numerical Computation of Particle-Laden Gas-Flows Past Staggered Tube Banks Undergoing Erosion. *Powder Technology,* 80**,** 1-10.

FAN, R., MARCHISIO, D. L. & FOX, R. O. 2004. Application of the direct quadrature method of moments to polydisperse gas-solid fluidized beds. *Powder Technology,* 139**,** 7-20.

FIROUZI, M., HOWES, T. & NGUYEN, A. V. 2015. A quantitative review of the transition salt concentration for inhibiting bubble coalescence. *Advances in Colloid and Interface Science,* 222**,** 305-318.

FORRET, A., SCHWEITZER, J. M., GAUTHIER, T., KRISHNA, R. & SCHWEICH, D. 2003. Influence of scale on the hydrodynamics of bubble column reactors: an experimental study in columns of 0.1, 0.4 and 1 m diameters. *Chemical Engineering Science,* 58**,** 719-724.

FRANK, T., ZWART, P. J., KREPPER, E., PRASSER, H. M. & LUCAS, D. 2008. Validation of CFD models for mono- and polydisperse air-water two-phase flows in pipes. *Nuclear Engineering and Design,* 238**,** 647-659.

FU, X. Y. & ISHII, M. 2003a. Two-group interfacial area transport in vertical air-water flow I. Mechanistic model. *Nuclear Engineering and Design,* 219**,** 143-168.

FU, X. Y. & ISHII, M. 2003b. Two-group interfacial area transport in vertical air-water flow II. Model evaluation. *Nuclear Engineering and Design,* 219**,** 169-190.

GRACE, J. R., CLIFT, R. & WEBER, M. E. 1978. *Bubbles, Drops, and Particles*, Academic Press.

GUEDON, G. R., BESAGNI, G. & INZOLI, F. 2017. Prediction of gas-liquid flow in an annular gap bubble column using a bi-dispersed Eulerian model. *Chemical Engineering Science,* 161**,** 138-150.

GUPTA, A. & ROY, S. 2013. Euler-Euler simulation of bubbly flow in a rectangular bubble column: Experimental validation with Radioactive Particle Tracking. *Chemical Engineering Journal,* 225**,** 818-836.

HAGESAETHER, L., JAKOBSEN, H. A. & SVENDSEN, H. F. 2002. A model for turbulent binary breakup of dispersed fluid particles. *Chemical Engineering Science,* 57**,** 3251-3267.

HARLOW, F. H. 1988. PIC and its progeny. *Computer Physics Communications,* 48.

HARLOW, F. H. & WELCH, J. E. 1965. Numerical calculation of time-dependent viscous incompressible flow of fluid with free surface. *The Physics of Fluids,* 8**,** 2182-2189.

HIBIKI, T., HOGSETT, S. & ISHII, M. 1998. Local measurement of interfacial area, interfacial velocity and liquid turbulence in two-phase flow. *Nuclear Engineering and Design,* 184**,** 287-304.

HILLS, J. H. 1974. Radial Nonuniformity of Velocity and Voidage in a Bubble Column. *Transactions of the Institution of Chemical Engineers,* 52**,** 1-9.

HIRT, C. W. & NICHOLS, B. D. 1981. Volume of fluid (VOF) method for the dynamics of free boundaries. *Journal of Computational Physics,* 39**,** 201-225.

HOUNSLOW, M. J., RYALL, R. L. & MARSHALL, V. R. 1988. A Discretized Population Balance for Nucleation, Growth, and Aggregation. *Aiche Journal,* 34**,** 1821-1832.

HUBERS, J. L., STRIEGEL, A. C., HEINDEL, T. J., GRAY, J. N. & JENSEN, T. C. 2005. X-ray computed tomography in large bubble columns. *Chemical Engineering Science,* 60**,** 6124-6133.

ISHII, M., PARANJAPE, S. S., KIM, S. & SUN, X. 2004. Interfacial structures and interfacial area transport in downward two-phase bubbly flow. *International Journal of Multiphase Flow,* 30**,** 779-801.

ISHII, M. & ZUBER, N. 1979. Drag Coefficient and Relative Velocity in Bubbly, Droplet or Particulate Flows. *Aiche Journal,* 25**,** 843-855.

ISMAIL, I., SHAFQUET, A. & KARSITI, M. N. Application of electrical capacitance tomography and differential pressure measurement in an air-water bubble column for online analysis of void fraction. 2011 Fourth International Conference on Modeling, Simulation and Applied Optimization, 19-21 April 2011 2011. 1-6.

JAKOBSEN, H. A. 2014. The Population Balance Equation. *Chemical Reactor Modeling: Multiphase Reactive Flows.* Cham: Springer International Publishing.

JAKOBSEN, H. A., LINDBORG, H. & DORAO, C. A. 2005. Modeling of bubble column reactors: Progress and limitations. *Industrial & Engineering Chemistry Research,* 44**,** 5107-5151.

JIN, H., WANG, M. & WILLIAMS, R. A. 2007. Analysis of bubble behaviors in bubble columns using electrical resistance tomography. *Chemical Engineering Journal,* 130**,** 179-185.

JIN, H. B., YANG, S. H., HE, G. X., GUO, Z. W. & TONG, Z. M. 2005. An experimental study of holdups in large-scale p-xylene oxidation reactors using the gamma-ray attenuation approach. *Chemical Engineering Science,* 60**,** 5955-5961.

JOSHI, J. B. 2001. Computational flow modelling and design of bubble column reactors. *Chemical Engineering Science,* 56**,** 5893-5933.

KEMOUN, A., ONG, B. C., GUPTA, P., AL-DAHHAN, M. H. & DUDUKOVIC, M. P. 2001. Gas holdup in bubble columns at elevated pressure via computed tomography. *International Journal of Multiphase Flow,* 27**,** 929-946.

KHAN, I., WANG, M., ZHANG, Y., TIAN, W., SU, G. & QIU, S. 2020. Two-phase bubbly flow simulation using CFD method: A review of models for interfacial forces. *Progress in Nuclear Energy,* 125.

KOLMOGOROV, A. N. 1991. The Local-Structure of Turbulence in Incompressible Viscous-Fluid for Very Large Reynolds-Numbers. *Proceedings of the Royal Society of London Series a-Mathematical Physical and Engineering Sciences,* 434**,** 9-13.

KRISHNA, R. & BATEN, J. M. V. 1999. Simulating the motion of gas bubbles in a liquid. *Nature,* 398**,** 208.

KRISHNA, R. & ELLENBERGER, J. 1996. Gas holdup in bubble column reactors operating in the churn-turbulent flow regime. *Aiche Journal,* 42**,** 2627-2634.

KRISHNA, R. & SIE, S. T. 2000. Design and scale-up of the Fischer-Tropsch bubble column slurry reactor. *Fuel Processing Technology,* 64**,** 73-105.

KRISHNA, R., URSEANU, M. I., VAN BATEN, J. M. & ELLENBERGER, J. 1999. Influence of scale on the hydrodynamics of bubble columns operating in the churn-turbulent regime: experiments vs. Eulerian simulations. *Chemical Engineering Science,* 54**,** 4903-4911.

KRISHNA, R. & VAN BATEN, J. M. 1999. Simulating the motion of gas bubbles in a liquid. *Nature,* 398**,** 208-208.

KRISHNA, R. & VAN BATEN, J. M. 2001a. Eulerian simulations of bubble columns operating at elevated pressures in the churn turbulent flow regime. *Chemical Engineering Science,* 56**,** 6249-6258.

KRISHNA, R. & VAN BATEN, J. M. 2001b. Scaling up bubble column reactors with the aid of CFD. *Chemical Engineering Research & Design,* 79**,** 283-309.

KULKARNI, A. A. & JOSHI, J. B. 2005. Bubble formation and bubble rise velocity in gas-liquid systems: A review. *Industrial & Engineering Chemistry Research,* 44**,** 5873-5931.

KUMAR, S. & RAMKRISHNA, D. 1996. On the solution of population balance equations by discretization .1. A fixed pivot technique. *Chemical Engineering Science,* 51**,** 1311-1332.

KUMAR, S. B., MOSLEMIAN, D. & DUDUKOVIC, M. P. 1997. Gas-holdup measurements in bubble columns using computed tomography. *Aiche Journal,* 43**,** 1414-1425.

LAIN, S. & SOMMERFELD, M. 2003. Turbulence modulation in dispersed two-phase flow laden with solids from a Lagrangian perspective. *International Journal of Heat and Fluid Flow,* 24**,** 616-625.

LANCE, M. & BATAILLE, J. 1991. Turbulence in the liquid phase of a uniform bubbly air–water flow. *Journal of Fluid Mechanics,* 222**,** 95-118.

LEE, D. J., LUO, X. & FAN, L. S. 1999. Gas disengagement technique in a slurry bubble column operated in the coalesced bubble regime. *Chemical Engineering Science,* 54**,** 2227-2236.

LEHR, F. & MEWES, D. 2001. A transport equation for the interfacial area density applied to bubble columns. *Chemical Engineering Science,* 56**,** 1159-1166.

LEHR, F., MILLIES, M. & MEWES, D. 2002. Bubble-size distributions and flow fields in bubble columns. *Aiche Journal,* 48**,** 2426-2443.

LIAO, Y., MA, T., KREPPER, E., LUCAS, D. & FRÖHLICH, J. 2019. Application of a novel model for bubble-induced turbulence to bubbly flows in containers and vertical pipes. *Chemical Engineering Science,* 202**,** 55-69.

LIAO, Y. X., RZEHAK, R., LUCAS, D. & KREPPER, E. 2015. Baseline closure model for dispersed bubbly flow: Bubble coalescence and breakup. *Chemical Engineering Science,* 122**,** 336-349.

LISTER, J. D., SMIT, D. J. & HOUNSLOW, M. J. 2004. Adjustable discretized population balance for growth and aggregation. *AIChE Journal,* 41**,** 591-603.

LIU, Y. F. & HINRICHSEN, O. 2014. Study on CFD-PBM turbulence closures based on k-epsilon and Reynolds stress models for heterogeneous bubble column flows. *Computers & Fluids,* 105**,** 91-100.

LIU, Z. Q. & LI, B. K. 2018. Scale-adaptive analysis of Euler-Euler large eddy simulation for laboratory scale dispersed bubbly flows. *Chemical Engineering Journal,* 338**,** 465-477.

LOPEZ DE BERTODANO, M. 1992. *Turbulent bubbly two-phase flow in a triangular duct.* Ph.D. thesis, Rensselaer Polytechnic Institute, Troy, New York.

LUO, H. 1993. *Coalescence, Breakup and Liuqid Circulation in Bubble Column Reactors.* PhD thesis PhD thesis, PhD thesis from the Norwegian Institute of Technology.

LUO, H. & SVENDSEN, H. F. 1996. Theoretical model for drop and bubble breakup in turbulent dispersions. *Aiche Journal,* 42**,** 1225-1233.

LUO, X. K., LEE, D. J., LAU, R., YANG, G. Q. & FAN, L. S. 1999. Maximum stable bubble size and gas holdup in high-pressure slurry bubble columns. *Aiche Journal,* 45**,** 665-680.

MA, T., ZIEGENHEIN, T., LUCAS, D. & FROHLICH, J. 2016. Large eddy simulations of the gas-liquid flow in a rectangular bubble column. *Nuclear Engineering and Design,* 299**,** 146-153.

MANJREKAR, O. N. & DUDUKOVIC, M. P. 2015. Application of a 4-point optical probe to a Slurry Bubble Column Reactor. *Chemical Engineering Science,* 131**,** 313-322.

MANJREKAR, O. N., SUN, Y. J., HE, L., TANG, Y. J. & DUDUKOVIC, M. P. 2017. Hydrodynamics and mass transfer coefficients in a bubble column photo-bioreactor. *Chemical Engineering Science,* 168**,** 55-66.

MARCHISIO, D. L., VIGIL, R. D. & FOX, R. O. 2003. Quadrature method of moments for aggregation-breakage processes. *Journal of Colloid and Interface Science,* 258**,** 322-334.

MAZZITELLI, I. M. & LOHSE, D. 2009. Evolution of energy in flow driven by rising bubbles. *Physical Review E,* 79**,** 066317.

MENDELSON HARVEY, D. 1967. The prediction of bubble terminal velocities from wave theory. *AIChE Journal,* 13**,** 250-253.

MENDEZ-DIAZ, S., C. SERRANO-GARCÍA, J., ZENIT, R. & HERNÁNDEZ-CORDERO, J. 2013. Power spectral distributions of pseudo-turbulent bubbly flows. *Physics of Fluids,* 25.

MENZEL, T., WEIDE, T. I. D., STAUDACHER, O., WEIN, O. & ONKEN, U. 1990. Reynolds Shear-Stress for Modeling of Bubble Column Reactors. *Industrial & Engineering Chemistry Research,* 29**,** 988-994.

MERCADO, J. M., GOMEZ, D. C., VAN GILS, D., SUN, C. & LOHSE, D. 2010. On bubble clustering and energy spectra in pseudo-turbulence. *Journal of Fluid Mechanics,* 650**,** 287-306.

METRAILLER, D., REBOUX, S. & LAKEHAL, D. 2017. Near-wall turbulence-bubbles interactions in a channel flow at Re-tau=400: A DNS investigation. *Nuclear Engineering and Design,* 321**,** 180-189.

MUDDE, R. F., GROEN, J. S. & VANDENAKKER, H. E. A. 1997. Liquid velocity field in a bubble column: LDA experiments. *Chemical Engineering Science,* 52**,** 4217-4224.

MUDDE, R. F. & SIMONIN, O. 1999. Two- and three-dimensional simulations of a bubble plume using a two-fluid model. *Chemical Engineering Science,* 54**,** 5061-5069.

MUKIN, R. V. 2014. Modeling of bubble coalescence and break-up in turbulent bubbly flow. *International Journal of Multiphase Flow,* 62**,** 52-66.

MUNIZ, M. & SOMMERFELD, M. 2020. On the force competition in bubble columns: A numerical study. *International Journal of Multiphase Flow,* 128.

MURAI, Y., KITAGAWA, A., SONG, X. Q., OHTA, J. & YAMAMOTO, F. 2000. Inverse energy cascade structure of turbulence in a bubbly flow (Numerical analysis using Eulerian-Lagrangian model equations). *Jsme International Journal Series B-Fluids and Thermal Engineering,* 43**,** 197-205.

NICENO, B., DHOTRE, M. T. & DEEN, N. G. 2008. One-equation sub-grid scale (SGS) modelling for Euler-Euler large eddy simulation (EELES) of dispersed bubbly flow. *Chemical Engineering Science,* 63**,** 3923-3931.

OEY, R. S., MUDDE, R. F. & VAN DEN AKKER, H. E. A. 2003. Sensitivity study on interfacial closure laws in two-fluid bubbly flow simulations. *Aiche Journal,* 49**,** 1621-1636.

OLMOS, E., GENTRIC, C., VIAL, C., WILD, G. & MIDOUX, N. 2001. Numerical simulation of multiphase flow in bubble column reactors. Influence of bubble coalescence and break-up. *Chemical Engineering Science,* 56**,** 6359-6365.

PAREKH, J. & RZEHAK, R. 2018. Euler-Euler multiphase CFD-simulation with full Reynolds stress model and anisotropic bubble-induced turbulence. *International Journal of Multiphase Flow,* 99**,** 231-245.

PATEL, A. K. & THORAT, B. N. 2008. Gamma ray tomography - An experimental analysis of fractional gas hold-up in bubble columns. *Chemical Engineering Journal,* 137**,** 376-385.

PFLEGER, D. & BECKER, S. 2001. Modelling and simulation of the dynamic flow behaviour in a bubble column. *Chemical Engineering Science,* 56**,** 1737-1747.

POELMA, C., WESTERWEEL, J. & OOMS, G. 2007. Particle-fluid interactions in grid-generated turbulence. *Journal of Fluid Mechanics,* 589**,** 315-351.

PRAKASH, V. N., MARTÍNEZ MERCADO, J., VAN WIJNGAARDEN, L., MANCILLA, E., TAGAWA, Y., LOHSE, D. & SUN, C. 2016. Energy spectra in turbulent bubbly flows. *Journal of Fluid Mechanics,* 791**,** 174-190.

PRINCE, M. J. & BLANCH, H. W. 1990. Bubble Coalescence and Break-up in Air-Sparged Bubble-Columns. *Aiche Journal,* 36**,** 1485-1499.

RAMPURE, M. R., KULKARNI, A. A. & RANADE, V. V. 2007. Hydrodynamics of bubble column reactors at high gas velocity: Experiments and computational fluid dynamics (CFD) Simulations. *Industrial & Engineering Chemistry Research,* 46**,** 8431-8447.

RANADE, V. V. & TAYALIA, Y. 2001. Modelling of fluid dynamics and mixing in shallow bubble column reactors: influence of sparger design. *Chemical Engineering Science,* 56**,** 1667-1675.

REICHARDT, T. & SOMMERFELD, M. Stereoscopic Imaging for Analysing Bubble Oscillation in Turbulence. 14th International Symposium Application of Laser Techniques to Fluid Mechanics, 2008 Lisbon.

REILLY, I. G., SCOTT, D. S., DEBRUIJN, T. J. W. & MACINTYRE, D. 1994. The Role of Gas-Phase Momentum in Determining Gas Holdup and Hydrodynamic Flow Regimes in Bubble-Column Operations. *Canadian Journal of Chemical Engineering,* 72**,** 3-12.

RENSEN, J., LUTHER, S. & LOHSE, D. 2005. The effect of bubbles on developed turbulence. *Journal of Fluid Mechanics,* 538**,** 153-187.

RIBOUX, G., LEGENDRE, D. & RISSO, F. 2013. A model of bubble-induced turbulence based on large-scale wake interactions. *Journal of Fluid Mechanics,* 719**,** 362-387.

RISSO, F. 2011a. Theoretical model for k−3 spectra in dispersed multiphase flows. *Physics of Fluids,* 23**,** 95.

RISSO, F. 2011b. Theoretical model for k(-3) spectra in dispersed multiphase flows. *Physics of Fluids,* 23.

ROGHAIR, I., MERCADO, J. M., ANNALAND, M. V., KUIPERS, H., SUN, C. & LOHSE, D. 2011. Energy spectra and bubble velocity distributions in pseudo-turbulence: Numerical simulations vs. experiments. *International Journal of Multiphase Flow,* 37**,** 1093-1098.

RUZICKA, M. C., DRAHOS, J., FIALOVA, M. & THOMAS, N. H. 2001. Effect of bubble column dimensions on flow regime transition. *Chemical Engineering Science,* 56**,** 6117-6124.

RUZICKA, M. C., DRAHOS, J., MENA, P. C. & TEIXEIRA, J. A. 2003. Effect of viscosity on homogeneous-heterogeneous flow regime transition in bubble columns. *Chemical Engineering Journal,* 96**,** 15-22.

RUZICKA, M. C., VECER, M. M., ORVALHO, S. & DRAHOS, J. 2008. Effect of surfactant on homogeneous regime stability in bubble column. *Chemical Engineering Science,* 63**,** 951-967.

RZEHAK, R. & KREPPER, E. 2013. CFD modeling of bubble-induced turbulence. *International Journal of Multiphase Flow,* 55**,** 138-155.

SATO, Y. & SEKOGUCHI, K. 1975. Liquid velocity distribution in two-phase bubble flow. *International Journal of Multiphase Flow,* 2**,** 79-95.

SCHILLER, L. & NAUMANN, A. 1935. A drag coefficient correlation. *Z. Ver. Deutsch. Ing,* 77**,** 318-320.

SCHLEGEL, J. P., HIBIKI, T. & ISHII, M. 2015. Two-group modeling of interfacial area transport in large diameter channels. *Nuclear Engineering and Design,* 293**,** 75-86.

SCHMIDT, D. & VELTEN, K. 2016. Numerical simulation of bubble flow homogenization in industrial scale wine fermentations. *Food and Bioproducts Processing,* 100**,** 102-117.

SHAH, Y. T., KELKAR, B. G., GODBOLE, S. P. & DECKWER, W. D. 1982. Design Parameters Estimations for Bubble Column Reactors. *Aiche Journal,* 28**,** 353-379.

SHINNAR, R. & CHURCH, J. M. 1960. Statistical Theories of Turbulence In ... Predicting Particle Size in Agitated Dispersions. *Industrial and Engineering Chemistry,* 52**,** 253-256.

SHU, S., EL BAHRAOUI, N., BERTRAND, F. & CHAOUKI, J. 2020. A bubble-induced turbulence model for gas-liquid bubbly flows in airlift columns, pipes and bubble columns. *Chemical Engineering Science,* 227**,** 115945.

SILVA, M. K., D'AVILA, M. A. & MORI, M. 2012. Study of the interfacial forces and turbulence models in a bubble column. *Computers & Chemical Engineering,* 44**,** 34-44.

SMITH, J. S., VALSARAJ, K. T. & THIBODEAUX, L. J. 1996. Bubble column reactors for wastewater treatment .1. Theory and modeling of continuous countercurrent solvent sublation. *Industrial & Engineering Chemistry Research,* 35**,** 1688-1699.

SOKOLICHIN, A., EIGENBERGER, G. & LAPIN, A. 2004. Simulation of buoyancy driven bubbly flow: Established simplifications and open questions. *AIChE Journal,* 50**,** 24-45.

SOKOLICHIN, A., EIGENBERGER, G., LAPIN, A. & LUBBERT, A. 1997. Dynamic numerical simulation of gas-liquid two-phase flows - Euler/Euler versus Euler/Lagrange. *Chemical Engineering Science,* 52**,** 611-626.

SOMMERFELD, M. & BRODER, D. 2009. Analysis of Hydrodynamics and Microstructure in a Bubble Column by Planar Shadow Image

Velocimetry. *Industrial & Engineering Chemistry Research,* 48**,** 330-340.

SUN, X. D., KIM, S., ISHII, M. & BEUS, S. G. 2004. Modeling of bubble coalescence and disintegration in confined upward two-phase flow. *Nuclear Engineering and Design,* 230**,** 3-26.

TABIB, M. V., ROY, S. A. & JOSHI, J. B. 2008. CFD simulation of bubble column - An analysis of interphase forces and turbulence models. *Chemical Engineering Journal,* 139**,** 589-614.

THAKRE, S. S. & JOSHI, J. B. 1999. CFD simulation of bubble column reactors: importance of drag force formulation. *Chemical Engineering Science,* 54**,** 5055-5060.

THANG, N. T. & DAVIS, M. R. 1979. Structure of Bubbly Flow through Venturis. *International Journal of Multiphase Flow,* 5**,** 17-37.

THORAT, B. N. & JOSHI, J. B. 2004. Regime transition in bubble columns: experimental and predictions. *Experimental Thermal and Fluid Science,* 28**,** 423-430.

THORAT, B. N., SHEVADE, A. V., BHILEGAONKAR, K. N., AGLAWE, R. H., VEERA, U. P., THAKRE, S. S., PANDIT, A. B., SAWANT, S. B. & JOSHI, J. B. 1998. Effect of sparger design and height to diameter ratio on fractional gas hold-up in bubble columns. *Chemical Engineering Research & Design,* 76**,** 823-834.

TOMIYAMA, A. 1998. Struggle with computational bubble dynamics. *Multiphase Science and Technology, Vol 10 Issue 4 1998***,** 369-405.

TOMIYAMA, A. 2004. *Drag, lift and virtual mass forces acting on a single bubble*.

TOMIYAMA, A., SOU, A., ZUN, I., KANAMI, N. & SAKAGUCHI, T. 1995. Effects of Eötvös Number and Dimensionless Liquid Volumetric Flux on Lateral Motion of a Bubble in a Laminar Duct Flow A2 - Serizawa, Akimi. *In:* FUKANO, T. & BATAILLE, J. (eds.) *Multiphase Flow 1995.* Amsterdam: Elsevier.

TOYE, D., FRANSOLET, E., SIMON, D., CRINE, M., L'HOMME, G. & MARCHOT, P. 2005. Possibilities and limits of application of electrical resistance tomography in hydrodynamics of bubble columns. *Canadian Journal of Chemical Engineering,* 83**,** 4-10.

TROSHKO, A. A. & HASSAN, Y. A. 2001. A two-equation turbulence model of turbulent bubbly flows. *International Journal of Multiphase Flow,* 27**,** 1965-2000.

TRYGGVASON, G., BUNNER, B., ESMAEELI, A., JURIC, D., AL-RAWAHI, N., TAUBER, W., HAN, J., NAS, S. & JAN, Y. J. 2001. A front-tracking method for the computations of multiphase flow. *Journal of Computational Physics,* 169**,** 708-759.

TSOURIS, C. & TAVLARIDES, L. L. 1994. Breakage and coalescence models for drops in turbulent dispersions. *AIChE Journal,* 40**,** 395–406.

VAN DEN BERG, T. H. 2006. *The effect of bubbles on developed turbulence.* PhD Thesis, University of Twente, The Netherlands.

VAN DEN HENGEL, E. I. V., DEEN, N. G. & KUIPERS, J. A. M. 2005. Application of coalescence and breakup models in a discrete bubble model for bubble columns. *Industrial & Engineering Chemistry Research,* 44**,** 5233-5245.

VANDU, C. O. & KRISHNA, R. 2004. Influence of scale on the volumetric mass transfer coefficients in bubble columns. *Chemical Engineering and Processing,* 43**,** 575-579.

VEERA, U. P. & JOSHI, J. B. 2000. Measurement of gas hold-up profiles in bubble column by gamma ray tomography - Effect of liquid phase properties. *Chemical Engineering Research & Design,* 78**,** 425-434.

VITANKAR, V. S., DHOTRE, M. T. & JOSHI, J. B. 2002. A low Reynolds number k-epsilon model for the prediction of flow pattern and pressure drop in bubble column reactors. *Chemical Engineering Science,* 57**,** 3235-3250.

WANG, T. F., WANG, J. F. & JIN, Y. 2003. A novel theoretical breakup kernel function for bubbles/droplets in a turbulent flow. *Chemical Engineering Science,* 58**,** 4629-4637.

WANG, T. F., WANG, J. F. & JIN, Y. 2006. A CFD-PBM coupled model for gas-liquid flows. *Aiche Journal,* 52**,** 125-140.

WARSITO, W., MARASHDEH, Q. & FAN, L. S. 2007. Electrical capacitance volume tomography. *Ieee Sensors Journal,* 7**,** 525-535.

WEGENER, P. P. & PARLANGE, J. Y. 1973. Spherical-Cap Bubbles. *Annual Review of Fluid Mechanics,* 5**,** 79-100.

WEGENER, P. P., SUNDELL, R. E. & PARLANGE, J. Y. 1971. Spherical Cap Bubbles Rising in Liquids. *Zeitschrift Fur Flugwissenschaften,* 19**,** 347-&.

WU, Q. & ISHII, M. 1999. Sensitivity study on double-sensor conductivity probe for the measurement of interfacial area concentration in bubbly flow. *International Journal of Multiphase Flow,* 25**,** 155-173.

WU, Q., KIM, S., ISHII, M. & BEUS, S. G. 1998. One-group interfacial area transport in vertical bubbly flow. *International Journal of Heat and Mass Transfer,* 41**,** 1103-1112.

YANG, N. & XIAO, Q. 2017. A mesoscale approach for population balance modeling of bubble size distribution in bubble column reactors. *Chemical Engineering Science,* 170**,** 241-250.

YANG, X., THOMAS, N. H., GUO, L. J. & HOU, Y. 2002. Two-way coupled bubble laden mixing layer. *Chemical Engineering Science,* 57**,** 555-564.

YAO, B. P., ZHENG, C., GASCHE, H. E. & HOFMANN, H. 1991. Bubble Behavior and Flow Structure of Bubble-Columns. *Chemical Engineering and Processing,* 29**,** 65-75.

YAO, W. & MOREL, C. 2004. Volumetric interfacial area prediction in upward bubbly two-phase flow. *International Journal of Heat and Mass Transfer,* 47**,** 307-328.

YOUSSEF, A. A., AL-DAHHAN, M. H. & DUDUKOVIC, M. P. 2013. Bubble Columns with Internals: A Review. *International Journal of Chemical Reactor Engineering,* 11.

ZAHRADNIK, J., FIALOVA, M., KASTANEK, F., GREEN, K. D. & THOMAS, N. H. 1995. The Effect of Electrolytes on Bubble Coalescence and Gas Holdup in Bubble-Column Reactors. *Chemical Engineering Research & Design,* 73**,** 341-346.

ZAHRADNIK, J., FIALOVA, M., RUZICKA, M., DRAHOS, J., KASTANEK, F. & THOMAS, N. H. 1997. Duality of the gas-liquid flow regimes in bubble column reactors. *Chemical Engineering Science,* 52**,** 3811-3826.

ZHANG, D., DEEN, N. G. & KUIPERS, J. A. M. 2006. Numerical simulation of the dynamic flow behavior in a bubble column: A study of closures for turbulence and interface forces. *Chemical Engineering Science,* 61**,** 7593-7608.

ZHANG, D. Z. & PROSPERETTI, A. 1997. Momentum and energy equations for disperse two-phase flows and their closure for dilute suspensions. *International Journal of Multiphase Flow,* 23**,** 425-453.

ZHAO, H. & GE, W. 2007. A theoretical bubble breakup model for slurry beds or three-phase fluidized beds under high pressure. *Chemical Engineering Science,* 62**,** 109-115.

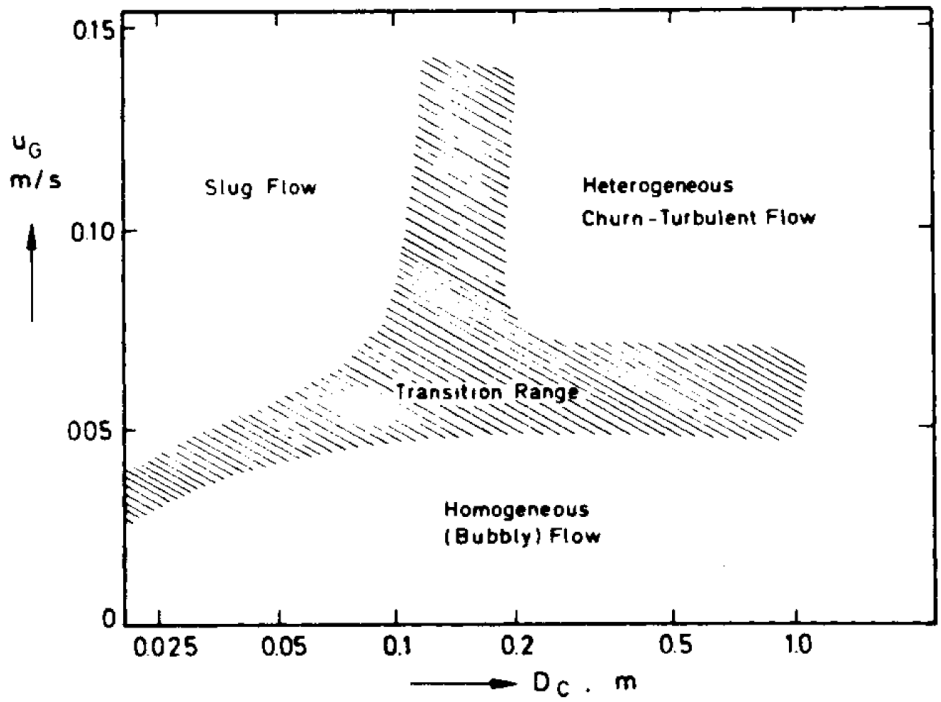

Figure 1- 1 Approximate dependence of flow regime on gas superficial velocity and the bubble column diameter (adapted from Shah et al. (1982))

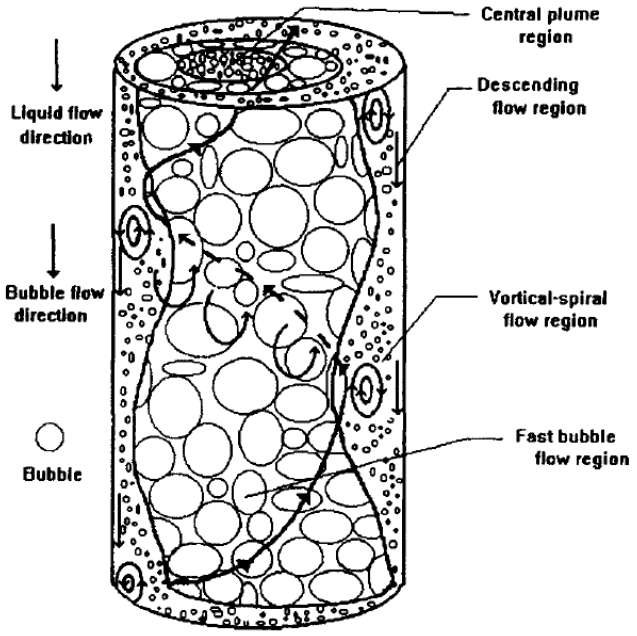

Figure 1- 2 Flow structure in the vortical-spiral flow regime in bubble column (taken from Fan et al. (1994))

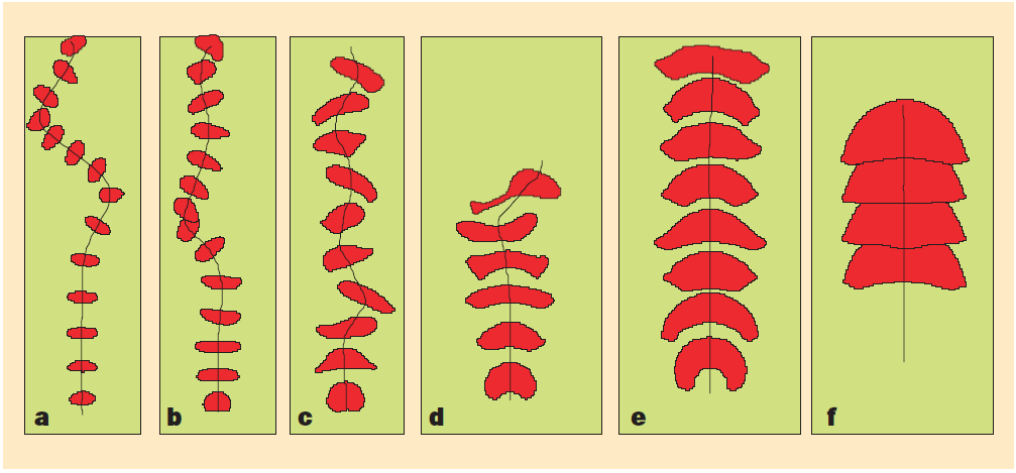

Figure 1- 3 Two-dimensional VOF simulations of the rise trajectories and the interface changes of bubbles (adapted from Krishna and van Baten (1999))

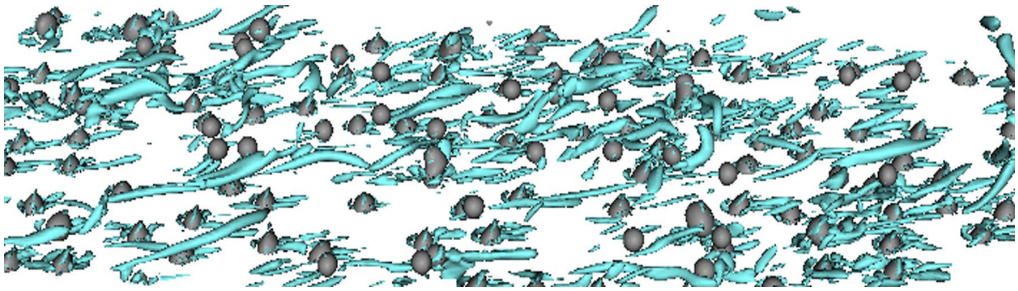

Figure 1- 4 Turbulent coherent structures affected by the bubbles while detaching from the wall (adapted from Metrailler et al. (2017))

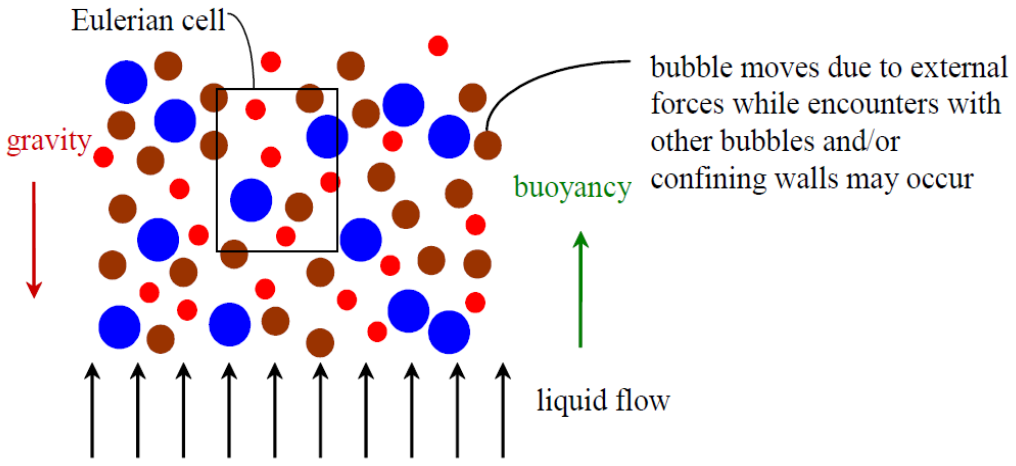

Figure 1- 5 Schematic diagram of Eulerian-Lagrangian method (adapted from Chen (2004))

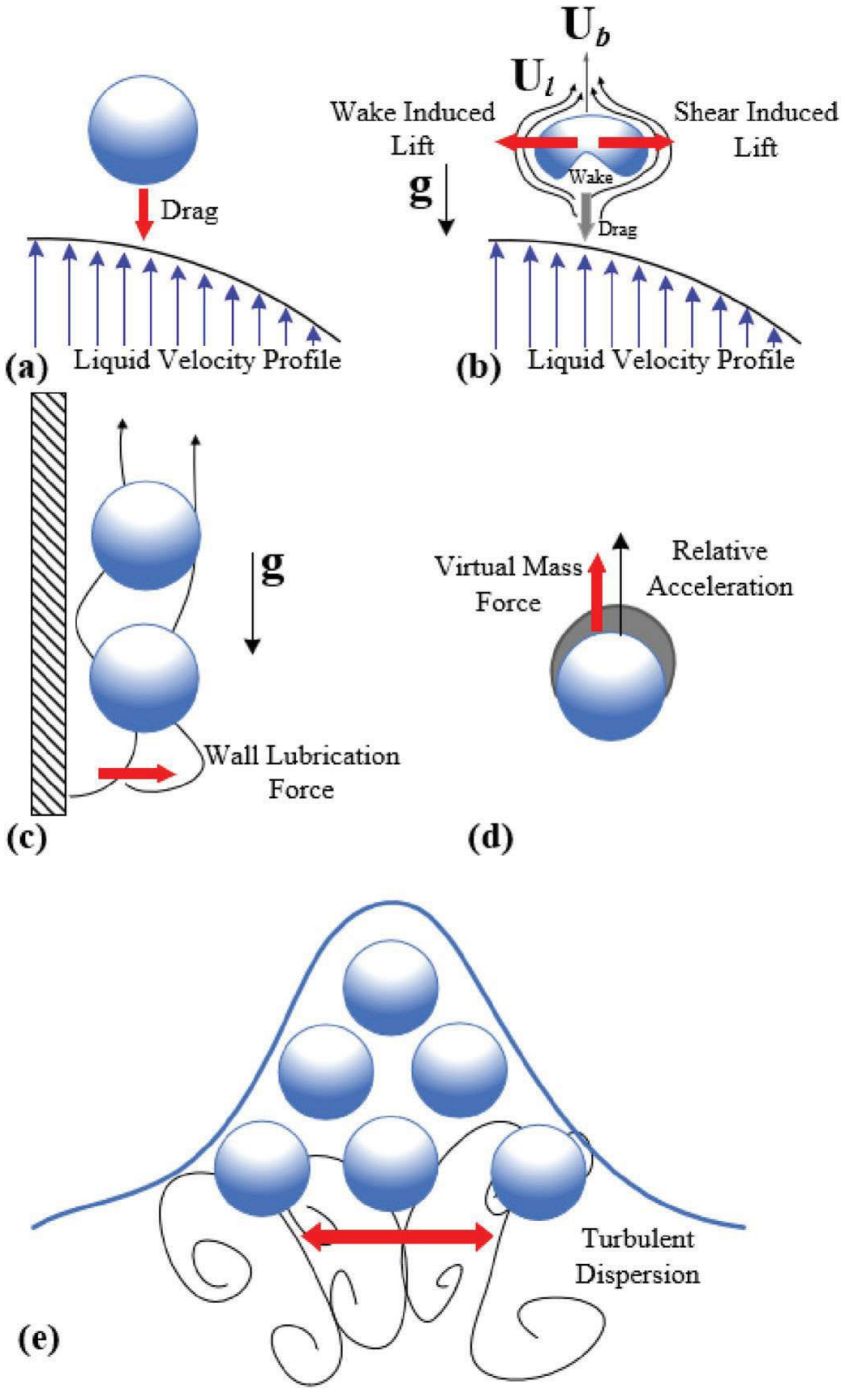

Figure 1- 6 The schematic of various force acting on bubbles in bubble column bubbly flow: (a) drag force; (b) lift force; (c) wall lubrication force; (d) virtual mass force; (d) turbulent dispersion force

(adapted from Khan et al. (2020))

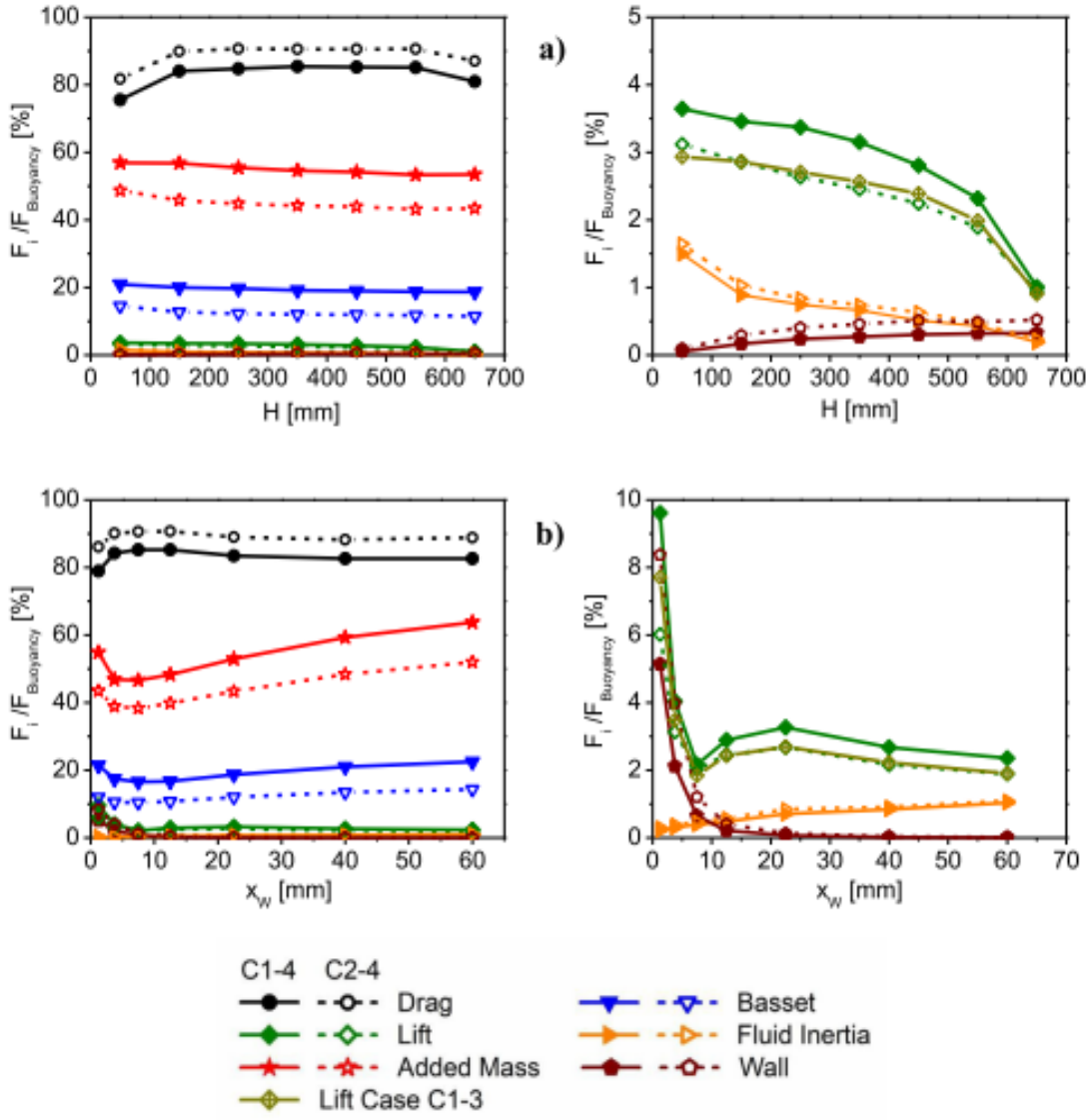

Figure 1- 7 Time-averaged local face ratios for C1-4 (1.26% gas holdup with 2.55mm diameter) C2-4 (1.40% gas holdup with 3.31mm diameter) against a) the height of bubble column; b) wall distance
(adapted from Muniz and Sommerfeld (2020))

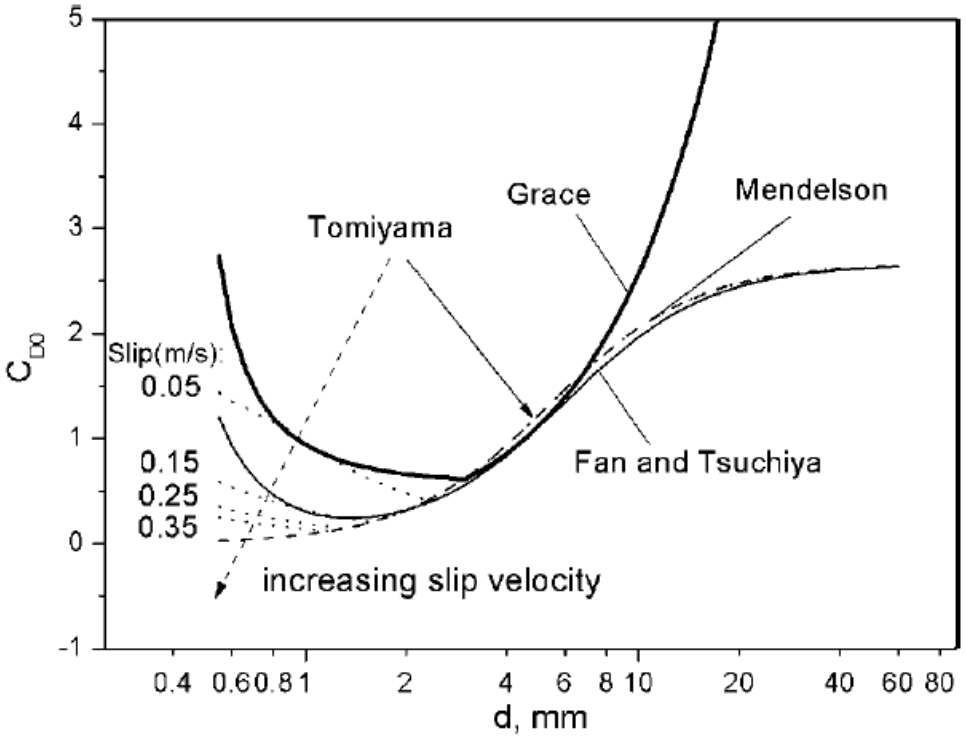

Figure 1- 8 Comparison of different drag coefficient correlations (adapted from Chen et al. (2009))

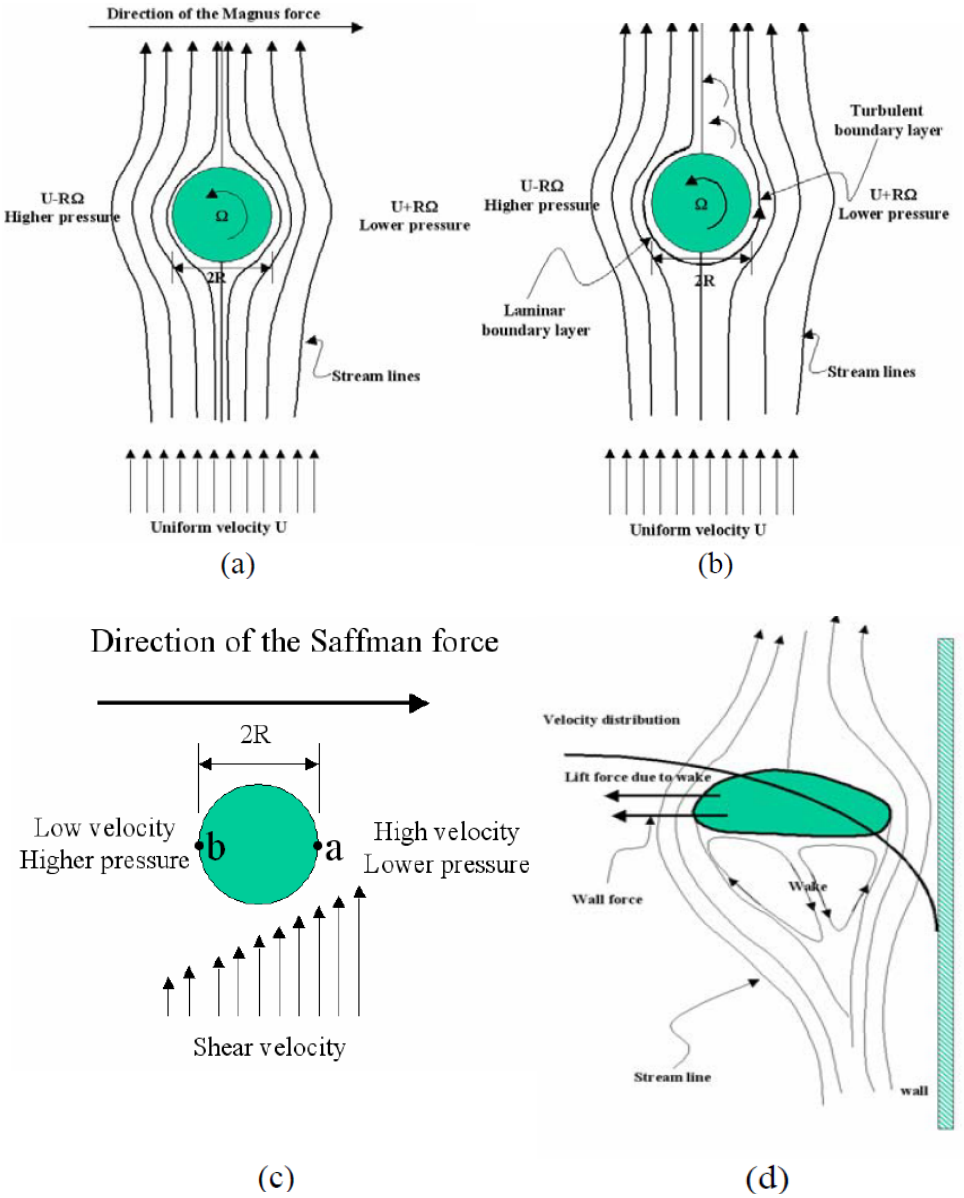

Figure 1- 9 Schematic diagram of lift force: (a) Magnus lift force in uniform flow field; (b) Magnus lift force with laminar boundary layer on one side and turbulent boundary layer on the other side of the bubble; (c) Saffman lift force; (d) lift force due to bubble deformation (U: uniform velocity; R: radius; Ω: rotational speed) (adapted from Chen (2004))

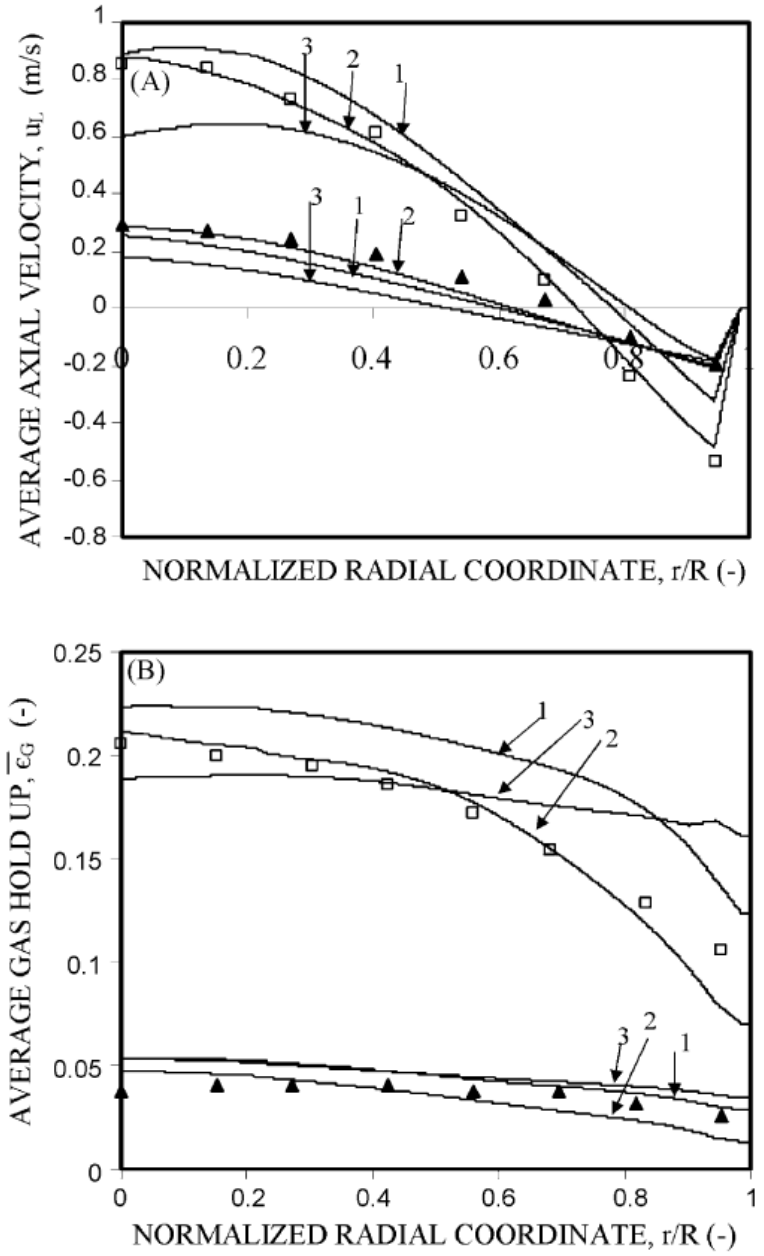

Figure 1- 10 Effect of lift force, (A) average liquid velocity; (B) gas holdup. (▲) Experimental data of Menzel et al. (1990) [U_g = 0.012 m/s], (□) experimental data of Menzel et al. (1990) [U_g = 0.096 m/s]; (1) C_L = 0 (2) C_L: negative value (3) C_L: positive value (adapted from (Tabib et al., 2008))

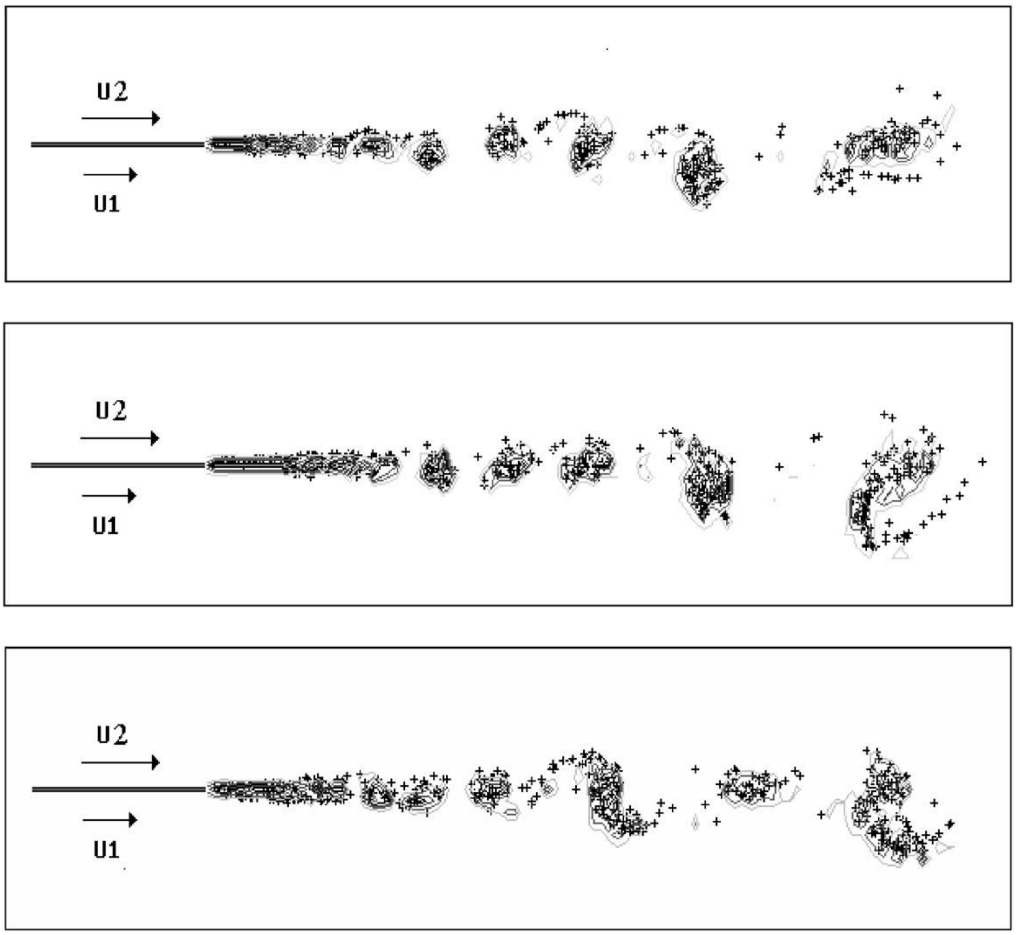

Figure 1- 11 Effect of lift force Instantaneous contours of bubble dispersion and vorticity at *St* = 1:1 and *Fr* = 2:887. "+" denotes the bubble position. From top to bottom: Bubble concentration = 0:08, 0.08 and 0.4 respectively (adapted from Yang et al. (2002))

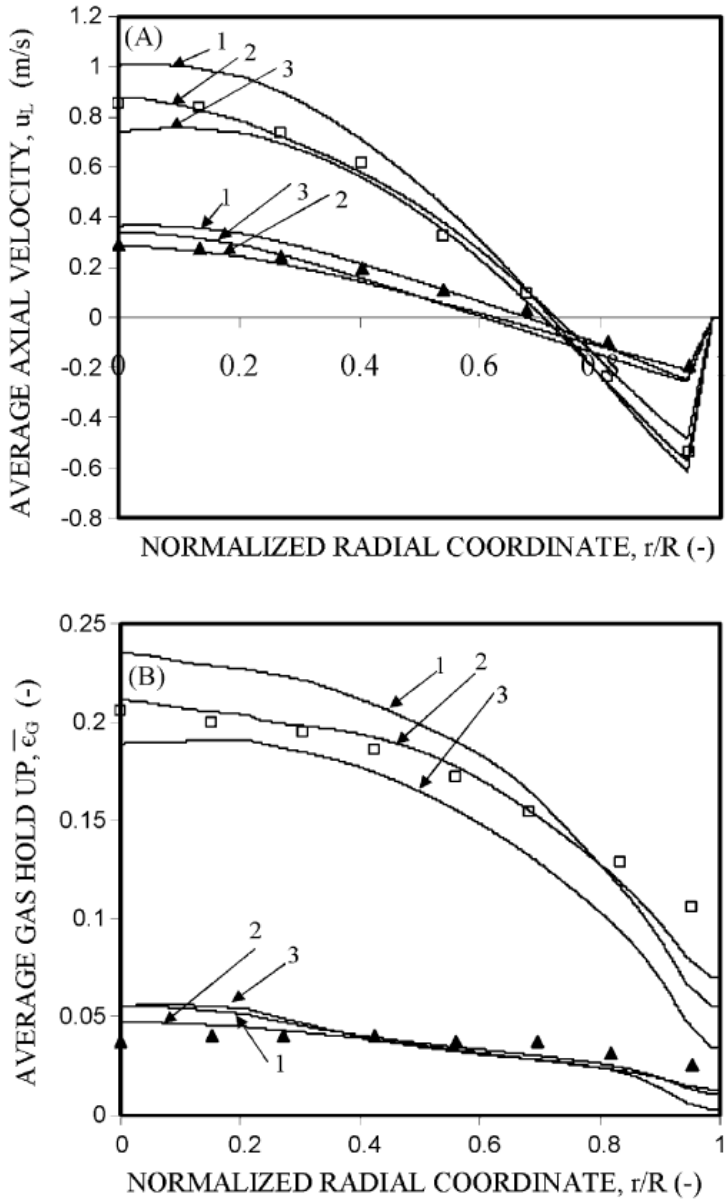

Figure 1- 12 Effect of turbulent dispersion force, (A) average liquid velocity; (b) gas holdup. (▲) Experimental data of Menzel et al. (1990) [U_g = 0.012 m/s], (□) experimental data of Menzel et al. (1990) [U_g = 0.096 m/s]; (1) C_{TD} = 0 (2) C_{TD} = 0.2 (3) C_{TD} = 0.5 (adapted from (Tabib et al., 2008))

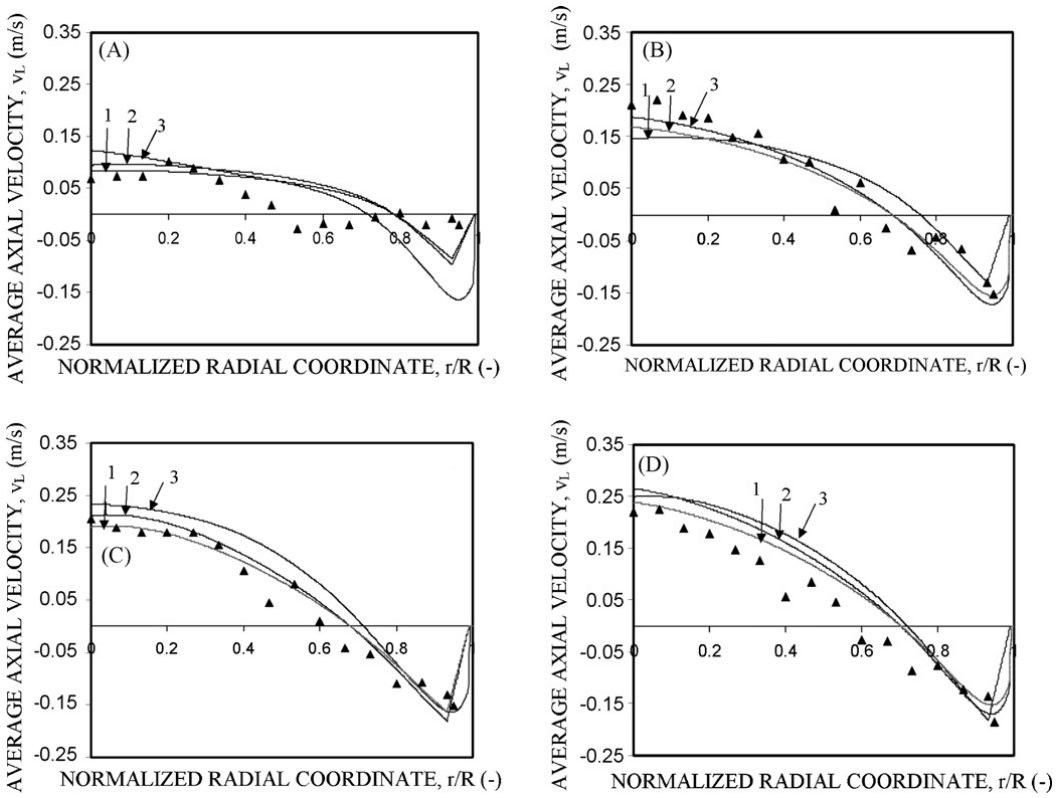

Figure 1- 13 Comparison between the simulated and experimental profiles of axial liquid velocity at different axial positions in a 150mm (i.d.) bubble column with sieve plate sparger at U_g = 20 mm/s (A) H/D= 1; (B) H/D= 2; (C) H/D= 3; (D) H/D=4. (▲) Experimental; (1) LES model; (2) RSM model and (3) k–ε model (adapted from Tabib et al. (2008))

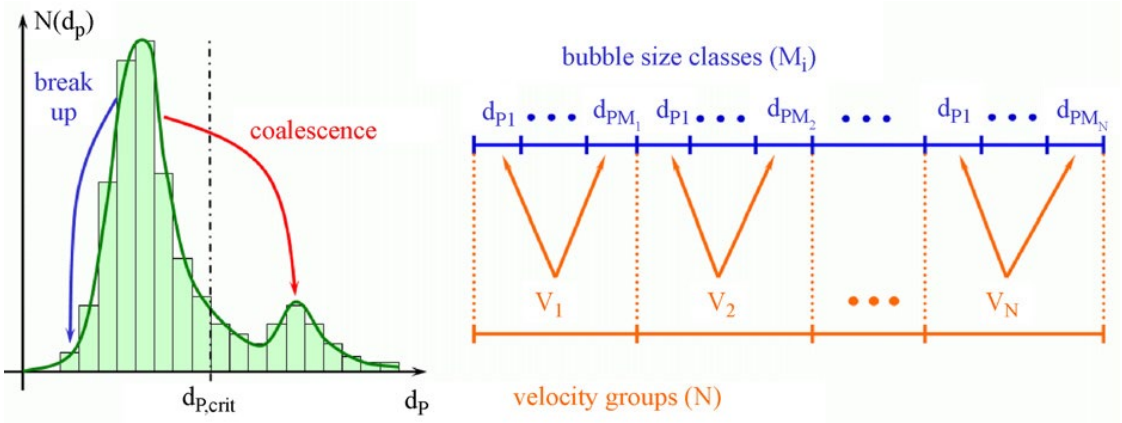

Figure 1- 14 Bubble size classes and velocity groups distribution (adapted from Frank et al. (2008))

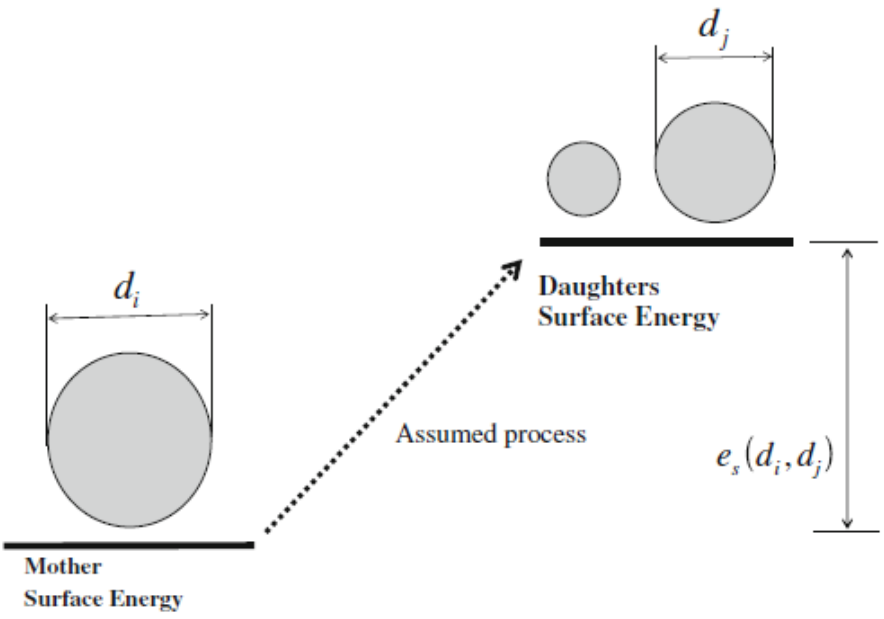

Figure 1- 15 A Sketch of the Surface Energy Balance during Bubble Breakage (adapted from Jakobsen (2014))

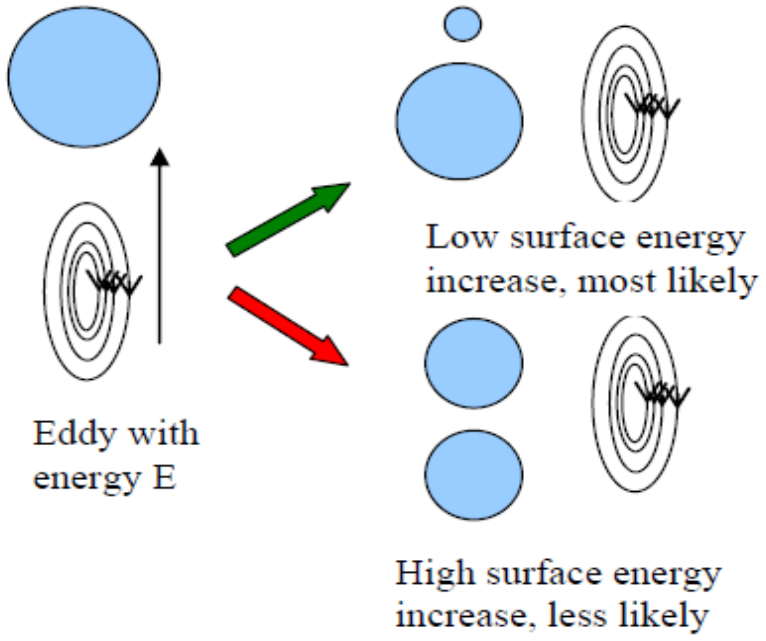

Figure 1- 16 Illustration of the Breakup Model by Luo and Svendsen (1996) (adapted from Chen (2004))

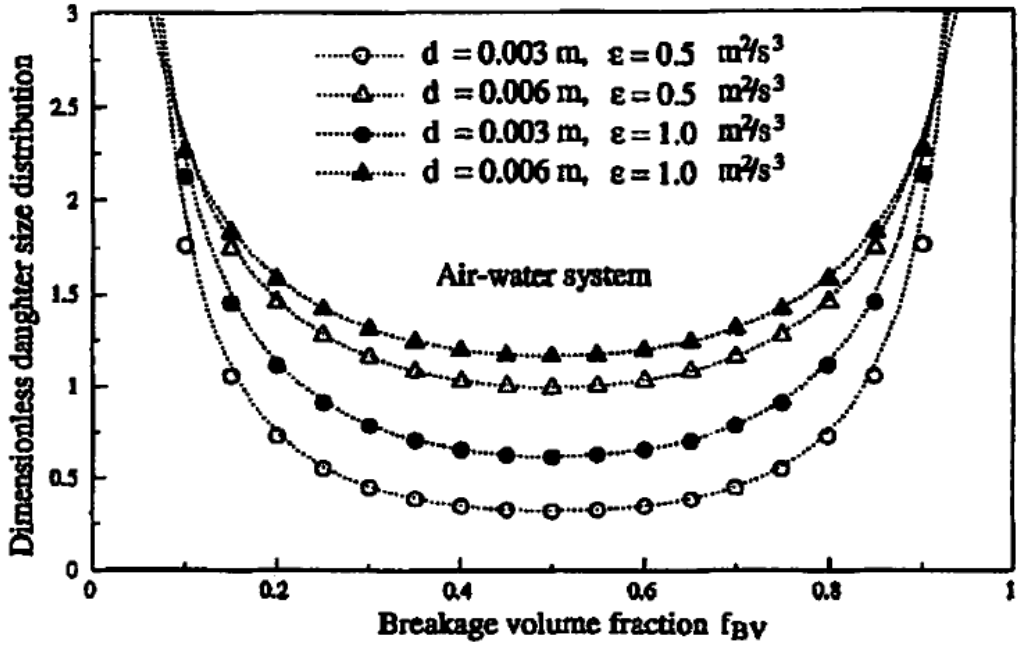

Figure 1- 17 Effect of bubble size and energy dissipation rate per unit mass on the dimensionless daughter bubble sized distribution for the air-water system (adapted from Luo and Svendsen (1996))

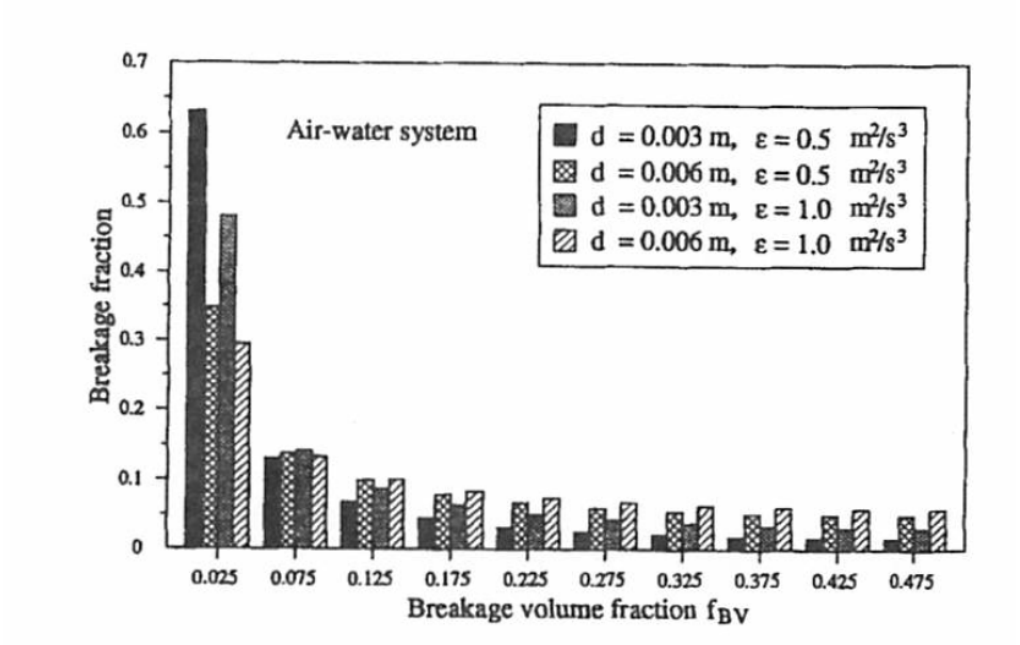

Figure 1- 18 Effect of bubble size and energy dissipation rate per unit mass on the breakage fraction as a function of the breakage volume fraction for the air-water system (adapted from Luo and Svendsen (1996))

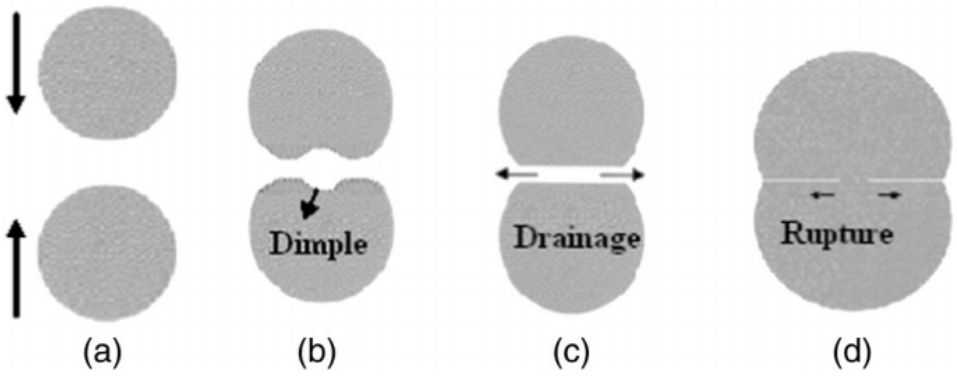

Figure 1- 19 Three consecutive stages of the binary bubble coalescence process under liquid film drainage model (adapted from Firouzi et al. (2015))

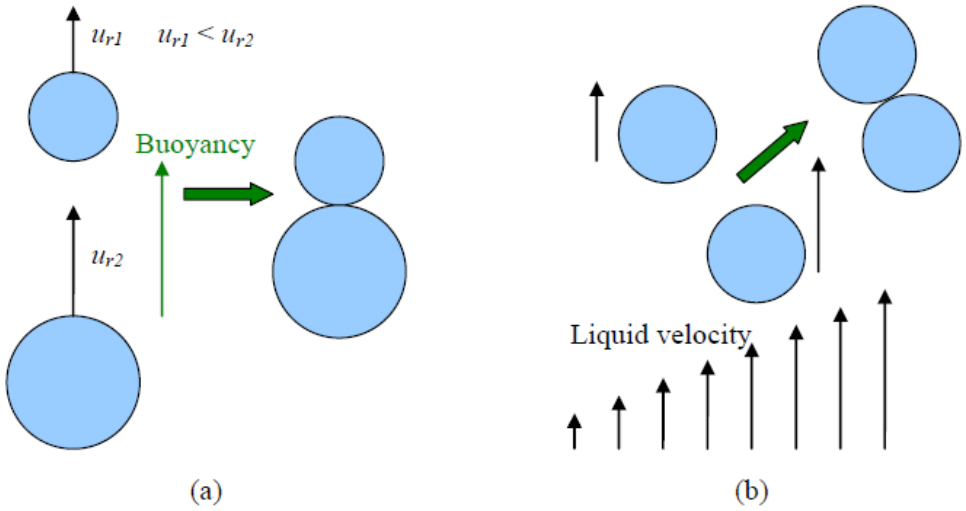

Figure 1- 20 Different driven forces of collision (adapted from Chen (2004))

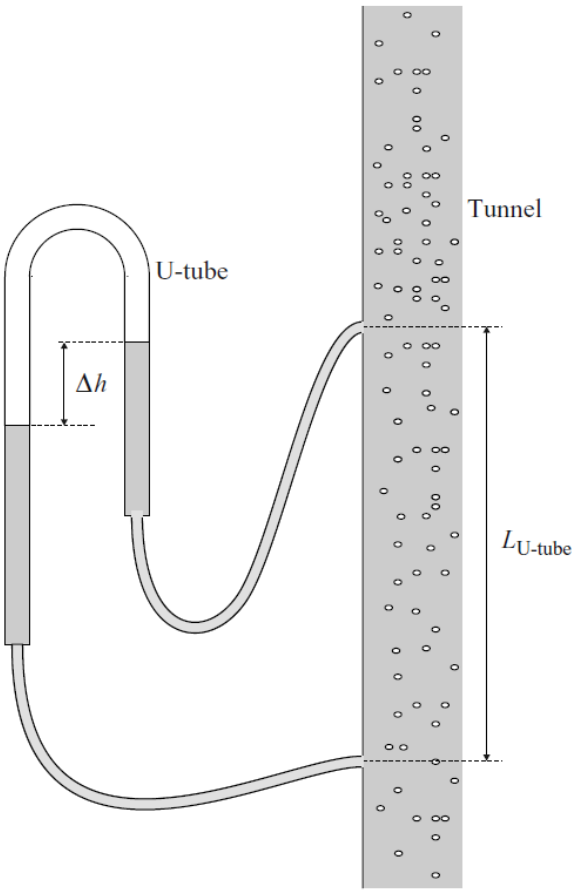

Figure 1- 21 Schematic diagram of using a U-tube to measure the pressure difference of the testing section (taken from Rensen et al. (2005)).

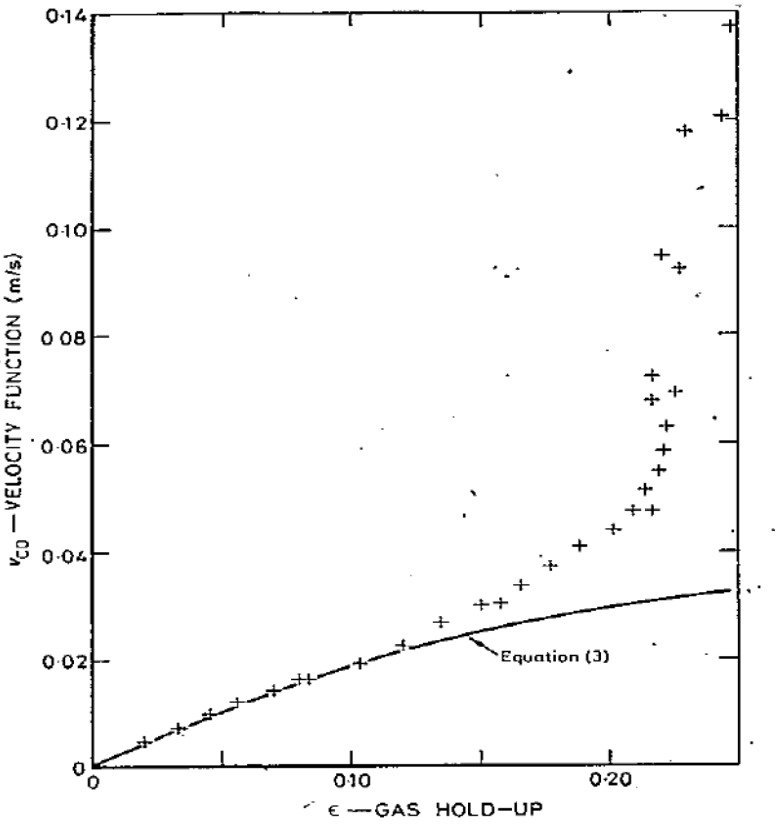

Figure 1- 22 Effect of gas superficial velocity on overall gas holdup (taken from Hills (1974)).

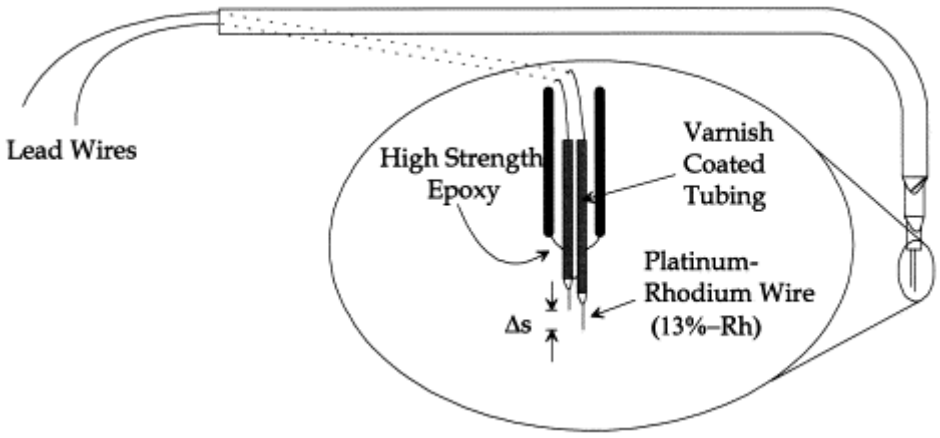

Figure 1- 23 Schematic diagram of a dual-tip conductivity probe (taken from Hibiki et al. (1998)).

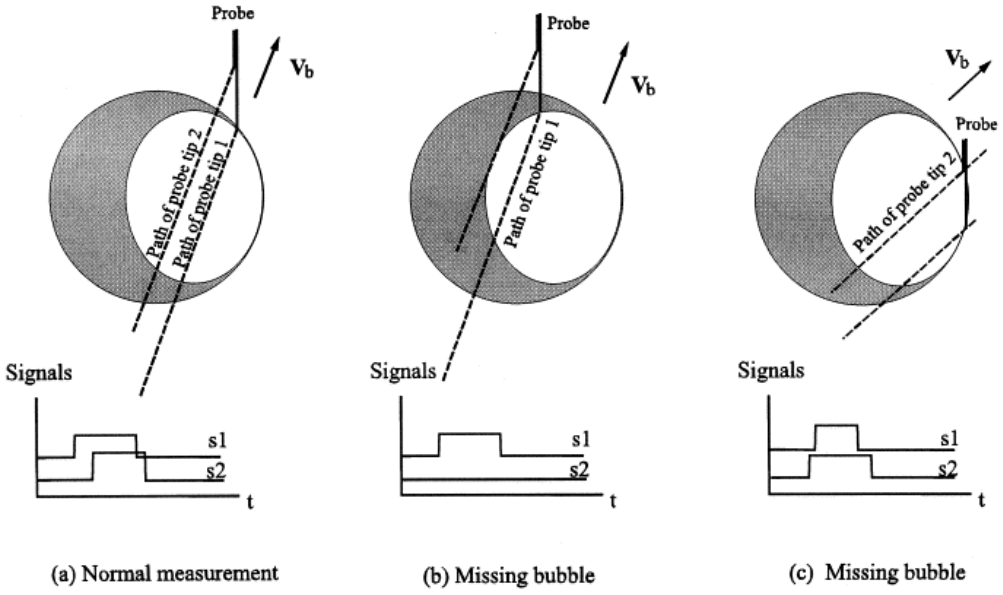

Figure 1- 24 Normal measurement and missing bubble of a dual-tip conductivity probe (taken from Wu and Ishii (1999)).

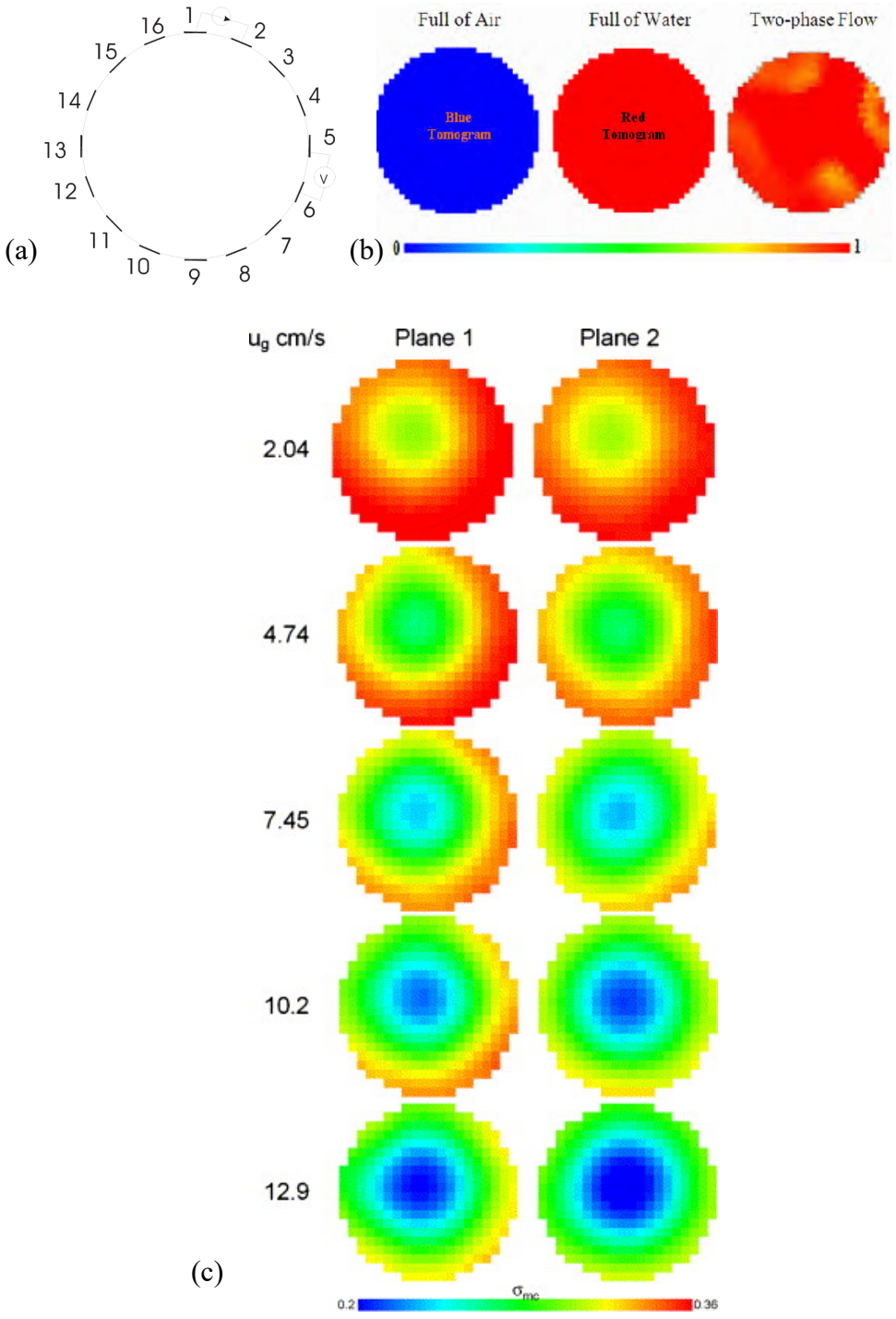

Figure 1- 25 (a) Typical arrangement of 16 electrodes (taken from Toye et al. (2005)); (b) calibration images of air-water system (taken from Ismail et al. (2011)); (c) gas holdup distributions of 2-layer ERT measurements for different superficial velocities (taken from Jin et al. (2007)).

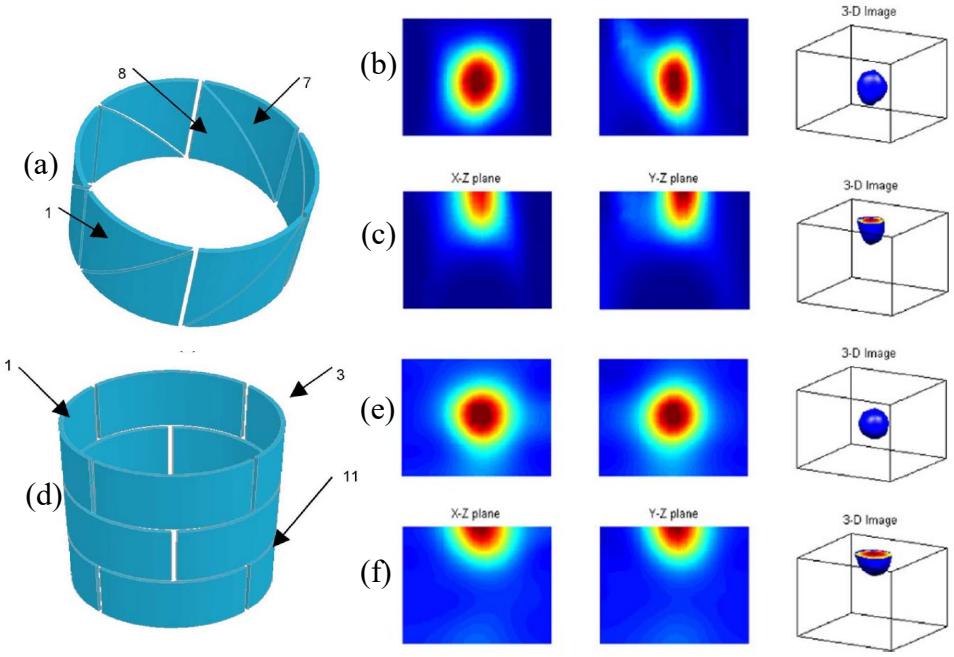

Figure 1- 26 ECVT Sensor designs and reconstruction results of a sphere in the centre of a cubic domain using NN-MOIRT algorithm: (a), (b), (c) single-plane triangular sensor; (d), (e), (f) triple-plane rectangular sensor (taken from Warsito et al. (2007)).

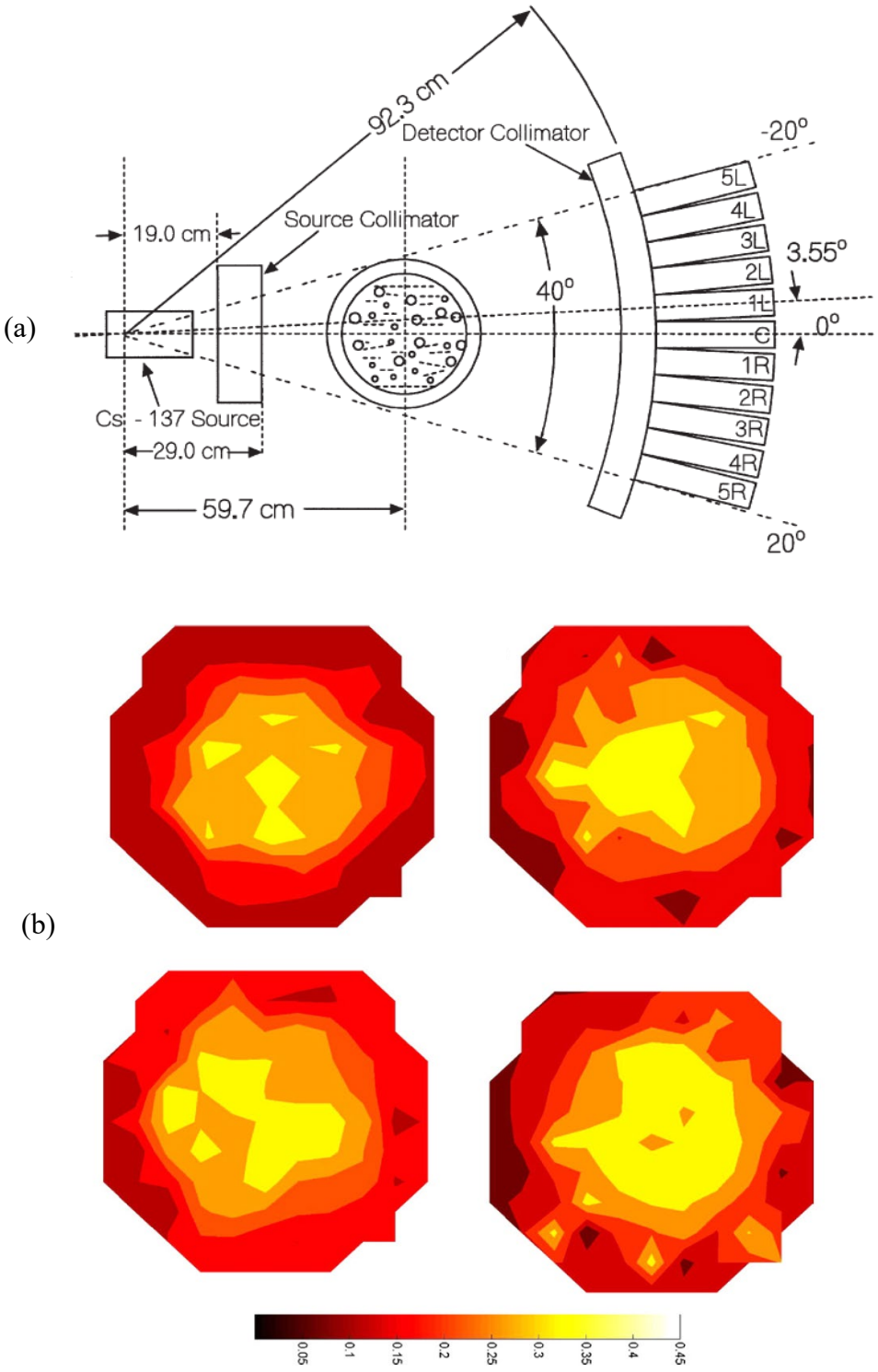

Figure 1- 27 (a) Typical source-detector configuration of CT systems (taken from Chen et al. (1998)); (b) Gas holdup profile at different cross sections measured by a γ-ray CT (taken from Patel and Thorat (2008)).

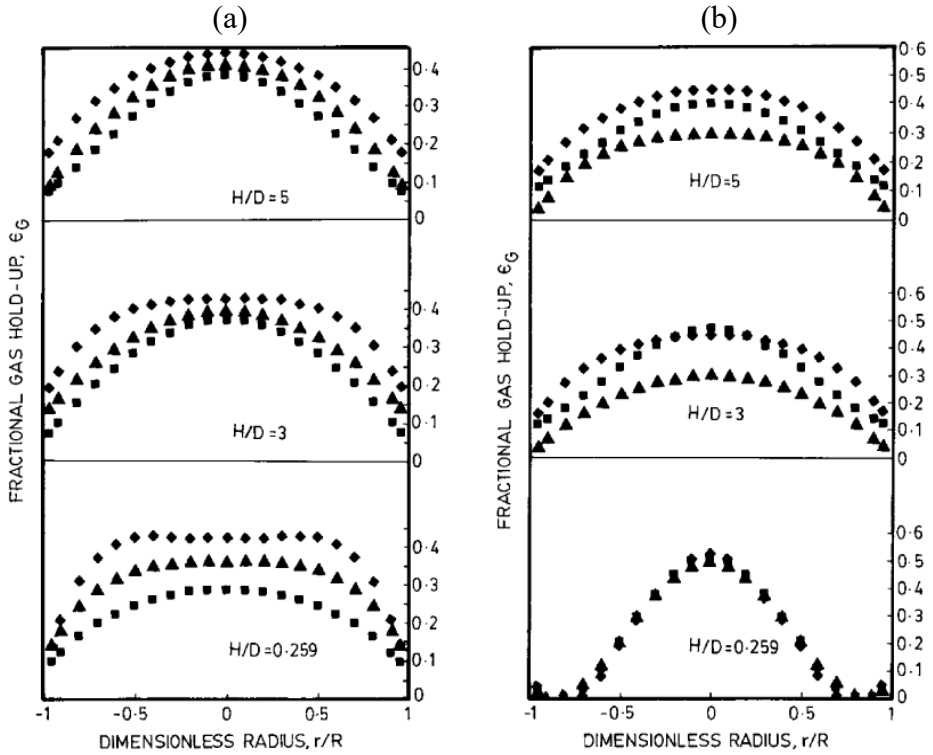

Figure 1- 28 Radial gas holdup profiles at various axial locations at Ug = 0.24 m/s for various liquid phases for the sparger plate: (a) d_o = 1 mm, and (b) d_o = 25 mm; ♦Coalescence inhabiting ▲Air-Water, ■ Coalescence promoting. (taken from Veera and Joshi (2000))

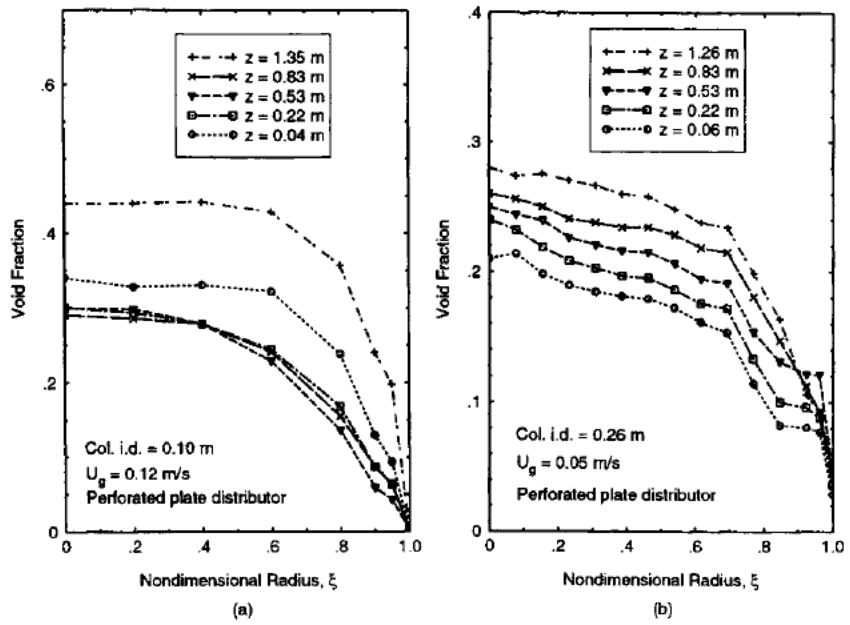

Figure 1- 29 Effect of axial distance on the radial distribution of gas holdup with bubble column diameter: (a) 0.1 m; (b) 0.26 m. (taken from Kumar et al. (1997))

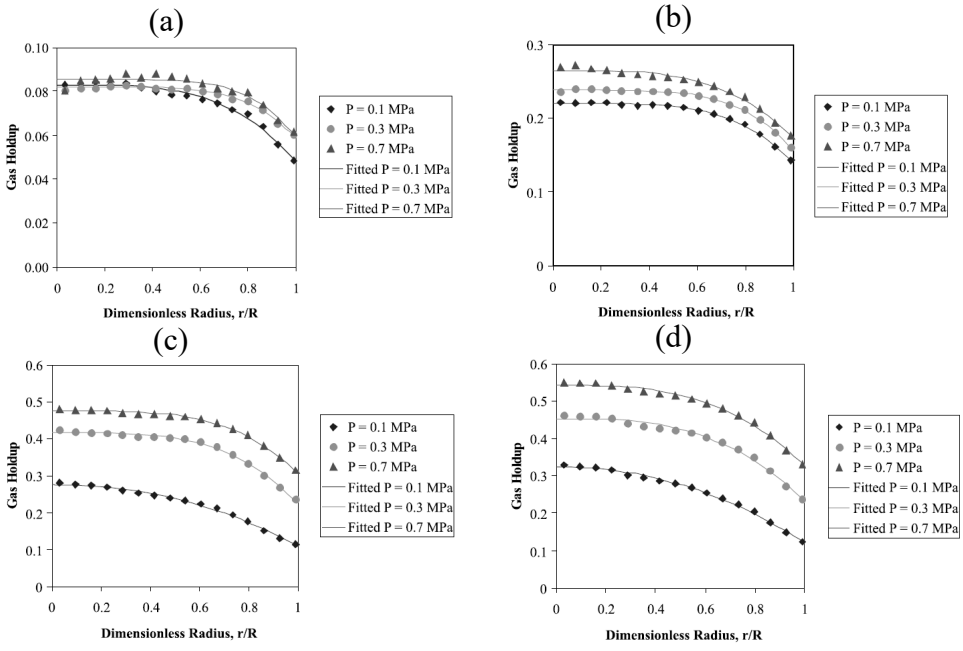

Figure 1- 30 Influence of different operating pressure on the radial distribution of gas holdup at different superficial gas velocities: (a) *Ug* = 0.02 m/s; (b) *Ug* = 0.05 m/s; (c) *Ug* = 0.12 m/s; (d) *Ug* = 0.18 m/s; (taken from Kemoun et al. (2001))

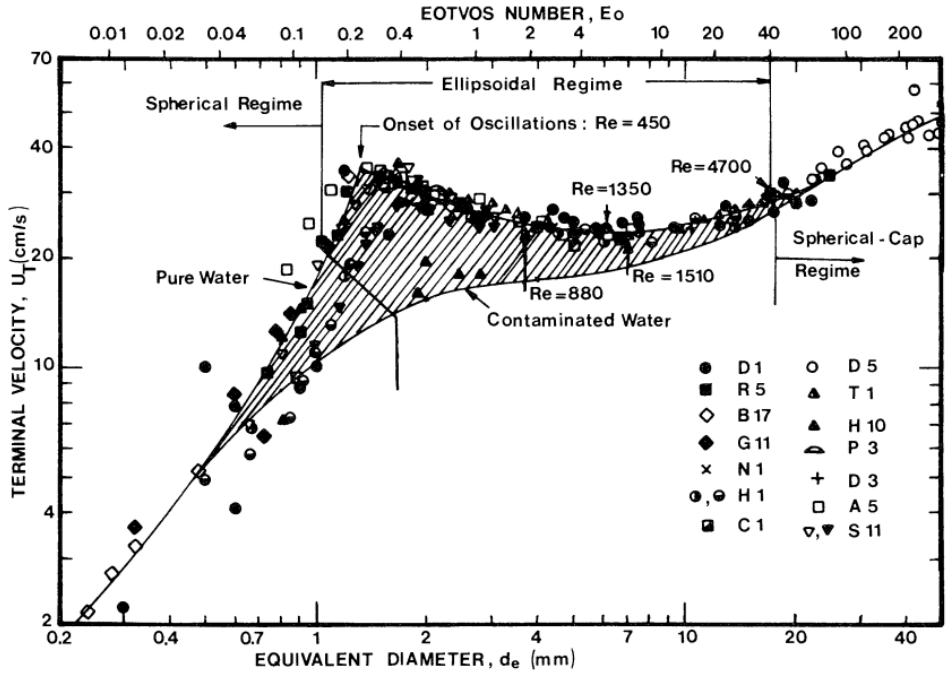

Figure 1- 31 Terminal velocity of airbubbles in water (taken from Clift et al. (1978)).

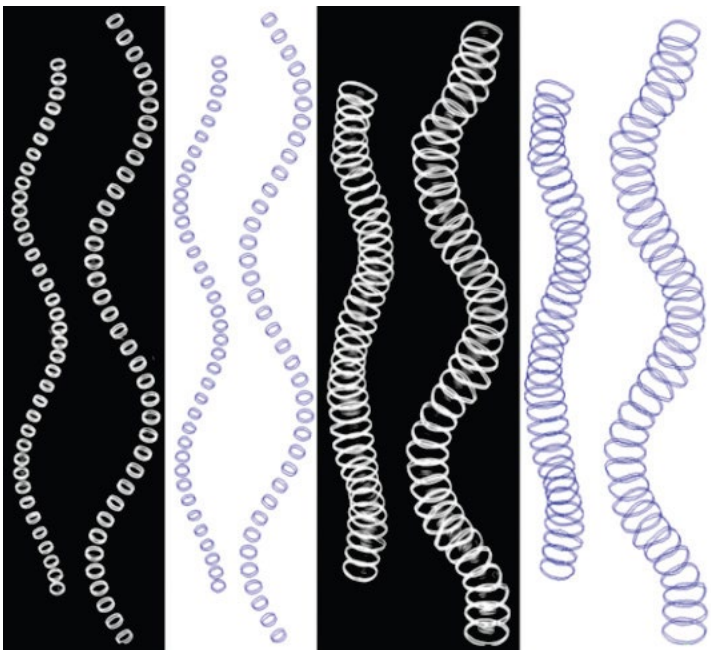

Figure 1- 32 Stereo imaging of bubble rise in stagnant liquid about 700 mm above the injection location for two bubble sizes given with their volume equivalent diameter, two images left) 2.3 mm, two images right) 5.2 mm (taken from Reichardt and Sommerfeld (2008)).

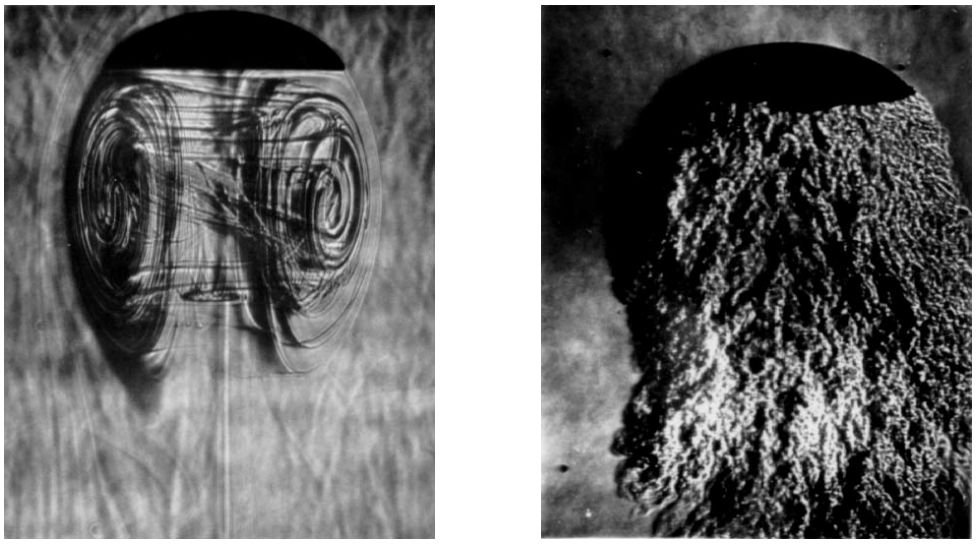

Figure 1- 33 Flow visualizations of spherical-cap bubbles: left) laminar wake at *Re* ≈ 180 (taken from Wegener and Parlange (1973)), and right) turbulent wake at Re ≈ 17,000 (taken from Wegener et al. (1971)).

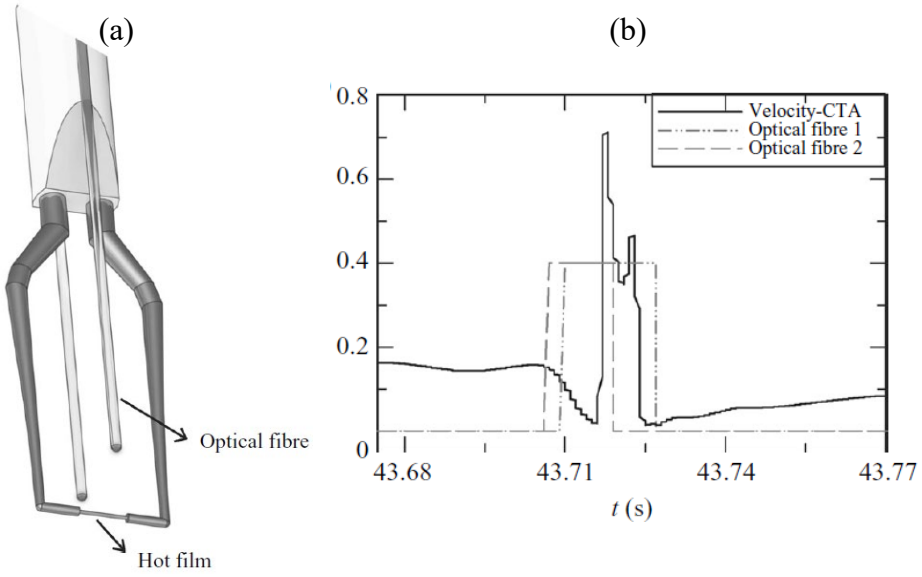

Figure 1- 34 Phase-sensitive CTA: (a) structure of the probe; (b) typical signals for bubble detection. (taken from Mercado et al. (2010))

(a)

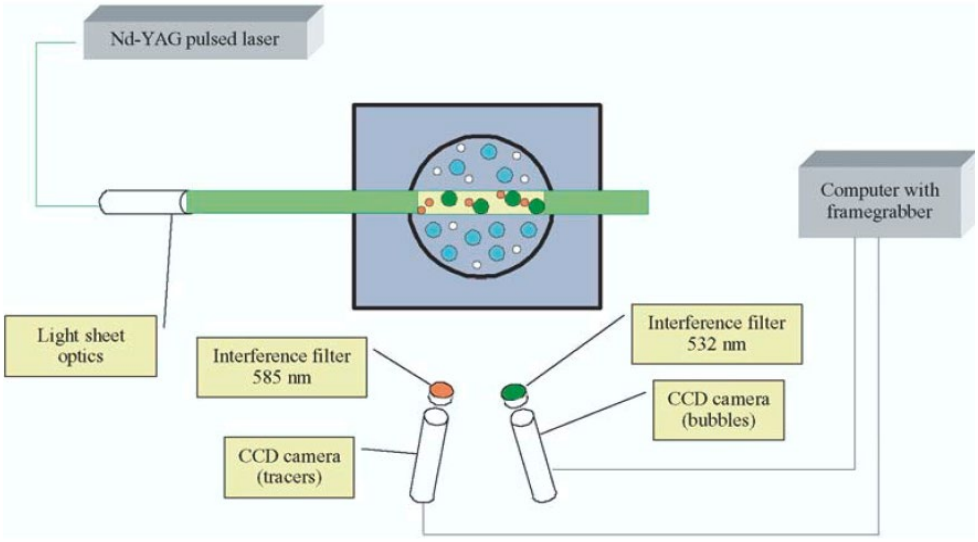

(b)

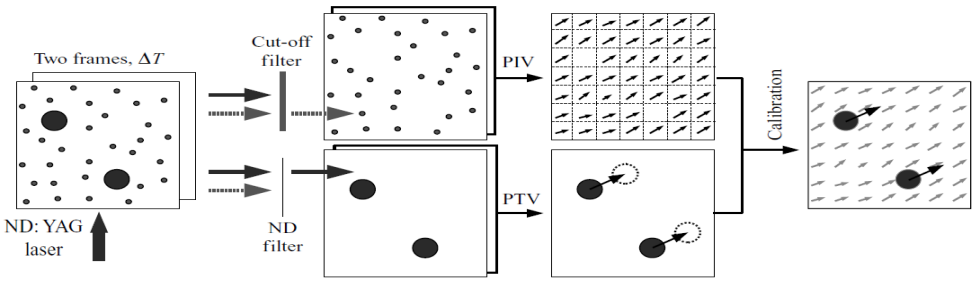

Figure 1- 35 Two-camera PIV system for bubble columns: (a) optical arrangement (taken from Broder and Sommerfeld (2002)); (b) schematic diagram of data processing (taken from Poelma et al. (2007)).

CHAPTER 2: CFD MODELLING OF THE POPULATION BALANCE FOR GAS-LIQUID TWO-PHASE FLOW IN BUBBLE COLUMN

SUMMARY

In Chapter 1, the current status and the methodology adopted for CFD simulation of two-phase bubbly flows together with the concerned modelling issues have been reviewed. Bubble size distribution, a main concern in bubble column simulation, is predicted by bubble breakup model. With the gain of understanding of flow nature, the modification for the classical bubble breakup model is required, which brings multiple integral, a tricky issue in numerical simulation due to the difficulty of achieving numerical integration and the high computational demand. This chapter will propose numerical method for bubble breakup model. The Eulerian-Eulerian CFD-PBM modelling of gas–liquid two-phase flow in a cylindrical bubble column reactor have been conducted. The results clearly show that this numerical method is time-saving with good performance of prediction, which provided a basis for the modification and validation of bubble breakup model when PBM is coupled in CFD simulation of bubble column.

1. INTRODUCTION

Bubble columns are intensively used as multiphase contactors for carrying out gas-liquid two-phase reactions in various industries, including chemical, pharmaceutical industries and nuclear power engineering. Due to the high efficiencies of heat and mass transfer, there has been an increasing interest in bubble column as its application in carbon neutral that is one of the most popular interests of research in recent years.

A large number of experimental studies have been conducted to investigate the flow dynamics in bubble column with different hydrodynamics parameters. However, most of the existing experimental studies focus on the lab-scale bubble columns whose diameter are not larger than 0.5m because the measurements inside large-diameter columns are difficult and extremely complex. As the understanding of fluid dynamics is crucial for the design and scale-up of bubble columns, with the help of numerical development and computer technology, CFD modelling has become an important approach in understand and predicting of the complexity of hydrodynamics. For CFD simulation, various aspects has been investigated individually or considered as interacting with each other.

There has been a number of literatures proposed and focused on various aspects in CFD modelling of bubble columns. Sokolichin and Eigenberger (1999) and Masood et al. (2014) assessed the influence of turbulence models, focusing on k-epsilon and Reynolds stress model respectively. The studies of Thakre and Joshi (1999), Burns et al. (2004) and Yang et al. (2011) describe the influence of drag

force with different closure models. Khan et al. (2020) reviewed different models of interfacial forces and Muniz and Sommerfeld (2020) evaluated the contributions of each interfacial force in fully development bubble column flows. Different models are proposed to investigate another important aspect in bubble column simulation, bubble breakup and coalescence phenomena (Chen et al., 2005, Bordel et al., 2006, Liao et al., 2015, Shi et al., 2019). Coupling of CFD simulation, the rate of mass transfer (Wiemann and Mewes, 2005, Bao et al., 2015) and reaction (Van Baten and Krishna, 2004, Rigopoulos and Jones, 2003, Troshko and Zdravistch, 2009) can also be modelled. Among above aspects, bubble size distribution is the key factor in CFD modelling due to its influence on heat and mass transfer, which is important to the application of bubble column.

Many literatures have been proposed to investigate bubble size distribution within bubble column. In earlier stage, CFD simulation have used the averaged bubble size, which can only be obtained from experimental measurements or determined by repetitive trial-and-error simulations. However, the averaged bubble size cannot shown the predictive nature of CFD modelling and the real inhomogeneity of bubble sizes in time and space aspects. Especially when the bubble columns are operated at the heterogeneous regime with high gas holdup and superficial velocity, the bubble sizes can be widely distributed. Therefore, Thakre and Joshi (1999), Vitankar et al. (2002), and Dhotre and Joshi (2007) have used the ratio of drag coefficient and bubble diameter C_D / d_B as a lumping coefficient to close the interphase momentum exchange term. However, the values of the lumping coefficient are usually determined based on semi-empirical or empirical correlations that developed from experiments, and which causes further difficulties

for other closure terms. For this reason, Krishna and Baten (1999) have proposed the two bubble groups model, which classified bubble sizes into large and small two groups, based on experimental observations by using dynamic gas disengagement (DGD) technique. It was observed that this model has significantly improved the simulation results especially at high superficial velocities (Krishna and van Baten, 2001, Krishna et al., 1999, Van Baten and Krishna, 2004, Guedon et al., 2017), however, it still cannot properly reflect dynamic changes of the bubble sizes and the momentum exchange between the large and small bubble. In recent years, the particle population balance model (PBM) has been applied to describe the dynamic changes of the number density of bubble groups. Wu et al. (1998) and Fu and Ishii (2003) have developed the interfacial area transport models by simplifying population balance model. Two assumptions are made in the simplification: firstly, the difference in daughter bubble breakup and coalescence rates within the same bubble group is not considered; secondly, the difference in velocity between daughter bubbles is ignored. Using the similar way, Lehr et al. (2002) developed a bubble volume transport model. Both the interfacial area transport models and the bubble volume transport model are the simplification of the population balance model, which have lower computational cost due to fewer equations (one or two) to be solved. However, the effect of sub-bubble size on the rate of bubble breakup and coalescence cannot be described in the derivation and the bubble size distribution cannot be predicted.

With the development of computational resources, instead of using simplified model, it becomes possible that solving the complete population balance equations for the grids with a large number of cells. Many models have been proposed to

describe bubble breakage and coalescence. For breakup process, based on the understanding of turbulent nature, a pioneering phenomenological model was proposed by Coulaloglou and Tavlarides (1977) with the assumption that the bubble breakup event occurs when the eddy-carried energy impacting on the bubble is greater than the bubble surface energy. As bubble collision is the main reason of bubble breakup, Prince and Blanch (1990) proposed that only the eddies with approximately same size as bubbles can lead bubble breakup, while the eddies at a much larger length scale have the tendency to transport bubbles rather than to break bubbles. Based on Prince and Blanch (1990) model, Tsouris and Tavlarides (1994) proposed a modified breakup model which defined the critical energy for breaking bubbles as the mean value of the surface energy increase for breakage into daughter bubbles with the same size and into a smallest and a biggest one. Luo and Svendsen (1996) proposed a theoretical model for bubble breakup based on the classical kinetic theory of gases. The model introduced the probability of bubble breakup which was the critical ratio of surface energy increased by bubble breakup and the mean turbulent kinetic energy of the eddies colliding to bubble. Based on the study of Luo and Svendsen (1996), Wang et al. (2003) proposed the model for bubble breakup with the constraints of energy and capillary pressure. The energy constrain is that bubble breakup occurs only when energy contained by bombarding eddies contains greater than or equal to the energy increased by bubble breakup. The capillary constraint is that the dynamic pressure of the arriving eddy is greater than the capillary pressure of the bubble. This model improved the accuracy of simulation results to practical observation in comparison of Luo and Svendsen (1996) model because the two breakup criteria add the restriction of the minimum size of the bubble that can breakup. The constraints of energy and

capillary pressure have also been adopted and extended in the recent studies reported by Zhao and Ge (2007) and Liao et al. (2015). Furthermore, Shi et al. (2018) proposed modified breakup models with the consideration of bubble shape variation.

The population balance equations can be numerically solved via different solution methods, such as the discrete method (DM) (Hounslow et al., 1988, Lister et al., 2004), the quadrature method of moments (QMOM) (Marchisio et al., 2003), and the direct quadrature method of moments (DQMOM) (Fan et al., 2004). It seems that all these solution methods are capable of mathematically resolving the population balance equations with different levels of complexity for each method. Therefore, the efficiency of each solution method is an important factor in CFD modelling as it affects the consuming time and computational demand.

The aim of this paper is to develop numerical methods for solving bubble breakage model as it is one of the most important and time-consuming processes in the CFD modelling. This method is time-saving and applicable of the modification of existing models. Section 2 will summarizes the mathematical framework in the current study while section 3 will present the numerical details in CFD simulations conducted in this work. Section 4 will present the simulation results and discussion, by the comparison of results of the simulations with error analysis numerical methods and on key parameters including gas holdup and bubble number density. Section 4 will present the conclusions derived from the study.

2. MATHEMATICAL MODELLING

2.1 Governing equations

A 3D transient CFD model is used in this work to simulate the local hydrodynamics of the gas-liquid two-phase bubble column. A Eulerian-Eulerian approach is adopted to describe the flow behaviours for both phases, i.e. water as the continuous phase, and air as the dispersed phase. The mass and momentum balance equations are given by equations (2-1) and (2-2) respectively,

$$\frac{\partial(\rho_k \alpha_k)}{\partial t} + \nabla \cdot (\rho_k \alpha_k \boldsymbol{u}_k) = 0 \quad (2\text{-}1)$$

$$\frac{\partial(\rho_k \alpha_k \boldsymbol{u}_k)}{\partial t} + \nabla \cdot (\rho_k \alpha_k \boldsymbol{u}_k \boldsymbol{u}_k) = -\alpha_k \nabla p + \nabla \cdot \boldsymbol{\tau}_k + \rho_k \alpha_k \boldsymbol{g} + \boldsymbol{F}_k \quad (2\text{-}2)$$

where ρ_k, α_k, $\boldsymbol{u}_k$, $\bar{\bar{\tau}}_k$, and $\boldsymbol{F}_k$ represent the density, volume fraction, velocity vector, viscous stress tensor and the inter-phase momentum exchange term for the *k* (liquid or gas) phase respectively. The sum of the volume fractions for both phases is equal to 1.

2.2 Interphase momentum transfer

For the closure of governing equations, the interfacial forces should be employed. In this study, only the drag force is considered because it is the predominant interfacial force in gas-liquid flows in bubble columns (Laborde-Boutet et al., 2009, Larachi et al., 2006). The drag force is calculated as:

$$\boldsymbol{F}_D = \frac{3}{4}\frac{C_D}{d_b}\rho_l \alpha_g \left|\boldsymbol{u}_g - \boldsymbol{u}_l\right|\left(\boldsymbol{u}_g - \boldsymbol{u}_l\right) \quad (2\text{-}3)$$

where C_D is the drag coefficient, which can be obtained from the model of Schiller and Naumann (1935). The Schiller and Naumann (1935) model is shown as

$$C_D = \begin{cases} 24(1 + 0.15Re_b^{0.687})/Re_b & Re_b \leq 1000 \\ 0.44 & Re_b > 1000 \end{cases} \quad (2\text{-}4)$$

where Re_b is the bubble Reynolds number given by $Re_b = \frac{\rho_L |\boldsymbol{u}_g - \boldsymbol{u}_L| d_b}{\mu_L}$

2.3 Turbulence modelling

In this work, turbulence model, the standard k-ε model, is employed as given below:

$$\frac{\partial(\alpha_l \rho_l k_l)}{\partial t} + \nabla \cdot (\alpha_l \rho_l k_l \boldsymbol{u}_k) = \nabla \cdot \left[\alpha_l \left(\mu_l + \frac{\mu_t}{\sigma_k}\right) \nabla k_l\right] + \alpha_l (G_{k,l} - \rho_l \varepsilon_l) \quad (2\text{-}5)$$

$$\frac{\partial(\boldsymbol{\alpha_l \rho_l \varepsilon_l})}{\partial t} + \boldsymbol{\nabla \cdot (\alpha_l \rho_l \varepsilon_l u_k)} = \boldsymbol{\nabla \cdot \left[\alpha_l \left(\mu_l + \frac{\mu_t}{\sigma_k}\right) \nabla \varepsilon_l\right] + \alpha_l \frac{\varepsilon_l}{k_l} \left(C_{1\varepsilon} G_{k,l} - C_{2\varepsilon} \rho_l \varepsilon_l\right)} \quad (2\text{-}6)$$

where k and ε represent the turbulent kinetic energy and the turbulent dissipation rate respectively. μ_t is the eddy viscosity and G_k represents the production of turbulent kinetic energy, as shown as

$$\mu_t = \rho_l C_\mu \frac{k_l^2}{\varepsilon} \quad (2\text{-}7)$$

$$G_{k,l} = \tau_l : \nabla \boldsymbol{u}_l \quad (2\text{-}8)$$

2.4 Population balance model

In this work, the population balance model is employed to predict the bubble size distribution, the bubbles are classified into groups with different size d_i for the discrete method.

The population balance equation is

$$\frac{\partial n_i}{\partial t} + \nabla \cdot \left(\boldsymbol{u}_{b,i} \cdot n_i\right) = S_i \tag{2-9}$$

where n is the number density of bubbles for, $\boldsymbol{u}_b$ is the bubble velocity vector, and S is the source term. The subscript i means the i-th group.

Bubble coalescence and breakage phenomena are taken into account, the source term can be expressed by the birth and death of bubbles due to coalescence, which is derived as:

$$S_i = B_{coalescence,i} - D_{coalescence,i} + B_{breakup,i} - D_{breakup,i}$$
$$= \sum_{V_j=V_{min}}^{\frac{V_i}{2}} \Omega_C\left(V_j : V_i - V_j\right) - \sum_{V_j}^{V_{max}-V_i} \Omega_C\left(V_j : V_i\right) + \sum_{V_j=V_i}^{V_{max}} \Omega_B\left(V_j : V_i\right) - \Omega_B(V_i) \tag{2-10}$$

where V_i is the volume for the i-th class.

The local gas volume fraction and the Sauter mean diameter d_{32} can be calculated as follows:

$$\alpha_g f_i = n_i V_i \tag{2-11}$$

$$d_{32} = 1 \Big/ \left(\sum_{i=1}^{N} \frac{f_i}{d_i}\right) \tag{2-12}$$

where f_i is the i-th class fraction of total volume fraction.

For describing the process of the coalescence between bubbles of size d_i and d_j, Luo (1993) coalescence model is implemented in this work, as shown as

$$\Omega_C(d_i:d_j) = n_i n_j \frac{\pi}{4}\left(d_i + d_j\right)^2\left(\bar{u}_i^2 + \bar{u}_j^2\right)^{\frac{1}{2}}$$

$$\exp\left(-c_1 \frac{\left[0.75\left(1+x_{ij}^2\right)\left(1+x_{ij}^3\right)\right]^{1/2}}{\left(\rho_g/\rho_l+0.5\right)^{1/2}\left(1+x_{ij}\right)^3} We_{ij}^{1/2}\right) \quad (2\text{-}13)$$

where c_1 is a constant of order unity that usually equals to, x_{ij} is the size ratio of two colliding bubbles $x_{ij}=d_i / d_j$ and We_{ij} the Weber number.

For the bubble breakup process, the binary breakage model by Luo and Svendsen (1996) is used in this work and shown as equation (2-14).

$$\Omega_B\left(d_i:d_j\right) = 0.923\left(1-\alpha_g\right)n_i\left(\frac{\varepsilon}{d_i^2}\right)^{\frac{1}{3}}\int_{\xi_{min}}^{1}\frac{(1+\xi)^2}{\xi^{11/3}}\exp\left(-\frac{12\sigma C_f}{\beta\rho_l\varepsilon^{2/3}d_i^{5/3}\xi^{11/3}}\right)d\xi$$

(2-14)

$$C_f = f_V^{2/3} + (1-f_V)^{2/3} - 1 \quad (2\text{-}15)$$

where ξ is the size ratio between an eddy and a bubble which is calculated from $\xi = \lambda / d_i$, $\beta \approx 2.0466$, C_f is the increase coefficient of surface area and f_V represents the breakage volume fraction as $f_V = d_j^3 / d_i^3$.

Since not only the interphase force closure, such as drag and lift force, but also the turbulence closure requires bubble size, the prediction of bubble size is essential in the numerical studies of bubble columns. The daughter bubble size distribution can be calculated directly from the Luo's breakup model (equation (2-14)) instead of using predefined distribution, as shown as

$$P = \frac{2\int_{\xi_{min}}^{1}\frac{(1+\xi)^2}{\xi^{11/3}}\exp\left(-\frac{12\sigma C_f}{\beta\rho_l\varepsilon^{2/3}d_i^{5/3}\xi^{11/3}}\right)d\xi}{V\int_0^1\int_{\xi_{min}}^{1}\frac{(1+\xi)^2}{\xi^{11/3}}\exp\left(-\frac{12\sigma C_f}{\beta\rho_l\varepsilon^{2/3}d_i^{5/3}\xi^{11/3}}\right)d\xi df_V}$$

(2-16)

Therefore, the Luo's breakage kernel can be expressed encompassing both the breakage frequency and the normalized daughter bubble size distribution function as known as the probability density function (PDF) of breaking bubble (Lehr et al., 2002).

As shown in equation (2-14) and (2-16), the breakup rate is expressed as the form of single integral, while bubble size distribution is as the combination of single integral and double integral. Due to the complexities of equations, the crucial point is how to solve these equations. In this work, a numerical solution is developed.

Take the single integral as example. Following the idea of Alopaeus (1999), the breakup kernel in integral expression can be rewritten into incomplete gamma function, as shown as

$$g(d_i: d_j) = -0.923\frac{3(1-\alpha_g)n_i}{11b^{\frac{6}{11}}}\left(\frac{\varepsilon}{d_i^2}\right)^{\frac{1}{3}}\Big\{\Gamma(8/11\,, t_m) - \Gamma(8/11\,, b) + 2b^{\frac{3}{11}}\big(\Gamma(5/11\,, t_m) - \Gamma(5/11\,, b)\big) + b^{\frac{6}{11}}\big(\Gamma(2/11\,, t_m) - \Gamma(2/11\,, b)\big)\Big\} \tag{2-17}$$

where $b = \frac{12\sigma C_f}{\beta\rho_l\varepsilon^{2/3}d_i^{5/3}}$ and $t_m = b(\eta/d_i)^{-11/3}$, η represents the Kolmogorov scale. The detail derivation process can be found in Appendix.

As Alopaeus's work was proposed for mixing tank, the change of boundary conditions should be considered when modelling multiphase bubble column

(Alopaeus et al., 1999). In this work, 5^{th} order Taylor expansion is employed to achieve the boundary convergences.

In this chapter, the efficiency and accuracy were evaluated by numerically modelling selected cases with different column diameters and great results were obtained. Furthermore, with the increase of understanding of flow nature within bubble column, many studies have proposed different models with the considerations of various factor. However, the population balance module in FLUENT, the most widely used commercial software in numerical simulation of bubble column, is set as a black box, the modification is usually set as sourceterms, not the kernel itself. In following chapters, a modified breakup model with the consideration of the bubble-induced turbulence energy spectrum distribution is employed, which proposes more complicate model and increases computation demand. This numerical method is the basis to implement the modification in simulation.

3. NUMERICAL MODELLING

To verify the reliability of this numerical scheme, firstly, the bubble breakup rate was evaluated numerically by both the Gauss-Kronrod quadrature with the relative error tolerance of 10^{-11} and the incomplete gamma function which was expressed in equation (2-17), the results was compared and got great agreement. Then, using the similar method, the double integral was numerically computed, hence the breakage frequency and PDF of breaking bubble could be calculated. The above process was repeated for every single bubble size and dissipation rate

and the values were summarized in a table with corresponding variables. Rather than calculating the time-consuming integral equation in each grid, this method directly searched the value with corresponding bubble size and dissipation rate in the generated table, which further shortened the simulation time while keeping the same precision level of prediction.

The proposed numerical method of bubble breakup model was validated by comparing the simulation results for the air-water bubble column systems as reported in Chen et al. (1999) and Guan and Yang (2017). The details of experiments are presented in Table 2-1.

Table 2- 1 Details of experimental set-up of selected numerical simulations

Experiment	Diameter (m)	Height (m)	Superficial Gas Velocity (m/s)	Static Liquid Height (m)	Observation Height (m)
Chen et al. (1999)	0.44	2.44	0.1	0.9	1.32
Guan and Yang (2017)	0.15	1.6	0.05	1.2	0.8

The 3D transient CFD-PBM modelling was performed by the ANSYS FLUENT 17.0. The constant time step size was 0.001s. For the population balance modelling, bubbles were divided discretely into 9 classes, The sizes of the bubble classes from small to large bubbles were increased in such a manner that $V_{i+1} = 4V_i$. The Luo's breakup model was solved by the numerical method

through the use of the user defined functions (UDF). All residual values including all phase bins are set to below 10^{-4} as the convergence criteria. The numerical method has been carefully tested as the simulation results were compared with the simulation from the FLUENT built-in PBM module of Luo's breakup model (Luo and Svendsen, 1996). The bottoms of columns were set as the velocity inlet, where the volume fraction for liquid and gas phases were specified as 0 and 1 respectively. The top of columns was set as the pressure outlet. No-slip conditions were applied for both liquid and gas phases at the bubble column wall.

As shown in Figure 2-1, the mesh set-up for the case of Chen et al. (1999), the height of the bubble column was extended to 3m to prevent overflow from the top. The computational grid (28(r)×64(θ)×100(z) equally distributed nodes in radial, circumferential and axial directions respectively) was fine enough to give mesh-independent results.

4. RESULTS AND DISCUSSION

4.1 Grid independency study

As shown in Figure 2-2, three grids, Grid 1 of 20(r)×40(θ)×80(z) nodes, Grid 2 of 28(r)×64(θ)×100(z) nodes, Grid 3 of 36(r)×72(θ)×126(z) nodes, were set to test the grid independence, as the total grid number increased doubly from the most coarser to the finest gradually.

The grid independence test was shown in Figure 2-3, the results for these three set-ups has yielded similar results quantitatively. However, Grid 2 and Grid 3 present very similar results in the normalized liquid axial velocity prediction while the coarser grid, Grid 1, has slightly deviated from both Grid 2 and Grid 3. Thus, Grid 2 shown in Figure 2-2 has been employed throughout the subsequent simulations.

4.2 Numerical integral validation

The normalized probability density function of bubble size is calculated numerically and illustrated in Figure 2-4 (a). It can be seen clearly that the dimensionless daughter bubble size distribution for air-water system has the great agreement with that reported in Luo and Svendsen (1996) under different conditions of parent bubble size and energy dissipation rate.

A benchmark case considering the breakup process only is conducted. As Figure 2-5 shows, the predicted number densities of different bubble classes have the acceptable error range with the results from the built-in module, and the error does not increase with the increase of time-steps. Therefore, the practicality of coupling the numerical method of breakage model is verified.

4.3 Predicted hydrodynamic properties

The case of Chen et al. (1999)

The gas-liquid two-phase in bubble columns is highly transient and turbulent, the bubbly flow consists of four flow regions including central plume region, descending flow region, vortical-spiral flow region and fast bubble flow region (Fan et al., 1994). Figure 2-6 shows the instantaneous velocity vectors and iso-surface of the gas volume fraction in the column, which clearly illustrates the vertical-spiral upward bubbly flow in the central region of bubble column and the descending flow region from the downward velocity vectors near the column wall. From Figure 2-6, it can be found that a large amount of vortices are oscillating throughout the bubble column, it is also shows the flow field predicted from the numerical method is highly similar with that from built-in PBM module.

Figure 2-7 shows a comparison of the simulated results solving from the numerical method and the built-in module at axial position H = 1.32 m which is the observation height in the stated experiment. Generally, as shown as Figure

2-7 (a), the averaged gas holdup decreases along the radial position, which further illustrates the bubble plume mainly occurs in the central region and is discretely distributed in the near wall region. For the radial distribution of the time-averaging gas holdup, it can be seen that the CFD simulation using the numerical method shows almost the same result with the built-in module. As shown in Figure 2-7(b), for the equivalent bubble diameter, the simulation using numerical method shows the similar distribution with the built-in module, while the specific values have slight differences. These differences may be caused by the spiral movement of bubbly flow, which can be eliminated by sampling more groups of data. In this work, it is considered to be sufficient for illustrating the time-averaged characteristics of the flow fields by carrying out the data sampling statistics for typically 120 seconds after quasi-steady state has been achieved, and the value of 120s is selected due to the balance of accuracy and computational demand. Figure 2-7 only illustrates the distribution in certain height to guarantee the consistency to experimental set-up. In order to evaluate the bubble size distribution in the whole column, the main concern of the population balance model, the volume-based bubble possibility density function is shown as Figure 2-8.

Figure 2-8 shows the overall bubble class probability distribution. The cumulative volume for each bubble class has been normalized by the total volume of all bubbles. It can be seen from Figure 2-8 that the bubble size mainly accumulates in the mid-size classes which are near the inlet bubble size. The reason is the breakup and coalescence process are in balance when the bubble column is in the equilibrium state. In addition, the results of the numerical

integral method and that of bubble breakup model shows similar bubble size distributions, in order to assess in detail, the relative error of each bubble size class is calculated, as shown in Figure 2-9. Most of them has the error under 10% which is in an acceptable error range. The greatest difference can be found in the largest bubble diameter class, however, as shown in Figure 2-8, the probability density of bubble with 40.32mm diameter is very small, the influence of difference in largest class can be neglected in the bubble breakup model.

The case of Guan and Yang (2017)

Above simulation results verifies the practicality of the numerical method for bubble column reported in Chen et al. (1999). Further CFD validations have been carried out for the bubble column used by Guan and Yang (2017) which has different flow characteristics due to the smaller column diameter. Figure 2-10 presents the time-averaged radial distribution of gas holdup and the equivalent bubble diameter d_{32} at the observation height of $H = 0.8$m. In general, the numerical method shows agreeable results with the built-in module in FLUENT in the prediction of key hydrodynamic parameters. As shown in Figure 2-10(a), the averaged gas holdup decreases from the central region to column wall, which demonstrates the bubble plume characteristics in the central region. With the average the value of gas hold-up on the cross-sectional plane, it can be clearly seen that the radial distribution of the time-averaging gas holdup simulated by using the numerical method shows almost the same result with the built-in module. However, such consistency can still be improved by

sampling with more groups of data, because the difference between numerical integration and built-in module is caused by the spiral movement of bubbly flow. In this work, the time-averaged statistics are based on 120 seconds after achieving the quasi-steady state for the balance of accuracy demand and computational demand. Figure 2-7(b) shows the equivalent bubble diameter, d_{32}, is uniformly distributed along radial direction. It is expected that the flow field may still be not fully developed at the observation height H = 0.8 m and would be influenced by the gas inlet condition. In fact, the air was introduced by a perforated plate in their experiments, which may cause uniform gas inlet distribution. For the radial distribution of equivalent bubble diameter, the simulation results with both using numerical method and built-in module are quite consistent, while the specific values have slight differences. These differences may be caused by the spiral movement of bubbly flow, which will be improved correspondingly with the improvement of gas holdup prediction.

The bubble size distribution, which is the main concern of using the population balance model, is illustrated in Figure 2-11, the cumulative volume for each bubble class has been normalized by the total volume of all bubbles. It can be seen from Figure 2-11 that the bubble size mainly accumulates in the mid-size classes which are close to the inlet bubble size. The reason is the breakup and coalescence process are in balance when the bubble column is in the equilibrium state. Comparing the results of bubble size probability density function of Guan and Yang (2017) with that of the case of Chen et al. (1999), the mid-class accumulation is more significant, the reason might include two aspects: the flow field is not fully developed at the observation height thus the influence of inlet

condition is dominant; the inlet superficially gas velocity is smaller than the case of Chen et al. (1999), thus the induced turbulent kinetic energy used for breakup is smaller and the breakup probability is affected correspondingly. In general, the results of the numerical integral method and that of bubble breakup model shows similar bubble size distributions, for deeper analysis, the relative error of each bubble size class is calculated, as shown in Figure 2-12. Most of them has the error under 6% which is in an acceptable error range. The reliability of the numerical method is thus validated.

4.4 The influence on computational time

As shown in previous sections, the results using this numerical method have great agreement with the build-in module in FLUENT. Therefore, the reliability of this numerical scheme is verified, which provides a basis of any modification on the breakup kernel itself. As mentioned above, the computation demand is another important factor in CFD modelling, therefore, the computational time of 1 iteration of the case of Chen et al. (1999) is recorded by the time monitor in ANSYS FLUENT, as shown as Table 2-2. It can be clearly seen that the numerical method significantly saves the computational time, with the saving rate of about 95%, and this finding is repeated and verified by three trails of simulation.

Table 2- 2 The computational time for 1 iteration (Chen's case)

	Built-in module	**Numerical method**
1st Attempt	2.997678 seconds	0.075164 seconds
2nd Attempt	3.040639 seconds	0.078919 seconds
3rd Attempt	3.010134 seconds	0.080293 seconds

In numerical simulation process, the computational time is influenced by the number of iterations and the convergence efficiencies. An automatic monitor is implemented to record the computational time of the two selected cases. The result is summarized in Figure 2-13. When implementing the built-in PBM module in FLUENT, with twenty-four parallel processes, the computational time is in billion level of both cases, in other words, the simulation of Chen et al. (1999) takes about 10 days while that of Guan and Yang (2017) takes approximate 6 days. However, when implementing this numerical method proposed in this chapter, the computational time significantly deceases to 6.8 hours of Chen's case and 4.9 hours of Guan and Yang's case. Therefore, the numerical integration method can save most computational time while keeping accuracy. Comparing the computational time of numerical method of the two cases, the computation resources are saved more significantly in Chen's case. As the number of cells in Chen's case is large than that of Guan and Yang's case, a likely reason is the numerical method uses incomplete gamma function and the discrete table to decrease the simulation time to achieve convergence, but the numerical simulation still needs to be derived grid by grid.

5. CONCLUSION

A numerical method of solving bubble breakup model is developed and verified by CFD simulation of gas-liquid flow in bubble column. In general, the numerical method successfully illustrates the flow nature in bubble column. Two cases of bubbly flow with different column diameter are simulated by the numerical method to validate its practicality. The simulation results of gas holdup, equivalent bubble diameter and bubble size distribution are verified by comparing with the simulation results using built-in PBM module, which got the great agreement. From the comparison of computational time cost between the proposed numerical integration method and built-in module, the result shows that the numerical method shortened the simulation time while keeping the same precision level of prediction, which provide the basis of following modification of bubble breakup and coalescence models.

REFERENCES

ALOPAEUS, V., KOSKINEN, J. & KESKINEN, K. I. 1999. Simulation of the population balances for liquid–liquid systems in a nonideal stirred tank. Part 1 Description and qualitative validation of the model. *Chemical Engineering Science,* 54**,** 5887-5899.

BAO, D., ZHANG, X., DONG, H. F., OUYANG, Z. L., ZHANG, X. P. & ZHANG, S. J. 2015. Numerical simulations of bubble behavior and mass transfer in CO2 capture system with ionic liquids. *Chemical Engineering Science,* 135**,** 76-88.

BORDEL, S., MATO, R. & VILLAVERDE, S. 2006. Modeling of the evolution with length of bubble size distributions in bubble columns. *Chemical Engineering Science,* 61**,** 3663-3673.

BURNS, A. D., FRANK, T., HAMILL, I. & SHI, J.-M. The Favre Averaged Drag Model for Turbulent Dispersion in Eulerian Multi-Phase Flows. Fifth International Conference on Multiphase Flow, ICMF-2004, 2004 Yokohama, Japan.

CHEN, J. W., LI, F., DEGALEESAN, S., GUPTA, P., AL-DAHHAN, M. H., DUDUKOVIC, M. P. & TOSELAND, B. A. 1999. Fluid dynamic parameters in bubble columns with internals. *Chemical Engineering Science,* 54**,** 2187-2197.

CHEN, P., SANYAL, J. & DUDUKOVIC, M. P. 2005. Numerical simulation of bubble columns flows: effect of different breakup and coalescence closures. *Chemical Engineering Science,* 60**,** 1085-1101.

COULALOGLOU, C. A. & TAVLARIDES, L. L. 1977. Description of Interaction Processes in Agitated Liquid-Liquid Dispersions. *Chemical Engineering Science,* 32**,** 1289-1297.

DHOTRE, M. T. & JOSHI, J. B. 2007. Design of a gas distributor: Three-dimensional CFD simulation of a coupled system consisting of a gas chamber and a bubble column. *Chemical Engineering Journal,* 125**,** 149-163.

FAN, J. R., ZHOU, D. D., HUA, Q. & CEN, K. F. 1994. Numerical Computation of Particle-Laden Gas-Flows Past Staggered Tube Banks Undergoing Erosion. *Powder Technology,* 80**,** 1-10.

FAN, R., MARCHISIO, D. L. & FOX, R. O. 2004. Application of the direct quadrature method of moments to polydisperse gas-solid fluidized beds. *Powder Technology,* 139**,** 7-20.

FU, X. Y. & ISHII, M. 2003. Two-group interfacial area transport in vertical air-water flow II. Model evaluation. *Nuclear Engineering and Design,* 219**,** 169-190.

GUAN, X. P. & YANG, N. 2017. Bubble properties measurement in bubble columns: From homogeneous to heterogeneous regime. *Chemical Engineering Research & Design,* 127**,** 103-112.

GUEDON, G. R., BESAGNI, G. & INZOLI, F. 2017. Prediction of gas-liquid flow in an annular gap bubble column using a bi-dispersed Eulerian model. *Chemical Engineering Science,* 161**,** 138-150.

HOUNSLOW, M. J., RYALL, R. L. & MARSHALL, V. R. 1988. A Discretized Population Balance for Nucleation, Growth, and Aggregation. *Aiche Journal,* 34**,** 1821-1832.

KHAN, I., WANG, M., ZHANG, Y., TIAN, W., SU, G. & QIU, S. 2020. Two-phase bubbly flow simulation using CFD method: A review of models for interfacial forces. *Progress in Nuclear Energy,* 125.

KRISHNA, R. & BATEN, J. M. V. 1999. Simulating the motion of gas bubbles in a liquid. *Nature,* 398**,** 208.

KRISHNA, R., URSEANU, M. I., VAN BATEN, J. M. & ELLENBERGER, J. 1999. Influence of scale on the hydrodynamics of bubble columns operating in the churn-turbulent regime: experiments vs. Eulerian simulations. *Chemical Engineering Science,* 54**,** 4903-4911.

KRISHNA, R. & VAN BATEN, J. M. 2001. Eulerian simulations of bubble columns operating at elevated pressures in the churn turbulent flow regime. *Chemical Engineering Science,* 56**,** 6249-6258.

LABORDE-BOUTET, C., LARACHI, F., DROMARD, N., DELSART, O. & SCHWEICH, D. 2009. CFD simulation of bubble column flows: Investigations on turbulence models in RANS approach. *Chemical Engineering Science,* 64**,** 4399-4413.

LARACHI, F., DESVIGNE, D., DONNAT, L. & SCHWEICH, D. 2006. Simulating the effects of liquid circulation in bubble columns with internals. *Chemical Engineering Science,* 61**,** 4195-4206.

LEHR, F., MILLIES, M. & MEWES, D. 2002. Bubble-size distributions and flow fields in bubble columns. *Aiche Journal,* 48**,** 2426-2443.

LIAO, Y. X., RZEHAK, R., LUCAS, D. & KREPPER, E. 2015. Baseline closure model for dispersed bubbly flow: Bubble coalescence and breakup. *Chemical Engineering Science,* 122**,** 336-349.

LISTER, J. D., SMIT, D. J. & HOUNSLOW, M. J. 2004. Adjustable discretized population balance for growth and aggregation. *AIChE Journal,* 41**,** 591-603.

LUO, H. 1993. *Coalescence, Breakup and Liuqid Circulation in Bubble Column Reactors.* PhD thesis PhD thesis, PhD thesis from the Norwegian Institute of Technology.

LUO, H. & SVENDSEN, H. F. 1996. Theoretical model for drop and bubble breakup in turbulent dispersions. *Aiche Journal,* 42**,** 1225-1233.

MARCHISIO, D. L., VIGIL, R. D. & FOX, R. O. 2003. Quadrature method of moments for aggregation-breakage processes. *Journal of Colloid and Interface Science,* 258**,** 322-334.

MASOOD, R. M. A., RAUH, C. & DELGADO, A. 2014. CFD simulation of bubble column flows: An explicit algebraic Reynolds stress model approach. *International Journal of Multiphase Flow,* 66**,** 11-25.

MUNIZ, M. & SOMMERFELD, M. 2020. On the force competition in bubble columns: A numerical study. *International Journal of Multiphase Flow,* 128.

PRINCE, M. J. & BLANCH, H. W. 1990. Bubble Coalescence and Break-up in Air-Sparged Bubble-Columns. *Aiche Journal,* 36**,** 1485-1499.

RIGOPOULOS, S. & JONES, A. 2003. A hybrid CFD - reaction engineering framework for multiphase reactor modelling: basic concept and application to bubble column reactors. *Chemical Engineering Science,* 58**,** 3077-3089.

SCHILLER, L. & NAUMANN, A. 1935. A drag coefficient correlation. *Z. Ver. Deutsch. Ing,* 77**,** 318-320.

SHI, W., YANG, J., LI, G., YANG, X., ZONG, Y. & CAI, X. 2018. Modelling of breakage rate and bubble size distribution in bubble columns accounting for bubble shape variations. *Chemical Engineering Science,* 187**,** 391-405.

SHI, W., YANG, X., SOMMERFELD, M., YANG, J., CAI, X., LI, G. & ZONG, Y. 2019. Modelling of mass transfer for gas-liquid two-phase flow in bubble column reactor with a bubble breakage model considering bubble-induced turbulence. *Chemical Engineering Journal,* 371**,** 470-485.

SOKOLICHIN, A. & EIGENBERGER, G. 1999. Applicability of the standard k-epsilon turbulence model to the dynamic simulation of bubble columns: Part I. Detailed numerical simulations. *Chemical Engineering Science,* 54**,** 2273-2284.

THAKRE, S. S. & JOSHI, J. B. 1999. CFD simulation of bubble column reactors: importance of drag force formulation. *Chemical Engineering Science,* 54**,** 5055-5060.

TROSHKO, A. A. & ZDRAVISTCH, F. 2009. CFD modeling of slurry bubble column reactors for Fisher-Tropsch synthesis. *Chemical Engineering Science,* 64**,** 892-903.

TSOURIS, C. & TAVLARIDES, L. L. 1994. Breakage and coalescence models for drops in turbulent dispersions. *AIChE Journal,* 40**,** 395–406.

VAN BATEN, J. M. & KRISHNA, R. 2004. Scale effects on the hydrodynamics of bubble columns operating in the heterogeneous flow regime. *Chemical Engineering Research & Design,* 82**,** 1043-1053.

VITANKAR, V. S., DHOTRE, M. T. & JOSHI, J. B. 2002. A low Reynolds number k-epsilon model for the prediction of flow pattern and pressure drop in bubble column reactors. *Chemical Engineering Science,* 57**,** 3235-3250.

WANG, T. F., WANG, J. F. & JIN, Y. 2003. A novel theoretical breakup kernel function for bubbles/droplets in a turbulent flow. *Chemical Engineering Science,* 58**,** 4629-4637.

WIEMANN, D. & MEWES, D. 2005. Calculation of flow fields in two and three-phase bubble columns considering mass transfer. *Chemical Engineering Science,* 60**,** 6085-6093.

WU, Q., KIM, S., ISHII, M. & BEUS, S. G. 1998. One-group interfacial area transport in vertical bubbly flow. *International Journal of Heat and Mass Transfer,* 41**,** 1103-1112.

YANG, N., WU, Z. Y., CHEN, J. H., WANG, Y. H. & LI, J. H. 2011. Multi-scale analysis of gas-liquid interaction and CFD simulation of gas-liquid flow in bubble columns. *Chemical Engineering Science,* 66**,** 3212-3222.

ZHAO, H. & GE, W. 2007. A theoretical bubble breakup model for slurry beds or three-phase fluidized beds under high pressure. *Chemical Engineering Science,* 62**,** 109-115.

APPENDIX

The breakup kernel from the model of Luo and Svendsen (1996) is shown as:

$$g(d_i, d_j) = k_1\beta_1(1-\alpha)\left(\frac{\varepsilon}{d_i^2}\right)^{\frac{1}{3}} \int_{\xi_{min}}^{1} \frac{(1+\xi)^2}{\xi^{\frac{11}{3}}} exp\left(-\frac{12c_f\sigma}{\beta_1\rho_l\varepsilon^{2/3}d_i^{5/3}\xi^{11/3}}\right) d\xi \tag{A-1}$$

Let $b = \frac{12c_f\sigma}{\beta_1\rho_l\varepsilon^{2/3}d_i^{5/3}}$, equation (A-1) can be written as:

$$g(d_i, d_j) = k_1\beta_1(1-\alpha)\left(\frac{\varepsilon}{d_i^2}\right)^{\frac{1}{3}} \int_{\xi_{min}}^{1} \frac{(1+\xi)^2}{\xi^{\frac{11}{3}}} e^{-\frac{b}{\xi^{11/3}}} d\xi \tag{A-2}$$

$$d\left(\frac{b}{\xi^{11/3}}\right) = b\left(-\frac{11}{3}\right)\xi^{-\frac{14}{3}} d\xi \tag{A-3}$$

Substituting (A-3) into (A-1),

$$g(d_i, d_j) = k_1\beta_1(1-\alpha)\left(\frac{\varepsilon}{d_i^2}\right)^{\frac{1}{3}} \int_{\xi_{min}}^{1} \frac{(1+\xi)^2}{b\left(-\frac{11}{3}\right)} b\left(-\frac{11}{3}\right)\xi\cdot\xi^{-\frac{14}{3}} e^{-\frac{b}{\xi^{11/3}}} d\xi$$

$$= -\frac{3k_1\beta_1(1-\alpha)}{11b}\left(\frac{\varepsilon}{d_i^2}\right)^{\frac{1}{3}} \int_{\xi_{min}}^{1} (\xi + 2\xi^2 + \xi^3)\, e^{-\frac{b}{\xi^{11/3}}} d\left(\frac{b}{\xi^{11/3}}\right) \tag{A-4}$$

Assume $t = b\xi^{-\frac{11}{3}} = b\left(\frac{\eta}{d_i}\right)^{-\frac{11}{3}}$,

$$g(d_i, d_j) = -\frac{3k_1\beta_1(1-\alpha)}{11b}\left(\frac{\varepsilon}{d_i^2}\right)^{\frac{1}{3}} \int_{b\xi_{min}^{-\frac{11}{3}}}^{b} (\xi + 2\xi^2 + \xi^3)\, \mathrm{e}^{-\mathrm{t}}\, dt \tag{A-5}$$

$$g(d_i, d_j) = -\frac{3k_1\beta_1(1-\alpha)}{11b^{\frac{8}{11}}}\left(\frac{\varepsilon}{d_i^2}\right)^{\frac{1}{3}} \int_{t_m}^{b} \left(t^{-\frac{3}{11}} + 2b^{\frac{3}{11}}t^{-\frac{6}{11}} + b^{\frac{6}{11}}t^{-\frac{9}{11}}\right) \mathrm{e}^{-\mathrm{t}}\, dt \tag{A-6}$$

From the gamma function definition, for any complex $u, v \neq 0$,

$$\int_u^v t^{s-1} e^{-t}\, dt = \Gamma(s, v) - \Gamma(s, u) \tag{A-7}$$

$$g(d_i : d_j) = -\frac{3k_1\beta_1(1-\alpha)}{11b^{\frac{8}{11}}}\left(\frac{\varepsilon}{d_i^2}\right)^{\frac{1}{3}}\Big\{\Gamma(8/11\,, t_m) - \Gamma(8/11\,, b) + 2b^{\frac{3}{11}}\big(\Gamma(5/11\,, t_m) - \Gamma(5/11\,, b)\big) + b^{\frac{6}{11}}\big(\Gamma(2/11\,, t_m) - \Gamma(2/11\,, b)\big)\Big\} \tag{A-8}$$

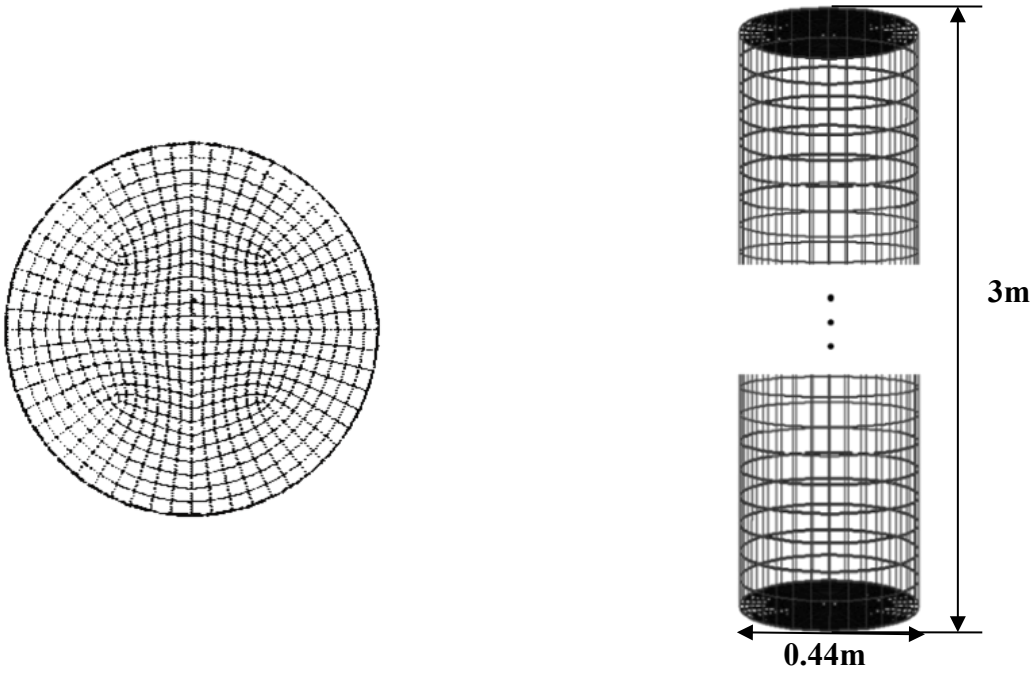

Figure 2- 1 Mesh set-up at cross-section and main body of the column

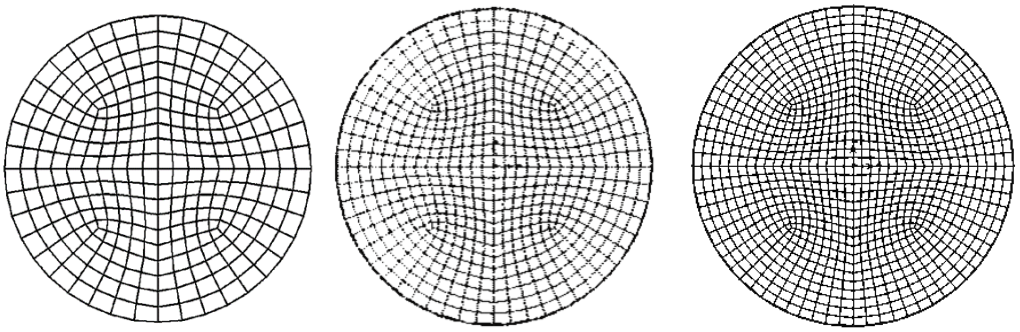

Grid 1 Grid 2 Grid 3

Figure 2- 2 The mesh set-up at the bottom surface of different grids

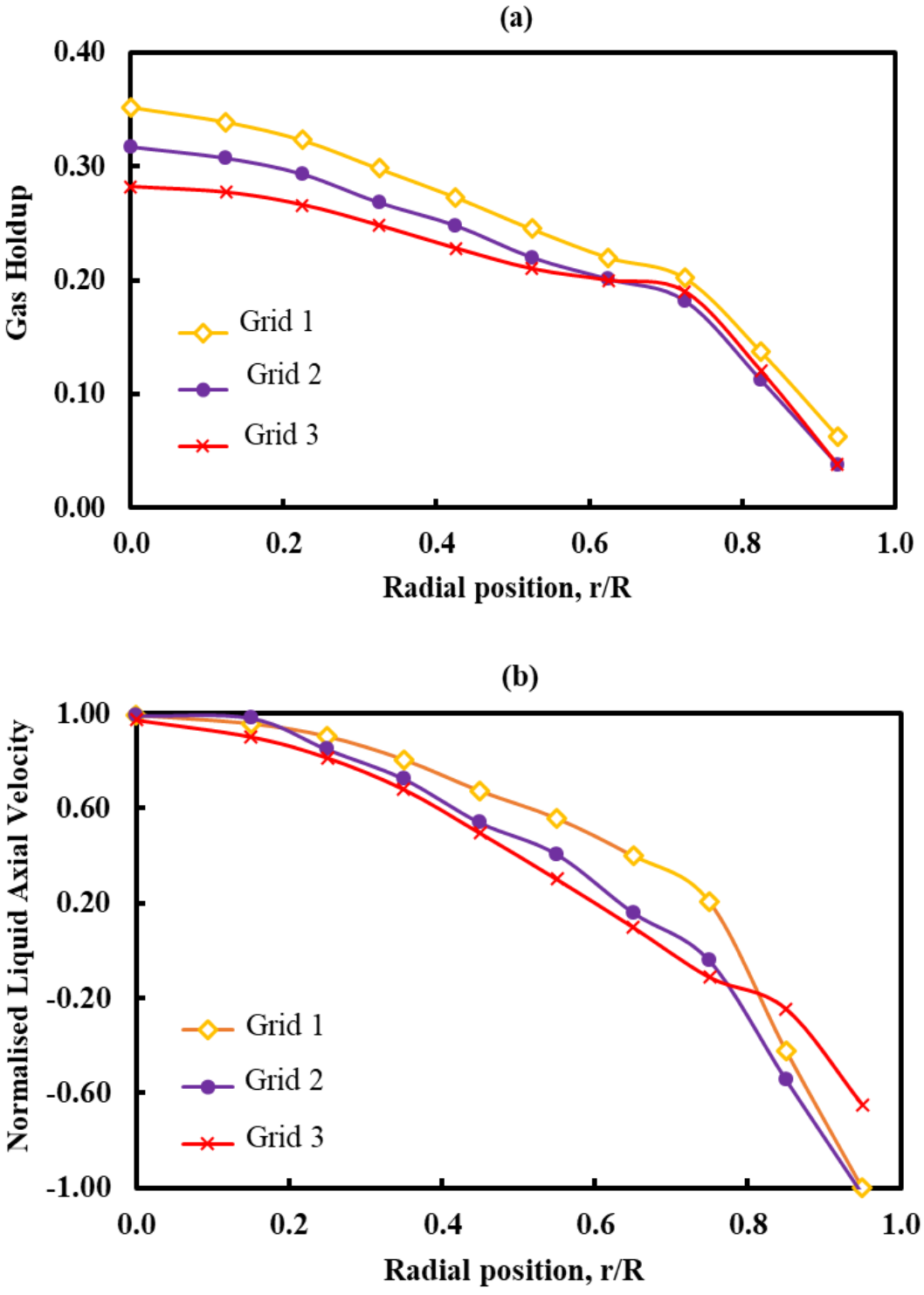

Figure 2- 3 Grid sensitivity test results on radial distribution of (a) gas holdup and (b) normalized liquid axial velocity

(a)

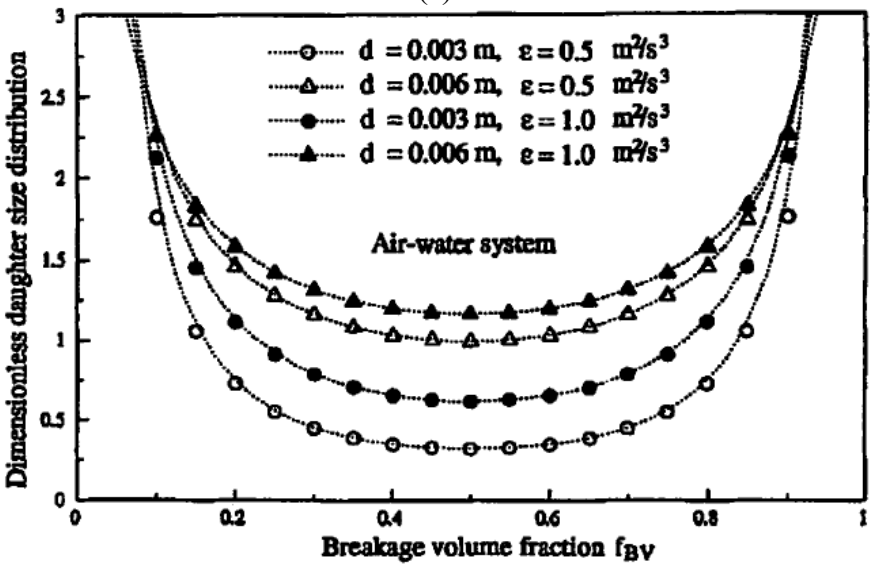

(b)

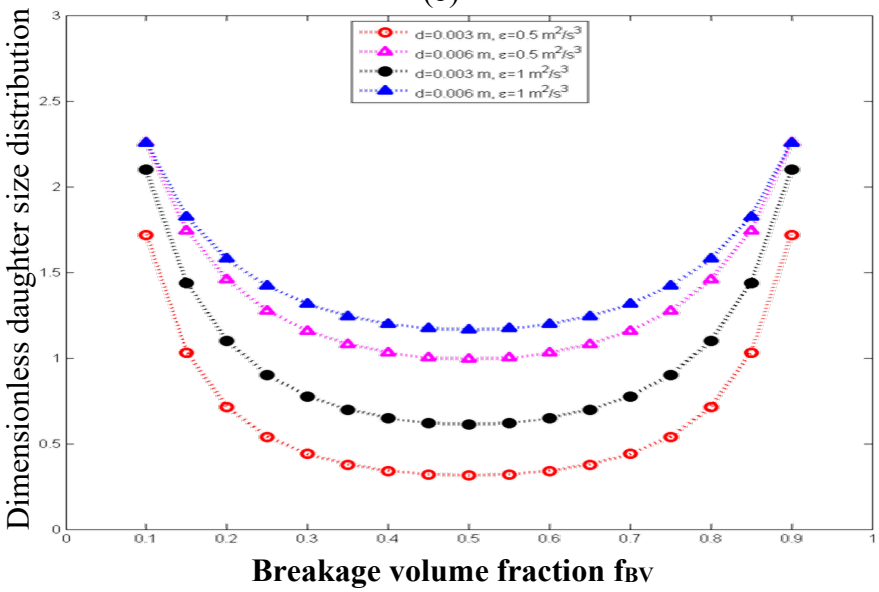

Figure 2- 4 Effect of bubble size and energy dissipation rate per unit mass on the dimensionless daughter bubble sized distribution for the air-water system: (a) is taken from Luo and Svendsen (1996) and (b) is calculated in this work (the symbols are used for distinguishing the different conditions)

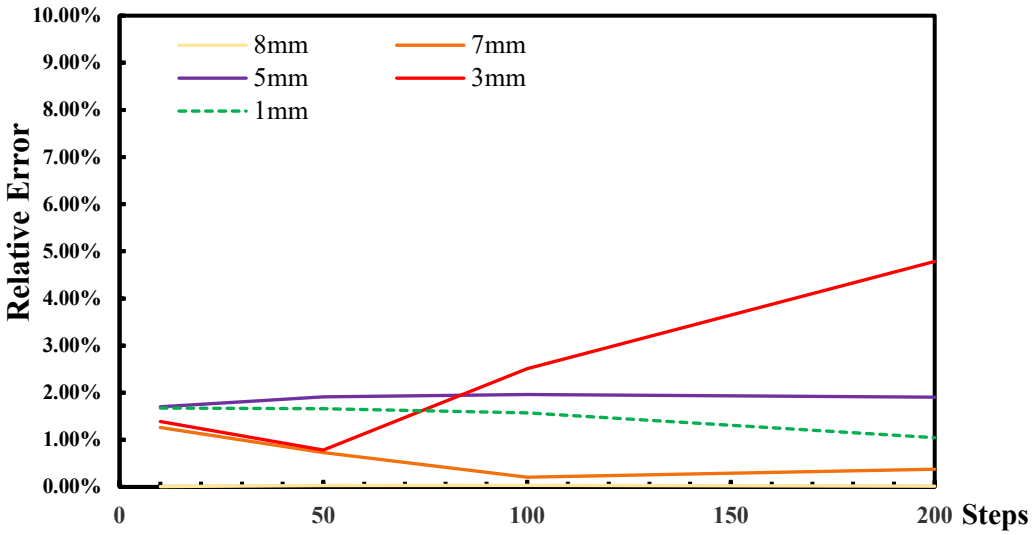

Figure 2- 5 Relative error of predicted bubble size distribution of numerical method to built-in module

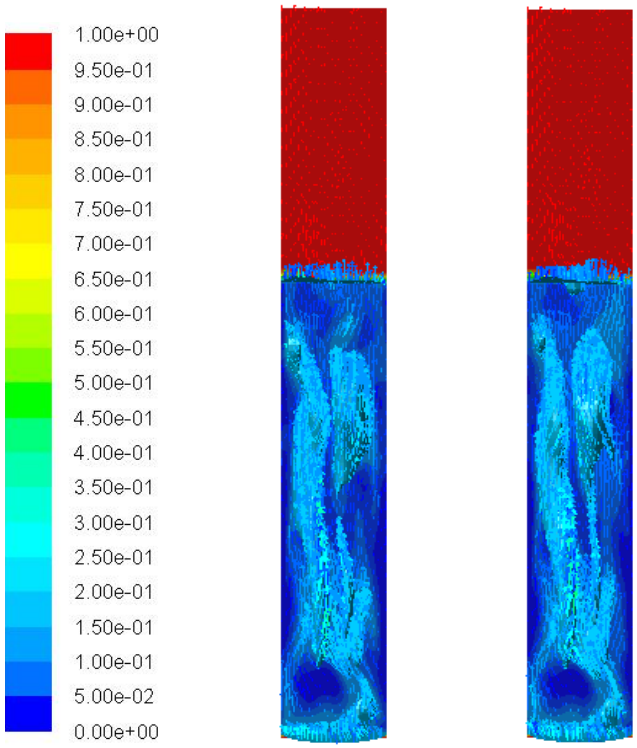

Figure 2- 6 Instantaneous iso-surface of the gas holdup α_g= 0.2 in x-plane

(Left: numerical method; Right: built-in module)

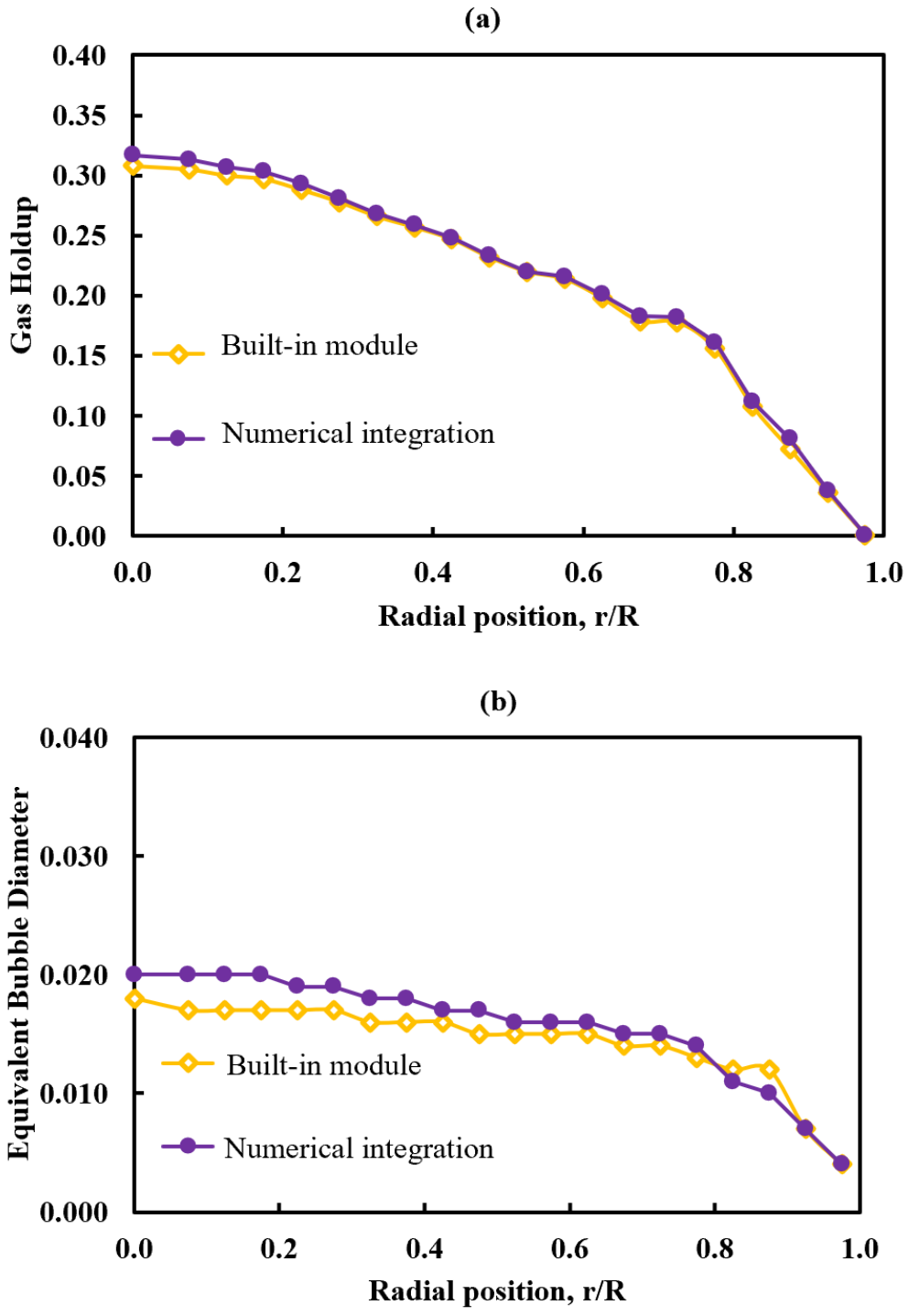

Figure 2- 7 Radial distribution of (a) gas holdup (b) equivalent bubble diameter d_{32}

* Built-in module represents the built-in 'population balance model' model in software ANSYS FLUENT 17.0

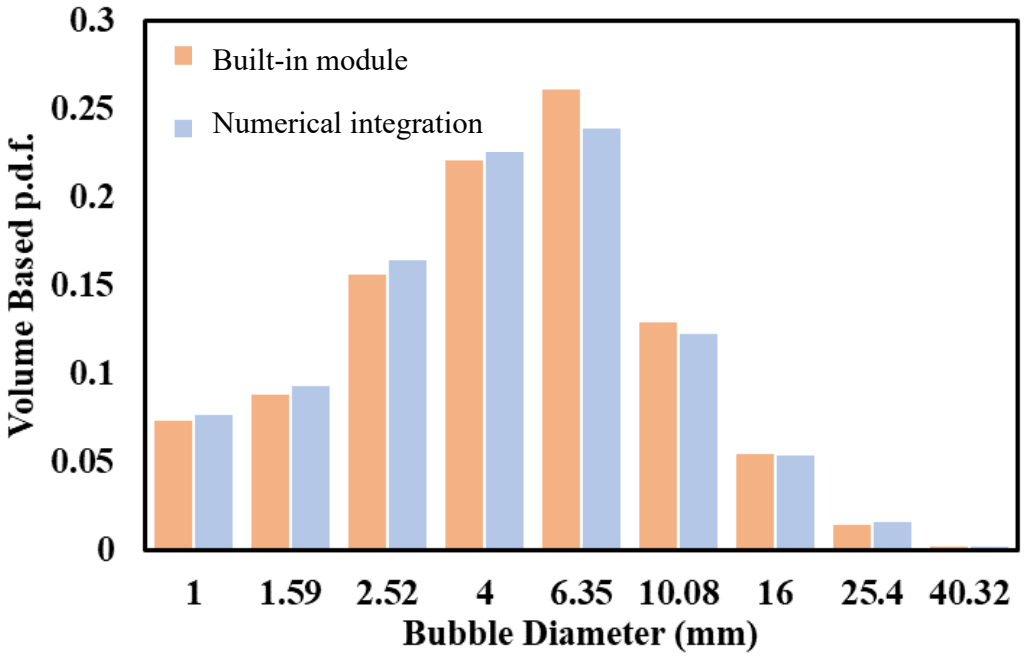

Figure 2- 8 Bubble class volume-based probability density function

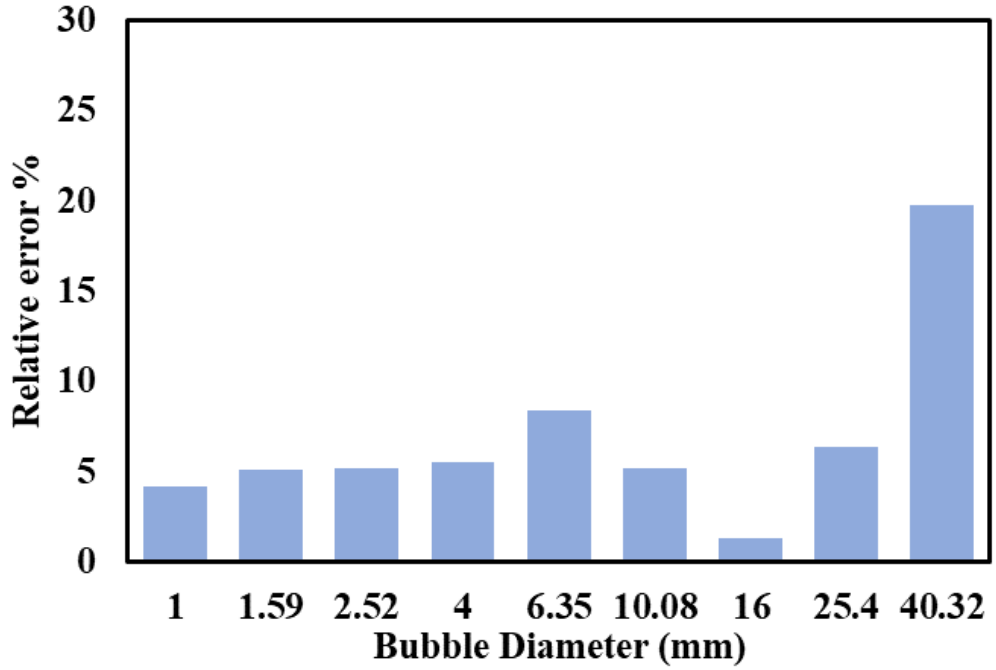

Figure 2- 9 Relative error of bubble size distribution

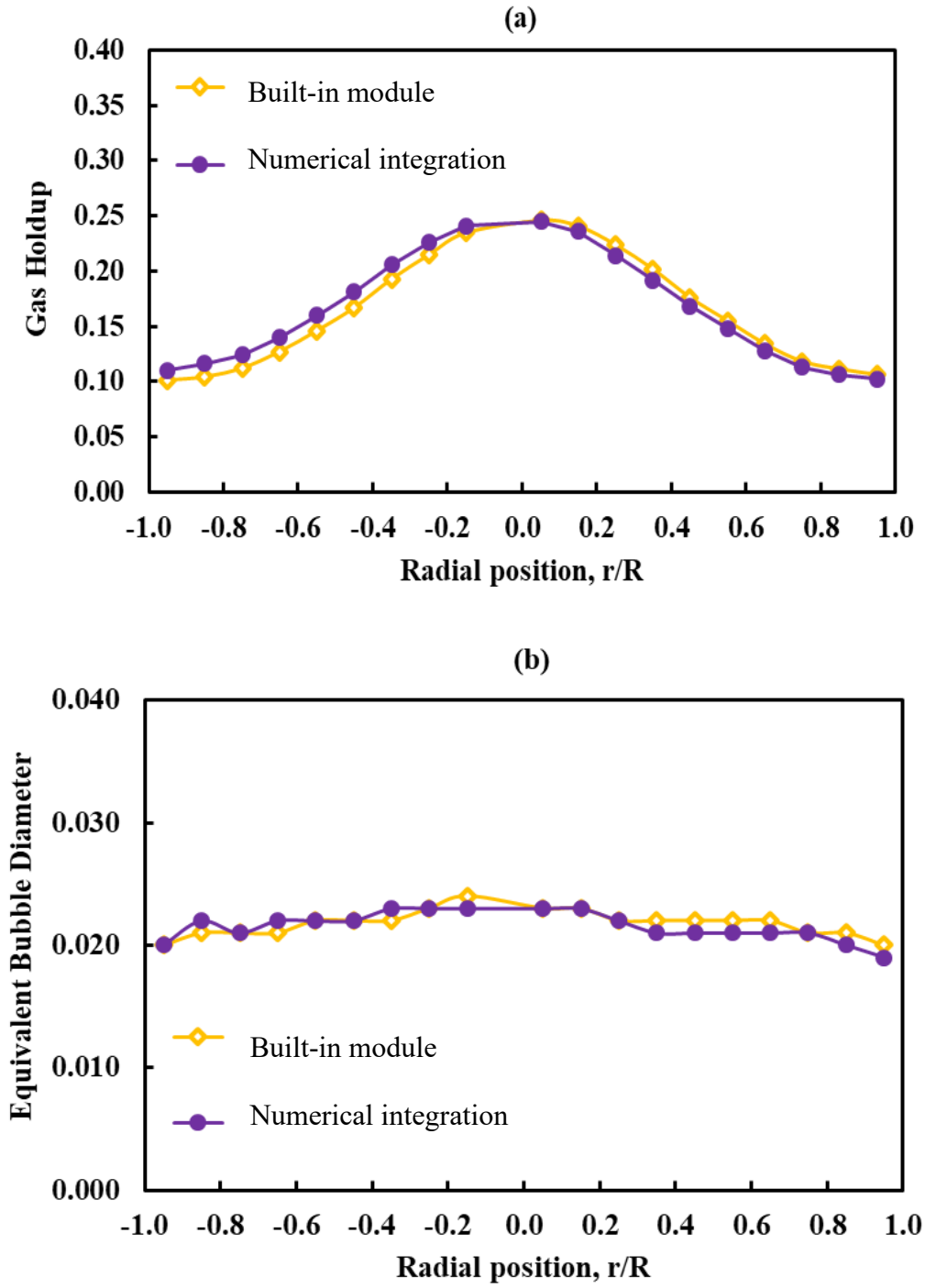

Figure 2- 10 Simulation result of (a) Time-averaged radial distribution of gas holdup, and (b) radial distribution of equivalent bubble diameter d_{32}

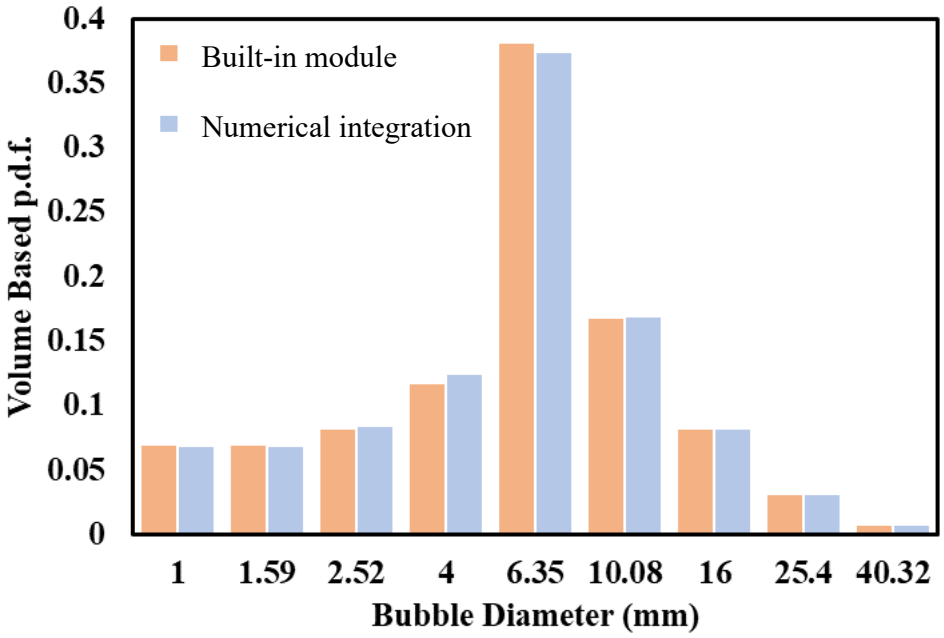

Figure 2- 11 Bubble class volume-based probability density function

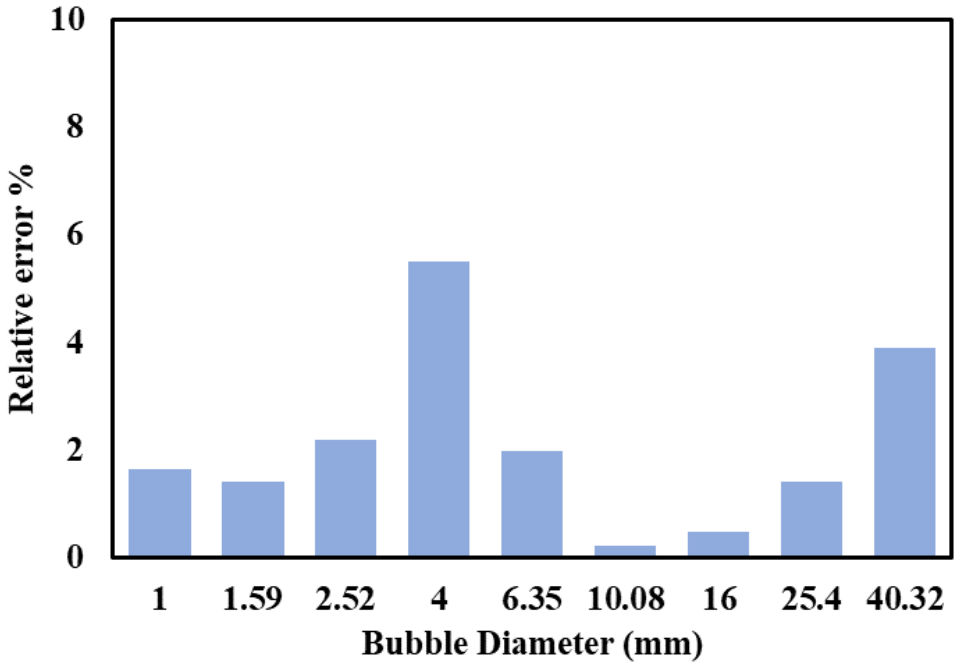

Figure 2- 12 Relative error of each class

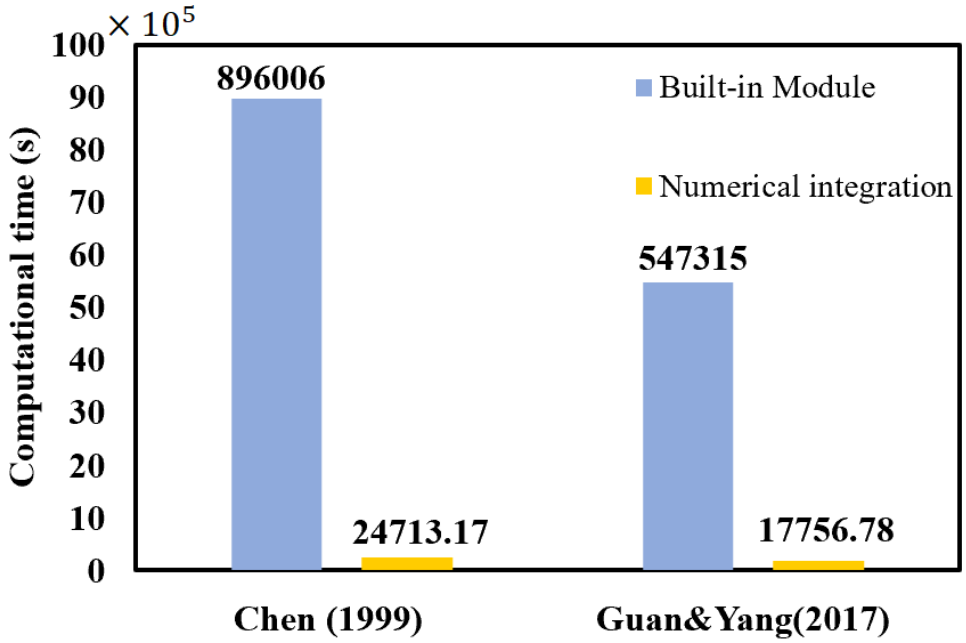

Figure 2- 13 Comparison of the computational time of two selected cases

CHAPTER 3: CFD-PBM MODELLING OF GAS-LIQUID TWO-PHASE FLOW IN BUBBLE COLUMN REACTOR ACCOUNTING THE EFFECT OF EDDY-BUBBLE INTERACTION AND BUBBLE-INDUCED TURBULENCE

SUMMARY

When studying the eddy-bubble interaction, the effect of bubble response to the surrounding eddies and bubble-induced turbulence cannot be neglected. This chapter will discuss this effect on CFD-PBM modelling. With the consideration of the bubble response to the eddies with a similar turbulence length scale, a modified turbulent viscosity model is proposed, while the bubble size distribution is predicted by a modified breakup model considering bubble-induced turbulence energy spectrum. The simulation results compare with the experimental data have clearly demonstrated that the modified model effectively describes the influence of bubble-eddy response in bubble columns. It is revealed that the interaction of bubbles with the bubble-induced turbulence eddies dominates the turbulence generated in in bubble column flows.

1. INTRODUCTION

Bubble columns are typical multiphase contacting system which are intensively used in chemical and biochemical industry due to the simple structure, high efficiencies of heat and mass transfer. Investigation of the behaviour and interaction of different phases is beneficial for achieving better performance, in which numerical modelling can play an important role.

CFD simulations of bubble columns mainly adopt two approaches, namely Eulerian-Eulerian (E-E) and Eulerian-Lagrangian (E-L). In the Eulerian-Lagrangian approach, the continuous phase is solved in Eulerian frame while the dispersed phase is simulated from the pathways of a large number of bubbles. This method can give the direct physical interpretation of the interaction between two phases, which can easily demonstrate the bubble-bubble interactions. Literatures of simulation using E-L approach can be found from Delnoij et al. (1999), Kuipers and van Swaaij (1998), Sokolichin et al. (1997)

Muniz and Sommerfeld (2020). However, in order to guarantee the simulating precision of bubble motion, the grid size of numerical simulation is limited by the bubble size, and the number of equations to be solved increases with the increase of the number density of bubbles. E-L approach is limited to low velocity and volume fraction of the dispersed phase (Tabib et al., 2008). On the other hand, the Eulerian-Eulerian approach, as known as two-fluid model, considers the two phases as interpenetrating continua (Zhang et al., 2006, Borchers et al., 1999, Ekambara et al., 2005, Pfleger et al., 1999). The computational demand is much

lower comparing with the E-L approach, therefore the E-E approach is more economical and more popular.

In bubble column simulation, an important area of interest is the modelling of bubble-induced turbulence. In bubble column, liquid fluctuations are induced when bubbles go up through the column, which is called as bubble induced turbulence or pseudo-turbulence. Bubble-induced turbulence fluctuations are reflected in energy spectrum, as the energy cascade of bubble-induced turbulence is different from that of homogeneous single-phase turbulence, especially for large-scale system (Roghair et al., 2011). In present state, most studies of bubbly flow have determined the kinetic energy of eddies by the classical Kolmogorov -5/3 scaling law for the inertial subrange which is the same as single-phase turbulence (Luo and Svendsen, 1996, Lehr et al., 2002, Andersson and Andersson, 2006, Wang et al., 2003, Hagesaether et al., 2002, Bhole et al., 2008, Zhao and Ge, 2007). However, this assumption may be not appropriate as the effect of bubble-induced turbulence would be the predominant part, especially for the system with high superficial gas velocity.

In order to investigate the characteristics of bubble-induced turbulence, Lance and Bataille (1991) measured the energy spectrum of the fluctuations caused by a swarm of bubbles rising through an imposed turbulent flow using hot-wire constant-temperature anemometry (CTA) and laser Doppler anemometry (LDV). They found the behaviour of energy spectrum in high wave number range obeys -8/3 scaling law, in contrast to the classical -5/3 energy spectrum scaling for homogeneous single-phase turbulence. They attributed the change of scaling to the

wake dissipation effect, in which eddies produced were dissipated rapidly before the spectral transfer has even taken place. They also have done scaling analysis and got an exponent of -3 which is close to the experimental value. The view of κ^{-3} in pseudo-turbulence is established in many research works in experimental method (Riboux et al., 2010, Murai et al., 2000, Bouche et al., 2014, Mercado et al., 2010, Prakash et al., 2016, Mendez-Diaz et al., 2013) and numerical simulations (Roghair et al., 2011, Sugiyama et al., 2001, Riboux et al., 2013, Bunner and Tryggvason, 2002). In these works, the effect of bubble-induced turbulence is reflected on the turbulence energy spectrum with the κ^{-3} scaling law in the inertial subrange, which is close to the range of the bubble size distribution (Risso et al., 2008, Roig and de Tournemine, 2007, Risso, 2011).

Due to the unneglectable effect on power law scaling of pseudo-turbulence, it is important to use proper turbulence models in bubbly flow modelling. The research on turbulence models for bubbly flow is still at the beginning stage, and there is still no a generally acceptable model for bubbly flows (Sokolichin et al., 2004). Some reported CFD simulation work consider the effect of bubble-induced turbulence on the effective viscosity, a typical model from Sato and Sekoguchi (1975) predicts the turbulent viscosity due to BIT by the bubble size and slip velocity. However, Shu et al. (2020) indicated that the total turbulence kinetic energy might be underestimated without the consideration of the contribution of bubble-induced turbulence on turbulence kinetic energy. In contrast, a source-term generated by bubble-induced turbulence is added directly in the transport equations of turbulent variables (Pfleger and Becker, 2001, Troshko and Hassan, 2001, Rzehak and Krepper, 2013).

There are different expressions of the source-terms of the contribution of BIT in transport equations, but most of them are proposed by assuming the contribution to turbulence kinetic energy from BIT is equal to power input generated by interfacial forces. The generation of turbulent kinetic energy leads to additional dissipation, thus the source-term representing the generation of turbulence dissipation rate due to the contribution of BIT is added by assuming that turbulence kinetic energy is dissipated at the characteristic timescale. Pfleger and Becker (2001) calculated that the characteristic timescale from the Kolmogorov length scale and the velocity scale from overall turbulent fluctuations. While Troshko and Hassan (2001) and Liao et al. (2019) proposed the model at macroscopic scale which employed bubble diameter and slip velocity as characteristic scale to find the characteristic timescale. However, these model adding source-terms in transport equations still not yield a better performance on both the mean flow field and turbulent quantities (Magolan et al., 2019). It can be assumed that the effect of BIT on bubbly flow may comprise two parts, the modulation in continuous phase and the interfacial interaction, represented as the term of turbulent viscosity and source-terms in transport turbulence variables in models respectively.

It should be pointed out that Sato's turbulent viscosity model accounting for the BIT in two-phase flow was derived from the assumption of the surrounding flow of a fixed bubble as the flow about a cylinder. Whereas, in reality, bubble may not follow the movement of turbulent eddy faithfully, thus there is response between bubble and the turbulent eddies entrain bubbles. Long et al. (2020) assessed bubble response in large eddy simulation by a modified Smagorinksy sub-grid scale model. This eddy-bubble response should also be taken into account in Eulerian-Eulerian

framework. When considering this type of bubbles' dynamic response to eddies, the bubble may be likely trapped by the eddy or escapes from the eddy trapping due to the buoyance effect. Hence, the slip velocity between the bubble and its surrounding turbulent eddies is influenced, especially when the eddy size is as the same order as bubble.

In addition, the bubble size distribution is the most important governing parameter to understand the hydrodynamics within bubble columns, proper prediction of bubble size distribution is crucial as it affects heat and mass transfer in bubble column. To determine the bubble size distribution, the population balance model (PBM) is employed to describe the bubble breakup and coalescence processes in bubble column in many literatures (Luo and Svendsen, 1996, Tsouris and Tavlarides, 1994). However, most proposed bubble breakup model ignore the contribution of bubble-induced turbulence and thus model the kinetic energy of the bombarding eddies to hit the bubbles by using the classical single-phase turbulence Kolmogorov -5/3 scaling law. With the consideration of the κ^{-3} scaling of the contribution of BIT energy spectrum on the bubble breakage, our previous work, Shi et al. (2019), proposed a modified breakage model accounting for the effect of the bubble-induced turbulence energy spectrum distribution,

Therefore, the aim of the current work is to implement a modified turbulent viscosity model considering eddy-bubble response and bubble breakup model with the consideration of bubble-induce turbulence energy spectrum into a CFD-PBM coupled simulation based on Eulerian-Eulerian frame. Section 2 will present the model development in the current study while Section 3 will present the numerical

details in CFD simulations conducted in this work. Section 4 will present the simulation results and discussion focusing on the effect of the bubble response to the surrounding turbulent eddies and the contribution bubble-induced turbulence on turbulent energy spectrum on the prediction of key parameters including gas holdup, bubble breakage rate and bubble size distribution function (PDF). Section 5 will present the conclusions derived from this study.

2. MODEL DEVELOPMENT

2.1 Governing equations

A three-dimensional transient CFD model is employed in this work to simulate the local hydrodynamics of the gas-liquid two-phase bubble column. An Eulerian-Eulerian approach is adopted to describe the flow behaviours for both phases, i.e. water as the continuous phase, and air as the dispersed phase. The mass and momentum balance equations are given by equations (3-1) and (3-2) respectively,

$$\frac{\partial(\rho_k \alpha_k)}{\partial t} + \nabla(\rho_k \alpha_k u_k) = 0 \tag{3-1}$$

$$\frac{\partial(\rho_k \alpha_k u_k)}{\partial t} + \nabla(\rho_k \alpha_k u_k u_k) = -\alpha_k \nabla p + \nabla \cdot \tau_k + \alpha_k \rho_k g + F_k \tag{3-2}$$

where the lower index k represents the phase (liquid or gas), with ρ_k, α_k, $\boldsymbol{u}_k$, $\boldsymbol{\tau}_k$, and $\boldsymbol{F}_k$ denote the density, volume fraction, velocity vector, viscous stress tensor and the inter-phase momentum exchange term respectively. The sum of the volume fractions for both phases is equal to 1. The stress term can be defined as equation (3-3),

$$\bar{\bar{\boldsymbol{\tau}}}_{\boldsymbol{k}} = -\mu_{eff}\left(\nabla \boldsymbol{u}_{\boldsymbol{k}} + (\nabla \boldsymbol{u}_{\boldsymbol{k}})^T - \frac{2}{3} I(\boldsymbol{\nabla} \cdot \boldsymbol{u}_k)\right) \tag{3-3}$$

where μ_{eff} represents the effective viscosity for liquid phase which is caused by the modelling of turbulent transport. According to Dhotre et al. (2008), the effective viscosity can be defined as the sum effect of the molecular viscosity μ_l, the turbulent viscosity μ_t and an additional term to model bubble induced turbulence μ_{BI}, as shown as:

$$\mu_{eff,l} = \mu_l + \mu_t + \mu_{BI}. \tag{3-4}$$

where μ_l is the molecular dynamic viscosity.

The bubble induced turbulence is considered by the model proposed by Sato et al. (1981), which is expressed as:

$$\mu_{BI} = \rho_l C_{\mu,BI} \alpha_g d_B \left|\boldsymbol{u}_g - \boldsymbol{u}_l\right|. \tag{3-5}$$

with a model constant $C_{\mu,BI} = 0.6$.

2.2 Turbulence modelling

In this work, turbulence model, the standard *k*-*ε* model, is employed as given below:

$$\frac{\partial(\alpha_l \rho_l k_l)}{\partial t} + \nabla \cdot (\alpha_l \rho_l k_l \boldsymbol{u}_k) = \nabla \cdot \left[\alpha_l \left(\mu_l + \frac{\mu_{eff,l}}{\sigma_k}\right) \nabla k_l\right] + \alpha_l \left(G_{k,l} - \rho_l \varepsilon_l\right) + S_k \tag{3-6}$$

$$\frac{\partial(\alpha_l \rho_l \varepsilon_l)}{\partial t} + \nabla \cdot (\alpha_l \rho_l \varepsilon_l \boldsymbol{u}_k) = \nabla \cdot \left[\alpha_l \left(\mu_l + \frac{\mu_{eff,l}}{\sigma_k}\right) \nabla \varepsilon_l\right] + \alpha_l \frac{\varepsilon_l}{k_l} \left(C_{1\varepsilon} G_{k,l} - C_{2\varepsilon} \rho_l \varepsilon_l\right) + S_\varepsilon \tag{3-7}$$

where k and ε represent the turbulent kinetic energy and the turbulent dissipation rate respectively. G_k represents the production of turbulent kinetic energy. S_k and S_ε are source terms.

2.3 Interphase momentum transfer

In this study, drag force and added mass force are considered as the main interactions between the continuous phase and dispersed phase.

Drag force

The drag force is generated due to the relative motion of bubbles and the surrounding liquid flow, which is calculated as:

$$\boldsymbol{F}_D = \frac{3}{4}\frac{C_D}{d_b}\rho_l \alpha_g \left|\boldsymbol{u}_g - \boldsymbol{u}_l\right|\left(\boldsymbol{u}_g - \boldsymbol{u}_l\right) \tag{3-8}$$

where C_D is the drag coefficient, which can be obtained from the model of Grace et al. (1978) model. Grace et al. (1978) drag model is shown as:

$$C_D = max\left(C_{D,sphere},\, min\left(C_{D,ellipse},\, C_{D,cap}\right)\right) \tag{3-9}$$

$$\begin{cases} C_{D,sphere} = \begin{cases} \dfrac{24}{Re_b} & Re_{eb} < 1000 \\ \dfrac{24}{Re_b}\left(1 + 0.15Re_b^{0.687}\right) & Re_{eb} \geq 1000 \end{cases} \\ C_{D,cap} = \dfrac{8}{3} \\ C_{D,ellipse} = \dfrac{4}{3}\dfrac{g d_{eq}}{U_t^2}\dfrac{\left(\rho_l - \rho_g\right)}{\rho_l} \end{cases}$$

where the relative number can be calculated as follows:

$$Re_b = \frac{\rho_l \left|\boldsymbol{u}_g - \boldsymbol{u}_l\right| d_b}{\mu_l} \qquad U_t = \frac{\mu_l}{\rho_l d} M_O^{-0.149}(J - 0.857)$$

$$M_O = \frac{\mu_l^4 \boldsymbol{g}\left(\rho_l - \rho_g\right)}{\rho_l^2 \sigma^3} \qquad J = \begin{cases} 0.94H^{0.757} & 2 < H < 59.3 \\ 3.42H^{0.441} & H \geq 59.3 \end{cases}$$

$$H = \frac{4}{3}E_O M_O^{-0.149}\left(\frac{\mu_l}{\mu_{ref}}\right)^{-0.14} \qquad \mu_{ref} = 0.0009\ kg/(ms)$$

Virtual mass force

Considering the relative acceleration of bubble surrounding liquid due to the acceleration induced bubble motion, the effect is modelled by virtual mass force. The mathematical expressions of virtual mass force have derived by Auton et al. (1988), as shown as equation (3-8)

$$\boldsymbol{F_{VM}} = \alpha_g \rho_l C_{VM} \left(\frac{D\boldsymbol{u_g}}{Dt} - \frac{D\boldsymbol{u_l}}{Dt} \right) \tag{3-10}$$

where C_{VM} is the virtual mass coefficient and a constant value of 0.5 is employed in this chapter.

2.4 Eddy-bubble response

The bubble motion equation, which only considers drag and virtual mass forces, is expressed as:

$$\rho_b V_b \frac{d\boldsymbol{u}_b}{dt} = \rho_b V_b \frac{\rho_l}{\rho_b} \frac{D\boldsymbol{u}_l}{Dt} + \frac{3}{4} \frac{\rho_l}{\rho_b d_b} \rho_b V_b C_D (\boldsymbol{u}_l - \boldsymbol{u}_b) |\boldsymbol{u}_l - \boldsymbol{u}_b| + C_{VM} \rho_b V_b \frac{\rho_l}{\rho_b} \left(\frac{D\boldsymbol{u}_l}{Dt} - \frac{d\boldsymbol{u}_b}{dt} \right) \tag{3-11}$$

As both the continuous phase and dispersed phase are solved in Eulerian frame, it can be assumed that $\frac{d\boldsymbol{u}_B}{dt} \sim \frac{D\boldsymbol{u}_B}{Dt}$. Most of researches, e.g. Prince and Blanch (1990), assumed the bubble velocity is same as that of a liquid eddy with bubble size, however, bubbles do not response the liquid eddy movement immediately, due to the slip velocity between two phases, the bubbles tend to escape from the controlling from the eddies where they are entrapped (Bhole et al., 2008). With the

consideration of the response of bubble fluctuation $\boldsymbol{u'}_b$ to eddy fluctuation $\boldsymbol{u'}_l$, the equation (3-11) is derived into:

$$(\rho_b + C_{VM}\rho_l)\frac{D\boldsymbol{u'}_{rel}}{Dt} = (\rho_l - \rho_b)\frac{D\boldsymbol{u}_l}{Dt} - \frac{3}{4}\frac{\rho_l C_D}{d_b}\boldsymbol{u'}_{rel}|\boldsymbol{u'}_{rel}| \qquad (3\text{-}12)$$

where the relative velocity in fluctuation motion $\boldsymbol{u'}_{rel}$ is defined as $\boldsymbol{u'}_{rel} = \boldsymbol{u'}_b - \boldsymbol{u'}_l$.

Considering the interaction mainly occurs between bubbles and the eddy with the same order of size which falls into the inertial subrange, Levich (1962) proposed the following relations of turbulence fluctuation: $\frac{d\boldsymbol{u'}_{rel}}{dt} = \frac{\boldsymbol{u'^2}_{rel}}{\lambda}$, $\boldsymbol{u'}_l = (\varepsilon\lambda)^{\frac{1}{3}}$, $d\boldsymbol{u'}_l/dt = \varepsilon^{\frac{2}{3}}/\lambda^{\frac{1}{3}}$, where λ is the turbulence eddy scale. By substituting these relations into equation (3-12), we can get

$$\boldsymbol{u'}_{rel} = \boldsymbol{u'}_b - \boldsymbol{u'}_l = \left(\frac{\rho_l - \rho_b}{\rho_b + C_{VM}\rho_l + \frac{\rho_b \lambda}{St_b \Delta}}\right)^{1/2}(\varepsilon\lambda)^{\frac{1}{3}} \qquad (3\text{-}13)$$

where St is stokes number and is given as $St_b = \frac{\tau_{\text{bubble}}}{\tau_l}$, the bubble response time scale is defined as $\tau_{\text{bubble}} = \frac{\rho_b d_b^2}{18\mu_l}$, and the liquid response time scale $\tau_l = \frac{\Delta}{\boldsymbol{u'}_{rel}}$. In this work, Reynolds averaging Navier-stokes model is employed, the length scale Δ can be considered as grid size.

Therefore, the modified bubble fluctuating velocity with the consideration of the bubble-eddy response is shown as:

$$\boldsymbol{u'}_b = \left(\frac{(\rho_l - \rho_b)^{1/2}}{(\rho_b + C_{VM}\rho_l + \frac{\rho_b \lambda}{St\,\Delta})^{1/2}} + 1\right)\boldsymbol{u'}_l \qquad (3\text{-}14)$$

According to Garcia (2001), the additional turbulence dissipation due to the bubbles corresponds to the inertial subrange can be assumed that mainly occurs

near the characteristic length scale λ^* where the relative fluctuating velocity is maximum, which can be represented by:

$$-\tau_{ij}\overline{S_{ij}}|_g \sim \rho_l C_D \left(\frac{\rho_l}{\rho_b}\right)\frac{u'^3_{\mathrm{rel}}}{d_b}\alpha_g \tag{3-15}$$

Substituting of relative fluctuating velocity into (3-15), and

$$-\tau_{ij}\overline{S_{ij}}|_g = C_g \rho_l \varepsilon \alpha_g \frac{\lambda}{d_b}\left(\frac{\rho_l-\rho_b}{\rho_b+C_{VM}\rho_l+\frac{\rho_b}{St_b}\frac{\lambda}{\Delta}}\right)^{3/2} \tag{3-16}$$

where the constant C_g is estimated by the comparison of series of trials with experimental results. Therefore, the total dissipation is calculated as:

$$-\tau_{ij}S_{ij} = \rho_l \varepsilon\left(1 + C_g \alpha_g \frac{\lambda}{d_b}\left(\frac{\rho_l-\rho_b}{\rho_b+C_{VM}\rho_l+\frac{\rho_b}{St_b}\frac{\lambda}{\Delta}}\right)^{3/2}\right) \tag{3-17}$$

Employing the eddy-viscosity model:

$$\mu_t = \rho_l C_\mu \frac{k^2}{\varepsilon} \tag{3-18}$$

The modified turbulent viscosity with the consideration of the bubble-eddy response can be estimated as:

$$\mu_{t,total} = \rho_l C_\mu \frac{k^2}{\varepsilon\left(1+C_g\alpha_g\frac{\lambda}{d_b}\left(\frac{\rho_l-\rho_b}{\rho_b+C_{VM}\rho_l+\frac{\rho_b}{St_b}\frac{\lambda}{\Delta}}\right)^{3/2}\right)} \tag{3-19}$$

Substituting equation (3-19) into (3-4), the effect viscosity is:

$$\begin{aligned}\mu_{eff,l} &= \mu_l + \mu_{t,total} + \mu_{BI,sato} \\ &= \mu_l + \rho_l C_\mu \frac{k^2}{\varepsilon\left(1 + C_g\alpha_g\frac{\lambda}{d_b}\left(\frac{\rho_l-\rho_b}{\rho_b+C_{VM}\rho_l+\frac{\rho_b}{St_b}\frac{\lambda}{\Delta}}\right)^{3/2}\right)} + \rho_l C_{\mu,BI}\alpha_g d_B\left|\boldsymbol{u}_g - \boldsymbol{u}_l\right|\end{aligned} \tag{3-20}$$

where μ_l is the molecular viscosity.

2.5 Bubble size distribution

MUSIG model, i.e. population balance model, is employed to determine the bubble size distribution under the consideration of bubble coalescence and breakup. Bubbles are divided into several size classes with different diameter d_i. For each class, an equation of number density of bubble is solved to show the population changes resulted from bubble coalescence and breakage. The equation is shown as equation (3-21),

$$\frac{\partial n_i}{\partial t} + \nabla \cdot (\boldsymbol{u}_i n_i) = S_i \tag{3-21}$$

where n_i is the number density of bubbles for i-th group, $\boldsymbol{u}_i$ is the mass average velocity vector, and S_i is the source term. Assuming each bubble group move with the same mean algebraic velocity, the source term can be expressed as the birth and death of bubbles due to coalescence and breakup respectively (Kumar and Ramkrishna, 1996), as shown as:

$$S_i = B_{coalescence,i} - D_{coalescence,i} + B_{breakup,i} - D_{breakup,i}$$
$$= \sum_{V_j=V_{min}}^{\frac{V_i}{2}} \Omega_C(V_j : V_i - V_j) - \sum_{V_j}^{V_{max}-V_i} \Omega_C(V_j : V_i) + \sum_{V_j=V_i}^{V_{max}} \Omega_B(V_j : V_i) - \Omega_B(V_i) \tag{3-22}$$

where V_i is the volume for the i-th class.

The local gas volume fraction and the Sauter mean diameter d_{32} can be calculated as follows:

$$\alpha_g f_i = n_i V_i \tag{3-23}$$

$$d_{32} = 1 \Big/ \left(\sum_{i=1}^{N} \frac{f_i}{d_i} \right) \tag{3-24}$$

where f_i is the i-th class fraction of total volume fraction.

Bubble breakup

The classical breakup model is proposed by Luo and Svendsen (1996), which considers eddy-bubble collision and probability of breakage due to bubble instability. The breakage rate for one individual parent bubble of size d_i breaking into daughter classes d_j can be expressed by equation (3-25),

$$\Omega_B(d_i: d_j) = \int_{\lambda_{min}}^{d} \omega_B^T(d_i, \lambda) p_B(d_i, d_j, \lambda) d\lambda \tag{3-25}$$

where p_B is the breakage probability function and ω_B^T is the eddy-bubble collision probability density which is determined by the eddy number density and mean turbulent fluctuation velocity based on the collision tube theory.

However, bubble breakage can be greatly affected by the hydrodynamics of the continuous phase and the interfacial interactions (Jakobsen et al., 2005). Considering the effect of bubble-induced turbulence, the eddy number density and mean turbulent fluctuation velocity are influenced due to the modified BIT energy spectrum. Based on the binary breakup model of Luo and Svendsen (1996), a modified bubble breakup model (Shi et al., 2019) is derived from BIT energy spectrum distribution, as shown as equation (3-26).

$$\Omega_B(d_i: d_j) = 0.923(1-\alpha_g) n_i \left(\frac{\varepsilon}{d_i^2}\right)^{\frac{1}{3}} \int_{\frac{\Lambda}{d_i}}^{1} \frac{(1+\xi)^2}{\xi^{\frac{11}{3}}} exp\left(-\frac{12\sigma C_f}{\beta \rho_l \varepsilon^{\frac{2}{3}} d_i^{\frac{5}{3}} \xi^{\frac{11}{3}}}\right) d\xi$$
$$+C_4(1-\alpha_g) n_i \sqrt{C_b \frac{\alpha_g g U_{Slip}}{\nu}} \int_{\xi_{min}}^{\frac{\Lambda}{d_i}} \frac{(1+\xi)^2}{\xi^{\frac{11}{3}}} exp\left(-\frac{12\sigma C_f}{\beta \rho_l C_b \frac{\alpha_g g U_{Slip}}{\nu} d_i^3 \xi^5}\right) d\xi \tag{3-26}$$

$$C_f = f_V^{2/3} + (1-f_V)^{2/3} - 1 \tag{3-27}$$

where ξ is the size ratio between an eddy and a bubble which is calculated from $\xi = \lambda / d_i$, and C_f is the increase coefficient of surface area which is determined by the breakage volume fraction $f_V = d_j^3 / d_i^3$. The lower integral limit is the minimum size of eddies falling into the inertial subrange $\xi_{min}=11.4\eta/d_i$, while the higher limit depends on the characteristic length scale Λ.

The bubble breakup model is derived based on binary breakage assumption, equation (3-26) is symmetrical with $f_V = 0.5$, therefore, the dimensionless daughter bubble size distribution can be derived from:

$$\beta(d_i: d_j) = \frac{2\Omega_B(d_i:d_j)}{\int_0^1 \Omega_B(d_i:d_j)df_V} \tag{3-28}$$

Bubble coalescence

When considering the effect of bubble-induced energy spectrum, the modification of the mean turbulent eddy velocity also has impact on the predicted coalescence rate in comparison of that of classical energy spectrum. However, the effect may not be as fundamental as that for bubble breakup prediction (Shi et al., 2019). Therefore, the influence of bubble-induced turbulence on the coalescence model is neglected. For describing the process of coalescence between bubbles of size d_i and d_j, Luo (1993) coalescence model is implemented in this work, which is based on the drainage of liquid films between two collision bubbles, as shown as

$$\Omega_C(d_i: d_j) = n_i n_j \frac{\pi}{4}(d_i + d_j)^2(\bar{u}_i^2 + \bar{u}_j^2)^{\frac{1}{2}} \exp\left(-c_1 \frac{\left[0.75\left(1+x_{ij}^2\right)\left(1+x_{ij}^3\right)\right]^{1/2}}{\left(\rho_g/\rho_l+0.5\right)^{1/2}\left(1+x_{ij}\right)^3} We_{ij}^{1/2}\right) \tag{3-29}$$

where c_1 is a constant of order unity that usually equals to, x_{ij} is the size ratio of two colliding bubbles $x_{ij}=d_i / d_j$ and We_{ij} the Weber number.

3. NUMERICAL MODELLING

To evaluate the effect of bubble-induced turbulence and eddy-bubble response, numerical simulations of liquid-gas bubble columns have been conducted based on the work of Chen et al. (1999) and Guan and Yang (2017). The details of experiments are presented in Table 3-1.

Table 3- 1 Details of experimental set-up of selected cases

Experiment	Diameter (m)	Height (m)	Superficial Gas Velocity (m/s)	Static Liquid Height (m)	Observation Height (m)
Chen et al. (1999)	0.44	2.44	0.1	0.9	1.32
Guan and Yang (2017)	0.15	1.6	0.05	1.2	0.8

The 3D transient CFD-PBM modelling was performed by the ANSYS FLUENT 17.0. The time step was set as 0.001s initially and gradually increased to 0.005s for all simulations, while the simulated results is averaged for typically 120s, which was considered to be sufficient for illustrating the time-averaged characteristics after achieving the quasi-steady state. The bottom of columns was set as the velocity inlet, where the volume fraction for liquid and gas phases were specified as 0 and 1 respectively. At inlet, the gas velocity was set as the same as superficial

velocity to simplify the problem with neglect of the effects of gas chamber and distributor, and the uniform bubble size distribution at the inlet was used. The top of columns was set as the pressure outlet. No-slip conditions were applied for both liquid and gas phases at the bubble column wall. The modified breakup model considering bubble-induced energy spectrum and the modified turbulent viscosity involving eddy-bubble response were implemented into the numerical simulation through the use of the user defined functions (UDF). In the case of Chen et al. (1999), for the population balance modelling, based on the geometry method $V_{i+1} = 4V_i$, bubbles were divided discretely into 9 classes. The bubble diameter varied from 1 to 40.32 mm.

As shown in Figure 2-2, the mesh set-up for the case of Chen et al. (1999), the height of the bubble column was extended to 3 m to prevent overflow from the top. In comparison of a coarser Grid 1 of 20(r)×40(θ)×80(z) nodes and a refined Grid 3 of 36(r)×72(θ)×126(z) nodes, the Grid 2 (28(r)×64(θ)×100(z) equally distributed nodes in radial, circumferential and axial directions respectively) was fine enough to give mesh-independent results. Detail grid independence results could be found in Chapter 2. In this chapter, the geometry was meshed with inflation layers created at the boundary of the column wall to accurately capture the flow effect in the near-wall region while keeping the same number of cells, the cross-sectional mesh set-up is shown in Figure 3-1.

4. RESULTS AND DISCUSSION

The gas-liquid two-phase in bubble columns is highly transient and turbulent, the bubbly flow consists of four flow regions including central plume region, descending flow region, vortical-spiral flow region and fast bubble flow region the proper prediction of hydrodynamic parameters is important in CFD modelling. The modified viscosity model is successfully implemented into CFD simulation of two selected cases.

The case of Chen et al. (1999)

The gas holdup distributions in radial direction at axial position obtained by implementing the modified model and standard model are shown in Figure 3-2. The data are taken at axial position H = 1.32 m which is the observation height in the experiment stated in the select literature, and is time-averaged. As shown in Figure 3-2, the gas holdup is maximum in the central region of bubble column and decreases gradually to the column wall, because bubble clusters in the central region. Comparing the simulation results, the predicted gas holdup from standard model is underestimated, while the profile from the modified model considering eddy-bubble response shows good agreement with the experimental data, for example, for the maximum gas holdup, the value from standard model is 0.2 m/s and that from experimental data and modified viscosity model is 0.245 m/s and 0.25 m/s respectively. It indicates that the standard model did not reflect properly the mechanism of eddy-bubble interactions in numerical simulation.

This modified model remarkably improved the prediction of gas holdup which is a crucial factor in bubble column as it directly affects the momentum and mass transfer efficiencies.

Figure 3-3 demonstrates the radial distribution of time-averaged profiles of liquid axial velocity. Generally, liquid velocity is maximum in the central region of column and decreases gradually with the movement to the column wall, which is similar to the gas holdup tendency, it further indicates the effect of bubble-induced turbulence. The predicted liquid velocity from the standard model is underestimated in the central region and overestimated in the near-wall region, a likely reason is that the total input energy is constant, with lower velocity in the central region, the wall effect will be enhanced. On the other hand, the modified turbulent viscosity model also shows the improvement of prediction in the continuous phase. From Figure 3-2 and 3-3, the need of considering the effect of eddy-bubble response on turbulent viscosity in CFD simulation of bubble column reactors is illustrated.

Chen (2004) found breakage rate was usually underestimated when implementing the classical bubble breakup model of Luo and Svendsen (1996), which is very likely result from the underestimation of the turbulent kinetic energy of the bombarding eddies. They artificially increased the breakup rate, shown as $\Omega_B'(d_i : d_j) = 10\Omega_B(d_i : d_j)$, and found the numerical results with tuning factor of 10 showed good agreement with experimental results, it is a good engineer method to achieve basic prediction. However, as shown in Equation (3-28), this tuning method would not change bubble size distribution, thus the

bubble size distribution still cannot be correctly predicted. In this work, the bubble size distribution is modelled by the breakup model considering bubble-induced turbulence energy spectrum. Figure 3-4 shows the comparison of the simulated results of overall bubble class probability distribution with different breakup models. The cumulative volume for each bubble class has been normalized by the total volume of all bubbles. The prediction by Luo and Svendsen's model shows the peak value at the 16 mm bubble class, which is not consistent with common sense. The peak values predicted by Chen's tuning method and breakup model with BIT move to 6.35 mm bubble class, which is much more reasonable. When using the modified model, the probability of small bubble classes (1mm ~ 1.59mm) is smaller than that of Chen (2004). One explanation is that the consideration of bubble-eddy interaction causes additional energy dissipation due to bubble response and an appropriate depiction of the energy carried by eddies. In reality, small bubbles do not tend to breakup due to the surface energy constrains. Although there is still a considerably large number of bubbles with small sizes in the simulation of modified model, the effect can be neglect because their contributions to the total volume are much smaller than large bubbles. In future work, breakage criteria can be considered to restrict the over-breakage of the small bubbles.

The case of Guan and Yang (2017)

The modified turbulent viscosity model coupled with bubble breakup model using bubble-induced turbulence energy spectrum has worked well in the simulation of bubble column reported in Chen et al. (1999). Further CFD

validations have been carried out for the bubble column used by Guan and Yang (2017) which has different flow characteristics due to the smaller column diameter.

Figure 3-5 presents the time-averaged radial distribution of gas holdup and the equivalent bubble diameter distribution d_{32} at H = 0.8 m which is the observation height in stated experiment. In general, the CFD simulations with the modified model have achieved agreeable results in the prediction of key hydrodynamic properties, gas holdup and equivalent bubble size. As shown in Figure 3-5(b), the distribution tendency of equivalent bubble diameter d_{32} is predicted well, however, the specific bubble size in the central region of column is over-predicted, it might be caused by the bubble swarm in central region. This requires further investigation that the proper number density of bubbles is need.

The bubble size distribution, which is the main concern of using the population balance model, is illustrated in Figure 3-6. The data sets are normalized by the total volume of the gas bubbles individually. As the gas holdup is significantly higher in central region, bubble size probability density function (PDF) centreline is chosen. As illustrate in the Figure 3-6, the predicted bubble sizes fall into a well-accepted range of PDF distribution. The prediction accuracy of the modified model is thus approved. The considerations of bubble response to eddy and bubble-induced turbulence in bubble column modelling have accurately reflected the nature of bubbly flow within bubble column. However, it should be note there are still some differences between the simulation and experimental results. One explanation is the consideration of bubble

coalescence model, because the coalescence model of Luo (1993) assumed that the mean turbulent approach velocity of bubbles that are carried by the fluid in bubble-bubble collisions is approximately the same as the mean turbulent velocity of eddies that have the same size as the bubbles. When taking bubble-induced turbulence energy spectrum into account, the approach bubble velocity is modified correspondingly. This requires further investigation and validation.

5. CONCLUSION

A modified turbulent viscosity model that considering bubble-eddy interaction has been proposed for modelling bubble column flows, and has been implemented in CFD simulation of a bubble column reactor, coupling with the bubble breakup model considering bubble-induced turbulence. The results of simulations clearly indicate that by employing the modified viscosity model, the prediction of velocity profile, gas holdup and bubble size distribution is improved.

1. The contribution to flow field due to the response of bubble to surrounding eddies has been reflected in simulation results.

2. The proposed viscosity model has been validated for two cases of bubble column flows with diameters of D = 0.44 m and D = 0.15 m, respectively. The simulation results for both cases are consistent with the experimental data. This suggests that the eddy-bubble response viscosity model may be appropriate for description of the mechanism of eddy-bubble interactions in the bubble columns

REFERENCES

ANDERSSON, R. & ANDERSSON, B. 2006. Modeling the breakup of fluid particles in turbulent flows. *Aiche Journal,* 52**,** 2031-2038.

AUTON, T. R., HUNT, J. C. R. & PRUDHOMME, M. 1988. The Force Exerted on a Body in Inviscid Unsteady Non-Uniform Rotational Flow. *Journal of Fluid Mechanics,* 197**,** 241-257.

BHOLE, M. R., JOSHI, J. B. & RAMKRISHNA, D. 2008. CFD simulation of bubble columns incorporating population balance modeling. *Chemical Engineering Science,* 63**,** 2267-2282.

BORCHERS, O., BUSCH, C., SOKOLICHIN, A. & EIGENBERGER, G. 1999. Applicability of the standard k–ε turbulence model to the dynamic simulation of bubble columns. Part II:: Comparison of detailed experiments and flow simulations. *Chemical Engineering Science,* 54**,** 5927-5935.

BOUCHE, E., ROIG, V., RISSO, F. & BILLET, A. M. 2014. Homogeneous swarm of high-Reynolds-number bubbles rising within a thin gap. Part 2. Liquid dynamics. *Journal of Fluid Mechanics,* 758**,** 508-521.

BUNNER, B. & TRYGGVASON, G. 2002. Dynamics of homogeneous bubbly flows Part 2. Velocity fluctuations. *Journal of Fluid Mechanics,* 466**,** 53-84.

CHEN, J. W., LI, F., DEGALEESAN, S., GUPTA, P., AL-DAHHAN, M. H., DUDUKOVIC, M. P. & TOSELAND, B. A. 1999. Fluid dynamic parameters in bubble columns with internals. *Chemical Engineering Science,* 54**,** 2187-2197.

CHEN, P. 2004. *Modeling the fluid dynamics of bubble column flows. Ph.D. Thesis.* Ph.D. Thesis.

CHEN, P., DUDUKOVIC, M. P. & SANYAL, J. 2005. Three-dimensional simulation of bubble column flows with bubble coalescence and breakup. *Aiche Journal,* 51**,** 696-712.

DELNOIJ, E., KUIPERS, J. A. M. & VAN SWAAIJ, W. P. M. 1999. A three-dimensional CFD model for gas–liquid bubble columns. *Chemical Engineering Science,* 54**,** 2217-2226.

DHOTRE, M. T., NICENO, B. & SMITH, B. L. 2008. Large eddy simulation of a bubble column using dynamic sub-grid scale model. *Chemical Engineering Journal,* 136**,** 337-348.

EKAMBARA, K., DHOTRE, M. T. & JOSHI, J. B. 2005. CFD simulations of bubble column reactors: 1D, 2D and 3D approach. *Chemical Engineering Science,* 60**,** 6733-6746.

GARCIA, J. 2001. Study of the turbulence modulation in particle-laden flows using LES. *Annual Research Briefs-2001***,** 177.

GRACE, J. R., CLIFT, R. & WEBER, M. E. 1978. *Bubbles, Drops, and Particles*, Academic Press.

GUAN, X. P. & YANG, N. 2017. Bubble properties measurement in bubble columns: From homogeneous to heterogeneous regime. *Chemical Engineering Research & Design,* 127**,** 103-112.

HAGESAETHER, L., JAKOBSEN, H. A. & SVENDSEN, H. F. 2002. A model for turbulent binary breakup of dispersed fluid particles. *Chemical Engineering Science,* 57**,** 3251-3267.

JAKOBSEN, H. A., LINDBORG, H. & DORAO, C. A. 2005. Modeling of bubble column reactors: Progress and limitations. *Industrial & Engineering Chemistry Research,* 44**,** 5107-5151.

KUIPERS, J. A. M. & VAN SWAAIJ, W. P. M. 1998. Computational Fluid Dynamics Applied To Chemical Reaction Engineering. *In:* WEI, J. (ed.) *Advances in Chemical Engineering.* Academic Press.

KUMAR, S. & RAMKRISHNA, D. 1996. On the solution of population balance equations by discretization—I. A fixed pivot technique. *Chemical Engineering Science,* 51**,** 1311-1332.

LANCE, M. & BATAILLE, J. 1991. Turbulence in the liquid phase of a uniform bubbly air–water flow. *Journal of Fluid Mechanics,* 222**,** 95-118.

LEHR, F., MILLIES, M. & MEWES, D. 2002. Bubble-size distributions and flow fields in bubble columns. *Aiche Journal,* 48**,** 2426-2443.

LEVICH, V. G. 1962. *Physicochemical Hydrodynamics,* EngelwoodCliffs, NJ, Prentice-Hall.

LIAO, Y., MA, T., KREPPER, E., LUCAS, D. & FRÖHLICH, J. 2019. Application of a novel model for bubble-induced turbulence to bubbly flows in containers and vertical pipes. *Chemical Engineering Science,* 202**,** 55-69.

LONG, S., YANG, J., HUANG, X., LI, G., SHI, W., SOMMERFELD, M. & YANG, X. 2020. Large-eddy simulation of gas–liquid two-phase flow in a bubble column reactor using a modified sub-grid scale model with the consideration of bubble-eddy interaction. *International Journal of Heat and Mass Transfer,* 161**,** 120240.

LUO, H. 1993. *Coalescence, Breakup and Liuqid Circulation in Bubble Column Reactors.* PhD thesis PhD thesis, PhD thesis from the Norwegian Institute of Technology.

LUO, H. & SVENDSEN, H. F. 1996. Theoretical model for drop and bubble breakup in turbulent dispersions. *Aiche Journal,* 42**,** 1225-1233.

MAGOLAN, B., LUBCHENKO, N. & BAGLIETTO, E. 2019. A quantitative and generalized assessment of bubble-induced turbulence models for gas-liquid systems. *Chemical Engineering Science: X,* 2**,** 100009.

MENDEZ-DIAZ, S., C. SERRANO-GARCÍA, J., ZENIT, R. & HERNÁNDEZ-CORDERO, J. 2013. Power spectral distributions of pseudo-turbulent bubbly flows. *Physics of Fluids,* 25.

MERCADO, J. M., GOMEZ, D. C., VAN GILS, D., SUN, C. & LOHSE, D. 2010. On bubble clustering and energy spectra in pseudo-turbulence. *Journal of Fluid Mechanics,* 650**,** 287-306.

MUNIZ, M. & SOMMERFELD, M. 2020. On the force competition in bubble columns: A numerical study. *International Journal of Multiphase Flow,* 128.

MURAI, Y., KITAGAWA, A., SONG, X. Q., OHTA, J. & YAMAMOTO, F. 2000. Inverse energy cascade structure of turbulence in a bubbly flow (Numerical analysis using Eulerian-Lagrangian model equations). *Jsme International Journal Series B-Fluids and Thermal Engineering,* 43**,** 197-205.

PFLEGER, D. & BECKER, S. 2001. Modelling and simulation of the dynamic flow behaviour in a bubble column. *Chemical Engineering Science,* 56**,** 1737-1747.

PFLEGER, D., GOMES, S., GILBERT, N. & WAGNER, H. G. 1999. Hydrodynamic simulations of laboratory scale bubble columns fundamental studies of the Eulerian–Eulerian modelling approach. *Chemical Engineering Science,* 54**,** 5091-5099.

PRAKASH, V. N., MERCADO, J. M., VAN WIJNGAARDEN, L., MANCILLA, E., TAGAWA, Y., LOHSE, D. & SUN, C. 2016. Energy spectra in turbulent bubbly flows. *Journal of Fluid Mechanics,* 791**,** 174-190.

PRINCE, M. J. & BLANCH, H. W. 1990. Bubble Coalescence and Break-up in Air-Sparged Bubble-Columns. *Aiche Journal,* 36**,** 1485-1499.

RIBOUX, G., LEGENDRE, D. & RISSO, F. 2013. A model of bubble-induced turbulence based on large-scale wake interactions. *Journal of Fluid Mechanics,* 719**,** 362-387.

RIBOUX, G., RISSO, F. & LEGENDRE, D. 2010. Experimental characterization of the agitation generated by bubbles rising at high Reynolds number. *Journal of Fluid Mechanics,* 643**,** 509-539.

RISSO, F. 2011. Theoretical model for k(-3) spectra in dispersed multiphase flows. *Physics of Fluids,* 23.

RISSO, F., ROIG, V., AMOURA, Z., RIBOUX, G. & BILLET, A. M. 2008. Wake attenuation in large Reynolds number dispersed two-phase flows. *Philosophical Transactions of the Royal Society a-Mathematical Physical and Engineering Sciences,* 366**,** 2177-2190.

ROGHAIR, I., MERCADO, J. M., ANNALAND, M. V., KUIPERS, H., SUN, C. & LOHSE, D. 2011. Energy spectra and bubble velocity distributions in pseudo-turbulence: Numerical simulations vs. experiments. *International Journal of Multiphase Flow,* 37**,** 1093-1098.

ROIG, V. & DE TOURNEMINE, A. L. 2007. Measurement of interstitial velocity of homogeneous bubbly flows at low to moderate void fraction. *Journal of Fluid Mechanics,* 572**,** 87-110.

RZEHAK, R. & KREPPER, E. 2013. CFD modeling of bubble-induced turbulence. *International Journal of Multiphase Flow,* 55**,** 138-155.

SATO, Y., SADATOMI, M. & SEKOGUCHI, K. 1981. Momentum and heat transfer in two-phase bubble flow—I. Theory. *International Journal of Multiphase Flow,* 7**,** 167-177.

SATO, Y. & SEKOGUCHI, K. 1975. Liquid velocity distribution in two-phase bubble flow. *International Journal of Multiphase Flow,* 2**,** 79-95.

SHI, W., YANG, X., SOMMERFELD, M., YANG, J., CAI, X., LI, G. & ZONG, Y. 2019. Modelling of mass transfer for gas-liquid two-phase flow in bubble column reactor with a bubble breakage model considering bubble-induced turbulence. *Chemical Engineering Journal,* 371**,** 470-485.

SHU, S., EL BAHRAOUI, N., BERTRAND, F. & CHAOUKI, J. 2020. A bubble-induced turbulence model for gas-liquid bubbly flows in airlift columns, pipes and bubble columns. *Chemical Engineering Science,* 227**,** 115945.

SOKOLICHIN, A., EIGENBERGER, G. & LAPIN, A. 2004. Simulation of buoyancy driven bubbly flow: Established simplifications and open questions. *AIChE Journal,* 50**,** 24-45.

SOKOLICHIN, A., EIGENBERGER, G., LAPIN, A. & LÜBERT, A. 1997. Dynamic numerical simulation of gas-liquid two-phase flows Euler/Euler versus Euler/Lagrange. *Chemical Engineering Science,* 52**,** 611-626.

SUGIYAMA, K., TAKAGI, S. & MATSUMOTO, Y. 2001. Multi-scale analysis of bubbly flows. *Computer Methods in Applied Mechanics and Engineering,* 191**,** 689-704.

TABIB, M. V., ROY, S. A. & JOSHI, J. B. 2008. CFD simulation of bubble column - An analysis of interphase forces and turbulence models. *Chemical Engineering Journal,* 139**,** 589-614.

TROSHKO, A. A. & HASSAN, Y. A. 2001. A two-equation turbulence model of turbulent bubbly flows. *International Journal of Multiphase Flow,* 27**,** 1965-2000.

TSOURIS, C. & TAVLARIDES, L. L. 1994. Breakage and coalescence models for drops in turbulent dispersions. *AIChE Journal,* 40**,** 395–406.

WANG, T. F., WANG, J. F. & JIN, Y. 2003. A novel theoretical breakup kernel function for bubbles/droplets in a turbulent flow. *Chemical Engineering Science,* 58**,** 4629-4637.

ZHANG, D., DEEN, N. G. & KUIPERS, J. A. M. 2006. Numerical simulation of the dynamic flow behavior in a bubble column: A study of closures for turbulence and interface forces. *Chemical Engineering Science,* 61**,** 7593-7608.

ZHAO, H. & GE, W. 2007. A theoretical bubble breakup model for slurry beds or three-phase fluidized beds under high pressure. *Chemical Engineering Science,* 62**,** 109-115.

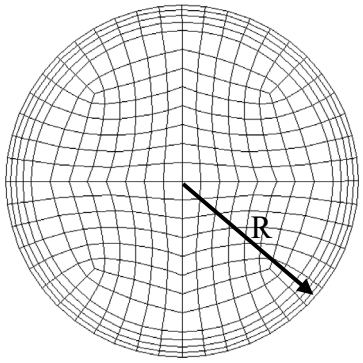

Figure 3- 1 Mesh set-up of the inlet of column (R=0.22m)

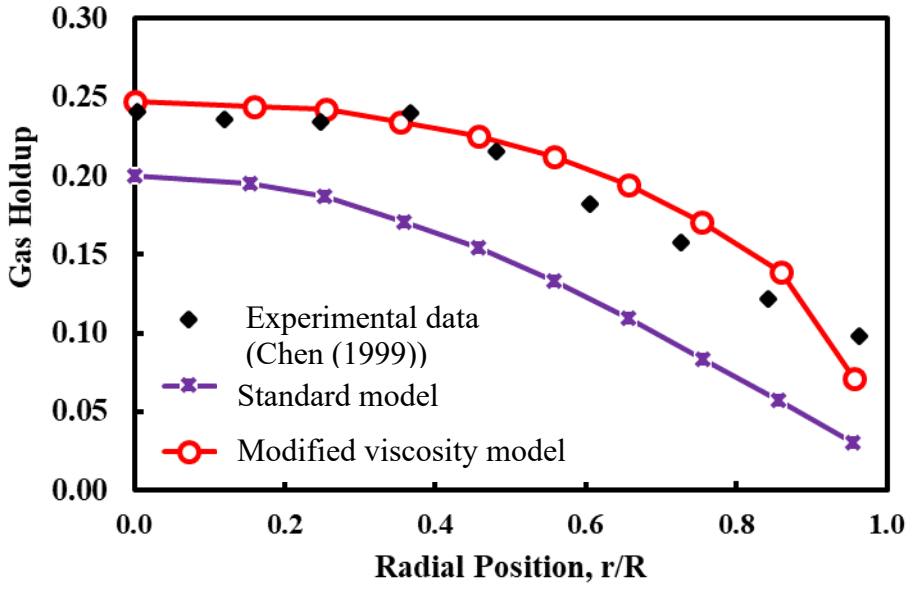

Figure 3- 2 Radial distribution of time-averaged profiles of gas holdup

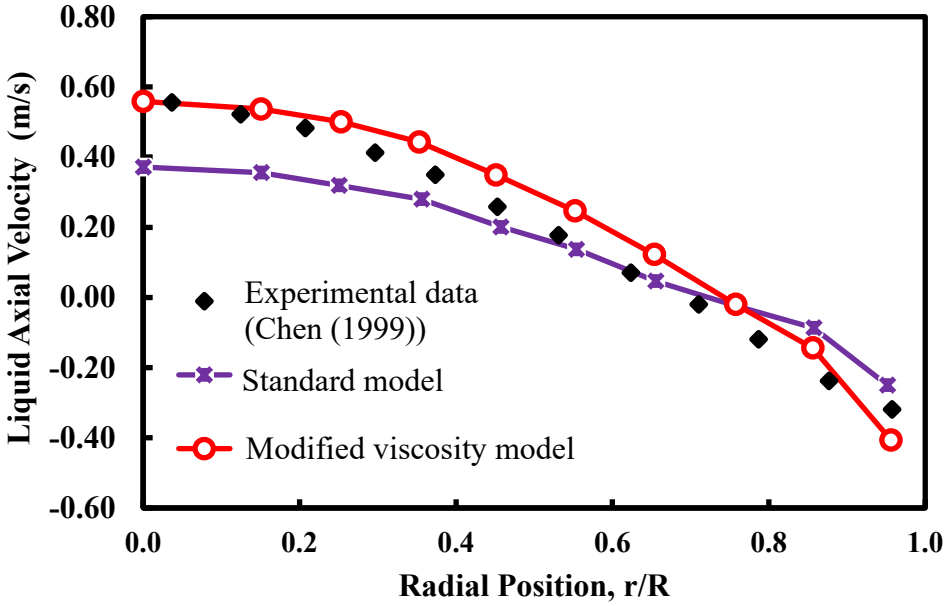

Figure 3- 3 Radial distribution of time-averaged profiles of liquid axial velocity

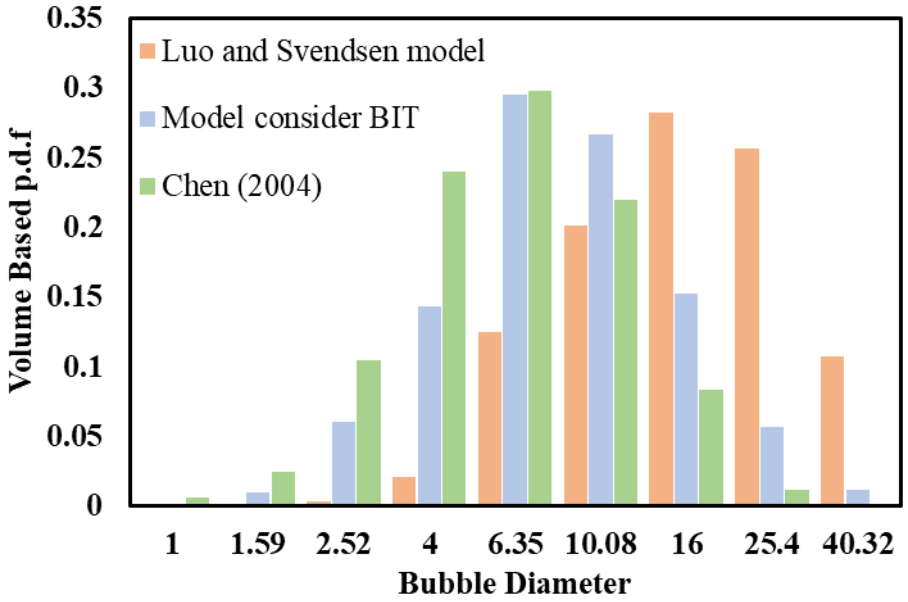

Figure 3- 4 Bubble class volume-based probability distribution

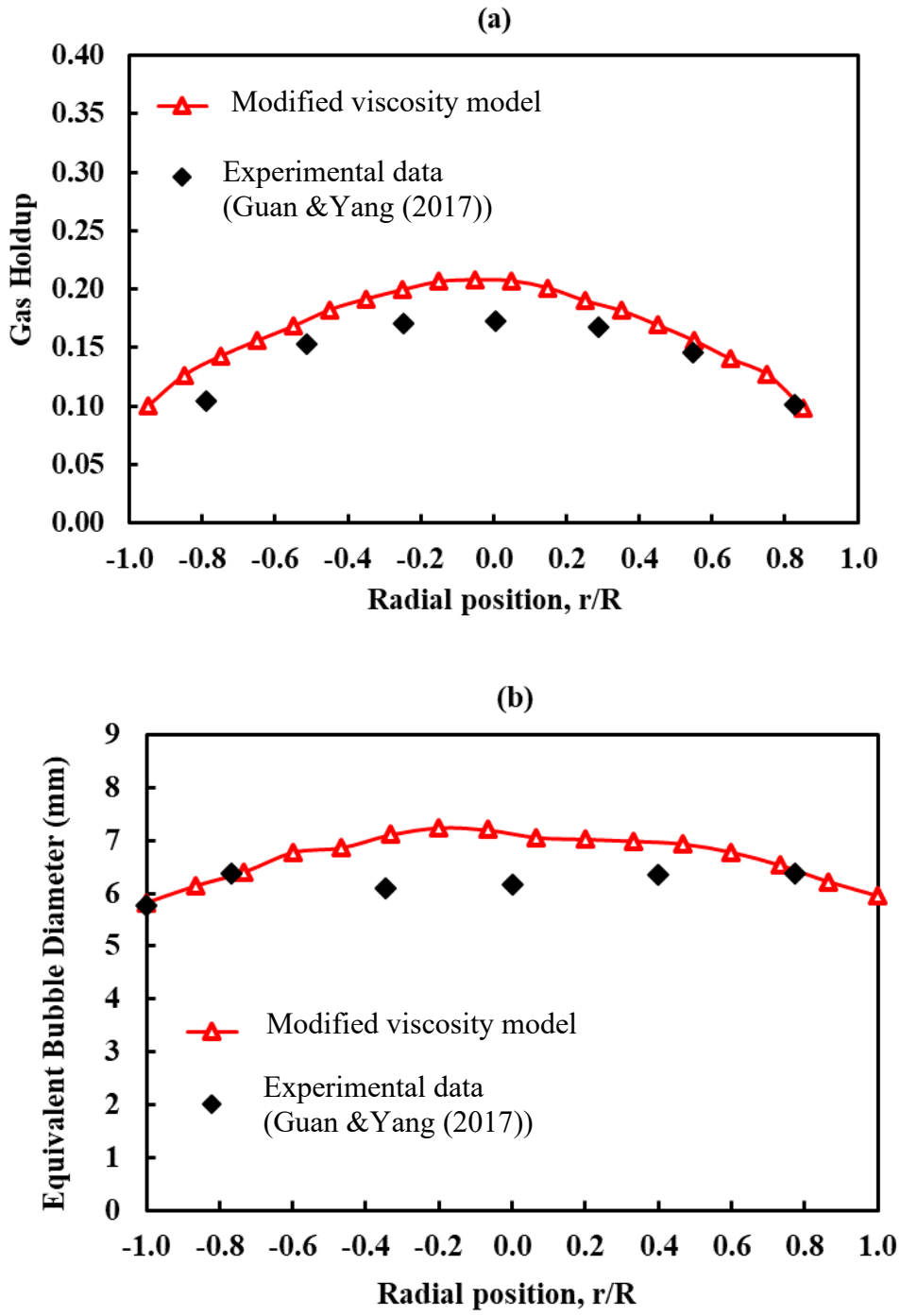

Figure 3- 5 Simulation result of (a) Time-averaged radial distribution of gas holdup, and (b) radial distribution of equivalent bubble diameter d_{32}.

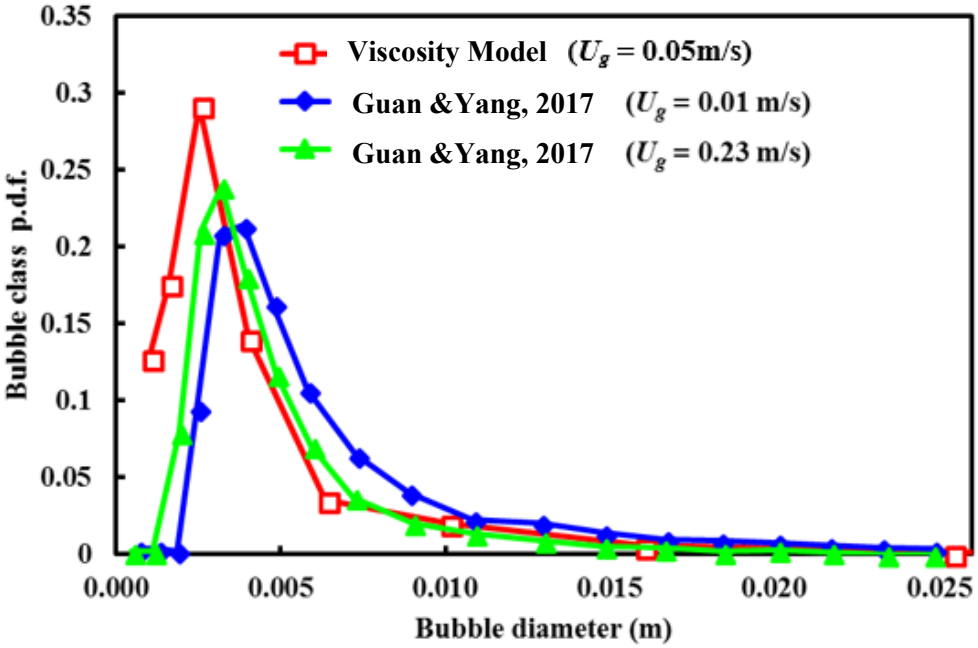

Figure 3- 6 Comparison of predicted bubble probability distribution with experimental data

CHAPTER 4: EXPERIMENTAL INVESTIGATION OF MULTI-PHASE FLOW IN THE BUBBLE COLUMN BY PIV

SUMMARY

In this chapter, the gas-liquid two-phase flow and gas-liquid-solid three-phase flow in the bubble column are experimentally studied and compared through 2D-PIV. The flow characteristics of bubbly flow in bubble column are well captured, the effect of central plume region and near-wall region is clearly illustrated. Bubble velocity promotes liquid velocity, which indicates the energy within bubble column results from bubble-induced turbulence. With the addition of particle, the velocities of both liquid and gas phase are reduced, which illustrates the particle modulation. In terms of the turbulent kinetic energy, the distribution of turbulent kinetic energy becomes more homogeneous under the effect of the solid phase. In addition, the energy spectrum clearly shows the combination of -5/3 scaling law of shear turbulence and -3 scaling law of bubble-induced turbulence in energy spectrum, thus the need of the consideration of the response between bubbles and eddies with similar size and the bubble-induced turbulence is verified.

1. INTRODUCTION

1.1 Two-phase flow

Bubble columns are frequently used in the fields of chemical, petrochemical and energy field. Their main advantages are large contact area between the liquid and gas phases and a good mixing efficiency within the liquid phase (Besagni and Inzoli, 2016b). The proper design of bubble columns relies on the correct prediction of the flow pattern and flow properties. For example, holdup, bubble rise velocity and bubble size distributions. The flow properties are related to two principal flow regimes in bubble column: mainly, the homogeneous and heterogeneous regimes (Kantarci et al., 2005). The homogeneous regime is created by small superficial gas velocities and is characterized by the presence of small, uniformly sized and less interacting bubbles (Besagni and Inzoli, 2016a). The heterogeneous regime is produced either by high gas flow rates, or by plates with large orifices. This regime is characterized by a wide variety of bubble size distribution and high coalescence and breakage phenomena are present.

A critical analysis proposed by Shah et al. (1982) involves non-adjustable parameters such as holdup, interfacial area, mass transfer, dispersion coefficient, flow regimes and transfer coefficient. All these parameters directly affect the design of bubble column device.

The holdup is a function of the axial and radial position in the bubble column. The research of local void fraction profiles could help in determining the flow regimes, liquid mixing, and heat and mass transfer. According to the gas and liquid superficial velocities, the bubble column and sparger design, and the operating conditions, local void fraction holdup profiles may be center peaked, wall peaked or flat. Many experimental measurements of holdup profiles have been reported in recent decades using various techniques (Joshi et al., 1998). In addition, the bubble column operation influences the holdup at high liquid velocities: the co-current mode reduces the holdup (Kumar et al., 2012, Shah et al., 2012, Pjontek et al., 2014), and the counter-current mode increases the holdup (Jin et al., 2010, Besagni et al., 2014, Besagni and Inzoli, 2016b).

In addition to the holdup, another important parameter of bubble column hydrodynamics is the Bubble Size Distribution (BSD). Due to coalescence and break-up, the BSD generated at the sparger gradually changes along the column until equilibrium/developed BSD is reached. The BSD- along with the holdup, enables an evaluation of the interfacial area (Kantarci et al., 2005) and is an important parameter for set-up CFD models (Lucas et al., 2016). In fact, when using Eulerian multi-fluid model, a bubble diameter or BSD information is requested as an input. In the literature, various intrusive and nonintrusive techniques have been proposed for measuring the BSD and bubble shape (Rodrigues and Rubio, 2003, Busciglio et al., 2010). Nonintrusive measurement techniques are more popular than intrusive methods because the flow conditions are undisturbed, and image analysis has attracted more and more attention because of its many advantages (Essadki et al., 1997, Guet et al., 2005).

1.2 Three-phase flow

Gas–liquid–solid three-phase bubble columns has also been studied for a long time. It can be considered as bubbly flows with the presence of solids, or, as liquid–solid flows with presence of bubbles (Mena et al., 2005). The presence of solids has a noteworthy influence on the gas-liquid bubble column, including gas holdup (Sarhan et al., 2018, Mokhtari and Chaouki, 2019, Lakhdissi et al., 2020), bubble formation (Yoo et al., 1997, Luo et al., 1998, Fan et al., 1999), bubble coalescence (Ojima et al., 2015), bubble rise (Bly and Worden, 1992, Luo et al., 1997b), axial (Gandhi et al., 1999) and radial (Ohkawa et al., 1997) profiles, mixing and dispersion (Smith and Ruether, 1985, Matsumoto et al., 1989), mass transfer (Koide et al., 1984, Quicker et al., 1984, Pandit and Joshi, 1986, Charinpanitkul et al., 1993), and flow regimes (Mena et al., 2005, Li et al., 2014, Rabha et al., 2014).

For example, some researchers observed a dual effect of solids on gas holdup (Kara et al., 1982, Pandit and Joshi, 1984, Bukur et al., 1990, Khare and Joshi, 1990, Mena et al., 2005). The dual effects of solid loads are attributed to two opposite processes, stabilizing, and destabilizing the three-phase systems (Mena et al., 2005). Khare and Joshi (1990) show that this dual effect results in a maxima at about c = 0.6% of fine alumina particles. Banisi et al. (1995) proposed that a small number of fine particles (inhibiting coalescence) and large number of large particles (break up of large bubbles) tend to increase the holdup. Sada et al. (1986) found that the addition of small particles (less than 10mm)

increases the gas holdup at very low particle load, while the particle load with particle size greater than 50mm reduces the gas holdup. Gandhi et al. (1999) proposed that the addition of solid can reduce the bubble breakup rate when the solid volume fraction is 40%; thus, the gas holdup decreases. Biń et al. (2001) reported that the gas holdup decreases in semi-batch and co-current mode, whereas it increased in counter-current mode.

Meanwhile, there are some research on the effects of solids on the flow regimes. Kara et al. (1982) found that increase the solids concentration and particle size can cause an earlier deviation from bubbly flow regime. Luo et al. (1997a) report stabilizing the homogeneous regime by increasing pressure in a three-phase bubble column. Mena et al. (2005) discussed the effect of solids on homogeneous–heterogeneous flow pattern transition in a bubble column. They found that at low solid loading (0–3%) the homogeneous regime is stabilized, while for higher solid loadings (>3%) destabilization occurs.

1.3 PIV technique

To characterize a bubble column, it is necessary to determine the liquid velocity induced by the bubble, the bubble rising velocity, the influence of the bubble column on the liquid and bubble characteristics. Thus, some measurement techniques have been developed in recent years. These techniques can be classified into two main categories: intrusive techniques, such as electrical resistivity probes, hot-film anemometer probes, and non-intrusive techniques including, electrochemical techniques, laser Doppler anemometry (LDA),

ultrasonic Doppler techniques, particle image velocimetry (PIV), particle tracking velocimetry (PTV), and holographic techniques (Pang and Wei, 2013). Wang et al. (1987), Serizawa and Kataoka (1990), Liu and Bankoff (1993a), Liu and Bankoff (1993b) and Shawkat et al. (2008) applied the hot-film anemometer probes to investigate the turbulent bubbly flow. Kashinsky et al. (1993), Nakoryakov et al. (1996) and Kashinsky and Randin (1999) used the electrochemical techniques to measure velocity fluctuations in turbulent flows laden with bubbles. Kato et al. (1999), So et al. (2002), Guet et al. (2004), Durst et al. (2006) and (Theofanous and Sullivan, 2006) used laser Doppler anemometry to investigate bubbly turbulence flows. Kawashima et al. (2004), Kitagawa et al. (2005) and Murai et al. (2006) investigated bubbly turbulence flows with PTV. Many researchers investigated the bubbly turbulence with PIV (Gui et al., 1997, Hassan et al., 1998, Delnoij et al., 1999, Tokuhiro et al., 1998, Hishida et al., 2001, Deen et al., 2002, Khalitov and Longmire, 2002, Lindken and Merzkirch, 2002, Nagaya et al., 2003, Fujiwara et al., 2004a, Fujiwara et al., 2004b, Kim et al., 2010, Pang and Wei, 2013, Murgan et al., 2017). Bröder and Sommerfeld (2000), Choi et al. (2002) and Akoi et al. (2006) analyzed turbulent bubbly flows with the combined techniques of PIV and PTV.

The principle of PIV technique is using fluorescent tracer particles to determine the fluid velocity field. Firstly, a pulsed laser is used to irradiate the flow field to form a sheet of light plane. Then the tracer particles evenly dispersed in the flow field can reflect light irradiated by the laser. Then using a camera to capture a pair of particle images with known time interval. Finally, the computer uses related algorithms to compare and analyze the two images to obtain the particle

displacement, and then obtain the velocity vector (Jahanmiri, 2011). As PIV was applied in multi-phase flow in our experiment, spherical polymer particles (polymethyl methacrylate – PMMA) coated with Rhodamine B fluorophore (RhB) were used.

Based on the above literature study, it is observed that the study of flow dynamics in a three-phase bubble column using PIV is limited and not comprehensive. Most of the work was done with the two-phase flow. Therefore, the purpose of the current work is to measure the flow dynamics in a three-phase bubble column with the aid of PIV technique. Section 2 will introduce the experimental method, followed by the phase discrimination methodology in Section 3. Section 4 will present the experimental results and discussion focusing on the solid effect on the flow within bubble column. Section 4 will present the conclusions derived from this study.

2. EXPERIMENTAL METHOD

2.1 Experimental setup

The experiments are performed in a transparent cylindrical bubble column of 150 mm inner diameter filled with deionized water. Since the reflection and refraction of lights in the surrounding environment should be minimized, in order to minimize distortions in the optical measurements, PIV, a transparent square vessel is installed outside the main column with de-ionised water filled

in the gap to reduce the effect of the curvature of the bubble column wall. The study was performed for a two-phase air-water flow and for a three-phase air-water-solid flow. The compressed air is pumped through a flowmeter with adjustable flow rate and finally into the gas chamber. In this experimental study, the air flow rate is Q=160 L/h. The gas is sparged into the main column through the gas distributor, which is a perforated plate with 16 orifices at the bottom of the bubble column.

During the three-phase experiment, 150mL transparent Polystyrene (PS) (volume void fraction 1%) was added in the bubble column. In order to prevent solids from falling under the sparger, a layer of iron mesh added above the sparger, as shown in Figure 4-1. Also, the experimental set-up arrangement is shown in Figure 4-2. The purpose of the experiment is to determine the water field velocity induced by the bubble column and the bubbles rising velocity in the two-phase air-water flow and in the three-phase air-water-solid flow, and investigate the influence of solid on the bubbly flow.

2.2 PIV measurement system

The 2D-PIV equipment (Dantec Dynamics) is composed of a Nd:YAG laser, a CCD camera, a timer box and the Dynamic-Studio software. The pulsed Nd:YAG laser (New Wave Gemini, @532nm, 2×30 MJ) is used to create a 3 mm thick laser sheet. The laser sheet illuminates the tracer particles on a sheet of light plane. Spherical polymer particles (polymethyl methacrylate – PMMA)

coated with Rhodamine B fluorophore (RhB) were used as tracer particles. The CCD camera (2048×2049 pixels) equipped with a Nikon lens (AF 50mm F/1.8D), positioned perpendicular to the laser plane, captures pairs of images at a frequency of 5 Hz by the synchronizer. Long-wave optical filter was used in front of the CCD camera, to weaken the laser wavelength from the light scattered by the fluorescent particles on the bubble. The time between the two images of each pair is 2000μs. The actual physical size of the image was about 150 mm × 150 mm. The cross-correlation method was used to compute the particle displacement with the interrogate window 8 pixels×8 pixels. For all experiments, 1000 image pairs were recorded to assure a statistical convergence of the velocity and the dissipation rate. In order to get the velocity distribution at different height of bubble column, three different height positions were measured. The center heights of the three positions were 200mm,325mm and 450mm from the bottom of column respectively.

3. PHASE DISCRIMINATION

The main difficulty in measuring bubbly flow is how to effectively distinguish bubbles from tracer particles representing the liquid phase. Although the size of bubbles is much larger than tracer particles, it is difficult to distinguish between the bubbles and the tracer particles due to the fact that the tracer particles can adhere to the bubble surface. The existing phase discrimination methods mainly include colour identification, image intensity identification, spatial frequency identification, correlation peak properties identification, spot size identification, and spot shape identification (Khalitov and Longmire, 2002). Bröder and

Sommerfeld (2002) considered that the colour identification is the most suitable and reliable method for the phase discrimination in bubbly flows. For the present measurement, another discrimination method is applied to discriminate bubbles and liquid containing tracer particles. The detailed description is presented as follows.

In order to measure the liquid velocity field, the flow was seeded with polyamide tracer particles (PMMA-RhB). In the present experiment, images of bubbles and tracer particles were simultaneously recorded by a CCD camera, as shown in Figure 4-3 (a). Then the full velocity field, Figure 4-3 (b), was obtained as described in section 2.2. As bubble rising velocity is larger than liquid velocity, so matlab is applied to delete the velocity value that larger than a threshold value, then the liquid velocity can be obtained in Figure 4-3 (c).

4. RESULTS AND DISCUSSION

4.1 Flow structure

The mean velocity vectors of liquid phase at different observation heights are shown in Figure 4-4. For both two-phase and three-phase flow, the upwards flow in the central region and downwards flow in near-wall region are well captured, which illustrates the central plume region and the descending flow region in the general macroscopic flow structures. In addition, the near-wall region, there are some local vortices (shown in the spiral manner) around the

discontinuity part in liquid phase, which is caused by the interaction with bubbles. It should be noted that the liquid velocity includes velocity of solid phase the gas-liquid-solid three-phase flow, because the density ratio and the response time ratio of solid particle to water are both in the order of 1, the current experiment cannot distinguish the liquid velocity from solid velocity, the mixture of liquid and solid phase is assumed as homogenous slurry. In general, the velocity of liquid phase in both gas-liquid two-phase flow and gas-liquid-solid three-phase flow varies from 0 m/s to 0.06 m/s. Comparing the two operating conditions, the velocity magnitude in three-phase flow is significant smaller than that in two-phase flow, which is caused by retardation effect of particle. Moreover, at high observation height, Z = 0.45 m, the velocity distribution of three-phase flow becomes irregular, the difference between central plume and backflow region becomes unclear, which further indicates the presence of the solid phase will weaken the driving effect of the bubbles on the liquid phase.

Correspondingly, the mean velocity of the gas phase at different heights is shown in Figure 4-5. In both two-phase flow and three-phase flow, the velocity distributions of gas phase are similar to the liquid velocity distributions in the corresponding positions and conditions, including the expected behaviour of central plume and descending region. It can be further illustrated that the liquid flow is induced by the injection of bubble, which shows the importance of the study on bubble-induced turbulence. Also, in the comparison of bubble velocity of two-phase flow and three-phase flow, the bubble rising velocity is significantly decreased by the addition of particle. In bubble column, the inject

energy is only from the bubble-induced energy, with the addition of solid phase, more energy dissipates in inter-phase interaction, therefore, the bubble velocity is reduced thus the induced liquid velocity. Another reason is the density of particle is much higher than the gas phase, the solid phase hinders the rise of the bubbles, thereby reducing the velocity of gas phase.

4.2 Induced flow velocity

In order to analyse quantitatively the effect of the solid phase on the flow in the bubble column, the liquid mean axial velocity and the radial velocity profiles in the radial direction are shown in Figure 4-6 and Figure 4-7 respectively. Since there are some points occupied by gas phase, the values become zero at the corresponding point on the exact observation height, the mean velocity here is obtained by averaging the velocity in the axial direction within a region of 6 mm height because the bubble diameter is obtained as 3mm in the experiment.

As shown in Figure 4-6, the mean liquid axial velocity is large in the central area and small in the near-wall region at three observation heights, it is caused by the following two reasons: bubbles tend to cluster as a bubble plume in the central region of bubble column, and the wall lubrication force generated by the asymmetric fluid flow surrounding bubbles push the bubbles away from the wall. From the velocity magnitude of liquid flow, the bubble-induced liquid velocity of three-phase flow reduces comparing with two-phase flow, which is mentioned in different literature in the above sections. In addition, the water velocity decreases with the increase of column height, which shows the

dissipation along the rising route. It should be noted that the mean liquid axial velocity distribution of gas-liquid two-phase flow is symmetric by the central line in ideal condition, in this experimental finding, the nonsymmetric flow results in the region of the strongest upward flow is shifted out of the central region of bubble column, a likely reason is there is some small disturbances during air injection which can be further improved in the future. Figure 4-7 shows the mean liquid radial velocity profile along the radial direction at different observation heights. Generally, the magnitude of radial velocity is small, therefore the difference between the two-phase flow and three-phase flow is not as large as axial velocity. When Z = 0.2 m, the maximum velocity of two-phase flow does not exceed 0.005m/s. However, the radial velocity in the three-phase flow is less than -0.005m/s near the right side, indicating that the radial motion is relatively severe here under the influence of solid particles. With moving up the observation window, the radial velocity in the two-phase flow exceeds 0.005m/s near the right side when Z = 0.325m, and the peak values of the radial velocities of both two-phase and three-phase flow are achieved when Z = 0.45m. It indicates that the radial motion is more severe with the increase of height. Moreover, as shown in Figure 4-7, the heterogeneity of radial velocity profile is caused by the turbulent dispersion, thus the need of considering turbulent dispersion force in the turbulent viscosity is proved.

4.3 Bubble raising velocity

For gas phase, the bubble axial velocity and radial velocity distribution in the radial direction is presented in Figure 4-8 and Figure 4-9 respectively. Figure 4-

8 and Figure 4-9 are generated by the similar averaging approach with the region of 6 mm in main direction to the keep the data region consistent. As shown in Figure 4-8(a), when Z = 0.2 m, the lower position, the radial distribution of bubble axial velocity is asymmetrical, which is caused by the disturbances in aeration. This effect becomes inapparent with the increase of observation height, as the profiles at 0.325m and 0.45m. From Figure 4-8, in general, the axial velocity of gas phase is in the range from -0.1 to 0.3 m/s and almost shows parabolic distribution. The velocity magnitude is high in a wide area in the central region and decreases sharply near the column wall, which is caused by the wall-lubrication force under boundary layer effect. Comparing the velocity profile of two-phase and three-phase flow, the profiles show similar tendencies, but the bubble velocity of three-phase flow is smaller than that of two-phase flow. As mentioned above, the addition of particles retard bubble motion as some particles hinder bubble rising up while some particles are trapped on the bubble surface. More energy is dissipated by particles in gas-liquid-solid three-phase flow. Figure 4-9 shows the bubble radial velocity profile. Basically, the radial velocity of gas phase in two-phase flow is greater than that in the three-phase flow, which verifies the retardation of particles on bubble motion. From the comparison of profiles at different heights, the velocity magnitude of bubble radial velocity gradually increases as the height increases generally, especially in the right side. To be specific, when Z = 0.2 m, the maximum velocity in the two-phase flow is not larger than 0.02m/s, and the minimum velocity in the three-phase flow is not less than -0.01m/s. When Z = 0.325 m, the radial velocity in the two-phase flow is larger than that in the three-phase flow in all regions. When Z = 0.45 m, the difference between radial velocity in the two-phase and

three-phase flow is not as significant as other two profiles. However, the maximum velocity in the two-phase flow exceeds 0.02m/s, and the minimum velocity in the three-phase flow is smaller than -0.01m/s. It can be seen that the radial motion at high height is more intense but the effect of particle on bubble radial velocity becomes less intense.

4.4 Turbulent characteristics

Due to the experimental apparatus limitation, there is no information about the third velocity component (U_y) in 2D PIV. In this work, based on the pseudo-isotropic assumption, the fluctuation velocity in y-direction is assumed as equation (4-1):

$$w' = \frac{1}{2}(u'^2 + v'^2) \tag{4-1}$$

the turbulent kinetic energy (TKE) is approximated as:

$$k = \frac{1}{2}(u'^2 + v'^2 + w'^2) = \frac{3}{4}(u'^2 + v'^2) \tag{4-2}$$

According to Khan et al. (2006), there is no significant differences between the maps obtained from the 2D and 3D PIV experimental results, thus this simplification is validated.

As mentioned in Equation (4-2), the turbulent kinetic energy is composed of the two components of the mean fluctuating velocity of liquid phase, therefore, the vertical velocity fluctuation $\boldsymbol{u'_{rms}}$ and horizontal velocity fluctuation $\boldsymbol{v'_{rms}}$ are shown in Figure 4-10 and Figure 4-11 show respectively. It can be seen from

the Figure 4-10 (a) that the vertical velocity fluctuation in the two-phase flow is relatively large on the right side while relatively small on the left side at both three heights. However, as shown in Figure 4-10(b), the vertical velocity fluctuation in the three-phase flow is approximately uniform distributed in the whole region expect the region with high wall effect. From above comparison, the effect of solid particle on the fluctuating velocity in main direction is strong, the velocity fluctuations in the three-phases are in relatively homogeneous distribution. Figure 4-11 is the horizontal velocity fluctuations. Overall, the distribution is roughly homogeneous. The main difference between two-phase and three-phase flow on the distribution of horizontal velocity fluctuations is that there are large velocity fluctuation areas on the left and right sides of the two-phase flow, while the high fluctuation only occurs in the right side in three-phase flow.

Similar to velocity of liquid phase, the velocity fluctuation profiles of vertical and horizontal components are generated by the averaging process and are shown in Figure 4-12 and Figure 4-13. Overall, vertical fluctuating velocity is higher in the right side, which is caused by the unstable air injection. If neglect this unsymmetric effect, the vertical fluctuating velocity is small in the near-wall region and increases sharply to a maximum value in a wide range in the middle region of column. In two-phase flow, the profile tendency changes insignificantly with the increase of height. Comparing the profile of two-phase flow and three-phase flow, the values of vertical fluctuating velocity increase with the addition of particle, thus solid phase enhances the mean velocity fluctuation in main direction in three-phase flow. Figure 4-13 shows the

horizontal fluctuating velocity profile in the radial direction. Different from the distribution of vertical velocity fluctuations, the horizontal velocity fluctuations of the two-phase and three-phase flow show similar distribution, the near-wall regions in both sides have large velocity fluctuations, and velocity fluctuations are small in the middle region of column. In addition, the fluctuating velocity profile shows similar distribution with the increase of observation height.

Using Equation (4-2), the turbulent kinetic energy of liquid phase is calculated and shown in Figure 4-14. As shown in Figure 4-14, the contour of turbulent kinetic energy of liquid phase shows different trend from the liquid velocity. The TKE values are relatively large on the near-wall regions, while the value becomes relatively small in the middle region of column. Comparing the liquid turbulent kinetic energy of two-phase flow and three-phase flow, although the liquid velocities are reduced in three-phase flow, there are more regions with high TKE values in the three-phase flow. It shows that the turbulent is enhanced with the addition of solid phase, as the turbulent kinetic energy is increased. In addition, the highest TKE region mainly occurs in the right side of column, which also results from the aeration turbulence, as higher turbulence leads to higher turbulent kinetic energy. To evaluate the enhancement quantitatively, the averaging approach over the region of 6 mm in main direction is applied to produce the TKE profile in radial direction, as shown in Figure 4-15. From left to right, the turbulent kinetic energy first increases from the left column side to about one fourth of the column diameter, then decreases in the middle region of column, then increases again to a maximum at about three fourths of the column diameter and the continuously decreases toward the right column wall.

Generally, the TKE profiles at different heights follow the similar trend which with two crests and one trough. From Figure 4-15(a), when the column height is 0.2m, the difference between peak and throughs reaches maximum, a likely reason is that the plume and surrounding liquid yield a strong shear flow, and thus the strong bubble agitation. With the increase of column height, as shown in Figure 4-15(b) and Figure 4-15(c), the difference decreases. Comparing the turbulent kinetic energy profile of the two-phase and three-phase flow, the difference of TKE value between the peaks and troughs of the two-phase flow is larger than that of the three-phase flow, the distribution of TKE becomes more homogeneous under the effect of the solid phase because of the additional momentum transfer between particle and liquid phase.

4.5 Energy Spectrum

In order to determine the energy spectra on the main direction of bubbles motion in two-phase bubble column, the velocity components and velocity fluctuations in the axial direction decomposed from the velocity vectors are shown in Figure 4-16. As discussed above, there is some small disturbances during air injection, to avoid such an error, as shown in Figure 4-16, polylines represent the vertical velocity components and fluctuations of the liquid phase at different horizontal positions on the PIV image. The centre of the image is allocated at the height of 0.45m, $H / D = 3$. The horizontal positions for line-1 to line-4 are selected as 26 mm, 55 mm, 74 mm and 95 mm from the left edge of the present PIV image, according to the existence of the preceding bubbles that just rise away from the measurement window. The velocity fluctuations are calculated by subtracting

the mean of each data set from the vertical velocities, such as $u'_z = u_z - \overline{U}_z$. The fluctuation is slightly higher at the top of the measurement window, which is closer to the rear of the bubbles or bubble swarm. The autocorrelation function in vertical direction can be defined as

$$f(z) = \frac{\overline{(u'_z)_A (u'_z)_B}}{\tilde{u}_z^2}, \tag{6-3}$$

where A and B refer to two points in the vertical column and the turbulence intensity $\tilde{u}_z$ can be defined as

$$\tilde{u}_z = \sqrt{\overline{u'^2_z}}. \tag{6-4}$$

When two points A and B are very close to each other, they can be considered to be under the influence of the same turbulent eddy. In this case, the velocity fluctuations are closely related, and the value of autocorrelation approximately equals to 1. With the increase of the distance between these two points, they might under the influence of different turbulent eddies. Therefore, it is expected that the correlation of velocity fluctuations is gradually diminished, and the values of autocorrelation function approach to 0. To demonstrate this trend clearly, the autocorrelation of line-2 is presented in Figure 4-17. It is noted that the curve has been cut-off at 64 mm away from the starting point. This is limited by the size of PIV measurement window, which leads to the loss of information in low wavenumber region ($\kappa = 2\pi / \lambda$) on the energy spectrum. However, this information loss may not be so important as the power law scaling behaviour has mainly taken place within the inertia subrange, while the low wavenumber region may have already been very close to the energy containing range. Taking all these considerations into account, the spatial spectra of the vertical velocity S_{zz} can be calculated using a fast Fourier transform (FFT) of the autocorrelation for each vertical column of the two-dimensional PIV velocity measurements.

The one-dimensional energy spectra in the wake of bubbles are presented in Figure 4-18. It can be clearly seen from Figure 6-6 that a slope of -3 can be found for all selected vertical columns in the wake of bubbles. The experimental results clearly show that the bubble-induced turbulence indeed exists, and its power law scaling behaviour is totally different from the homogeneous isotropic single-phase turbulence. It can also be found that the characteristic length scale that corresponds to the slope -3 scaling is approximately the same as the size of bubbles that generate the wake. For turbulent eddies with wavelength much larger than the characteristic length scale, the slope of -5/3 is still observed. This indicates that the shear turbulence and bubble-induced turbulence both exists in bubble column turbulent bubbly flows. However, the influence of bubbles is only on the turbulent eddies that are approximately the same size or smaller than the size of bubbles. Therefore, the need of the consideration of the response between bubbles and eddies with similar size and the bubble-induced turbulence is verified.

5. CONCLUSION

In this chapter, an experimental study is proposed which compared the gas-liquid two-phase flow and gas-liquid-solid three-phase flow in the bubble column by 2D-PIV. The most prominent flow features in both gas-liquid two-phase flow and gas-liquid-solid three-phase bubble column flow are:

i) The higher velocity in the central region of column, namely central plume region, and the lower velocity in the near-wall region.

ii) With the increase of column height, the velocity decreases due to dissipation along the rising route.

iii) The change of liquid velocity is followed the trend of gas velocity, in other words, bubble velocity promotes liquid velocity, which indicates the energy within bubble column results from bubble-induced turbulence.

From the comparison of gas-liquid two-phase flow and gas-liquid-solid three-phase flow, with the addition of particle, the velocities of both liquid and gas phase are reduced, which illustrates the particle modulation, particle retards bubble movement. In terms of the turbulent kinetic energy, the distribution of turbulent kinetic energy becomes more homogeneous under the effect of the solid phase because the additional momentum transfer between particle and liquid phase causes the more dissipation in liquid phase.

In addition, a turbulent energy spectrum is generated and clearly shows the combination of -5/3 scaling law of shear turbulence and -3 scaling law of bubble-induced turbulence in energy spectrum, thus the need of the

consideration of the response between bubbles and eddies with similar size and the bubble-induced turbulence is verified.

REFERENCES

AKOI, K., HISHIDA, K. & KODAMA, Y. Measurements of near wall turbulent structure in a microbubble flow using a highly magnifying telecentric PIV/PTV system. Proceedings of the 13th International Symposium on Applications of Laser Techniques to Fluid Mechanics Lisbon, Portugal, 2006. Citeseer, 26-29.

BANISI, S., FINCH, J. A., LAPLANTE, A. R. & WEBER, M. E. 1995. Effect of solid particles on gas holdup in flotation columns—I. Measurement. *Chemical Engineering Science,* 50**,** 2329-2334.

BESAGNI, G., GUÉDON, G. & INZOLI, F. 2014. Experimental investigation of counter current air-water flow in a large diameter vertical pipe with inners. *Journal of Physics: Conference Series,* 547**,** 012024.

BESAGNI, G. & INZOLI, F. 2016a. Bubble size distributions and shapes in annular gap bubble column. *Experimental Thermal and Fluid Science,* 74**,** 27-48.

BESAGNI, G. & INZOLI, F. 2016b. Comprehensive experimental investigation of counter-current bubble column hydrodynamics: Holdup, flow regime transition, bubble size distributions and local flow properties. *Chemical Engineering Science,* 146**,** 259-290.

BIŃ, A. K., DUCZMAL, B. & MACHNIEWSKI, P. 2001. Hydrodynamics and ozone mass transfer in a tall bubble column. *Chemical Engineering Science,* 56**,** 6233-6240.

BLY, M. J. & WORDEN, R. M. 1992. The effects of solids density and void fraction on the bubble rise velocity in a liquid-solid fluidized bed. *Chemical Engineering Science,* 47**,** 3281-3288.

BRÖDER, D. & SOMMERFELD, M. A PIV/PTV system for analysing turbulent bubbly flows. Proceedings of the 10th International Symposium Application of Laser Techniques to Fluid Mechanics, Lisbon, Portugal, 2000. Citeseer.

BRÖDER, D. & SOMMERFELD, M. 2002. An advanced LIF-PLV system for analysing the hydrodynamics in a laboratory bubble column at higher void fractions. *Experiments in Fluids,* 33**,** 826-837.

BUKUR, D. B., PATEL, S. A. & DALY, J. G. 1990. Gas holdup and solids dispersion in a three-phase slurry bubble column. *AI Ch. E. Journal (American Institute of Chemical Engineers);(United States),* 36.

BUSCIGLIO, A., GRISAFI, F., SCARGIALI, F. & BRUCATO, A. 2010. On the measurement of local gas hold-up and interfacial area in gas–liquid contactors via light sheet and image analysis. *Chemical Engineering Science,* 65**,** 3699-3708.

CHARINPANITKUL, T., TSUTSUMI, A. & YOSHIDA, K. 1993. Gas-liquid mass transfer in a three-phase reactor. *Journal of chemical engineering of Japan,* 26**,** 440-442.

CHOI, H. M., KURIHARA, T., MONJI, H. & MATSUI, G. 2002. Measurement of particle/bubble motion and turbulence around it by hybrid PIV. *Flow Measurement and Instrumentation,* 12**,** 421-428.

DEEN, N. G., WESTERWEEL, J. & DELNOIJ, E. 2002. Two-Phase PIV in Bubbly Flows: Status and Trends. *Chemical Engineering & Technology,* 25**,** 97-101.

DELNOIJ, E., WESTERWEEL, J., DEEN, N. G., KUIPERS, J. A. M. & VAN SWAAIJ, W. P. M. 1999. Ensemble correlation PIV applied to bubble plumes rising in a bubble column. *Chemical Engineering Science,* 54**,** 5159-5171.

DURST, F., SCHÖNUNG, B., SELANGER, K. & WINTER, M. 2006. Bubble-driven liquid flows. *Journal of Fluid Mechanics,* 170**,** 53-82.

ESSADKI, H., NIKOV, I. & DELMAS, H. 1997. Electrochemical probe for bubble size prediction in a bubble column. *Experimental Thermal and Fluid Science,* 14**,** 243-250.

FAN, L. S., YANG, G. Q., LEE, D. J., TSUCHIYA, K. & LUO, X. 1999. Some aspects of high-pressure phenomena of bubbles in liquids and liquid–solid suspensions. *Chemical Engineering Science,* 54**,** 4681-4709.

FUJIWARA, A., DANMOTO, Y., HISHIDA, K. & MAEDA, M. 2004a. Bubble deformation and flow structure measured by double shadow images and PIV/LIF. *Experiments in Fluids,* 36**,** 157-165.

FUJIWARA, A., MINATO, D. & HISHIDA, K. 2004b. Effect of bubble diameter on modification of turbulence in an upward pipe flow. *International Journal of Heat and Fluid Flow,* 25**,** 481-488.

GANDHI, B., PRAKASH, A. & BERGOUGNOU, M. A. 1999. Hydrodynamic behavior of slurry bubble column at high solids concentrations. *Powder Technology,* 103**,** 80-94.

GUET, S., LUTHER, S. & OOMS, G. 2005. Bubble shape and orientation determination with a four-point optical fibre probe. *Experimental Thermal and Fluid Science,* 29**,** 803-812.

GUET, S., OOMS, G., OLIEMANS, R. V. A. & MUDDE, R. F. 2004. Bubble size effect on low liquid input drift–flux parameters. *Chemical Engineering Science,* 59**,** 3315-3329.

GUI, L., LINDKEN, R. & MERZKIRCH, W. Phase-separated PIV measurements of the flow around systems of bubbles rising in water. ASME FEDSM, 1997. Citeseer, 22-26.

HASSAN, Y. A., SCHMIDL, W. & ORTIZ-VILLAFUERTE, J. 1998. Investigation of three-dimensional two-phase flow structure in a bubbly pipe flow. *Measurement Science and Technology,* 9**,** 309-326.

HISHIDA, K., FUJIWARA, A., NAGAYA, S., KAKUGAWA, A. & KODAMA, Y. Measurement of turbulent micro-structure in bubbly flows using combined PIV/LIF/IST technique. Proceedings of the Second Symposium on Smart Control of Turbulence, Tokyo, Japan, 2001. 69-78.

JAHANMIRI, M. 2011. Particle image velocimetry: Fundamentals and its applications. Citeseer.

JIN, H., YANG, S., HE, G., WANG, M. & WILLIAMS, R. A. 2010. The effect of gas-liquid counter-current operation on gas hold-up in bubble columns using electrical resistance tomography. *Journal of Chemical Technology & Biotechnology,* 85**,** 1278-1283.

JOSHI, J., PARASU, U., PRASAD, C., PHANIKUMAR, D., DESHPANDE, N. & THORAT, B. 1998. Gas hold-up structures in bubble column reactors. *Proceedings of the Indian National Science Academy,* 64**,** 441-567.

KANTARCI, N., BORAK, F. & ULGEN, K. O. 2005. Bubble column reactors. *Process Biochemistry,* 40**,** 2263-2283.

KARA, S., KELKAR, B. G., SHAH, Y. T. & CARR, N. L. 1982. Hydrodynamics and axial mixing in a three-phase bubble column. *Industrial & Engineering Chemistry Process Design and Development,* 21**,** 584-594.

KASHINSKY, O. N. & RANDIN, V. V. 1999. Downward bubbly gas–liquid flow in a vertical pipe. *International Journal of Multiphase Flow,* 25**,** 109-138.

KASHINSKY, O. N., TIMKIN, L. S. & CARTELLIER, A. 1993. Experimental study of "laminar" bubbly flows in a vertical pipe. *Experiments in Fluids,* 15**,** 308-314.

KATO, H., IWASHINA, T., MIYANAGA, M. & YAMAGUCHI, H. 1999. Effect of microbubbles on the structure of turbulence in a turbulent boundary layer. *Journal of Marine Science and Technology,* 4**,** 155-162.

KAWASHIMA, H., FUJIWARA, A., SAITOH, Y., HISHIDA, K. & KODAMA, Y. Experimental study of frictional drag reduction by microbubbles: laser measurement and bubble generator. Proceedings of the fifth symposium on smart control of turbulence, Tokyo, 2004.

KHALITOV, D. A. & LONGMIRE, E. K. 2002. Simultaneous two-phase PIV by two-parameter phase discrimination. *Experiments in Fluids,* 32**,** 252-268.

KHAN, F., RIELLY, C. & BROWN, D. 2006. Angle-resolved stereo-PIV measurements close to a down-pumping pitched-blade turbine. *Chemical engineering science*, 61, 2799-2806.

KHARE, A. S. & JOSHI, J. B. 1990. Effect of fine particles on gas hold-up in three-phase sparged reactors. *The Chemical Engineering Journal,* 44**,** 11-25.

KIM, H. D., YI, S. J., KIM, J. W. & KIM, K. C. 2010. Structure analysis of bubble driven flow by time-resolved PIV and POD techniques. *Journal of Mechanical Science and Technology,* 24**,** 977-982.

KITAGAWA, A., HISHIDA, K. & KODAMA, Y. 2005. Flow structure of microbubble-laden turbulent channel flow measured by PIV combined with the shadow image technique. *Experiments in Fluids,* 38**,** 466-475.

KOIDE, K., TAKAZAWA, A., KOMURA, M. & MATSUNAGA, H. 1984. Gas holdup and volumetric liquid-phase mass transfer coefficient in solid-suspended bubble columns. *Journal of chemical engineering of Japan,* 17**,** 459-466.

KUMAR, S., KUMAR, R. A., MUNSHI, P. & KHANNA, A. 2012. Gas Hold-up in Three Phase Co-current Bubble Columns. *Procedia Engineering,* 42**,** 782-794.

LAKHDISSI, E. M., SOLEIMANI, I., GUY, C. & CHAOUKI, J. 2020. Simultaneous effect of particle size and solid concentration on the hydrodynamics of slurry bubble column reactors. *AIChE Journal,* 66**,** e16813.

LI, W., ZHONG, W., JIN, B., LU, Y. & HE, T. 2014. Flow patterns and transitions in a rectangular three-phase bubble column. *Powder Technology,* 260**,** 27-35.

LINDKEN, R. & MERZKIRCH, W. 2002. A novel PIV technique for measurements in multiphase flows and its application to two-phase bubbly flows. *Experiments in Fluids,* 33**,** 814-825.

LIU, T. J. & BANKOFF, S. G. 1993a. Structure of air-water bubbly flow in a vertical pipe—I. liquid mean velocity and turbulence measurements. *International Journal of Heat and Mass Transfer,* 36**,** 1049-1060.

LIU, T. J. & BANKOFF, S. G. 1993b. Structure of air-water bubbly flow in a vertical pipe—II. Void fraction, bubble velocity and bubble size distribution. *International Journal of Heat and Mass Transfer,* 36**,** 1061-1072.

LUCAS, D., RZEHAK, R., KREPPER, E., ZIEGENHEIN, T., LIAO, Y., KRIEBITZSCH, S. & APANASEVICH, P. 2016. A strategy for the qualification of multi-fluid approaches for nuclear reactor safety. *Nuclear Engineering and Design,* 299**,** 2-11.

LUO, X., JIANG, P. & FAN, L. S. 1997a. High-pressure three-phase fluidization: Hydrodynamics and heat transfer. *AIChE Journal,* 43**,** 2432-2445.

LUO, X., YANG, G., LEE, D. J. & FAN, L.-S. 1998. Single bubble formation in high pressure liquid—solid suspensions. *Powder Technology,* 100**,** 103-112.

LUO, X., ZHANG, J., TSUCHIYA, K. & FAN, L.-S. 1997b. On the rise velocity of bubbles in liquid-solid suspensions at elevated pressure and temperature. *Chemical Engineering Science,* 52**,** 3693-3699.

MATSUMOTO, T., HIDAKA, N. & MOROOKA, S. 1989. Axial distribution of solid holdup in bubble column for gas-liquid-solid systems. *AIChE Journal,* 35**,** 1701-1709.

MENA, P. C., RUZICKA, M. C., ROCHA, F. A., TEIXEIRA, J. A. & DRAHOŠ, J. 2005. Effect of solids on homogeneous–heterogeneous flow regime transition in bubble columns. *Chemical Engineering Science,* 60**,** 6013-6026.

MOKHTARI, M. & CHAOUKI, J. 2019. New technique for simultaneous measurement of the local solid and gas holdup by using optical fiber probes in the slurry bubble column. *Chemical Engineering Journal,* 358**,** 831-841.

MURAI, Y., OISHI, Y., TAKEDA, Y. & YAMAMOTO, F. 2006. Turbulent shear stress profiles in a bubbly channel flow assessed by particle tracking velocimetry. *Experiments in Fluids,* 41**,** 343.

MURGAN, I., BUNEA, F. & CIOCAN, G. D. 2017. Experimental PIV and LIF characterization of a bubble column flow. *Flow Measurement and Instrumentation,* 54**,** 224-235.

NAGAYA, S., HISHIDA, K., KAKUGAWA, A. & KODAMA, Y. PIV/LIF measurement of wall turbulence modification by microbubbles. Proceedings of the 4th International Symposium on Smart Control of Turbulence, Tokyo, Japan, 2003. 69-78.

NAKORYAKOV, V. E., KASHINSKY, O. N., RANDIN, V. V. & TIMKIN, L. S. 1996. Gas-Liquid Bubbly Flow in Vertical Pipes. *Journal of Fluids Engineering,* 118**,** 377-382.

OHKAWA, W. M., MAEZAWA, A. & UCHIDA, S. 1997. Flow structure and phase distributions in a slurry bubble column. *Chemical Engineering Science,* 52**,** 3941-3947.

OJIMA, S., SASAKI, S., HAYASHI, K. & TOMIYAMA, A. 2015. Effects of Particle Diameter on Bubble Coalescence in a Slurry Bubble Column. *JOURNAL OF CHEMICAL ENGINEERING OF JAPAN,* 48**,** 181-189.

PANDIT, A. & JOSHI, J. 1984. Three phase sparged reactors—some design aspects. *Reviews in Chemical Engineering,* 2**,** 1-84.

PANDIT, A. & JOSHI, J. 1986. Mass and heat transfer characteristics of three phase sparged reactors. *Chemical Engineering Research and Design,* 64**,** 125-157.

PANG, M. & WEI, J. 2013. Experimental investigation on the turbulence channel flow laden with small bubbles by PIV. *Chemical Engineering Science,* 94**,** 302-315.

PJONTEK, D., PARISIEN, V. & MACCHI, A. 2014. Bubble characteristics measured using a monofibre optical probe in a bubble column and freeboard region under high gas holdup conditions. *Chemical Engineering Science,* 111**,** 153-169.

QUICKER, G., SCHUMPE, A. & DECKWER, W. D. 1984. Gas-liquid interfacial areas in a bubble column with suspended solids. *Chemical Engineering Science,* 39**,** 179-183.

RABHA, S., SCHUBERT, M. & HAMPEL, U. 2014. Regime transition in viscous and pseudo viscous systems: A comparative study. *AIChE Journal,* 60**,** 3079-3090.

RODRIGUES, R. T. & RUBIO, J. 2003. New basis for measuring the size distribution of bubbles. *Minerals Engineering,* 16**,** 757-765.

SADA, E., KUMAZAWA, H. & LEE, C. 1986. Influences of suspended fine particles on gas holdup and mass transfer characteristics in a slurry bubble column. *AI Ch. EJ;(United States),* 32.

SARHAN, A. R., NASER, J. & BROOKS, G. 2018. Effects of particle size and concentration on bubble coalescence and froth formation in a slurry bubble column. *Particuology,* 36**,** 82-95.

SERIZAWA, A. & KATAOKA, I. 1990. Turbulence suppression in bubbly two-phase flow. *Nuclear Engineering and Design,* 122**,** 1-16.

SHAH, M., KISS, A. A., ZONDERVAN, E., VAN DER SCHAAF, J. & DE HAAN, A. B. 2012. Gas Holdup, Axial Dispersion, and Mass Transfer Studies in Bubble Columns. *Industrial & Engineering Chemistry Research,* 51**,** 14268-14278.

SHAH, Y. T., KELKAR, B. G., GODBOLE, S. P. & DECKWER, W. D. 1982. Design Parameters Estimations for Bubble Column Reactors. *Aiche Journal,* 28**,** 353-379.

SHAWKAT, M. E., CHING, C. Y. & SHOUKRI, M. 2008. Bubble and liquid turbulence characteristics of bubbly flow in a large diameter vertical pipe. *International Journal of Multiphase Flow,* 34**,** 767-785.

SMITH, D. N. & RUETHER, J. A. 1985. Dispersed solid dynamics in a slurry bubble column. *Chemical Engineering Science,* 40**,** 741-753.

SO, S., MORIKITA, H., TAKAGI, S. & MATSUMOTO, Y. 2002. Laser Doppler velocimetry measurement of turbulent bubbly channel flow. *Experiments in Fluids,* 33**,** 135-142.

THEOFANOUS, T. G. & SULLIVAN, J. 2006. Turbulence in two-phase dispersed flows. *Journal of Fluid Mechanics,* 116**,** 343-362.

TOKUHIRO, A., MAEKAWA, M., IIZUKA, K., HISHIDA, K. & MAEDA, M. 1998. Turbulent flow past a bubble and an ellipsoid using shadow-image and PIV techniques. *International Journal of Multiphase Flow,* 24**,** 1383-1406.

WANG, S. K., LEE, S. J., JONES, O. C. & LAHEY, R. T. 1987. 3-D turbulence structure and phase distribution measurements in bubbly two-phase flows. *International Journal of Multiphase Flow,* 13**,** 327-343.

YOO, D. H., TSUGE, H., TERASAKA, K. & MIZUTANI, K. 1997. Behavior of bubble formation in suspended solution for an elevated pressure system. *Chemical Engineering Science,* 52**,** 3701-3707.

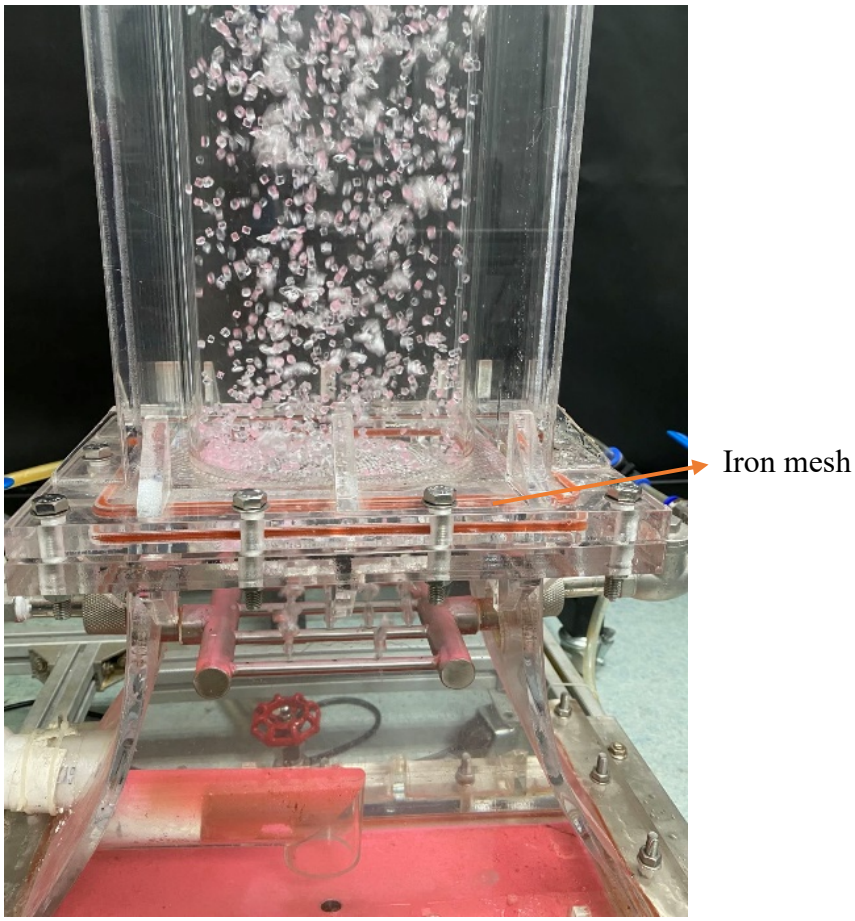

Figure 4- 1 Bubbles generation by air injection through an iron mesh

(a)

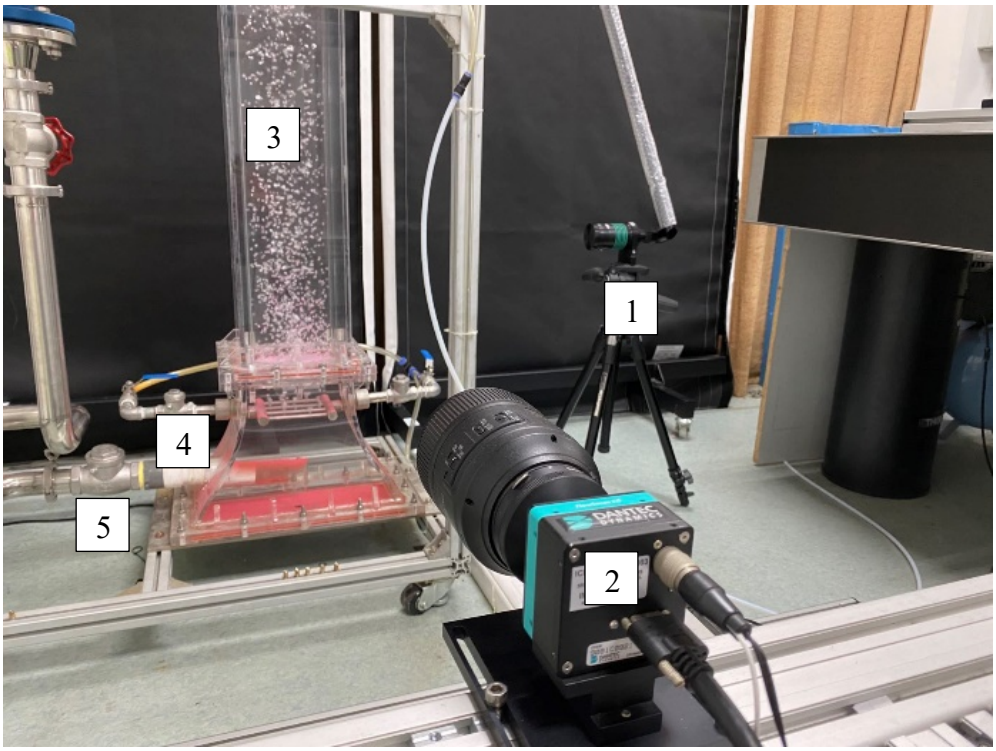

1: Laser Transmitter; 2: CCD camera; 3: Bubble column; 4: Gas inlet;

5: Liquid inlet valve; Red particle within bubble column: Tracer particle

(b)

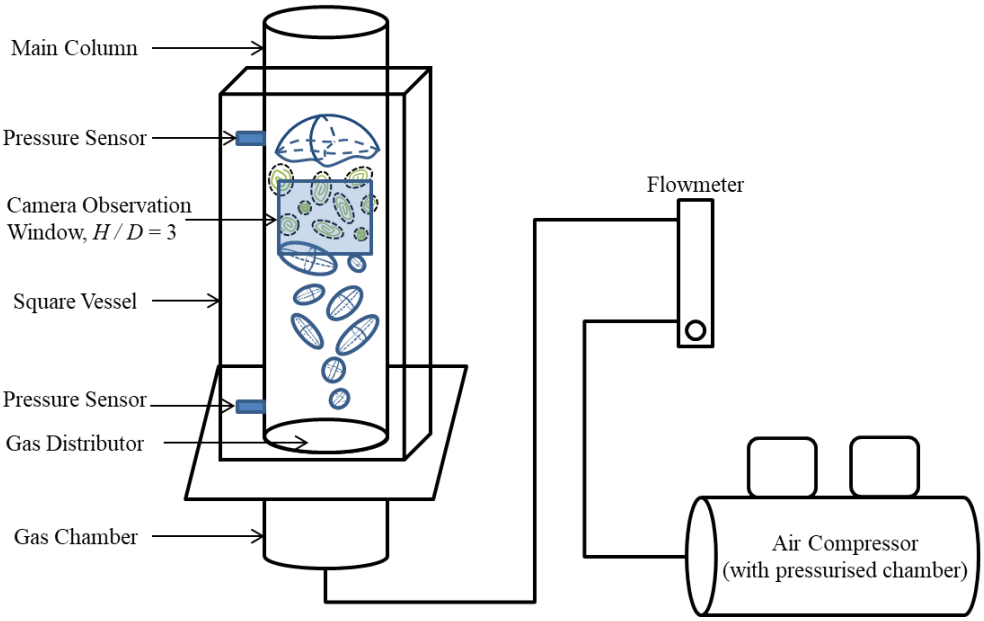

Figure 4- 2 Experimental set-up arrangement

(a) digital photograph (b) schematic diagram

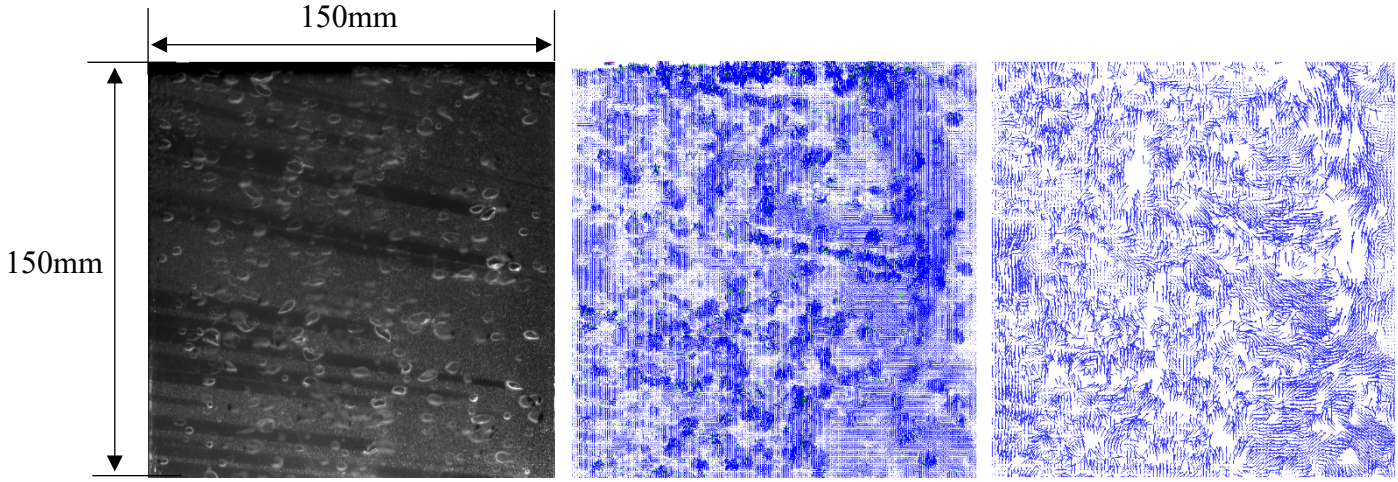

(a) Original image (b) Full velocity (c) Liquid velocity

Figure 4- 3 Bubble discrimination method of PIV images

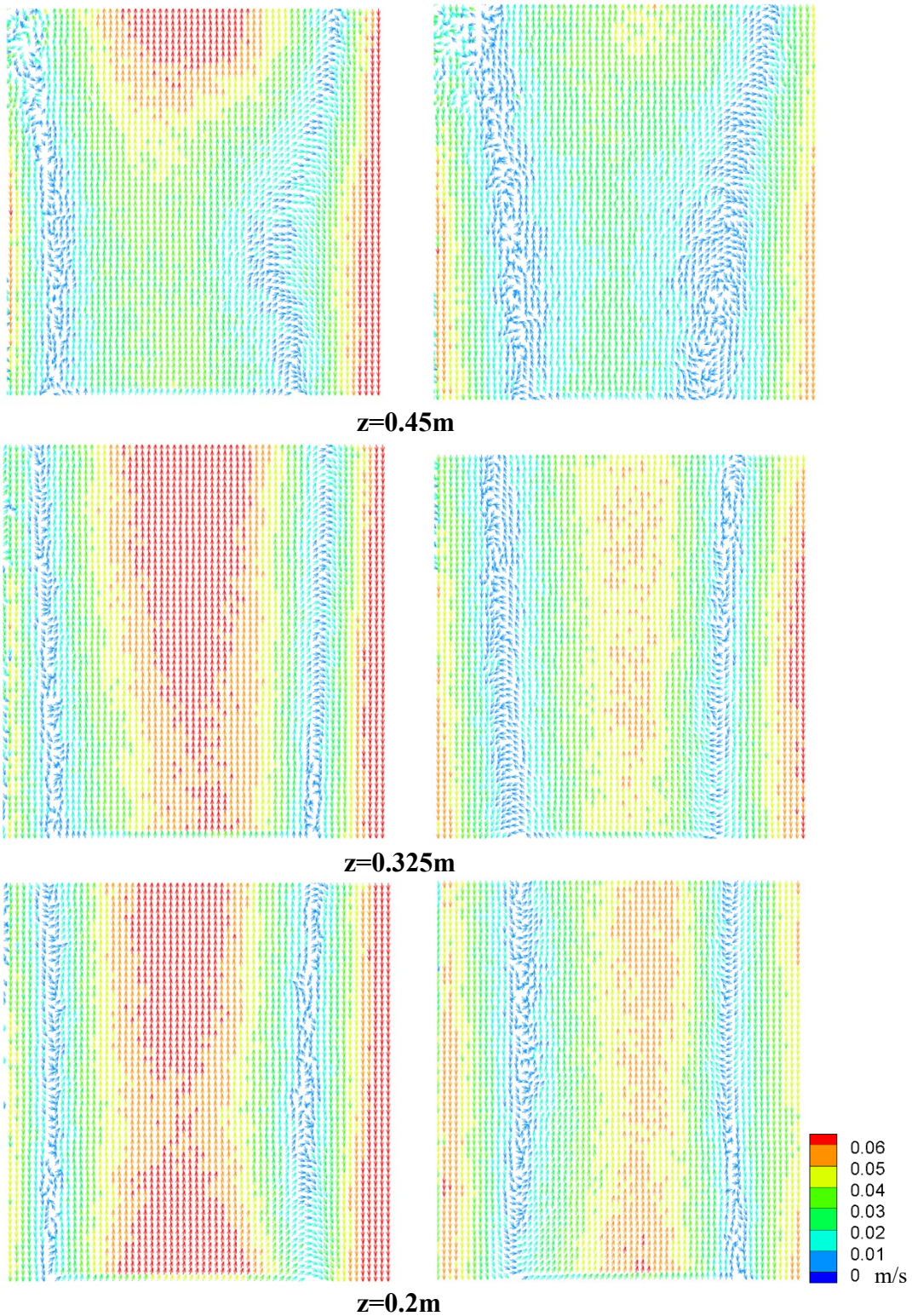

Figure 4- 4 Mean liquid velocity vector of (a) gas-liquid two-phase flow and (b) gas-liquid-solid three-phase flow

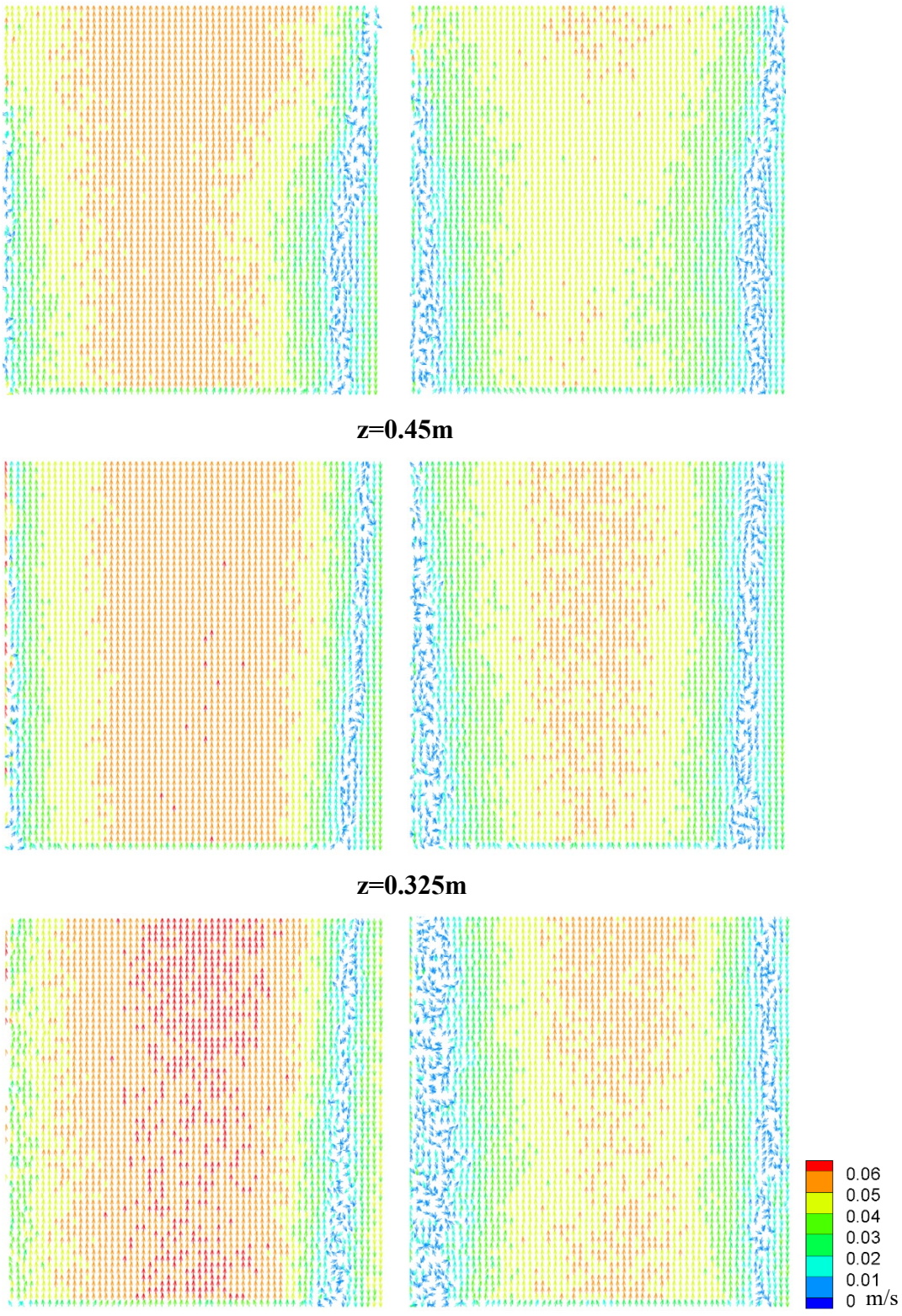

Figure 4- 5 Mean bubble rising velocity vector of (a) gas -liquid two-phase flow and (b) gas -liquid-solid three-phase flow

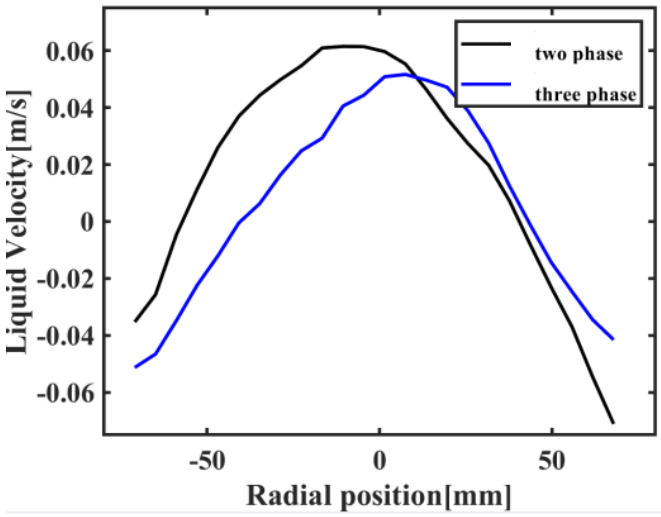

(a)

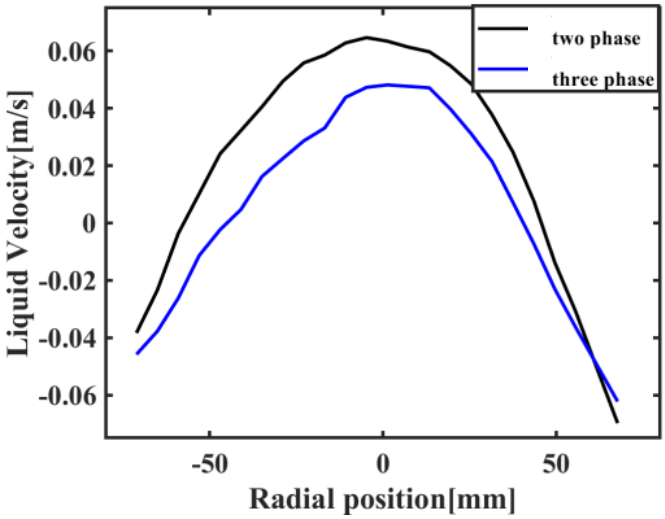

(b)

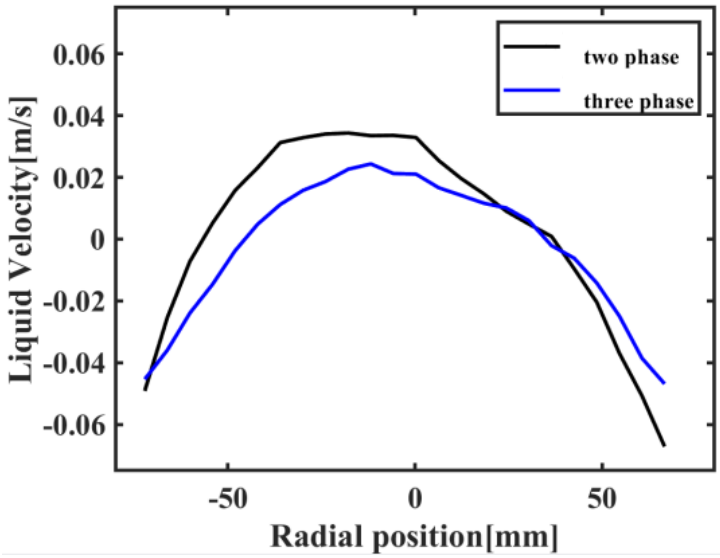

(c)

Figure 4- 6 Mean liquid axial velocity profile in the radial direction at different height. (a) z=0.2m, (b) z=0.325m, (c) z=0.45m.

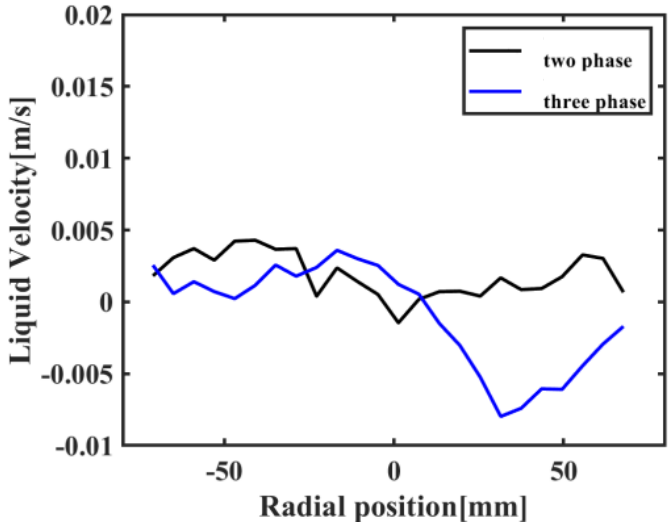

(a)

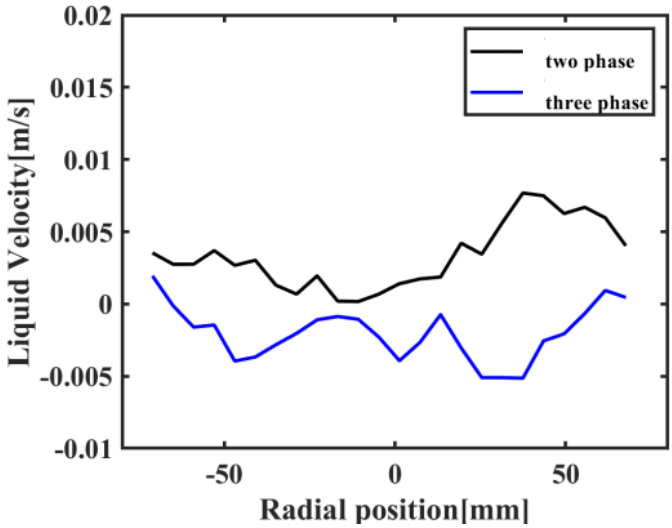

(b)

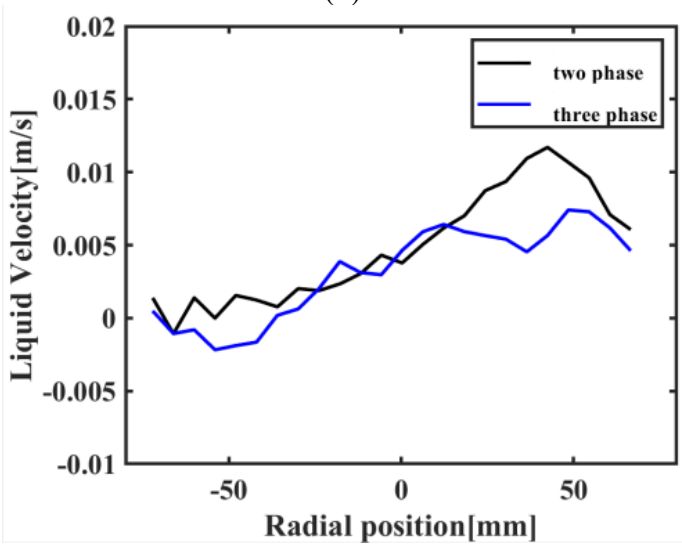

(c)

Figure 4- 7 Mean liquid radial velocity profile in the radial direction at different height. (a) z=0.2m, (b) z=0.325m, (c) z=0.45m

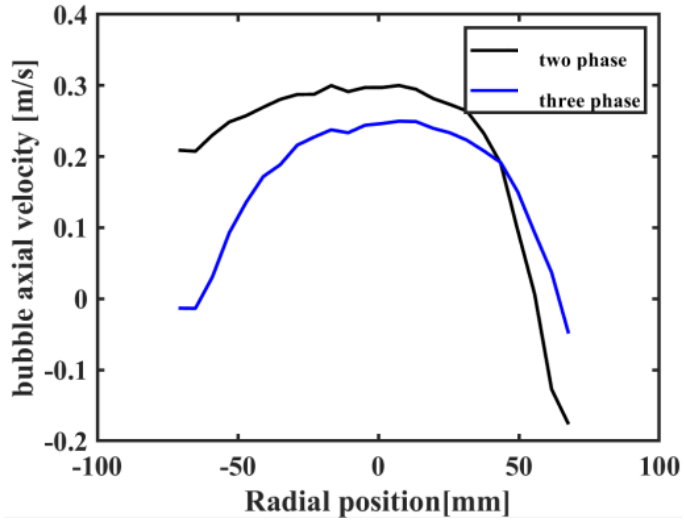

(a)

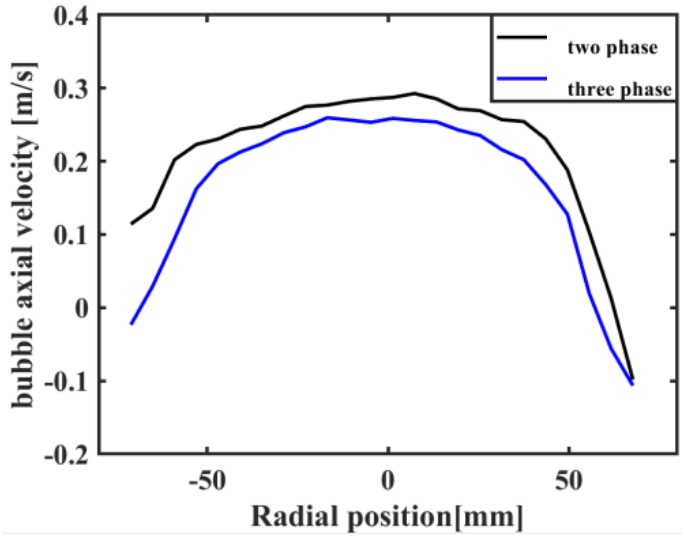

(b)

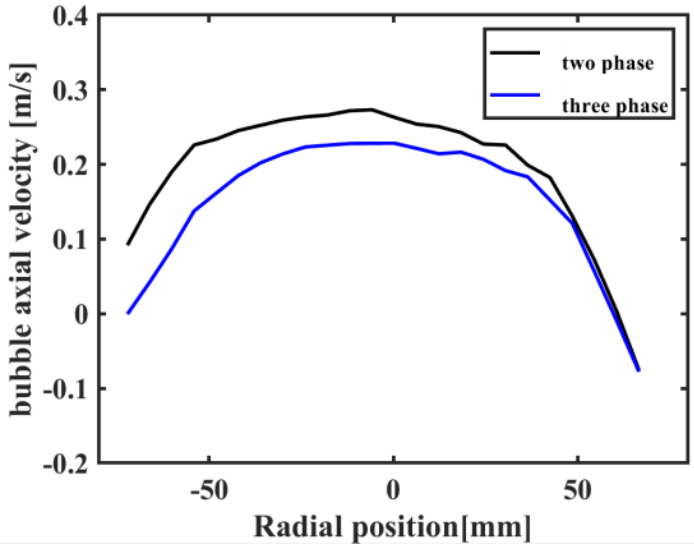

(c)

Figure 4- 8 The mean bubble axial velocity in the radial direction at different height. (a) z=0.2m, (b) z=0.325m, (c) z=0.45m

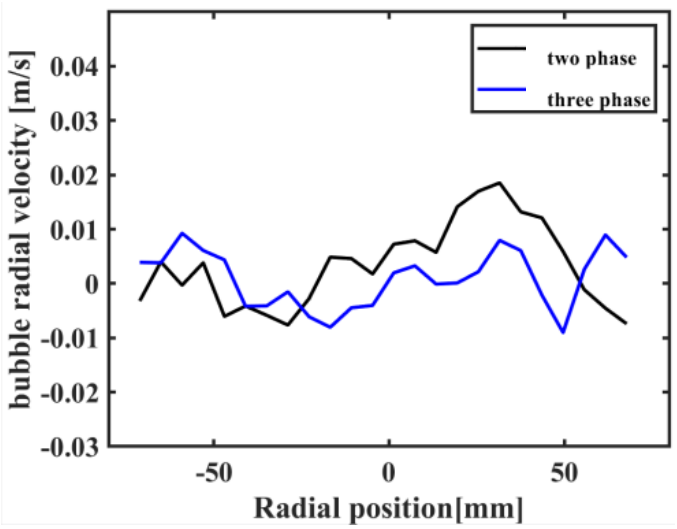

(a)

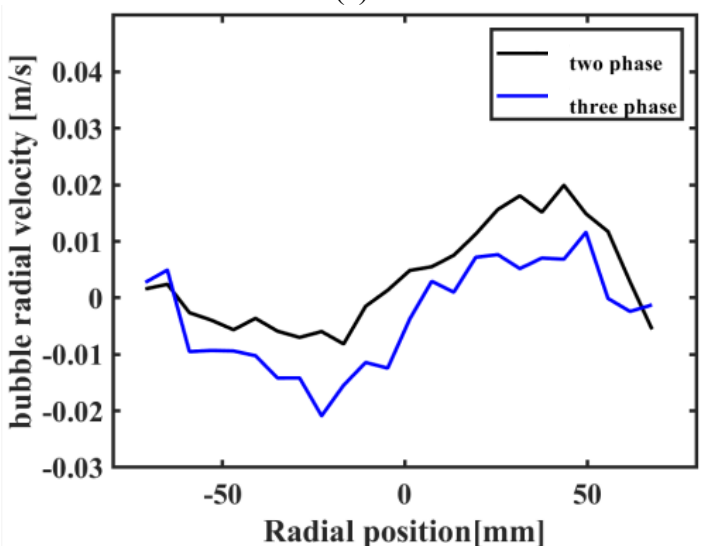

(b)

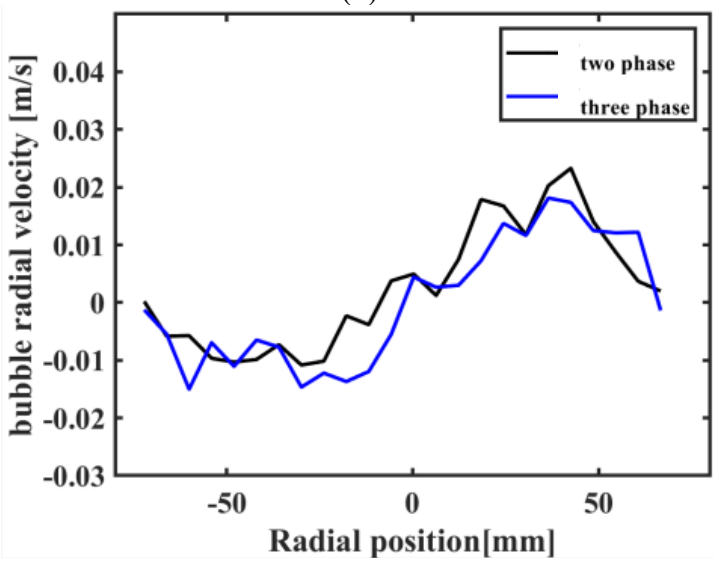

(c)

Figure 4- 9 The mean bubble radial velocity in the radial direction at different height. (a) z=0.2m, (b) z=0.325m, (c) z=0.45m

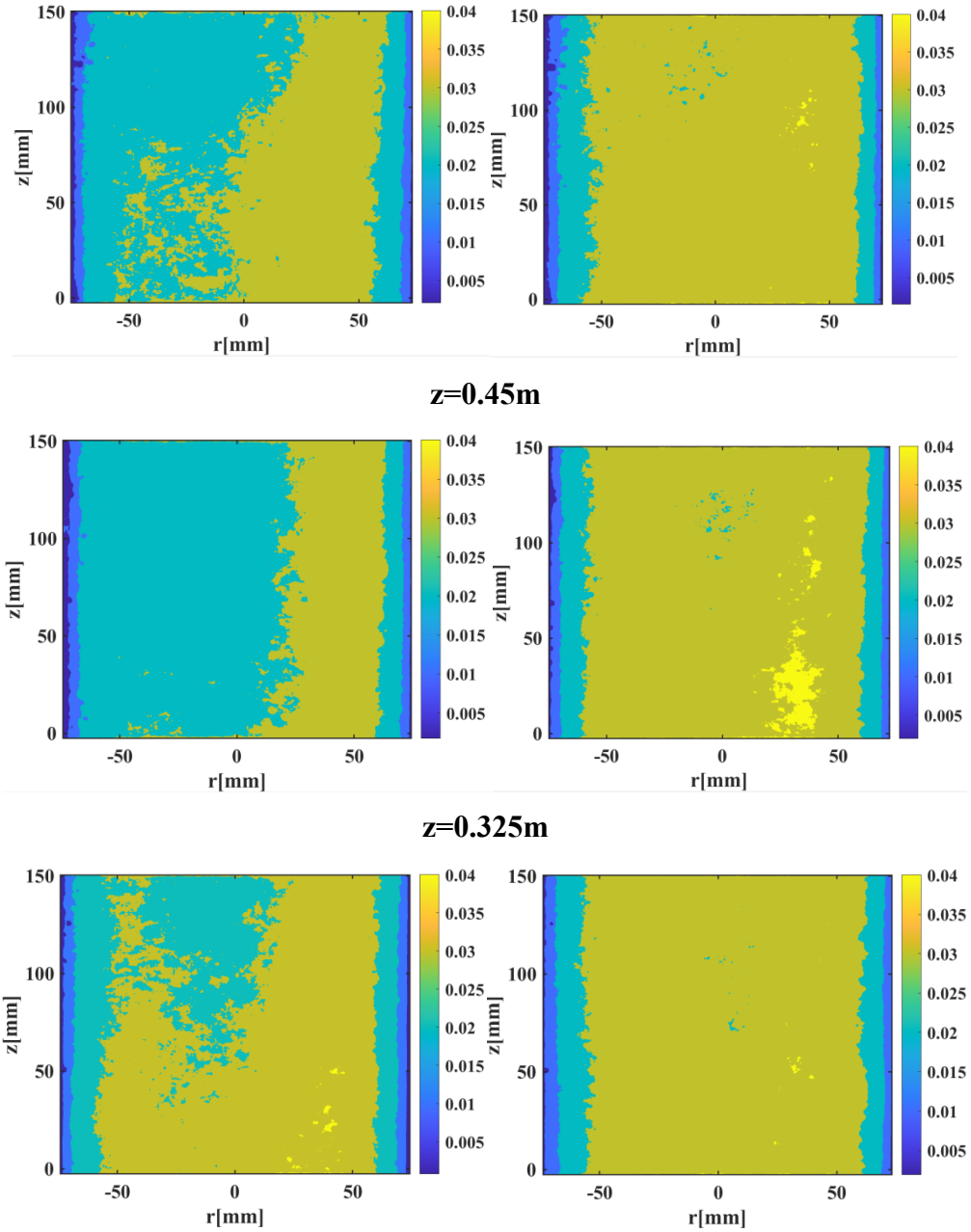

Figure 4- 10 liquid velocity fluctuations u'_{rms} contour. (a) gas-liquid two-phase flow and (b) gas-liquid-solid three-phase flow.

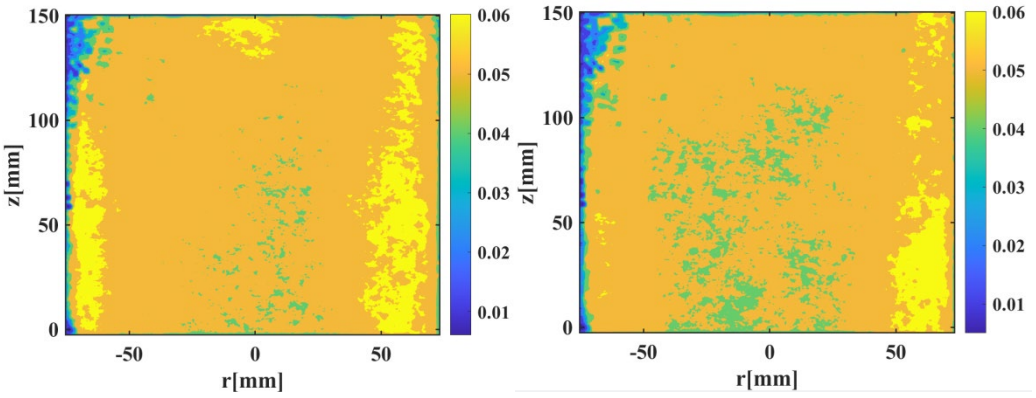

z=0.45m

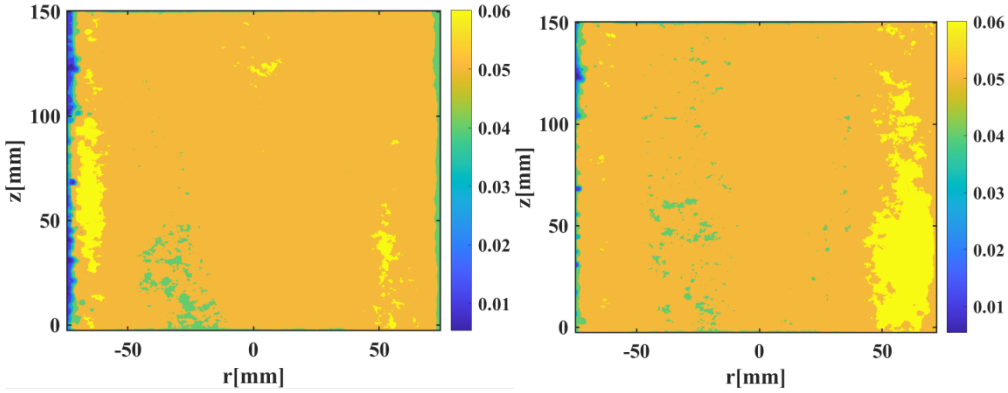

z=0.325m

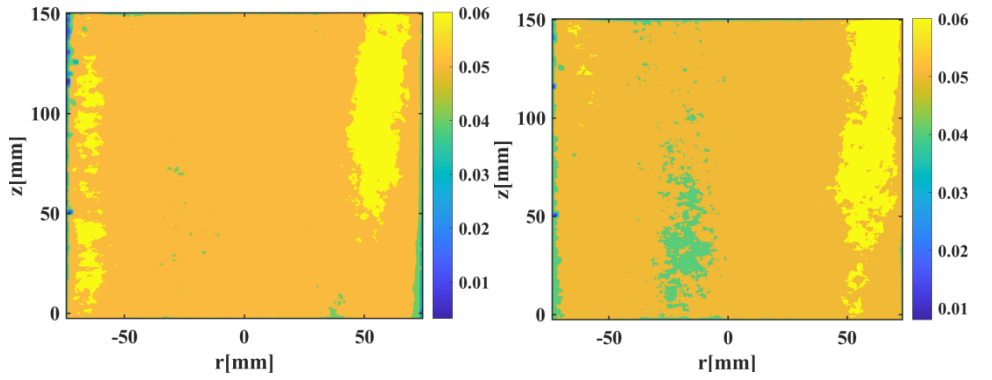

z=0.2m

(a) (b)

Figure 4- 11 Liquid velocity fluctuations v'_{rms} contour. (a) gas-liquid two-phase flow and (b) gas-liquid-solid three-phase flow.

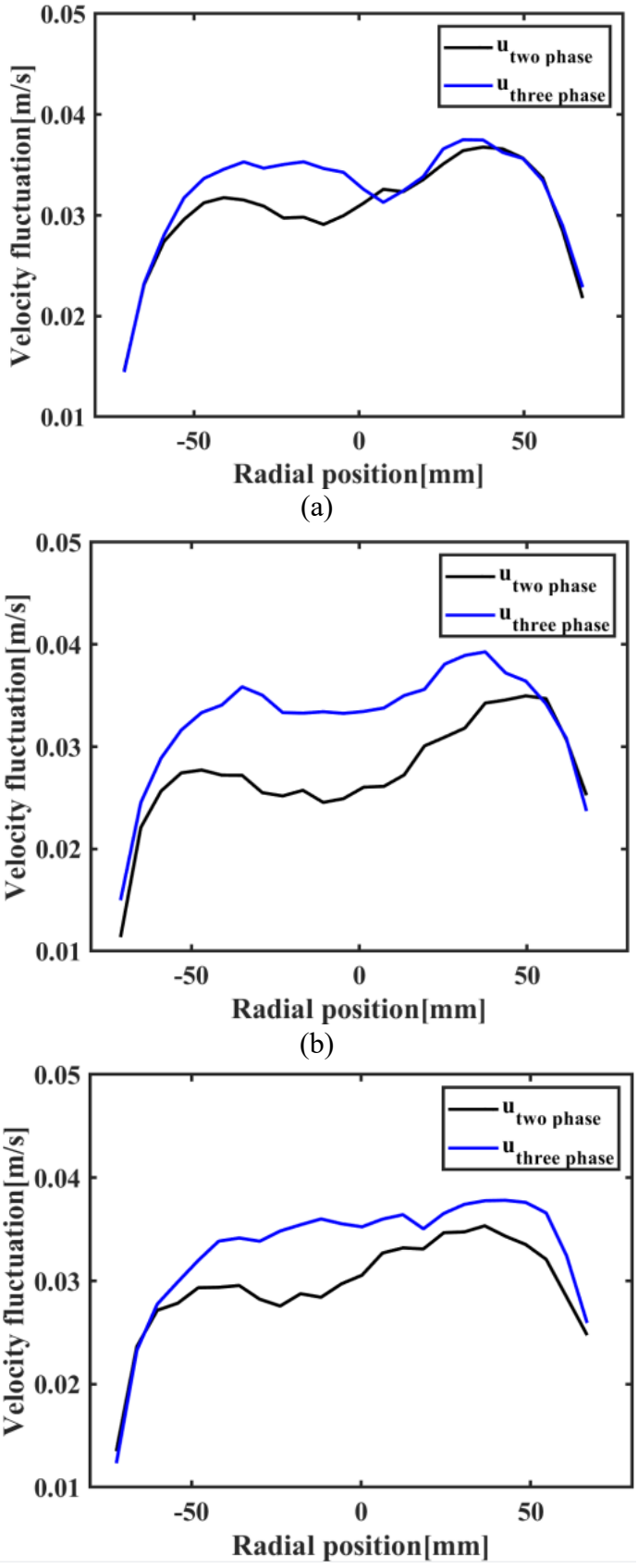

Figure 4- 12 Fluctuation velocity u'_{rms} profile of liquid phase. (a) z=0.2m, (b) z=0.325m, (c) z=0.45m.

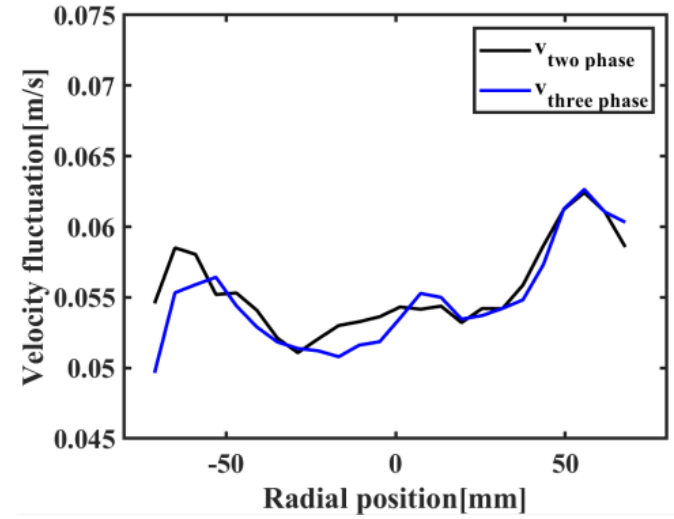

(a)

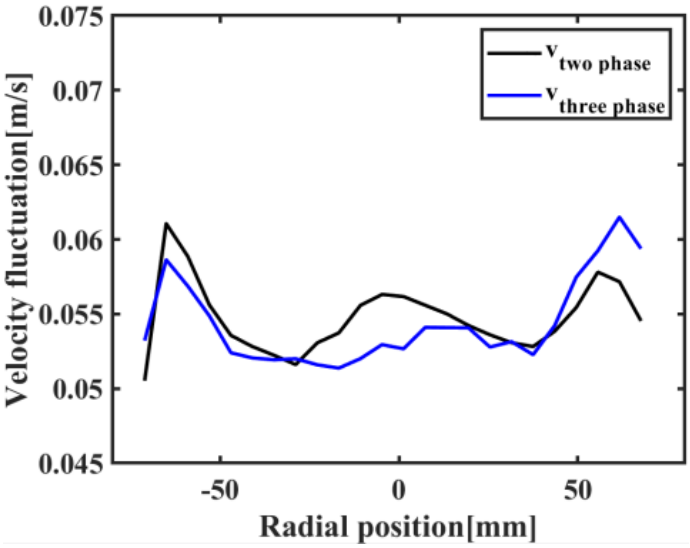

(b)

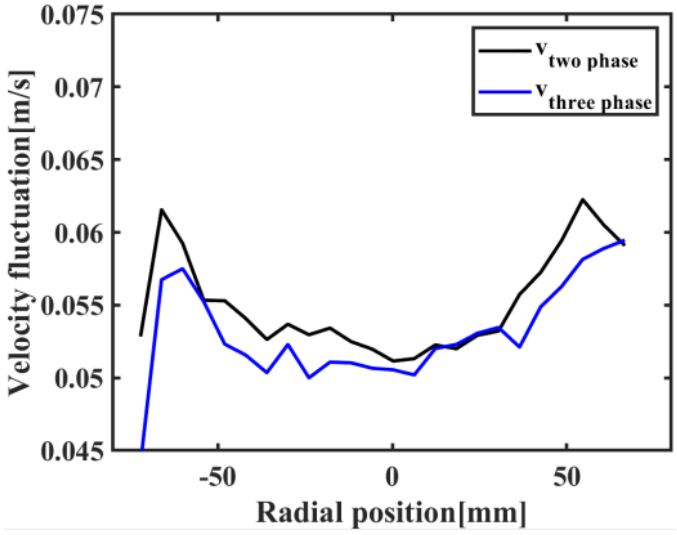

(c)

Figure 4- 13 Fluctuation velocity v'_{rms} profile of liquid phase. (a) z=0.2m, (b) z=0.325m, (c) z=0.45m.

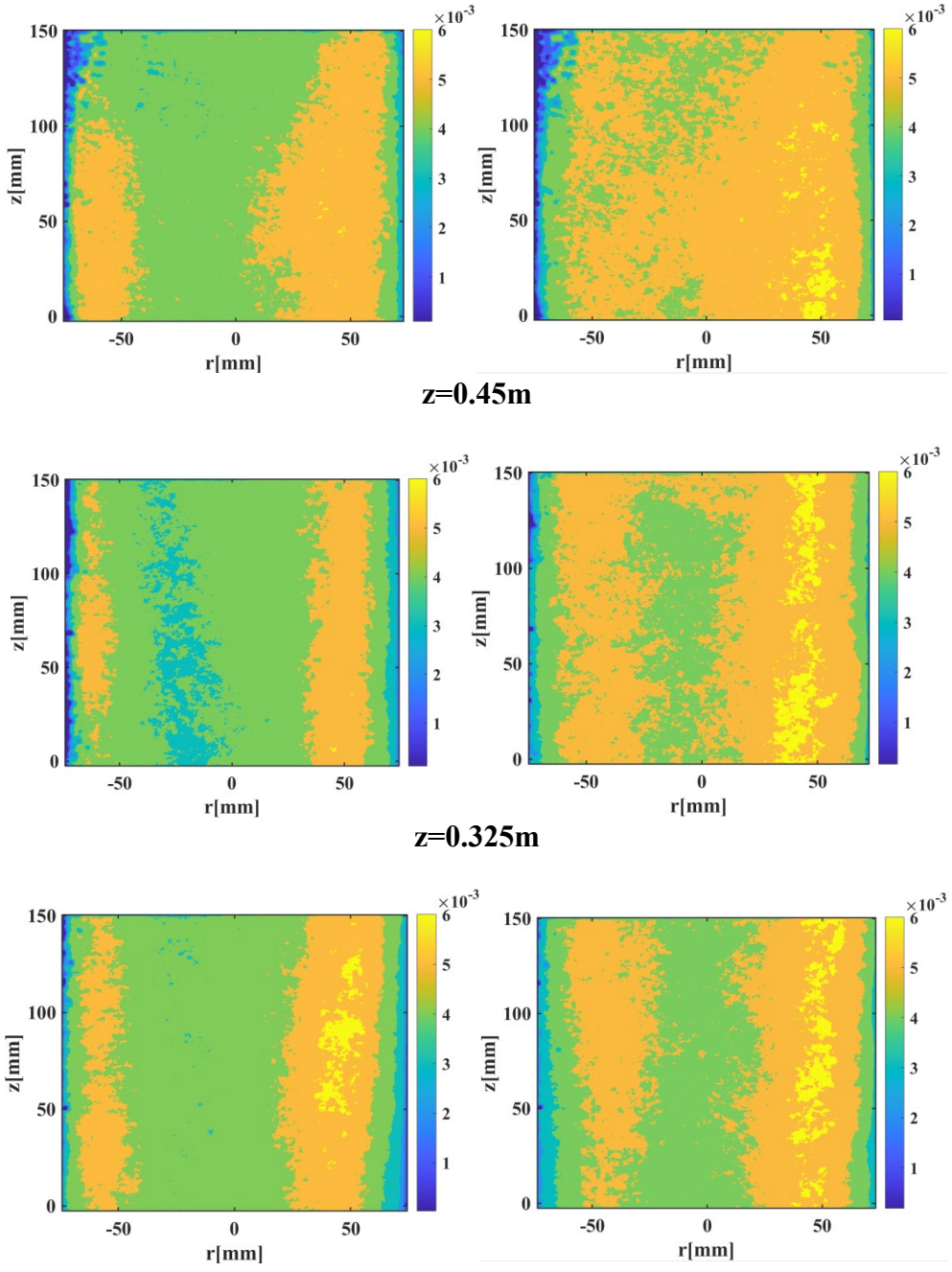

Figure 4- 14 The turbulent kinetic energy of the continuous phase. (a) gas-liquid two-phase flow and (b) gas-liquid-solid three-phase flow

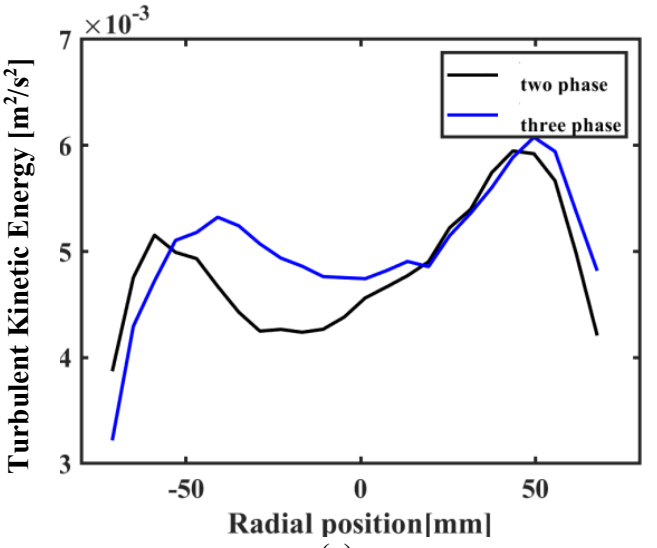

(a)

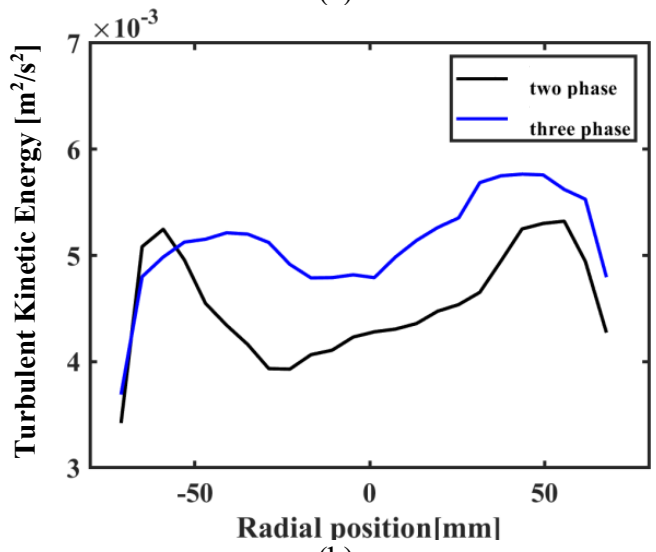

(b)

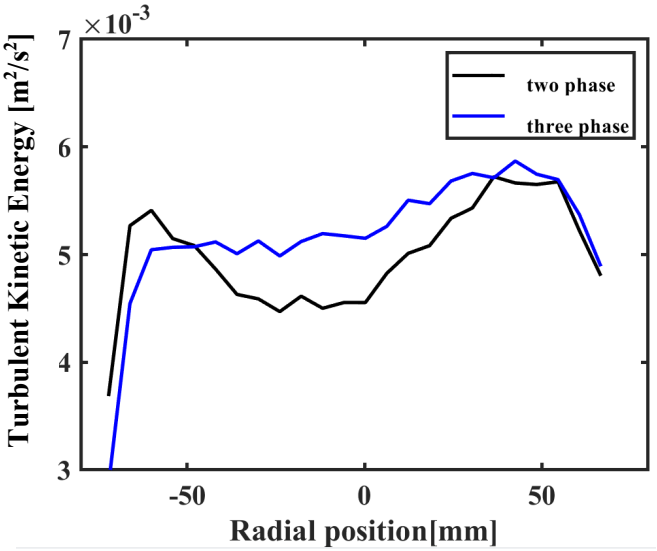

(c)

Figure 4- 15 The turbulent kinetic energy in the radial direction at different height. (a) z=0.2m, (b) z=0.325m, (c) z=0.45m.

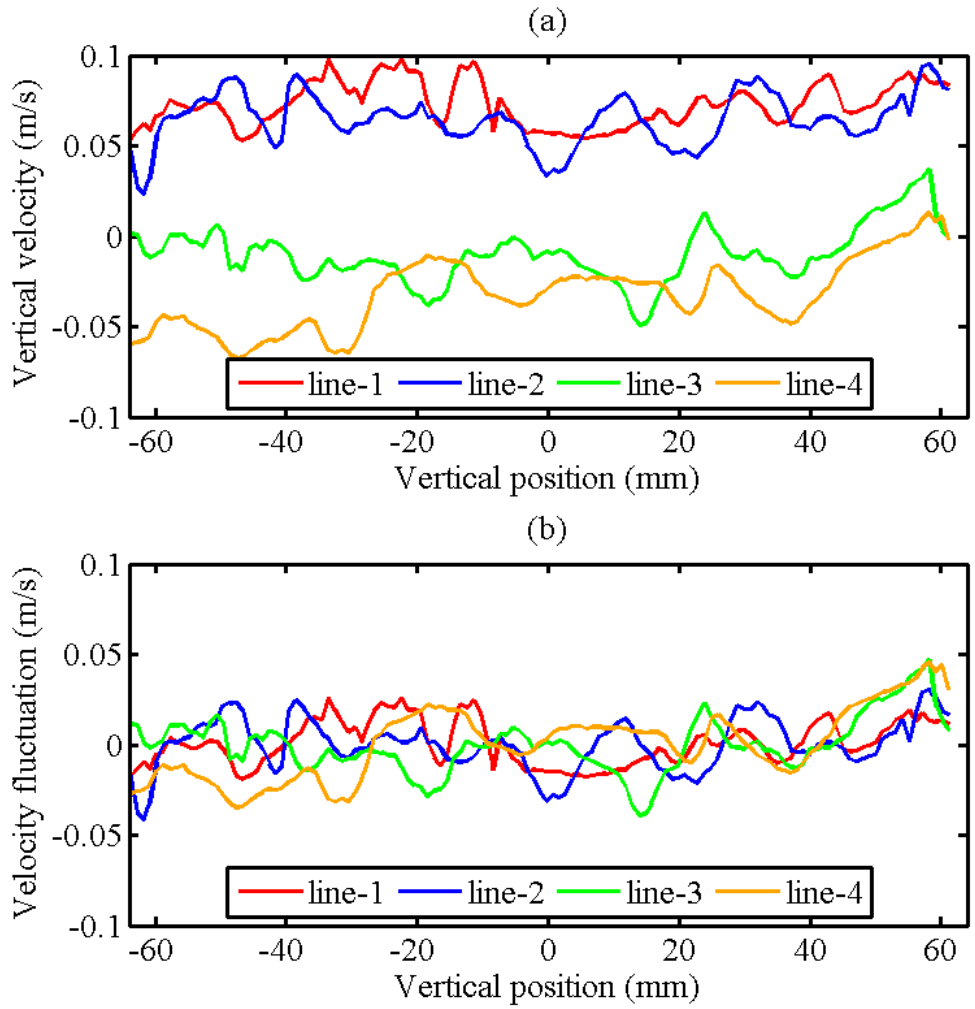

Figure 4- 16 (a) axial liquid velocity and (b) velocity fluctuation at different radial positions.

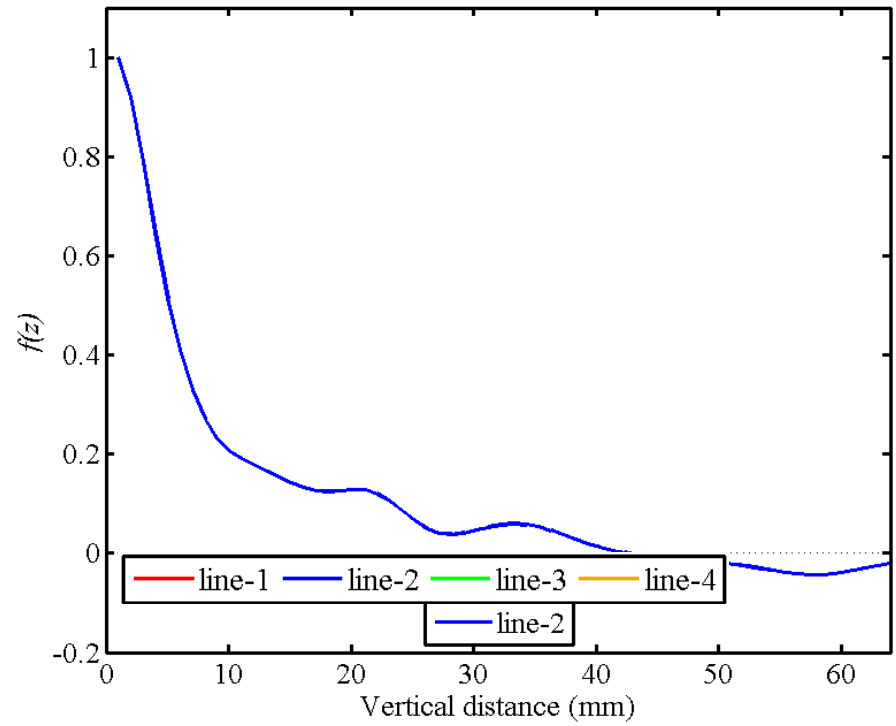

Figure 4- 17 Autocorrelation function in vertical direction.

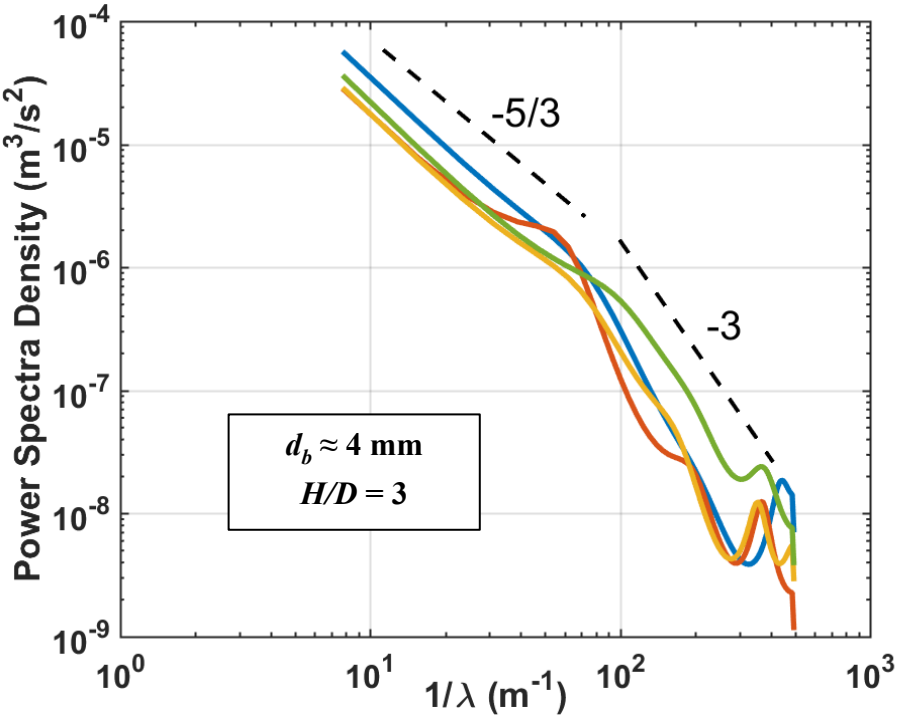

Figure 4- 18 One-dimensional energy spectra in the wake of bubbles.

CHAPTER 5: RECAPITULATION AND RECOMMENDATIONS

1. NUMERICAL MODELLING OF BUBBLE COLUMN REACTORS

The aims of this PhD project are to investigate the hydrodynamics inside the bubble column based on CFD modelling in Eulerian-Eulerian approach and experimental method, focusing on interactions between eddy and bubble. To investigate the effect of eddy/bubble interaction, the CFD modelling implements the modification of bubbles response to their surrounding eddies into turbulent viscosity model and modification of bubble-induced turbulence into bubble breakup model, and experimental studies of multiphase flow. The current research status of CFD modelling in bubble column together with related models and corresponding experimental studies, has been comprehensively reviewed in Chapter 1. As two or three phase flows in bubble column reactors involve complicated transport phenomena such as strong interactions between bubbles and turbulent eddies and bubble-induced turbulence, the hydrodynamic properties cannot be predicted well by CFD modelling using the standard turbulence model without the aforementioned couplings and modifications. Although several researches have considered the effect of bubble-eddy interaction and successfully implemented into multiphase flow simulation in bubble column reactors, majority of them focus on the interphase forces. It remains very challengeable for accurate predicting those important parameters for multiphas e flows in the bubble columns such as liquid

velocities, bubble volume fraction, flow pattern and bubble size distribution. The present PhD project has attempted to consider the effect of bubble response to the surrounding eddies with similar scale on turbulent viscosity and the effect of bubble-induced turbulence on bubble breakup model, and has conducted an experimental study to investigate flow pattern.

The main concluding remarks are summarized as follows:

i. The CFD-PBM method can be implemented to investigate the bubble breakup and coalescence. However, the bubble breakup models with different consideration result in multiple integral, a tricky issue in numerical simulation due to the difficulty of achieving numerical integration and the high computational demand. In Chapter 2, a numerical method for bubble breakup model is proposed. This method adopted for numerical integrations has been used for the acceleration of CFD-PBM modelling. Two cases of bubble columns with different column diameters have been simulated for validations. The results show that this numerical method is time-saving with good performance of prediction in different scale of bubble column. This has provided a basis for the modification and validation of bubble breakup model when PBM is coupled in CFD simulation of bubble column.

ii. The effect of eddy-bubble interactions is considered in Chapter 3. The proposed modified turbulent viscosity model involving bubble response to the surrounding eddies is successfully implemented into Eulerian-Eulerian bubbly flow, while the bubble size distribution is predicted by a breakup

model considering the bubble-induced turbulence kinetic energy spectrum. The simulation results demonstrate improvements in the predictions of gas holdup, liquid velocity and bubble size distribution. The modified model properly addresses the influence of bubble-induced turbulence and bubble response to turbulent eddies.

iii. In Chapter 4, the multiphase flow in the bubble column is experimentally studied and compared through 2D-PIV. The flow characteristics of bubbly flow in bubble column are well capture. From the comparison of gas-liquid two-phase flow and gas-liquid-solid three-phase flow, the particle modulation is illustrated. In terms of the turbulent kinetic energy, the energy distribution is influenced by dispersed phase

The specific realizations of the above claims are described in detail in the following section.

2. SPECIFIC REALIZATIONS

In Chapter 2, a numerical method for bubble breakup model is proposed. From the review of the current status and the methodology adopted for CFD simulation of two-phase bubbly flows together with the concerned modelling issues, bubble size distribution, a main concern in bubble column simulation, is predicted by bubble breakup model. With the gain of understanding of flow nature, the modification for the classical bubble breakup model is required,

which brings multiple integral, a tricky issue in numerical simulation due to the difficulty of achieving numerical integration and the high computational demand. The Eulerian-Eulerian CFD-PBM modelling of gas–liquid two-phase flow in a cylindrical bubble column reactor have been conducted. The results clearly show that this numerical method is time-saving with good performance of prediction, which provided a basis for the modification and validation of bubble breakup model when PBM is coupled in CFD simulation of bubble column.

In Chapter 3, effect of bubble response to the surrounding eddies and bubble-induced turbulence is investigated by CFD-PBM modelling. When studying the eddy-bubble interaction, the effect of bubble response to the surrounding eddies and bubble-induced turbulence cannot be neglected. However, rare research focus on this aspect. With the consideration of the bubble response to the eddies with a similar turbulence length scale, a modified turbulent viscosity model is proposed, while the bubble size distribution is predicted by a modified breakup model considering bubble-induced turbulence energy spectrum. It is revealed that the interaction of bubbles with the bubble-induced turbulence eddies dominates the turbulence generated in in bubble column flows. The contribution to flow field due to the response of bubble to surrounding eddies has been reflected in simulation results. The proposed viscosity model has been validated for two cases of bubble column flows with diameters of D = 0.44 m and D = 0.15 m, respectively. The simulation results for both cases are consistent with the experimental data, which suggests that the eddy-bubble response viscosity

model may be appropriate for description of the mechanism of eddy-bubble interactions in the bubble columns

In Chapter 4, the gas-liquid two-phase flow and gas-liquid -solid three-phase flow in the bubble column are experimentally studied and compared through 2D-PIV. The flow characteristics of bubbly flow in bubble column are well capture. For both liquid mean velocity and bubble mean velocity, the velocity in the middle area is large, and there are low velocity regions near both sides. The velocity in the two-phase flow is greater than that in the three-phase flow. The radial motion at high height is more intense for both two-phase flow and three-phase flow. From the comparison of gas-liquid two-phase flow and gas-liquid-solid three-phase flow, the particle modulation is illustrated. In terms of the turbulent kinetic energy, the energy distribution is influenced by dispersed phase.

3. RECOMMENDATIONS FOR FUTURE WORK

This PhD project has concentrated on one key issue, the gas-liquid interactions of the turbulent bubbly flows in bubble column reactors, and has investigated the effects of bubble response to the surrounding eddies and the effect of bubble-induced turbulence on the bubble breakage, bubble size distributions, turbulence kinetic energy, dissipation rate and other related hydrodynamic parameters. However, there are still some issues that need to be further addressed in order to understand the flow nature. To the best of the author's knowledge, these issues can be classified as follows:

i. In corresponding to the anisotropic feature of the bubble-induced turbulence, the turbulence generation source terms for the Reynolds stress equations also have to be anisotropic. Although the current models have considered the decomposition of isotropic source term S^k into S^R in all three directions, the expression of S^k is still based on the work done by drag force in the direction of the main flow. However, it is believed that the turbulence generations in two transverse directions are strongly affected by the forces acting on the transverse directions, such as lift and wall lubrication forces. Therefore, the effects of transverse forces need to be considered in the turbulence generation term S^R to appropriately address the anisotropic nature of the bubble-induced turbulence. Although the dissipation source term S^ε can be calculated by the dissipation in the wake of bubble ε_w divided by some time scale t, it seems that there is not such a widely accepted expression for this time scale. It is suggested that the time scale should only correspond to that of the turbulent eddies in the wake of bubbles. Therefore, the in-depth understanding regarding the characteristic time scale of the bubble-induced turbulence is further required.

ii. The CFD simulations conducted in the current work are based on the two-fluid model with two-equation $k \sim \varepsilon$ turbulence model. Clearly, the local turbulence structures still have not been resolved sufficiently using these simulation approaches. In order to further understand the inherent structures of the two-phase turbulence, large eddy simulation (LES) may be a more promising modelling strategy. In Euler/Euler LES approach, the

grid size should be larger than the bubble size (0.75 - 0.8Δ) so that the simulation results of Euler/Euler LES modelling can be trusted and reliable. However, when involving bubble coalescence process, bubble size may exceed the limitation, it has impeded the further implementation of the LES to investigate the turbulent bubbly flow because the bubble breakup and coalescence events are important especially for high superficial gas velocity. Developing a reliable method of separating a large bubble into several gridstwo-phase is strongly suggested, which will assist to accurately depict the gas-liquid interactions in the bubble column reactors.

iii. The studies on modelling gas-liquid-solid three-phase bubble column reactors are still rarely reported in the open literature. Most of proposed literature assume liquid and solid phase together as a pseudo-homogeneous phase, which is still two phase modelling in nature. Although some promising results are obtained, a systematic understanding of how density difference in three-phase flows contributes to the interfacial forces closures is still lacking. The density difference of gas-liquid and solid-liquid may lead to significant difference in the directions of bubble and solid particle movements. As a result, seeking the proper drag force relationships which can reflect the interaction between the bubbles and solid.

LIST OF PUBLICATIONS AND CONFERENCES

Journal articles

SHI, W., YANG, X., SOMMERFELD, M., YANG, J., CAI, X. & LI, G. 2020. A Modified Bubble Breakage and Coalescence Model Accounting the Effect of Bubble-Induced Turbulence for CFD-PBM Modelling of Bubble Column Bubbly Flows. *Flow Turbulence Combustion*, 105, 1197–1229.

SHI, W., YANG, J., LI, G., YANG, X., ZONG, Y. & CAI, X. 2018. Modelling of breakage rate and bubble size distribution in bubble columns accounting for bubble shape variations. *Chemical Engineering Science*, 187, 391-405.

SHI, W., YANG, X., SOMMERFELD, M., YANG, J., CAI, X., LI, G. & ZONG, Y. 2019. Modelling of mass transfer for gas-liquid two-phase flow in bubble column reactor with a bubble breakage model considering bubble-induced turbulence. *Chemical Engineering Journal*, 371, 470-485.

SHI, W., LONG, S. YANG, X., & CAI, X. 2022. 计及气泡诱导与剪切湍流的气泡破碎、湍流相间扩散及传质模型.*化工学报*.

Conference proceedings and presentations

CAI, X., YANG, X., SOMMERFELD, M., YANG, J., SHI, W. & LI, G. 2019. CFD-PBM Modelling of Gas-Liquid-Solid Three-phase flow in Bubble Columns with Consideration of Bubble-induced Turbulence Energy Spectrum Distribution and Phase Interaction. *10th Inter-national Conference on Multiphase Flow,* Rio de Janeiro, Brazil, May 19 – 24.

CAI, X., YANG, X., SOMMERFELD, M., YANG, J., SHI, W. & LI, G. 2019. CFD-PBM Modelling of Gas-Liquid-Solid Three-phase flow in Bubble Columns with Consideration of Bubble-induced Turbulence Energy Spectrum Distribution and Particle Modulation. *14th International Conference on Gas-Liquid and Gas-Liquid-Solid Reactor Engineering*, Guilin, China, May 30 – June 3. (Best Poster Award)

CAI, X., YANG, X., YANG, J., SHI, W. & LI, G. 2019. CFD 耦合群平衡方法模拟鼓泡塔中气液固三相流动及颗粒与介尺度湍流涡旋相互作用的研究. *2019 中国化工年会*, 青岛, October 17-19.